IMPACT OF HEPATIC TRANSPORTER MULTIPLICITY AND LOSS-OF-FUNCTION ON HEPATOCELLULAR DISTRIBUTION AND EXCRETION OF DRUGS

Nathan D. Pfeifer

A dissertation submitted to the faculty of the University of North Carolina at Chapel Hill
in partial fulfillment of the requirements for the degree of Doctor of Philosophy
in the Eshelman School of Pharmacy

Chapel Hill
2013

Approved by:

Kim L.R. Brouwer

Dhiren Thakker

Roy Hawke

Gary Pollack

Giulia Ghibellini

ABSTRACT

Nathan D. Pfeifer: Impact of Hepatic Transporter Multiplicity and Loss-of-Function on Hepatocellular Distribution and Excretion of Drugs
(Under the direction of Kim L.R. Brouwer)

The objective of this research project was to develop preclinical and clinical tools to assess hepatocellular exposure and multiplicity of transport. A variety of model systems were employed, including membrane vesicles, sandwich-cultured hepatocytes (SCH), rat isolated perfused livers (IPLs), and *in vivo* human studies; a truly translational approach. This research focused primarily on three drugs to evaluate transporter function: ^{99m}Technetium-mebrofenin (MEB), ritonavir (RTV), and rosuvastatin (RSV). A semi-physiologically-based pharmacokinetic (semi-PBPK) modeling and *in vitro* systems translational approach suggested a transporter-mediated drug-drug interaction (DDI) between MEB and RTV at both hepatic and extrahepatic sites of MEB distribution, observed using a novel clinical protocol. Rather than a specific multidrug resistance-associated protein (MRP) 2 probe, this clinical study demonstrated the utility of MEB as a model organic anion to evaluate DDIs in overall (uptake and efflux) transporter-mediated hepatobiliary clearance. A novel application of classic approaches to determine whole tissue distribution (differential centrifugation, equilibrium dialysis) was investigated with a set of probe drugs in the SCH model system, highlighting the finding that total tissue accumulation and intracellular unbound concentrations can be predicted using SCH, including the relative contribution of active transport vs. binding/sequestration as potential mechanisms of hepatocellular accumulation. A novel uptake and efflux protocol in SCH, coupled with pharmacokinetic modeling, was developed in order to elucidate the relative contribution of basolateral and biliary efflux to the hepatocellular elimination of RSV. This approach, along with IPL data, revealed that basolateral and biliary efflux represent alternative pathways with a quantitatively similar contribution to total hepatocellular excretion

of RSV; the role of basolateral efflux in the hepatocellular disposition of RSV has not been investigated previously. RSV transport was evaluated in human SCH and membrane vesicles prepared from MRP3- and MRP4-overexpressing cells, demonstrating that RSV is an efficient MRP4 substrate. This research resulted in a number of important and novel contributions to the preclinical and clinical "toolkit" available to study hepatic drug disposition. These developments will significantly enhance the ability to assess and predict altered hepatobiliary drug disposition due to DDIs, genetic variation and/or disease states, and will ultimately lead to improved safety and efficacy of medications.

ACKNOWLEDGEMENTS

I want to thank Dr. Kim Brouwer for guiding my personal and scientific development, and for the opportunities she has provided in the course of this research project and my future career in science. I also want to thank all the members of my dissertation advisory committee who have been instrumental in the progression of this project and my scientific development: Dr. Thakker, for taking over as my chair and the timely guidance at critical moments; Dr.Pollack, for serving as my early chair and all of the modeling advice; Dr. Hawke, for all of the support through my clinical experience; and Giulia, for sharing your first-hand knowledge of working with ^{99m}Tc-mebrofenin.

I could not have done this without the help of my colleagues, Brouwer lab members past and present, with whom I have shared countless days and nights in the lab: Brandon Swift for showing me the ropes, Jin Lee, Tracy Marion, Grace Yan, LaToya Griffin, Wei Yue, Kevin Watt and Jason Slizgi. My contemporary partners in crime, humor, science and PK modeling: Brian Ferslew, Kyunghee Yang, Kathleen Köck and Rhiannon Hardwick. The best undergraduate research assistant, with whom I had the opportunity to work and share my only Duke-UNC basketball game, Kevin Harris. All of our undergraduate work-study students over the years who have graciously cleaned our glassware and helped with many experiments, notably: Travis Brown, Chastity Caulder, Rhabia Choudhary and Pearl Nguyen. PK/PD, drug development and T32 fellows from whom I have learned a great deal: Ahsan Rizwan, Noelia Nebot, Dora Dumitrescu, Christina Mayer, Mario Sampson, Curtis Johnston, and Danny Gonzalez. The best, smartest, and funniest cohort I could imagine; thanks for bringing me, and all of us, to the top of our game: Scott Brantley, Jasmine Talameh, Bob Schuck and Dan Hertz. I want to thank a number of other DPET members who have helped me a great deal to relate across narrow lines of age,

interests and responsibility: Christina Won, Melanie Nicol, Christine Walko, Amanda Corbett, and my blast from the past, Julie Dumond - the only person in these walls who knows from whence I came and I never had to explain myself.

Of course I need to thank many people outside the ESoP who reminded me that there was another world out there, and kept me grounded and sane. Ghassan Hamra, for many a coffee break (RIP Global Cup!), as well as my other Bitter Dose and local cycling companions. My early "roomie," and relocation partner, Eliza Peterson, and my recent "roomie" and sounding board, Jimi Radabaugh. Friends who have known me well through many obstacles, including this one, and supported me through many phone calls, emails, and/or trips: Drs. Carly Efros and Thomas Rutkoski (Champs' Champs!) and Tom Leidecker; Renée, for truly rounding out this time of growth for me. Finally, and most importantly, my family: Uncle Jeff and Aunt Kim, who inspired this strangely confluent path; Nana and Papa Stoen, from whom these values of (over-) education and achievement have come down the line; Jordan and Meredith, for relating on so many levels. Erin, thank you for your support in so many things over the years and being such an inspiring sibling, including this whole "pharmacy" thing. Dad, thanks for all your support and demonstrating how to follow one's passions and the capacity for change. Mom, this one's for you; I could not have done this without your support.

TABLE OF CONTENTS

LIST OF TABLES

LIST OF FIGURES

CHAPTER 1

Introduction

Role of Hepatic Efflux Transporters in Regulating Systemic and Hepatocyte Exposure to Xenobiotics

Introduction

The liver is arguably the single most important organ for drug disposition, serving as the primary site of drug metabolism in the body, providing a "gatekeeper" function for systemic exposure following first-pass of portal blood, and being one of the major routes for final elimination of substances from the body. Compounds are presented to hepatocytes via sinusoidal blood, and gain access to the intracellular space by passive diffusion and/or active uptake mediated by transport proteins expressed on the basolateral membrane. The propensity and relative contribution of these mechanisms depends largely on physicochemical properties of the compound. Once inside hepatocytes, the fate of compounds depends on susceptibility to the diverse strategies available for the cell to regulate concentrations of useful and potentially harmful chemicals constantly present in the cellular milieu. This includes subcellular sequestration and mechanisms of elimination, such as biotransformation (metabolism) and/or excretion. It has become clear that transport proteins are responsible for the hepatocellular disposition of highly polar or charged drugs and metabolites, which cannot exit hepatocytes at a sufficient rate without the aid of an active efflux mechanism.

This review provides a summary of transporter-mediated efflux of drugs and metabolites from

---

This work will be published, in part, in *Annual Review of Pharmacology and Toxicology (ARPT)*

hepatocytes into sinusoidal blood and/or bile. The impact of altered transport function, resulting from drug-drug interactions (DDIs), genetic variation and disease states, on systemic and hepatic exposure is discussed. Related issues including multiplicity of transporters, interplay of metabolism and transport, and model systems used to elucidate the role of hepatic efflux on drug disposition are addressed and updated with recent contributions to this area of active research.

Canalicular Efflux

Canalicular efflux transporters include several well-known drug transporters such as ABCB1 (P-gp; MDR1), ABCC2 (MRP2), and ABCG2 (BCRP); in addition, ABCB11 (BSEP), ABCB4 (MDR3), ABCG5/G8, and SLC47A (MATE1) are responsible for bile acid, phosphatidylcholine, and sterol excretion(1-3). MRP2, BCRP, and P-gp are important determinants of biliary excretion of organic anions, organic cations, and Phase II xenobiotic products including glutathione, glucuronide, and sulfate conjugates.

MRP2 is responsible for the bile acid-independent portion of bile flow via secretion of reduced glutathione(1; 4). Additionally, MRP2 is responsible for biliary excretion of organic anions and sulfate-, glucuronide-, and glutathione-conjugates such as methotrexate, etoposide, and acetaminophen-glucuronide, as well as glucuronide and sulfate bile acid conjugates(4-6). Perhaps more importantly, MRP2 transports bilirubin conjugates into bile. Deleterious polymorphisms in the ABCC2 gene lead to the condition known as Dubin-Johnson Syndrome, which is characterized by hyperbilirubinemia despite normal secretion of bile acids via BSEP(5; 6). BCRP is a half transporter containing six transmembrane domains and one ATP-binding cassette in contrast to the common twelve transmembrane domains and two ATP-binding cassettes that comprise other ABC transporters(7; 8). Studies have shown that in order to be functional, BCRP most likely needs to homodimerize or oligomerize(7; 8). BCRP mediates the biliary excretion of sulfate and glucuronide conjugates and bile acids(4; 9). Additionally, BCRP appears to be responsible for the partial compensatory excretion of such conjugates in scenarios of diminished MRP2 function(6). P-gp transports a wide variety of substrates including immunosuppressants, antibiotics, steroids, anticonvulsants, and Ca^{2+} channel blockers, among others.(10) Although it is postulated that P-gp does not normally play a primary

role in biliary excretion of drug conjugates, it is one of the major determinants of cation excretion into bile(6; 10). Unlike MRP2 and BCRP, P-gp is not considered as having a major role in the formation of bile flow(4).

Due to their wide substrate specificity, canalicular efflux transporters play a central role in limiting systemic exposure to xenobiotics and their conjugates. In the classic view, xenobiotics and conjugates are excreted into bile by canalicular transporters for delivery to the intestine and removal from the body via fecal excretion. However, some xenobiotics and conjugates that undergo biliary excretion evade fecal elimination, at least in part, by reabsorption in the intestine and re-delivery to the liver. This process, which may occur numerous times for a given compound, is known as enterohepatic recirculation (ER). ER can lead to a prolonged half-life of compound in the systemic circulation, and frequently is manifested by multiple peaks in the plasma concentration-time profile.(11; 12) ER often involves cleavage of phase II conjugates in the gut and reabsorption of parent drug, a process that can be facilitated by intestinal microflora.(12; 13) Drugs (or their metabolites) that are known to undergo ER to a significant extent include mycofenolic acid(14), glycyrrhizic acid(15), morphine(12), warfarin(12), amlodipine(16), indomethacin(17; 18), spironolactone(12), sulindac(12), sorafenib(19), valproic acid(20), and the irinotecan metabolite, SN-38(21).

Enterohepatic recirculation is an important process for the regulation of bile acid synthesis in the liver, thus any event leading to perturbation of normal biliary secretion has implications not only for xenobiotic excretion, but also for the circulating bile acid pool and hepatocellular homeostasis(22). BSEP dominates bile acid and bile acid conjugate excretion into bile; however, the affinity and capacity of BSEP for individual bile acid conjugates differs between species, necessitating caution in the interpretation of mechanistic rodent studies(2; 4). Mutations in the ABCB11 gene can result in the lack of protein expression, improper localization of the transporter in the canalicular membrane, or overall decreased expression(2). Such mutations lead to the accumulation of bile acids within hepatocytes and subsequently, hepatocellular damage and cholestasis(2). This condition, which is known as progressive familial intrahepatic cholestasis (PFIC), is a collection of cholestatic disorders resulting from mutations in ABCB11 (PFIC2), ATP8B1

(PFIC1), or ABCB4 (PFIC3). On the other hand, xenobiotic inhibition of BSEP can result in an acquired cholestatic condition, which may also lead to severe hepatocellular damage, toxicity, and liver failure, known as drug-induced liver injury (DILI), which will be discussed below(2; 23).

Basolateral/Sinusoidal Efflux

Basolateral efflux commonly is regarded as a compensatory route of elimination to protect hepatocytes in the setting of cholestasis or otherwise impaired biliary excretion, by mediating excretion of endo- and xenobiotics from hepatocytes into the sinusoidal blood. Transport proteins that have been shown to mediate basolateral efflux of drugs are limited primarily to MRP3 and MRP4. These transporters serve also to facilitate systemic exposure and resulting efficacy, toxicity and/or non-hepatic (e.g., renal) elimination of metabolites that are formed in the liver. This is particularly true of phase II metabolites such as sulfate, glucuronide and glutathione conjugates(6). A classic example is acetaminophen, which undergoes extensive conversion to glucuronide and sulfate conjugates that are recovered largely in urine, and are known to be substrates for MRP3 and/or MRP4(6). Another example is enalaprilat, the dicarboxylic acid and active metabolite of enalapril, which is formed primarily in the liver and relies on active transport for efflux into the systemic circulation(24). Additionally, increased systemic concentrations of the pharmacologically active phase II metabolite, ezetimibe-glucuronide, correlated with increased expression of Mrp3 and altered localization (internalization) of Mrp2 in a rodent model of NASH(25). This shift from biliary excretion to plasma by basolateral efflux transporters diverts the active ezetimibe-glucuronide metabolite away from the site of action in the intestine, and illustrates a mechanism of altered efficacy as a result of disrupted hepatobiliary efflux. Basolateral efflux transporters also may play a role in the disposition of parent drugs, such as fexofenadine. The loss of Abcc3 (but not Abcc4) in mice reduced outflow perfusate recovery in the isolated perfused liver system(26). Another example is methotrexate, which will be discussed under Interplay of Multiple Hepatic Efflux Systems (below).

The importance of basolateral efflux in regulating systemic versus hepatocyte exposure, routes of drug elimination, and the detoxification function of the liver has been described recently for bilirubin

glucuronides by Schinkel and colleagues(27). The interplay of Oatp-mediated hepatic uptake and efflux by Mrp2 and Mrp3 was investigated by observing alterations in the disposition of bilirubin glucuronides in single- and multiple-knockout mice(27-29). These studies elegantly challenged the prevailing perception that extensive biliary excretion of bilirubin glucuronides results from efficient vectorial transport from sinusoidal blood to bile on the level of an individual hepatocyte. The relative contribution of basolateral vs. canalicular excretion may be much greater than previously thought. Rather than efficient excretion from the cellular space into bile, it is possible that multiple rounds of less efficient cycling, or "hepatocyte hopping," along the length of the liver sinusoid result in extensive biliary excretion. In this way, basolateral efflux was suggested to be a major contributor to the efficiency of the liver as a "flexible and robust" organ of detoxification, "potentially distributing the biliary excretion load over all hepatocytes within the liver lobule"(27).

A number of other efflux transporters are known to be expressed on the basolateral/sinusoidal membrane of hepatocytes, including ABCC5 (MRP5) and ABCC6 (MRP6). Although expression levels are generally low in healthy individuals, there is evidence of upregulation in disease states(30; 31), suggesting that these proteins may play an important compensatory role in the setting of impaired biliary excretion pathways, or otherwise compromised hepatocellular function. Although a number of drugs and endogenous compounds have been identified as substrates and/or inhibitors in isolated expression systems(32), there are no known examples where these transport proteins play a significant role in the disposition of compounds *in vivo*. It may be that these proteins are responsible (in part or in whole) for the significant "residual" basolateral efflux of sulfate and glucuronide conjugates observed in Abcc3$^{-/-}$, Abcc4$^{-/-}$ and Abcc3$^{-/-}$/Abcc4$^{-/-}$ animals(33).

In addition to the unidirectional, ATP-driven ABC family transporters, a number of facilitated diffusion mechanisms exist that can participate in uptake or efflux depending on the electrochemical gradient of substrates and co-substrates. One example is SLC51 (polyspecific organic solute carrier, OSTα/β), which is thought to be involved in bile acid and sterol reabsorption under normal circumstances, but displays bidirectional transport *in vitro*(34-37). The substrate specificity of OSTα/β is

limited currently to bile acids, steroid conjugates and eicosanoids, but the ability to transport digoxin suggests that further characterization of potential drug substrates is needed. It has been suggested that the SLC isoforms (OATPs, OATs and OCTs) are capable of bidirectional transport under certain conditions(38; 39), which would open the door to a large number of well-known substrate drugs, including the statins. However, the role of bi-directional transport by OATPs and other SLC family members is controversial and has not been shown definitively to play a role for drug molecules.

Functional Impairment Mechanisms

Drug Interactions Involving Hepatic Efflux Transport

Inhibition of hepatocellular efflux activity affects normal hepatic function, including excretion of endogenous substances such as glutathione, bile acids and bilirubin, and can alter the pharmacokinetic profile of drugs(40). Therefore, affinity of drug candidates for hepatic efflux transporters may represent a liability to serve as victims and/or perpetrators of drug interactions(40). For example, clinically-significant differences in mycophenolic acid (MPA) pharmacokinetics are observed when this medication is co-administered with the calceiunurin inhibitors tacrolimus or cyclosporine A (CsA) for maintenance of immunosuppression following solid organ transplant(14; 41). MPA is metabolized primarily to the inactive phenolic glucuronide conjugate, MPAG, which is excreted into bile via MRP2, hydrolyzed back to MPA in the gut, and undergoes ER(14; 41; 42). Inhibition of MRP2-mediated biliary excretion and decreased ER explains some of the ~50% decrease in MPA trough concentrations in patients co-administered CsA(14; 41). One challenge in distinguishing biliary excretion as the definitive mechanism responsible for DDIs and altered pharmacokinetics is that many of the same transport proteins are present at the apical border of the intestine and kidney(6; 40; 43-46). In the absence of mechanistic information, such as bile-duct cannulated animals, it can be difficult to deconvolute the relative contribution of impaired canalicular versus intestinal or renal excretion(47; 48). Definitive examples of reduced biliary clearance in the presence of inhibitors remain limited. Erythromycin decreased the biliary excretion of fexofenadine in rat isolated perfused livers(49), while elacridar (GF120918, an BCRP and P-gp inhibitor)

decreased the biliary excretion of DPDPE (a metabolically stable opioid peptide) in isolated perfused livers from Abcc2-/Mrp2-deficient TR$^-$ rats(50). P-gp inhibition may contribute to other DDIs, such as the reduced biliary excretion of colchicine, doxorubicin and digoxin by erythromycin or ketoconazole(44; 45). The role of Mrp2 and Bcrp as the primary mechanisms for biliary excretion of rosuvastatin was confirmed in rat livers from wild-type and TR$^-$ rats in the presence and absence of GF120918, which had been suggested previously using *in vitro* systems and single knockout animals.(51; 52) A number of drugs have been shown to inhibit biliary excretion of conjugated bile salts mediated by BSEP, which can result in DILI, as demonstrated by several cases of drug withdrawals or black-box warnings (*e.g.*, troglitazone, bosentan, erythromycin, nefazodone)(53-58). In addition to BSEP, MRP3 and MRP4 also are involved in the export of bile acids and drugs/metabolites. Recent studies suggest that inhibition of MRP4 is a risk factor for the development of DILI; considering the potential for drug candidates to inhibit MRP4, in addition to BSEP, could aid in predicting compounds with liability for DILI at an earlier stage in drug development(59).

For lists of compounds that inhibit hepatic efflux transporters, the reader is directed to a number of excellent reviews that have collated available data for individual ABC family transport proteins: MRP2(5; 32; 60), BCRP(7; 60-62), P-gp(60; 63), BSEP(64), MRP3(6; 32) and MRP4(6; 32). These reviews typically include information such as the model system that was used to generate inhibition data, the probe substrate, and a mathematical value corresponding to the inhibitory potential of the compound of interest, such as a percent inhibition at a given concentration, IC_{50} or K_i. These data tend to be collected from reports of individual or small sets of inhibitors generated in different experimental systems/conditions. As such, it can be difficult to compare the relative inhibitory potential of compounds from different sources. In addition to these reviews, several large-scale, public, web-based efforts are underway to curate the historic and growing body of experimental data reporting interactions between chemicals and transport proteins. These databases include "TP-Search" (www.tp-search.jp)(65), the Transporter Classification Database (TCDB; www.tcdb.org)(66), TransporterDB (www.membranetransport.org)(67) and the UCSF pharmacogenetics database

(pharmacogenetics.ucsf.edu)(68). A large-scale QSAR modeling effort was reported recently by Tropsha and colleagues, which included automated curation of the aforementioned databases and literature sources, resulting in the largest known repository of transporter inhibition data(69).

Mechanisms of DDIs Involving Hepatic Efflux Transporters

The vast majority of data describing transporter DDIs suggest a competitive inhibition mechanism, resulting from the aforementioned wide and overlapping substrate specificity of transport proteins. However, drugs may interact with transport proteins by a variety of mechanisms and, therefore, cis-inhibition as well as mechanism-based and trans-inhibition, allosteric-induced modulation and induction of transport function may be important mechanisms of transporter-mediated DDIs(70). For example, trans-inhibition of BSEP has been demonstrated for estrogens, possibly contributing to cholestasis of pregnancy(71; 72). Time-dependent inhibition of hepatic uptake transporters has been shown with cyclosporine A(73; 74). Of the multiple binding sites proposed for P-gp, some are reported to interact in a positive cooperative manner, resulting in mutual stimulation of P-gp-mediated transport of several substrates, including rhodamine 123, anthracyclines, some flavonoids, and the p53 inhibitors QB102 and QB11(75). Similarly, in 2003, two groups independently reported potentiation of estradiol-17-β-D-glucuronide transport by MRP2, which was followed by additional reports from large-scale screening approaches(76). Another classic mechanism leading to increased transport activity is induction. Treatment of cultured primary rat hepatocytes with the chemical carcinogen 2-acetylaminofluorene (2-AAF), the antineoplastic drug cisplatin, and the protein-synthesis inhibitor cycloheximide led to a dose-dependent and time-dependent increase in gene expression of Mrp2, with corresponding plasma membrane localization(77). Although this effect is likely to be of relevance mostly for the acquisition of multidrug resistance during chemotherapy, potential implications exist for the hepatobiliary disposition of drugs and metabolites. P-gp also is induced by a number of drugs, including ritonavir(78). In the case of P-gp, many drugs overlap in their ability to interact with CYP3A and P-gp (as substrates, inhibitors and/or inducers). Due to the often sequential detoxification chain represented by these mechanisms, the effect of inducers or inhibitors can be synergistic, thereby resulting in extreme changes in xenobiotic

elimination(45). Although many of these atypical mechanisms have been observed only in *in vitro* systems, it is clear that competitive inhibition should not be regarded as the only mechanism of DDIs resulting in modulation of transporter function/activity.

Effect of Genetic Polymorphisms on Transporter Expression and Function

Several studies have investigated the impact of transporter polymorphisms on drug pharmacokinetics; however, difficulty exists in demonstrating reproducible functional effects *in vitro* with successful clinical translation. A brief description of selected polymorphisms in specific efflux transporters, and some of the controversies surrounding them, will be discussed. For a more detailed review of transporter pharmacogenetics, the reader is directed elsewhere.(5; 10; 79-81)

ABCC2/MRP2

ABCC2, next to ABCB1, is one of the most illustrious of the efflux transporters with regard to pharmacokinetics. Several polymorphisms in the ABCC2 gene locus have been associated with the hyperbilirubinemic disorder known as Dubin-Johnson Syndrome including the R412G, I1173F, R1392del, and M1393del protein variants(5). Of those associated with Dubin-Johnson Syndrome, the I1173F, R1392del, and M1392del variants lead to improper trafficking of MRP2 protein to the apical membrane of hepatocytes and loss of transport function(82; 83). Two independent groups identified the 2366C>T (S789F) and 4348G>A (A1450T) alleles as conferring decreased ATPase and transport activity, along with altered membrane localization(84; 85). In contrast, the 1249G>A (V417I) allele was shown to decrease affinity(85), or have little effect on transport function *in vitro*.(84) Additional *in vitro* experiments discovered a reduction in transport activity for the K324A, K483A, R1210A, and R1257A MRP2 protein variants as well as diminished protein expression of the K578A variant(86). The 4544G>A allele has been associated with susceptibility to nonalcoholic fatty liver and cholestatic liver diseases, resulting in decreased ATPase activity and diminished transport of lopinavir, calcein, and carboxydichlorofluorescien diacetate(87; 88). ABCC2 promoter variants and haplotypes have been associated with susceptibility to hepatotoxicity(89). Haplotypes containing the -1774Gdel variant have been linked to cholestatic and mixed-type hepatotoxicity in a Korean population, while the -1774Gdel/-

1549G>A/-24C>T haplotype appears to reduce promoter activity(89). In contrast, the -24C>T allele alone and within the -24C>T/-1019A>G/-1549G>A haplotype leads to an increase in promoter activity(90). Additional ABCC2 haplotype studies investigating the -24C>T, 1249G>A, and 3972C>T alleles identified the -24C/1249A/3972C haplotype as conferring an increase in MRP2 protein levels, which corresponded to transport activity *in vitro* and altered bioavailability of talinolol *in vivo*(91). In contrast, the -24C/1249G/3972T, -24T/1249G/3972C, and -24T/1249G/3972T haplotypes resulted in diminished protein expression *in vitro*(91). Still others have shown a preference for transcription of the 3972C allele in comparison to 3972T, which did not correlate with hepatic or renal MRP2 expression(90).

ABCC3/MRP3

In 2004, Lang and colleagues determined that homo- and heterozygous carriers of the -211C>T variant exhibited decreased hepatic mRNA expression of ABCC3, and that this promoter variant affected binding of transcription factors(92). The investigators concluded that the -211C>T allele affected hepatic expression of the transporter, although this effect has been controversial(93). Additional studies using reporter gene activity experiments discovered that the length of the promoter, rather than the -211C>T variant affected gene expression(94). A later study discovered improper post-translational processing and localization of the MRP3 R1381S protein variant *in vitro*(95). Additionally, investigators identified the MRP3 S346F and S407N protein variants to confer decreased transport activity in Sf9 membrane vesicles, the three polymorphisms were postulated to be possible risk factors for hepatotoxicity(95). In an effort to translate *in vitro* polymorphism studies to *in vivo* pharmacokinetics, Sasaki, et al., utilized a reporter gene assay to identify decreased transcriptional activity of the -1767A>G allele(96). However, the -1767A>G variant did not appear to affect human hepatic ABCC3 mRNA expression, nor was it associated with 4-methylumbelliferone-glucuronide pharmacokinetics(96).

ABCC4/MRP4

Experiments utilizing site-directed mutagenesis and transfected HEK293 cells identified a decrease in the transport of azidothymidine and adefovir for the MRP4 G187W and G487E protein variants(97). Additionally, the G187W variant was associated with decreased expression in the

transfected cell system(97); however, the clinical significance of these variants has not been determined. Others identified the -1393T>C allele to be associated with improved event-free survival and decreased methotrexate plasma concentrations in pediatric acute lymphoblastic leukemia as opposed to an association between the 934A>C allele with decreased event-free survival and increased toxicity(98). In contrast, a later study tested the results of Ansari, et al., in adult ALL patients and found no association between event-free survival and genotype(99). The impact of age of disease-onset and the discrepancies in these two findings have not been determined.

ABCB1/P-gp

The majority of the >100 ABCB1 polymorphisms have been studied in the context of gut expression of P-gp protein and altered bioavailability of drugs such as digoxin, talinolol, and fexofenadine(10; 100). However, Elens, et al., investigated ABCB1 polymorphisms in ~150 liver donors and their subsequent effects on blood and hepatic tacrolimus concentrations(101). This study found that ABCB1 polymorphisms, specifically the 1199G>A and 2677G>T/A alleles, independently exerted a significant effect on tacrolimus liver, but not plasma concentrations, the primary endpoint used for therapeutic monitoring(101). Owen, et al., when investigating the 3435C>T and 2677T>G alleles determined that the large variation observed in human hepatic ABCB1 mRNA and P-gp protein expression could not be attributed to genetic variation alone(102). In contrast, Song, et al., identified an increase in hepatic ABCB1 mRNA for homozygous carriers of the 3435C allele, and a decrease in those homozygous for the 2677T allele(103).

ABCG2/BCRP

Of the polymorphisms identified in the ABCG2 gene, the 421C>A allele resulting in the Q141K amino acid substitution appears to be the most important for adverse drug events(104). The ABCG2 421C>A allele appears to decrease BCRP-associated ATPase activity and cause alterations in diflomotecan, imatinib, sulfasalazine, atorvastatin, rosuvastatin, nitrofurantoin, lamuvidine, and pitavastatin pharmacokinetics, among others(104; 105). Additionally, the 34G>A allele resulted in the V12M amino acid substitution, which results in the improper processing and cellular localization of

BCRP protein *in vitro*(105). The Q141K variant also has been implicated in improper membrane localization of BCRP protein(106).

Despite major advances in the field of molecular biology and pharmacogenomics, the ability to translate *in vitro* polymorphic effects on transporter expression and function to the clinic remains a daunting task.

Expression of Hepatic Efflux Transporters in Disease States

Historically, investigations to determine the effect of liver disease on efflux transporter expression have sought to provide insight to disease pathogenesis. However, alterations in the expression of efflux drug transporters can have significant effects on the elimination of xenobiotics and endogenous molecules. It has been proposed that upregulation of efflux transporters may serve as an adaptive mechanism to limit cellular exposure to hepatotoxicants(107); however, systematic, comprehensive investigations of efflux transporter expression are severely limited for several disease states. The following will provide a brief overview of efflux transporter expression in human liver tissue from selected liver diseases. A summary of the effects discussed is provided in Table *1* below to aid in comparisons among diseases.

Primary Biliary Cirrhosis

Primary biliary cirrhosis (PBC) arises from inflammation and irritation of bile ducts leading to stasis of bile flow (cholestasis) which can severely damage hepatocytes and ultimately lead to cirrhosis. Much work has been done to understand the effects of cholestasis on transporter expression and function. ABCC2 mRNA remains largely unchanged in PBC compared to normal liver(107-109). While some have reported no change in ABCC4 mRNA(110), others have discovered an increase in ABCC4 mRNA in cholestasis(111). There is overall agreement that MRP3 and MRP4 protein are elevated in cholestasis(107; 111). Additionally, ABCB1 and ABCC1 mRNA levels appear to be elevated compared to normal liver(109).

Nonalcoholic Fatty Liver Disease & Nonalcoholic Steatohepatitis

Nonalcoholic fatty liver disease (NAFLD) and nonalcoholic steatohepatitis (NASH) represent a spectrum of liver damage that has emerged recently as a prevalent condition due to its association with the obesity epidemic. It is characterized by the accumulation of lipids within hepatocytes, termed simple steatosis. NAFLD progresses via inflammation, oxidative stress, and increased lipid accumulation to NASH, which also may incorporate fibrosis and eventual cirrhosis(31). ABCC1, ABCC3, ABCC4, ABCB1, and ABCG2 mRNA levels are increased with progression of NAFLD from simple steatosis to NASH, while ABCC2 mRNA levels remain unchanged(31). Protein levels of all efflux transporters appear to be increased with disease progression, although the localization of MRP2 most likely shifts to the subapical region, away from the plasma membrane(31).

Hepatitis C Virus

Hepatitis C virus (HCV) induces several response pathways in hepatocytes including oxidative and endoplasmic reticulum stress(112). Chronic HCV infection can lead to fibrosis and development of severe cirrhosis, propagating hepatocellular injury with potential for numerous alterations in gene expression patterns(113). In comparisons of HCV-positive tissue with HCV-negative, ABCC1, ABCC3, ABCC4, and ABCB1 mRNA are elevated in non-cirrhotic tissue(113; 114). ABCG2 and ABCC2 mRNA expression is diminished in HCC(113; 114) with ABCC2 mRNA decreasing as fibrosis severity increases(112). Studies comparing mRNA expression in cirrhotic HCV tissue with HCV-negative, noncirrhotic tissue are in agreement with those comparing HCV-positive to noncirrhotic, HCV-negative tissue, suggesting that the changes in gene expression are driven primarily by infection status. ABCB1, ABCC1, ABCC4 mRNA is elevated, while ABCC2 and ABCG2 levels are decreased(114). Additionally, ABCC2 mRNA has been demonstrated to be reduced in HCV/HCC-positive tissues compared to HCC/HCV-negative tissues(115). Comparisons of protein levels in this disease are limited; however, MRP4 protein is elevated in HCV-positive tissue versus noncirrhotic, HCV-negative tissue(114).

Hepatocellular Carcinoma

Hepatocellular carcinoma (HCC) is a common form of cancer that arises from cirrhosis due to chronic liver disease(116). Studies have shown an increase in mRNA levels of several efflux transporters including ABCC1, ABCC2, ABCC4, and ABCB1(116; 117). ABCG2 mRNA remains unchanged in comparison to healthy adjacent tissue(116). However, ABCC3 mRNA increased(116) or remain unaltered(117). Information regarding protein levels of efflux transporters in HCC as compared to normal tissue remains limited.

Progressive Familial Intrahepatic Cholestasis.

Progressive familial intrahepatic cholestasis (PFIC) refers to a group of autosomal recessive disorders affecting biliary membrane proteins including ATP8B1, BSEP, and MDR3, referred to as PFIC1, 2, and 3, respectively. The resultant dysfunction in each generally culminates in disrupted formation of bile. Investigations assessing the expression of efflux transporters in PFIC are limited to small groups of patients. Keitel, et al., determined mRNA levels in PFIC 2 and 3 for a number of efflux transporters and discovered an increase in ABCC4 mRNA in both PFIC2 and 3, while protein was increased in PFIC3(118). ABCC1 and ABCB1 mRNA was increased in PFIC3 as well(118). ABCC2 mRNA was unaltered in PFIC2 and 3, but protein may be decreased in PFIC3(118). ABCC3 mRNA was unaltered in both PFIC2 and PFIC3(118). Unfortunately, due to low patient numbers (n=4-5) and thus low statistical power, generalizations on efflux transporter expression due to PFIC are tentative at best.

Though systematic studies including both mRNA and protein data for efflux transporters are minimal, a significant obstacle in the application of findings from such studies remains the ability to absolutely quantify transporter protein. Understanding the absolute expression level of one specific efflux transporter compared to another may provide better insight regarding which transporters may exert a more dominant function in various disease states and enable better prediction of drug response.

Trafficking of Hepatic Efflux Transporters

An important concept in transporter regulation is that of intracellular pools from which membrane transporters can be swiftly recruited and inserted into the membrane as a result of xenobiotic treatment or

physiological demand(119). It has been postulated that these intracellular reservoirs of transporters serve as a means of increasing transporter expression in the membrane, and thus transport activity, without initiating the energetically expensive processes of transcription and translation(120). In contrast, other studies have demonstrated the endocytic retrieval of transporters from the membrane as a consequence of xenobiotic treatment or disease states. Whether changes involve transporter delivery to, or internalization from, the membrane, the net result is alteration of the steady-state levels of efflux transporters residing in the membrane, and thus modulation of their transport function. However, the majority of such studies have focused on canalicular efflux transporters including P-gp and MRP2, with less attention directed towards sinusoidal efflux transporters.

Much work has been done to determine the mechanisms governing P-gp trafficking from large intracellular pools to the canalicular membrane. Administration of cAMP or taurocholate to rats results in increased levels of hepatic P-gp in the membrane(120-122). Furthermore, *in vivo* pulse-chase experiments revealed that newly-synthesized P-gp is targeted directly from the Golgi apparatus to the canalicular membrane rather than progressing through the transcytotic pathway via temporary insertion in the sinusoidal membrane(123). Additional studies in HepG2 cells revealed the involvement of protein kinase A (PKA)-RIIα, which can be activated by cAMP, in the trafficking of newly-synthesized P-gp to the membrane(124). Interestingly, the basal rate of P-gp delivery to the membrane in HepG2 cells differed from that of MRP2(124). Non-hepatic cell lines have provided further insight into the proteins responsible for regulating the insertion into and endocytic retrieval of ABCB1/P-gp from the membrane via perimembranous pools. Concomitant overexpression of green fluorescent-tagged P-gp in HeLa cells with constitutively-active forms of the small GTPases Rab5 or RalA resulted in an increase in intracellular P-gp localization, which correlated with increased intracellular accumulation of the fluorescent P-gp substrate, daunorubicin(125). However, whether Rab5 and RalA were involved in the process of exocytic insertion, or endocytic retrieval of P-gp from the membrane is unclear. A recent study involving membrane expression of P-gp in K562 cells identified the small GTPase Rab4 as a negative regulator in the exocytic insertion of P-gp in the membrane(126). Similar to studies in transfected HeLa

cells, Rab4-mediated retrieval of P-gp correlated with increased intracellular levels (reduced efflux) of an P-gp substrate(126).

Extensive investigations have focused on the dynamic regulation of MRP2 in the canalicular membrane. Several experimental cholestatic and oxidative stress-inducing conditions such as bile duct ligation or treatment with estradiol-17β-D-glucuronide, lipopolysaccharide, phalloidin, ethacrynic acid, or buthionine sulfoximine, are known to induce endocytic retrieval of Mrp2 from the canalicular membrane in rats(127-129). Additionally, disrupted canalicular localization of MRP2 has been demonstrated in primary biliary cirrhosis, drug-induced liver injury, poorly drained obstructive jaundice, autoimmune hepatitis, sclerosing cholangitis, and nonalcoholic steatohepatitis patients(31; 130; 131). The specific mechanisms governing the endocytic retrieval and exocytic insertion ofMRP2 in the canalicular membrane are convoluted and involve multiple kinases. Ethacrynic acid-induced oxidative stress resulting in depletion of glutathione leads to rapid internalization of Mrp2 which can be rescued by subsequent glutathione treatment(127; 132). Estradiol-17β-D-glucuronide-induced cholestasis also causes internalization of Mrp2 resulting in diminished biliary excretion of Mrp2 substrates; however, this process is reversed by cAMP administration(133). The endocytic retrieval of Mrp2 from the membrane is largely a microtubule-independent process involving activation of Ca^{2+}-dependent protein kinase C (PKC), and de-phosphorylation of radixin, which is responsible for tethering actin filaments to membrane proteins(128; 134-137). De-phosphorylation of radixin destabilizes its interaction with Mrp2 leading to their dissociation and movement away from the membrane(134; 136). Once internalized, phosphatidylinositol 3-kinase (PI3K) has been proposed to regulate Mrp2 retention within the cell via interactions with extracellular signal-regulated kinases 1 and 2(137; 138). Furthermore, sustained buthionine sulfoximine-induced oxidative stress has been shown to lead to not only internalization of Mrp2, but increased ubiquitination and subsequent degradation of the protein(129). Conversely, reinsertion of Mrp2 into the membrane is a microtubule-dependent process that is sensitive to colchicine treatment and stimulated by cAMP, taurocholate, tauroursodeoxycholate, and hypoosmotic buffer(128; 133). Protein kinase A (PKA) may be involved in the phosphorylation of radixin; however, PKC isoforms

also have been implicated in the exocytic reinsertion of Mrp2 in the membrane through signaling events involving p38 mitogen activated protein kinase(132; 134; 138; 139).

Glycosylation has been implicated as an additional factor affecting the membrane localization of efflux transporters. N-linked glycosylation of BCRP has been implicated as a possible mechanism affecting protein stabilization, proper routing of the transporter to the membrane, and functional activity(140-142). Others have shown full glycosylation of MRP2 to be necessary for proper localization within the membrane and effective transport activity(143; 144). The interconnection of glycosylation pathways regulating transporter routing to the membrane and kinase pathways involved in the dynamic localization of efflux transporters remains to be determined.

Localization studies investigating sinusoidal efflux transporters are beginning to emerge; however, there is a substantial gap between the breadth of knowledge of canalicular efflux transporter trafficking and that of sinusoidal efflux transporters. Recent studies have identified Na^+/H^+ exchanger regulatory factor 1 (NHERF1) and nexin 27 as binding partners of MRP4 necessary for internalization of the transporter(145; 146). Further studies are necessary to determine the pathways involved and clinically relevant states of MRP4 internalization. Nonetheless, whether reduced membrane expression of efflux transporters is the result of improper post-translational processing and trafficking to the membrane or endocytic retrieval and intracellular sequestration, the net result is diminished extrusion of substrates out of the hepatocyte.

Interplay Between Multiple Hepatic Efflux Systems

As one of the main eliminating organs of the body, the liver has evolved to excrete a wide range of endo- and xenobiotics. In order to perform this essential excretory function, an array of transport proteins with overlapping substrate specificity exist to handle a wide range of endo- and xenobiotics (Figure 1.1). This includes multiple complimentary proteins on the same membrane transporting in the same direction, as well as proteins on the opposite, or alternative, membrane. Due to the potential

involvement of multiple transporters, it can be challenging to predict the impact of altered function of one or more transport proteins on hepatic and systemic exposure of a given substrate.

The quantitative impact of excretory transport modulation on the hepatic, systemic, and biliary exposure to xenobiotics and derived metabolites was formalized recently by Zamek-Gliszyznski based on work conducted in our laboratory(147). Experimental data and theoretical relationships indicated that the fold change in exposure is governed by the relationship, $1/(1 - f_e)$, where f_e is the fraction excreted by a particular transport protein. Loss-of-function of a transport pathway associated with a $f_e < 0.5$ will have minimal consequences on exposure, but exponential changes can be expected in response to loss-of-function of one or more transport pathways with $f_e > 0.5$. It should be noted that the impact of f_e on exposure depends on the compartment of interest (systemic, hepatic or bile), the directionality of the impaired pathway (canalicular or sinusoidal), and the existence of an alternative route of excretion. For example, when a transport protein is impaired, the increased excretion in the alternative direction is a function of the fraction of total hepatocellular clearance mediated by the impaired pathway. The resulting increase in excretion over the alternative membrane is caused by the decrease in total excretory clearance, which produces elevated cellular concentrations that serve as a driving force for increased excretion by the remaining available pathways. The relationship between exposure and f_e also can be extended to partial inhibition scenarios by modifying the equation with the ratio of inhibitor concentration and inhibition constant ($[I]/K_i$). Figure 1.2 depicts the relationship between exposure and f_e, including the effect of partial inhibition(147).

$$\text{Fold change in exposure} = \frac{1}{\frac{f_e}{(1 + {}^{[I]}/_{K_i})} + (1 - f_e)} \qquad (1)$$

In a series of reports, Vlaming and colleagues characterized the role of multiple hepatic efflux transporters in the elimination of methotrexate and its main toxic metabolite, 7-hydroxymethotrexate, *in vivo* using single and multiple knockout mouse models(148-150). Biliary excretion of methotrexate and the 7-hydroxy metabolite were reduced ~20-fold in Abcc2:Abcg2$^{-/-}$ mice, indicating that these proteins are the main determinants of canalicular efflux(149). The role of Mrp3 in compensatory excretion of

methotrexate and 7-hydroxymethotrexate from the liver into sinusoidal blood was demonstrated by increased plasma concentrations and urinary excretion in the absence of Mrp2 and/or Bcrp, which was reversible in Abcc2:Abcc3$^{-/-}$ mice(150). Mrp3 appeared to be required for increased plasma concentrations in the absence of Bcrp(148). Despite initial hepatic accumulation of methotrexate in the absence of one or two proteins, the mass recovered in was similar to wild-type by 2 hours. However, in the absence of all three proteins, hepatic accumulation was further increased and prolonged in Abcc2:Abcg2:Abcc3$^{-/-}$ mice (7- and 90-fold increase for parent and metabolite at 2 h)(148). Also in Abcc2:Abcg2:Abcc3$^{-/-}$ mice, 7-hydroxymethotrexate still exited the liver, resulting in a 10-fold increase in plasma exposure, potentially due to up-regulation of Mrp4. The role of multiple efflux transporters in the enterohepatic circulation and related efficacy of ezetimibe and its glucuronide conjugate was explored using a variety of model systems, demonstrating that enterohepatic circulation strongly depends on the joint function of Mrp3, Mrp2 and Bcrp(151). Although biliary excretion of ezetimibe glucuronide was minimally altered in Abcg2$^{-/-}$ mice, Bcrp clearly functions to compensate for loss of Mrp2, as demonstrated in Abcc2:Abcg2$^{-/-}$(151). Interestingly, the role of Mrp3 in absorption of ezetimibe from the intestine was shown in Abcc3$^{-/-}$ mice, which displayed greatly reduced enterohepatic circulation(151). The overlapping function of P-gp, MRP2 and MRP3 in protection against trabectedin-mediated hepatotoxicity by clearing harmful metabolites formed by CYP3A was shown using a combination of single- and multiple-knockout animals with translation to humans using MRP2- and MRP3-transfected MDCK cells(152; 153). Multiple efforts to characterize the hepatobiliary disposition of fexofenadine have shown the overlapping roles of P-gp, BSEP and MRP2, but not BCRP in facilitating biliary excretion, and the significant contribution of MRP3 but not MRP4 in the sinusoidal efflux from liver into blood(26; 154-156). Using a combination of Mrp2-deficient TR^{-} rats and chemical "knockdown" of Abcb1/P-gp by elacridar (GF120918), Mrp2 was identified as the primary mechanism for biliary excretion of the metabolically stable opioid peptide, DPDPE, in rats, with P-gp facilitating biliary excretion only in the absence of Mrp2(45; 50). These studies also suggested that GF120918 inhibited a basolateral excretion mechanism for DPDPE. Using chemical inhibitors alone, increased hepatocyte

concentrations of valproate glucuronide were observed in isolated perfused rat livers following probenecid and valproate co-administration.(157) Mathematical modeling of the data revealed that probenecid inhibited both the basolateral and canalicular excretion of generated valproate glucuronide.

For most drugs where multiple pathways are available for hepatocellular egress into bile or blood, the safety is maintained when only one pathway is impaired. However, as demonstrated by the f_e concept and various experimental models used to study multiple transporters, significant changes begin to occur as more pathways are impaired and the hepatoprotective effect of transporter multiplicity is diminished. That is why it is important to characterize the multiplicity and relative contribution of transport pathways for new chemical entities (NCEs), as a way to asses risk in the setting of impaired function of one or more transporters, whether due to DDIs (with NCE as victim and/or perpetrator), disease states or genetic variation.

Relationship Between Hepatic Efflux Transport and Intracellular Unbound Concentrations

Measurement of unbound blood or plasma concentrations is convenient and may correlate with unbound tissue/cellular concentrations for compounds with sufficient passive permeability. However, for compounds that are poorly permeable or otherwise violate the assumption of rapid equilibration, the ratio of intracellular to extracellular (blood or plasma) $C_{unbound}$ ($Kp_{u,u}$) may be highly disparate. Since the liver is frequently a primary site of drug elimination from the body, hepatocellular $C_{unbound}$ greatly influences drug efficacy and toxicity on a systemic as well as local level. As such, predictions of clinical efficacy, toxicity and drug-drug interactions (DDIs) could be improved by accounting for $C_{unbound}$ *in vitro* and *in vivo*, as well as between cell-free and whole cell *in vitro* systems used to assess mechanisms/targets of efficacy, toxicity and drug disposition, including transporter activity.

Altered function of efflux mechanisms described in this review can influence hepatocellular exposure of drugs, with implications for altered efficacy, toxicity and DDI potential. This includes the effect of interplay between drug transport and metabolizing enzymes, in which intracellular $C_{unbound}$ drives elimination of parent drug; however, metabolic/elimination pathway "switching" can occur in the setting

of impaired efflux, leading to increases in hepatic and/or systemic metabolite exposure.(6; 147; 158-161) In contrast, subcellular binding/sequestration can limit access of drugs to mechanisms of elimination and constrain the ability of efflux and/or metabolism to "clear" drug from the hepatocytes. It is assumed that only the $C_{unbound}$ within the cell is available for elimination.

Although hepatocellular $C_{unbound}$ is assumed to be the relevant concentration driving elimination, a number of exceptions exist, particularly in the case of efflux transport. A preponderance of evidence suggests that ABCB1/P-gp has multiple binding sites, including the ability to remove compounds from the inner leaflet of the plasma membrane and function as a "membrane vacuum" for compounds that partition into the lipid bilayer.(162; 163) An elegant piece of pharmacokinetic modeling by Korzekwa, et al., supports this mechanism, and suggests that a portion of the ABCB1/P-gp-mediated efflux process is driven by drug accumulation and concentration within the membrane, although this would not be regarded as a component of $C_{unbound}$ within the cell.(164) As integral membrane proteins, transporters are transferred to the plasma membrane following synthesis through dynamic and complex vesicle trafficking pathways.(123; 165-168) Likewise, plasma membrane regions and their contents are continuously cycled on and off the membrane, leading to pools of transporter-containing vesicles.(122; 169) As a result, substrates for efflux transporters are constantly accumulating within these vesicles, as has been shown with fluorescent ABCC2/MRP2 substrates, demonstrating characteristic punctate vesicular structures, which are absent in Abcc2-/Mrp2-deficient cells and sensitive to known inhibitors, such as cyclosporine A.(169-171) Although the initial transport into these vesicles is presumed to be driven by intracellular $C_{unbound}$, the terminal release (efflux) of accumulated drug results from fusion of the vesicles with the plasma membrane, which may occur at a very different rate compared to direct efflux across the plasma (canalicular or basolateral) membrane.(169; 172) This vesicular fusion pathway offers yet another level of complexity to hepatic efflux that is subject to altered function, as vesicle trafficking in hepatocytes is known to be altered by a number of disease states (see above).

Model Systems for Evaluating the Role of Hepatic Efflux

For a comprehensive list of experimental models used to measure transporter activity in general, the reader is referred to a recent review by the International Transporter Consortium(173). While vesicle systems and transfected systems are useful to determine whether a transporter may be involved for a particular substrate, the more challenging aspect is to determine the role of a particular transporter in the presence of other competing transporters and pathways of cellular elimination. The only cells that truly express all of the relevant transporters of interest are primary cells from the organ of interest.

Primary Hepatocytes

Freshly isolated or cryopreserved primary hepatocytes are not polarized and require long-term culture in a sandwich configuration to recapitulate polarized architecture, including formation of bile networks and appropriate expression and localization of efflux transporters on the respective apical (canalicular) and basolateral membrane domains.(174) Sandwich-cultured hepatocytes (SCH) typically are used to evaluate vectorial transport into bile and differentiate the roles of active uptake and biliary excretion. This is accomplished by modulating tight junctions in the presence (cells+bile) or absence (cells) of divalent cations (Ca^{2+} and Mg^{2+}) in the experimental buffer system (B-CLEAR® technology, Qualyst Transporter Solutions, Research Triangle, NC). These studies are performed routinely by applying substrates in the presence or absence of inhibitors for a period of 10 min, and a number of pharmacokinetic parameters can be calculated from the resulting data, including the total accumulation in cells+bile and cells, biliary excretion index (BEI) and *in vitro* clearance values for uptake and/or biliary excretion, which can be scaled to predict *in vivo* clearance values based on scaling factors such as protein content and hepatocellularity(174).

The SCH model has many advantages including expression of relevant transport mechanisms, which enables accurate prediction/assessment of efflux processes, since the panoply of mechanisms mediating hepatocellular entry and egress are represented. However, it should be noted that transporter expression may be altered compared to whole tissue, depending on the culture conditions, as shown for rat SCH with (~5-fold) downregulation of SLCO/OATP expression and 5-fold increase in expression of

efflux transporters such as P-gp and Mrps(175-178). Presently, estimation/prediction of transport processes may be improved by taking these changes into account upon scaling of data from *in vitro* to *in vivo(179; 180)*. Less frequently, the SCH model has been used to assess efflux by various strategies of preloading the cells with substrates (± inhibitors), followed by a brief wash and application of "blank" buffer for an efflux phase, which may involve sampling/observation of substrate in cells+bile, cells and/or appearance in buffer(181; 182). However, the SCH system remains to be characterized under these conditions.

In a "simplified" conception of the SCH system, maintenance of tight junctions in the presence of Ca^{2+} would completely seal the bile networks, and appearance in buffer during an efflux experiment would reflect only basolateral efflux. Efflux in the absence of Ca^{2+} with disrupted tight junctions would reflect basolateral plus biliary efflux, and would be greater than that in $+Ca^{2+}$ conditions. In reality, the SCH model is dynamic, with regular and extensive "pulsing" of the bile canaliculi, similar to reports in hepatocyte couplets and cultured hepatocytes(183; 184) (video: http://www.pharmacy.unc.edu/research/labs/kim-brouwer-lab/bile-canalicular-contractions-in-sandwich-cultured-rat-hepatocytes) This means that appearance of substrate in buffer in the $+Ca^{2+}$ condition reflects basolateral efflux plus the flux of accumulated substrate within the bile spaces. In order to deconvolute these data and elucidate the relative contribution of basolateral versus biliary efflux, one can apply a pharmacokinetic modeling approach to the SCH data(161; 185-188).

At least two potential schemes exist for the design of efflux studies in SCH (Figure 1.3). One is to pre-incubate and/or perform the uptake phase exclusively in standard ($+Ca^{2+}$) Hanks' Balanced Salt Solution (HBSS), followed by a brief wash and efflux in $\pm Ca^{2+}$ HBSS [Fig. 1.3, (A)](181; 182). A potential limitation of this approach is that substrate accumulation in the bile networks during the uptake phase may not be washed away completely before initiating the efflux phase in $-Ca^{2+}$ HBSS. The time required for "complete" opening of bile networks is unclear, although disappearance of carboxydichlorofluorescein (CDF) fluorescence intensity in bile networks suggests a time frame of ~5-6 min (Figure 1.4). Prior to this time, efflux in the $-Ca^{2+}$ condition in part reflects dumping of bile networks. A potential solution is to

incubate in ±Ca^{2+} HBSS long enough to complete opening/dumping of bile spaces in -Ca^{2+} (~5-6 min), and then replace buffer again and observe efflux. However, it may be difficult to detect cellular content for compounds that are rapidly excreted (e.g. taurocholate)(186). Another potential experimental design for efflux studies in SCH involves maintaining tight junction modulation throughout the study period by pre-incubating in ±Ca^{2+} HBSS, then performing an uptake phase in +Ca^{2+} HBSS (<30 min) to provide relief from -Ca^{2+}/EGTA , followed by a brief wash and efflux in ±Ca^{2+} HBSS [Fig. 1.3, (B)]. A limitation with this method is potential re-sealing of the tight junctions during Ca^{2+} repletion in the uptake phase. This has been characterized previously(186), and is of concern for compounds with extensive biliary excretion (BEI), such as taurocholate(186). However, imaging with CDF suggests that re-sealing of the tight junctions allowing substrate accumulation in the bile networks is minimal over a 20-min loading/uptake phase (Figure 1.4). Another potential issue relates to cell integrity in prolonged and repeated -Ca^{2+} conditions; this does not appear to be an issue in rat SCH as judged by LDH release (<5% of total cellular content over the study period). The advantages and limitations associated with these two approaches suggest that maintaining tight junction modulation throughout the study period [Fig. 1.3, (B)] is the most appropriate method for conducting efflux studies in the SCH system. It should be noted that a modeling and simulation approach to data analysis is required in order to differentiate basolateral and biliary efflux from flux out of bile spaces in +Ca^{2+} conditions. Using this approach, it is possible to elucidate the relative contribution of basolateral and biliary efflux to the total hepatocellular elimination of probe drugs.

Whole Tissue and Animal Models

Isolated perfused livers (IPLs) are considered the "gold standard" for studying the hepatobiliary system in isolation, without the influence of extrahepatic components(189). Single-pass and recirculating configurations are possible, both offering direct sampling of bile and determination of biliary excretion. A useful feature of the single-pass method in the context of hepatic efflux is that it allows continuous sampling of outflow perfusate. When coupled with a protocol in which drug is added to the perfusate ("loading" phase) and then switched over to blank buffer ("efflux" phase), the single-pass method is an

established approach to measure basolateral efflux directly(26; 190). However, when coupled with an appropriate experimental design and pharmacokinetic modeling of generated data, recirculating and single-pass IPLs are both useful for investigating hepatobiliary transport. In theory, liver tissue can be used from any species or strain, including those with natural or targeted disruption of genes encoding transport proteins, as described in further detail below.

A common paradigm for evaluating the role of transport proteins in the hepatobiliary disposition of drugs is to use a combination of single- and multiple-knockout animal models, as discussed above. Although there exist a number of naturally-occurring mutant animal strains in which transporter genes are disrupted, such as Abcc2-/Mrp2-deficient rats (TR^- Wistar or EHBR Sprague-Dawley), targeted knockout of transporter genes has been limited primarily to mice. A recent development has been the application and marketing of zinc-finger nuclease technology, allowing efficient, targeted editing of the genome in a variety of preclinical species. This technology is offered from Sigma (St. Louis, MO) under the SAGE (Sigma Advanced Genetic Engineering) line of products. These models have been adopted for a variety of biomedical research applications, including ADME and drug transport, with various single- and multiple-knockout models available. $Abcb1^{-/-}$, $Abcg2^{-/-}$ and $Abcc2^{-/-}$ SAGE rat models were characterized recently using loperamide, paclitaxel, sulfasalazine and carboxydichlorofluorescein.(191) One limitation to knockout animal models is that compensatory regulation of other transport mechanisms may confound the interpretation of generated data. Another challenge in distinguishing the role of hepatic excretion *in vivo* as the definitive mechanism responsible for DDIs and altered pharmacokinetics is that many of the same transport proteins are present at other epithelial barriers, most notably the apical border of the intestine and kidney. For example, $Abcb1^{-/-}$ and $Abcg2^{-/-}$ rats, along with chemical inhibitors (GF-120918) and bile-duct cannulation were used to differentiate the role of Abcb1/P-gp and Abcg2/Bcrp in the biliary excretion/enterohepatic recirculation versus direct excretion from the circulation into the intestinal lumen of intravenously-administered apixaban, a Factor Xa inhibitor.(192) Similarly, the biliary excretion of nitrofurantoin, sulfasalazine and a proprietary compound were decreased 70-90% in Bcrp knockout rats, with differential effects on systemic clearance, urinary excretion and oral absorption

depending on clearance pathways and compound properties.(193) These studies highlight the fact that transport proteins contributing to hepatocellular efflux exist in other tissues, and altered function may be global (germline genetic variation) or local (DDIs, tissue-specific disease states or epigenetic regulation), with implications for hepatic or systemic exposure and alternative clearance pathways. In addition, since transport proteins are responsible for the disposition of many endogenous and exogenous substances, and vectorial transport from blood to bile is often a result of overlapping substrate specificity and reliance on multiple mechanisms, a complex network of cellular regulation is often perturbed along with transport function, leading to compensatory/additional changes in disposition mechanisms.

General Strategies

While animal models are useful and convenient for evaluating transporter activity, translating these data to humans can be challenging and must be done with caution, due to potential species differences in substrate and/or inhibitor affinity. A common strategy for strengthening the extrapolation of animal data to human conditions is to perform studies in systems (*e.g.*, membrane vesicles, transfected cell lines) containing the human-specific homologues/isoforms that were shown to be important in animals(151; 152). A common paradigm for exploring the involvement of multiple transporters is a combination of genetic knockout and chemical "knockdown" in cultured hepatocytes, isolated livers and whole animals. Perhaps the most common application is the use of naturally-occurring Abcc2-/Mrp2-deficient rats (TR^- Wistar or EHBR Sprague-Dawley), combined with an inhibitor, such as GF120918 (elacridar) for modulation of Abcb1/P-gp and/or Abcg2/Bcrp.(50; 52; 192) In this way, one can elucidate the role of some of the most common transporters involved in the biliary excretion of drugs. The only major biliary excretion mechanism excluded in this paradigm is Abcb11/Bsep. Chemical inhibition is used commonly with the intention to assess the impact of individual transport pathways on the pharmacokinetics of drugs. However, when inhibitors are used in complex systems such as intact organs and whole animals, they often interact with multiple transport pathways. Thus, the use of chemical inhibitors intended to disrupt single mechanisms may reveal the involvement of multiple transport pathways in the hepatobiliary disposition of compounds(157).

Future Challenges

Tools to Study Xenobiotic Transport

One of the complexities and challenges of studying drug transport is the overlapping substrate specificity and redundant transporter activity in a given tissue. As a result, there remain no truly selective substrates or inhibitors to study the role of individual transporters in complex *in vitro* or *in vivo* models, including clinical DDI studies in humans(173). In addition, there is an urgent need for probes and methods to measure and characterize definitively the consequences of altered transport function on organ and tissue exposure of chemicals *in vivo* in humans(173). For these reasons, efforts must continue to further characterize existing and prospective probe substrates and inhibitors for their potential to interact with the panoply of transporters and mechanisms of regulation.

In Vitro-In Vivo Correlations

Scaling of *in vitro* transporter data into accurate *in vivo* predictions remains a significant challenge. It is widely accepted that one of the primary gaps currently precluding successful extrapolation is knowledge concerning the quantitative differences in transport protein expression amongst the *in vitro* systems used to evaluate transport protein function, and between these *in vitro* models and whole tissue expression *in vivo*(194). Mass spectrometry-based quantitative proteomics efforts are underway by a number of investigators to fill this gap for the major proteins involved in the hepatobiliary disposition of drugs. These efforts have been advanced greatly by the work of Terasaki and colleagues(195-199) in an academic setting, as well as Lai and colleagues(177; 178; 200-202) in the pharmaceutical industry. This work has focused primarily on whole-cell or -tissue expression(178; 198), often following isolation of crude membrane fractions(177; 202) in order to reduce background interference from the cell and tissue milieu. These reports have proven useful to improve or confirm previous scaling efforts that used empirical approaches based on directly scaling transport activity of prototypical substrates between systems(51; 179; 180; 196; 200; 201; 203-208). However, future efforts will continue to refine the quantitative proteomics methods to distinguish the transporter expression at the plasma membrane, which is believed to be the appropriate input to establish an accurate stoichiometric

relationship for single molecule-transporter interactions. Further characterization might include subcellular transporter localization in the vesicular network, which may play a role in the cellular accumulation of some drugs and their ultimate excretion by vesicle trafficking and plasma membrane fusion, as discussed above. Additionally, the role of post-translational modifications of transport proteins as they migrate through the antero- and retrograde vesicle pathways may be elucidated by the sensitive capabilities of mass spectrometry. One of the challenges associated with characterizing the subcellular distribution of transporter expression is assessing and correcting for the efficiency of the methods used to isolate various subcellular components. Although these methods have been established and incorporated into other quantitative proteomics efforts, the application of this technology to drug transporters remains in an early stage.

Emerging transporters

It is generally assumed that the transporters commonly involved in efflux of drugs and metabolites from hepatocytes into blood or bile have been identified. However, transporters that were previously disregarded, or entirely unknown, continue to emerge as the field of drug transport moves forward. One such example is the SLC47A, or Multidrug and Toxin Extrusion (MATE), family, which was first discovered in 1999 and cloned in 2005(209-212). MATE1 has quickly come to prominence after reports describing its role in the renal handling of metformin and cisplatin, with associated alterations in efficacy and toxicity due to DDIs in humans and in knockout animals(213-215). Interestingly, MATE1 also is localized in the liver on the canalicular membrane, but the interactions observed in renal proximal cells do not appear to occur to an appreciable degree in hepatocytes. The reasons for this remain unclear, but the understanding of MATE1 in the liver is likely to evolve. Similarly, the organic solute transporter (OSTα/β), SLC51, was discovered in 2001 and subsequently characterized in humans and rodents(216; 217). Expression and localization of OST includes the basolateral membrane of the liver and small intestine, where it plays a significant role in bile acid transport and homeostasis(35). Although known substrates of OST are limited currently to bile acids, steroid conjugates, eicosanoids and digoxin, additional drugs are likely to interact with this pathway(34-

37). These are just the latest transporters to be identified and characterized, but other proteins are likely to emerge as important players in hepatic efflux of xenobiotics.

Conclusions

The field of drug transport is evolving rapidly. The growing body of knowledge, including substrates and inhibitors, has revealed a pattern of broad and overlapping substrate specificity for the various transport proteins. While the majority of transport proteins mediating hepatic efflux have been identified and characterized with regard to tissue expression and localization, the interplay of multiple efflux transporters remains poorly understood and limits our ability to predict hepatocellular accumulation and/or routes of excretion when the function of one or more proteins is impaired, as outlined in the recent International Transporter Consortium White Paper(294). However, advances in quantitative proteomics, determination of intracellular concentrations, in vitro-in vivo extrapolation and pharmacokinetic modeling will continue to enable cutting-edge research in this critical area. The ultimate goal is to improve the safety and efficacy of medications through a better understanding of hepatic efflux and its impact on the pharmacokinetics of drugs.

Table 1.1. Summary of hepatic efflux transporter expression changes in disease states.

Transporter	PBC	NAFLD/ NASH	HCV	HCV/ Cirrhosis	HCC (mixed etiology)	PFIC3
ABCC1/MRP1						
mRNA	↑ (109)	↑ (31)	↑ (114)	↑(114)	↑ (116; 117)	↑ (118)
Protein		↑ (31)				
ABCC2/MRP2						
mRNA	↔ (108; 109)	↔(31)	↓ (114)	↓(114)	↑ (116; 117)	
Protein	↔ (107)	↑ (31)				↓ (118)
ABCC3/MRP3						
mRNA	↑ (109)	↑ (31)	↑ (113) ↔ (114)	↔ (114)	↑ (109; 116) ↔ (117)	↔ (118)
Protein	↑ (107)	↑ (31)				
ABCC4/MRP4						
mRNA	↔ (107)	↑ (31)	↑(113; 114)	↑(114)	↑ (116)	↑ (118)
Protein	↑ (107)	↑ (31)		↑(114)		↑ (118)
ABCB1/P-gp						
mRNA	(109)	↑ (31)	↑(113; 114)	↑(114)	↑ (109; 116; 117)	↑ (118)
Protein	↔ (107)	↑ (31)				
ABCG2/BCRP						
mRNA		↑ (31)	↓(113; 114)	↓(114)	↔ (116)	
Protein		↑ (31)				

Figure 1.1. Localization of Human Transport Proteins Involved in Hepatocellular Disposition of Drugs. (Adapted from Chandra and Brouwer, Pharm Res, 21:719, 2004)

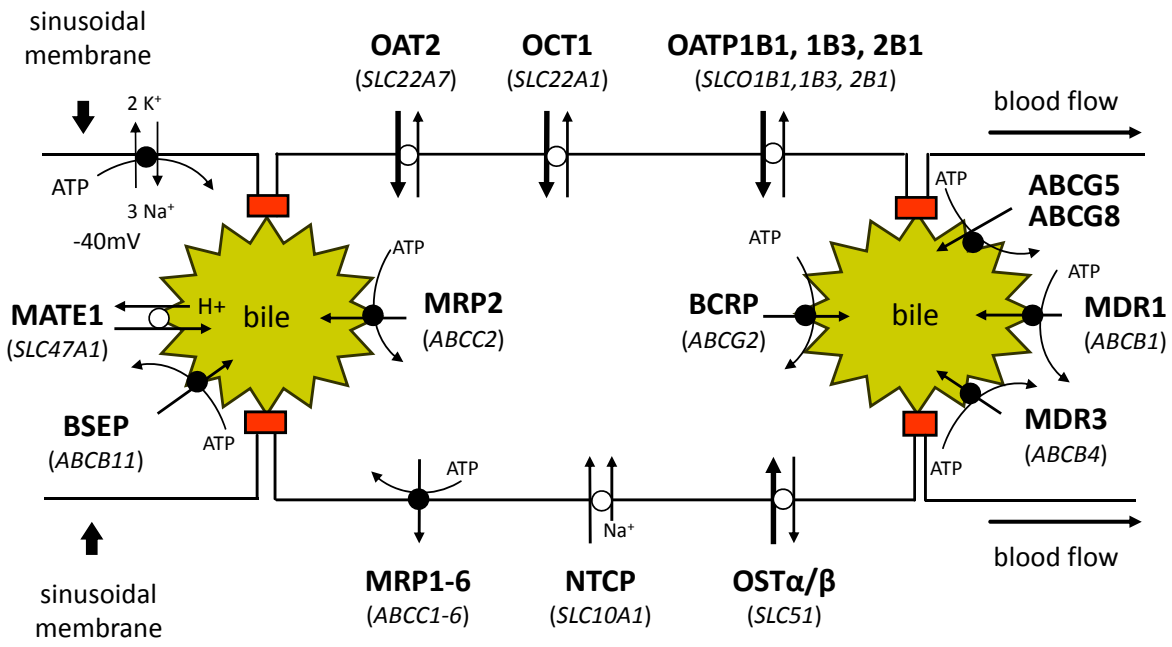

Figure 1.2. Fold change in exposure as a function of f_e at various $[I]/K_I$ ratios as described by eq. 1. (Reprinted with permission from Zamek-Gliszczynski, et al. Drug Metab Dispos 37:386, 2009)

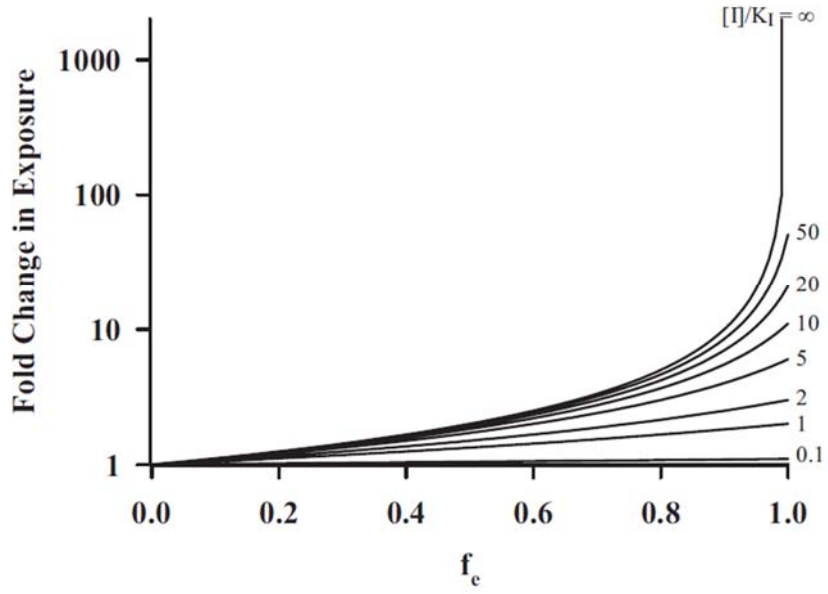

Figure 1.3. Scheme depicting potential experimental uptake/efflux protocols in the sandwich-cultured hepatocyte (SCH) model. Gray shading represents inclusion of substrate in the Hanks' Balanced Salt Solution (HBSS) buffer during the uptake phase.

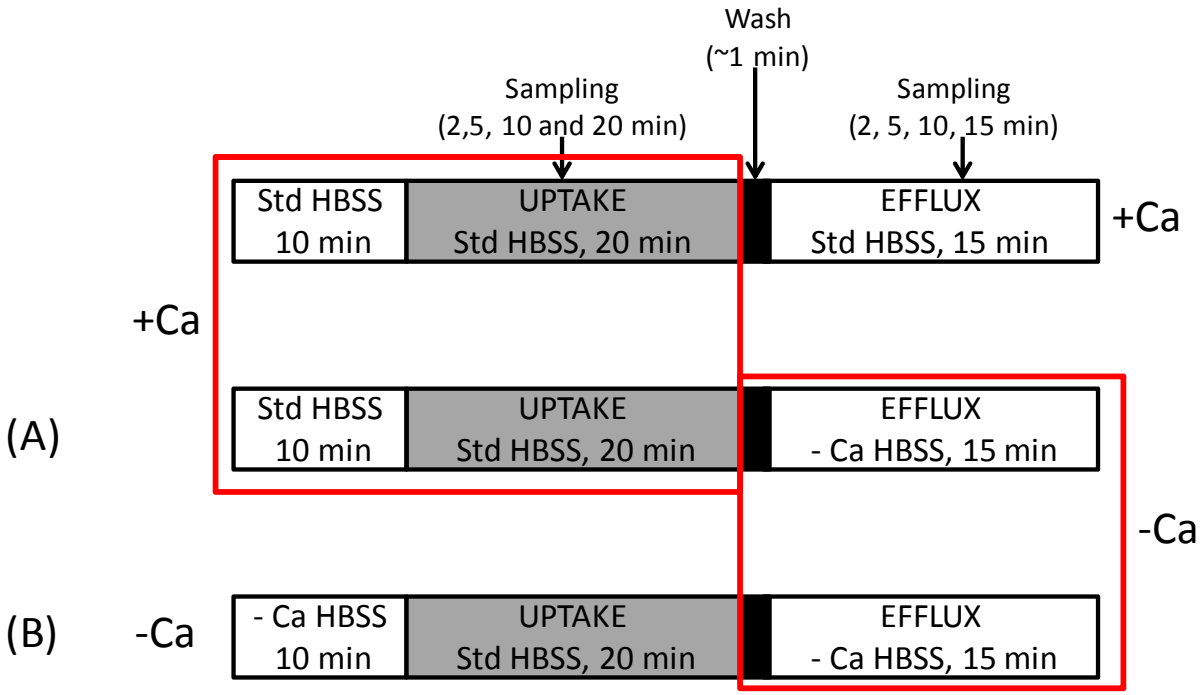

Figure 1.4. Fluorescence intensity in bile networks observed following administration of 1 μM carboxydichlorofluorescein diacetate (CDFDA) according to the schemes depicted in Figure 1.4 for the uptake (**A.**) and efflux (**B.**) phase.

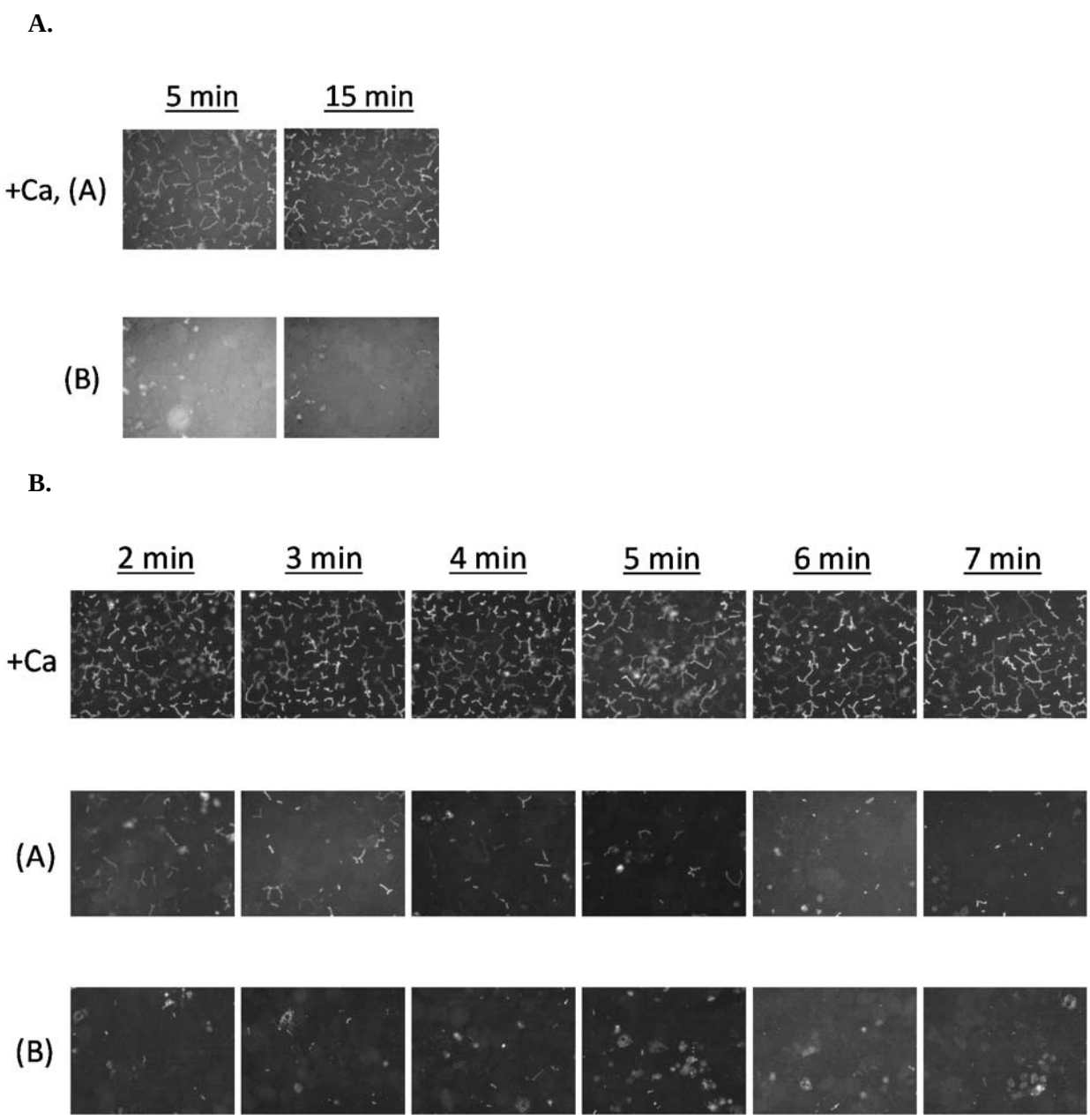

Project Rationale and Specific Aims

The objective of this research project is to develop preclinical and clinical (translational) tools to assess hepatocellular exposure, identify the role of altered hepatic transport function, and explain the change(s) that would be expected. This includes improving our mechanistic understanding of hepatobiliary drug disposition, specifically the role of overlapping substrate specificity (multiplicity of transport) and impact of impaired function of one or more transport proteins (due to genetic variation, drug interactions or disease states) on drug disposition. In order to describe and predict hepatic exposure of drugs, including the effects of altered transport function, intracellular disposition of substrates and inhibitors must be better understood.

In summary, the first aim of this research project was to administer ^{99m}Tc-mebrofenin (MEB) to human subjects, and measure changes in biliary excretion, as well as hepatic and systemic exposure, in order to elucidate the impact of ritonavir (RTV) coadministration, an inhibitor of multiple transport processes (**Aim #1**). A second objective was to develop methods in the SCH model to evaluate intracellular disposition of a set of probe drugs, including the determination of unbound concentrations in total lysate and hepatic cytosol, and subcellular localization of each compound (**Aim #2**). Finally, rosuvastatin (RSV) was used as a probe to estimate the relative contribution of basolateral vs. biliary excretion, and the impact of impaired transport function on hepatocellular accumulation and routes of excretion. Candidate transporters that mediate basolateral efflux of RSV in humans were evaluated. *In vitro* methods for estimating basolateral efflux in the SCH model system also were developed (**Aim #3**).

Aim #1. Quantify the influence of hepatic transport protein modulation by ritonavir (RTV) on the hepatic exposure, systemic disposition and biliary excretion of ^{99m}Technetium-mebrofenin (MEB) in humans.

Hypothesis: *RTV modulates one or more canalicular and/or basolateral transport proteins responsible for MEB disposition. This modulation can be measured in humans using a novel oral tube method for bile collection and noninvasive imaging technology to quantify tissue exposure in vivo. Mechanistic understanding of the interaction can be gleaned using in vitro and in vivo data coupled with pharmacokinetic modeling/simulation.*

1.a. Quantify the effects of the transport protein inhibitor RTV on MEB hepatic exposure, biliary excretion and systemic disposition *in vivo* in healthy volunteers.

1.b. Characterize, in human SCH, the effects of RTV on MEB hepatocellular accumulation and excretion.

1.c. Use *in vitro* and *in vivo* data (1.a.,b. and Aim #2) with PK modeling/simulation to gain a mechanistic understanding of the impact of RTV-mediated transporter modulation on MEB disposition in humans.

Aim #2. Examine the utility of sandwich-cultured hepatocytes (SCH) to assess the role of intracellular binding/sequestration in the hepatic accumulation of probe drugs.

Hypothesis: *Intracellular binding/sequestration contributes to the hepatic accumulation of RTV and other drugs, and influences their ability to interact with enzyme systems (metabolism and transport) involved in their own hepatic disposition, and the disposition of other drugs (DDI potential).*

2.a. Determine uptake, efflux and hepatocellular accumulation (including fraction unbound and subcellular localization) of probe drugs in rat SCH, and compare with available *in vivo* data and/or data generated in 2.b.

2.b. Determine the hepatic accumulation, unbound fraction and subcellular localization of ritonavir in rat isolated perfused livers (IPLs), and compare results with data generated in 2.a. and available *in vivo* data.

Aim #3. Evaluate the role of basolateral efflux in hepatocellular accumulation of rosuvastatin (RSV) in the setting of impaired biliary excretion.

Hypothesis: *Impaired biliary excretion will increase hepatocellular accumulation and shift excretory routes based on the relative involvement of basolateral efflux, which may be mediated by MRP3 and/or MRP4 in humans.*

3.a. Define the role of basolateral and canalicular efflux in the hepatocellular disposition of RSV in SCH under conditions of impaired function of Mrp2 (TR^- rats) and Bcrp (GF120918), alone and in combination, compared to control.

3.b. Define the role of basolateral and canalicular efflux in the hepatobiliary disposition of RSV using rat isolated perfused livers (IPLs), and establish scaling factors for clearance values determined in SCH (3.a.).

3.c. Determine the potential of MRP3 and MRP4 to mediate basolateral efflux of RSV in human liver using the membrane vesicle system.

REFERENCES

1. Esteller A. 2008. Physiology of bile secretion. *World J Gastroenterol* 14:5641-9

2. Stieger B. 2010. Role of the bile salt export pump, BSEP, in acquired forms of cholestasis. *Drug Metab Rev* 42:437-45

3. Kubitz R, Droge C, Stindt J, Weissenberger K, Haussinger D. 2012. The bile salt export pump (BSEP) in health and disease. *Clin Res Hepatol Gastroenterol* 36:536-53

4. Pauli-Magnus C, Meier PJ. 2006. Hepatobiliary transporters and drug-induced cholestasis. *Hepatology* 44:778-87

5. Jemnitz K, Heredi-Szabo K, Janossy J, Ioja E, Vereczkey L, Krajcsi P. 2010. ABCC2/Abcc2: a multispecific transporter with dominant excretory functions. *Drug Metab Rev* 42:402-36

6. Zamek-Gliszczynski MJ, Hoffmaster KA, Nezasa K, Tallman MN, Brouwer KL. 2006. Integration of hepatic drug transporters and phase II metabolizing enzymes: mechanisms of hepatic excretion of sulfate, glucuronide, and glutathione metabolites. *Eur J Pharm Sci* 27:447-86

7. Robey RW, To KK, Polgar O, Dohse M, Fetsch P, et al. 2009. ABCG2: a perspective. *Adv Drug Deliv Rev* 61:3-13

8. Koshiba S, An R, Saito H, Wakabayashi K, Tamura A, Ishikawa T. 2008. Human ABC transporters ABCG2 (BCRP) and ABCG4. *Xenobiotica* 38:863-88

9. Robey RW, Ierano C, Zhan Z, Bates SE. 2011. The challenge of exploiting ABCG2 in the clinic. *Curr Pharm Biotechnol* 12:595-608

10. Cascorbi I. 2011. P-glycoprotein: tissue distribution, substrates, and functional consequences of genetic variations. *Handb Exp Pharmacol*:261-83

11. Fagerholm U. 2008. Prediction of human pharmacokinetics-biliary and intestinal clearance and enterohepatic circulation. *J Pharm Pharmacol* 60:535-42

12. Roberts MS, Magnusson BM, Burczynski FJ, Weiss M. 2002. Enterohepatic circulation: physiological, pharmacokinetic and clinical implications. *Clin Pharmacokinet* 41:751-90

13. Stieger B, Meier PJ. 2011. Pharmacogenetics of drug transporters in the enterohepatic circulation. *Pharmacogenomics* 12:611-31

14. Cremers S, Schoemaker R, Scholten E, den Hartigh J, Konig-Quartel J, et al. 2005. Characterizing the role of enterohepatic recycling in the interactions between mycophenolate mofetil and calcineurin inhibitors in renal transplant patients by pharmacokinetic modelling. *Br J Clin Pharmacol* 60:249-56

15. Ploeger BA, Meulenbelt J, DeJongh J. 2000. Physiologically based pharmacokinetic modeling of glycyrrhizic acid, a compound subject to presystemic metabolism and enterohepatic cycling. *Toxicol Appl Pharmacol* 162:177-88

16. Rausl D, Fotaki N, Zanoski R, Vertzoni M, Cetina-Cizmek B, et al. 2006. Intestinal permeability and excretion into bile control the arrival of amlodipine into the systemic circulation after oral administration. *J Pharm Pharmacol* 58:827-36

17. Duggan DE, Hooke KF, Noll RM, Kwan KC. 1975. Enterohepatic circulation of indomethacin and its role in intestinal irritation. *Biochem Pharmacol* 24:1749-54

18. Kouzuki H, Suzuki H, Sugiyama Y. 2000. Pharmacokinetic study of the hepatobiliary transport of indomethacin. *Pharm Res* 17:432-8

19. Jain L, Woo S, Gardner ER, Dahut WL, Kohn EC, et al. 2011. Population pharmacokinetic analysis of sorafenib in patients with solid tumours. *Br J Clin Pharmacol* 72:294-305

20. Pollack GM, Brouwer KL. 1991. Physiologic and metabolic influences on enterohepatic recirculation: simulations based upon the disposition of valproic acid in the rat. *J Pharmacokinet Biopharm* 19:189-225

21. Chabot GG, Abigerges D, Catimel G, Culine S, de Forni M, et al. 1995. Population pharmacokinetics and pharmacodynamics of irinotecan (CPT-11) and active metabolite SN-38 during phase I trials. *Ann Oncol* 6:141-51

22. Chiang JY. 2009. Bile acids: regulation of synthesis. *J Lipid Res* 50:1955-66

23. Padda MS, Sanchez M, Akhtar AJ, Boyer JL. 2011. Drug-induced cholestasis. *Hepatology* 53:1377-87

24. de Lannoy IA, Barker F, 3rd, Pang KS. 1993. Formed and preformed metabolite excretion clearances in liver, a metabolite formation organ: studies on enalapril and enalaprilat in the single-pass and recirculating perfused rat liver. *J Pharmacokinet Biopharm* 21:395-422

25. Hardwick RN, Fisher CD, Street SM, Canet MJ, Cherrington NJ. 2012. Molecular mechanism of altered ezetimibe disposition in nonalcoholic steatohepatitis. *Drug Metab Dispos* 40:450-60

26. Tian X, Swift B, Zamek-Gliszczynski MJ, Belinsky MG, Kruh GD, Brouwer KL. 2008. Impact of basolateral multidrug resistance-associated protein (Mrp) 3 and Mrp4 on the hepatobiliary disposition of fexofenadine in perfused mouse livers. *Drug Metab Dispos* 36:911-5

27. Iusuf D, van de Steeg E, Schinkel AH. 2012. Hepatocyte hopping of OATP1B substrates contributes to efficient hepatic detoxification. *Clin Pharmacol Ther* 92:559-62

28. Iusuf D, van de Steeg E, Schinkel AH. 2012. Functions of OATP1A and 1B transporters in vivo: insights from mouse models. *Trends Pharmacol Sci* 33:100-8

29. van de Steeg E, van Esch A, Wagenaar E, van der Kruijssen CM, van Tellingen O, et al. 2011. High impact of Oatp1a/1b transporters on in vivo disposition of the hydrophobic anticancer drug paclitaxel. *Clin Cancer Res* 17:294-301

30. Barnes SN, Aleksunes LM, Augustine L, Scheffer GL, Goedken MJ, et al. 2007. Induction of hepatobiliary efflux transporters in acetaminophen-induced acute liver failure cases. *Drug Metab Dispos* 35:1963-9

31. Hardwick RN, Fisher CD, Canet MJ, Scheffer GL, Cherrington NJ. 2011. Variations in ATP-binding cassette transporter regulation during the progression of human nonalcoholic fatty liver disease. *Drug Metab Dispos* 39:2395-402

32. Zhou SF, Wang LL, Di YM, Xue CC, Duan W, et al. 2008. Substrates and inhibitors of human multidrug resistance associated proteins and the implications in drug development. *Curr Med Chem* 15:1981-2039

33. Zamek-Gliszczynski MJ, Nezasa K, Tian X, Bridges AS, Lee K, et al. 2006. Evaluation of the role of multidrug resistance-associated protein (Mrp) 3 and Mrp4 in hepatic basolateral excretion of sulfate and glucuronide metabolites of acetaminophen, 4-methylumbelliferone, and harmol in Abcc3-/- and Abcc4-/- mice. *J Pharmacol Exp Ther* 319:1485-91

34. Boyer JL, Trauner M, Mennone A, Soroka CJ, Cai SY, et al. 2006. Upregulation of a basolateral FXR-dependent bile acid efflux transporter OSTalpha-OSTbeta in cholestasis in humans and rodents. *Am J Physiol Gastrointest Liver Physiol* 290:G1124-30

35. Ballatori N, Li N, Fang F, Boyer JL, Christian WV, Hammond CL. 2009. OST alpha-OST beta: a key membrane transporter of bile acids and conjugated steroids. *Front Biosci* 14:2829-44

36. Ballatori N, Christian WV, Wheeler SG, Hammond CL. 2013. The heteromeric organic solute transporter, OSTalpha-OSTbeta/SLC51: A transporter for steroid-derived molecules. *Mol Aspects Med* 34:683-92

37. Ballatori N, Christian WV, Lee JY, Dawson PA, Soroka CJ, et al. 2005. OSTalpha-OSTbeta: a major basolateral bile acid and steroid transporter in human intestinal, renal, and biliary epithelia. *Hepatology* 42:1270-9

38. Li L, Meier PJ, Ballatori N. 2000. Oatp2 mediates bidirectional organic solute transport: a role for intracellular glutathione. *Mol Pharmacol* 58:335-40

39. Mahagita C, Grassl SM, Piyachaturawat P, Ballatori N. 2007. Human organic anion transporter 1B1 and 1B3 function as bidirectional carriers and do not mediate GSH-bile acid cotransport. *Am J Physiol Gastrointest Liver Physiol* 293:G271-8

40. Tang W. 2007. Drug metabolite profiling and elucidation of drug-induced hepatotoxicity. *Expert Opin Drug Metab Toxicol* 3:407-20

41. Shaw LM, Figurski M, Milone MC, Trofe J, Bloom RD. 2007. Therapeutic drug monitoring of mycophenolic acid. *Clin J Am Soc Nephrol* 2:1062-72

42. Kobayashi M, Saitoh H, Tadano K, Takahashi Y, Hirano T. 2004. Cyclosporin A, but not tacrolimus, inhibits the biliary excretion of mycophenolic acid glucuronide possibly mediated by multidrug resistance-associated protein 2 in rats. *J Pharmacol Exp Ther* 309:1029-35

43. Kruh GD, Belinsky MG. 2003. The MRP family of drug efflux pumps. *Oncogene* 22:7537-52

44. Ayrton A, Morgan P. 2001. Role of transport proteins in drug absorption, distribution and excretion. *Xenobiotica* 31:469-97

45. Hoffmann U, Kroemer HK. 2004. The ABC transporters MDR1 and MRP2: multiple functions in disposition of xenobiotics and drug resistance. *Drug Metab Rev* 36:669-701

46. Konig J, Nies AT, Cui Y, Leier I, Keppler D. 1999. Conjugate export pumps of the multidrug resistance protein (MRP) family: localization, substrate specificity, and MRP2-mediated drug resistance. *Biochim Biophys Acta* 1461:377-94

47. Sparreboom A, van Asperen J, Mayer U, Schinkel AH, Smit JW, et al. 1997. Limited oral bioavailability and active epithelial excretion of paclitaxel (Taxol) caused by P-glycoprotein in the intestine. *Proc Natl Acad Sci U S A* 94:2031-5

48. van Asperen J, van Tellingen O, Sparreboom A, Schinkel AH, Borst P, et al. 1997. Enhanced oral bioavailability of paclitaxel in mice treated with the P-glycoprotein blocker SDZ PSC 833. *Br J Cancer* 76:1181-3

49. Milne RW, Larsen LA, Jorgensen KL, Bastlund J, Stretch GR, Evans AM. 2000. Hepatic disposition of fexofenadine: influence of the transport inhibitors erythromycin and dibromosulphothalein. *Pharm Res* 17:1511-5

50. Hoffmaster KA, Zamek-Gliszczynski MJ, Pollack GM, Brouwer KL. 2004. Hepatobiliary disposition of the metabolically stable opioid peptide [D-Pen2, D-Pen5]-enkephalin (DPDPE): pharmacokinetic consequences of the interplay between multiple transport systems. *J Pharmacol Exp Ther* 311:1203-10

51. Kitamura S, Maeda K, Wang Y, Sugiyama Y. 2008. Involvement of multiple transporters in the hepatobiliary transport of rosuvastatin. *Drug Metab Dispos* 36:2014-23

52. Hobbs M, Parker C, Birch H, Kenworthy K. 2012. Understanding the interplay of drug transporters involved in the disposition of rosuvastatin in the isolated perfused rat liver using a physiologically-based pharmacokinetic model. *Xenobiotica* 42:327-38

53. Ho RH, Kim RB. 2005. Transporters and drug therapy: implications for drug disposition and disease. *Clin Pharmacol Ther* 78:260-77

54. Kostrubsky SE, Strom SC, Kalgutkar AS, Kulkarni S, Atherton J, et al. 2006. Inhibition of hepatobiliary transport as a predictive method for clinical hepatotoxicity of nefazodone. *Toxicol Sci* 90:451-9

55. Fattinger K, Funk C, Pantze M, Weber C, Reichen J, et al. 2001. The endothelin antagonist bosentan inhibits the canalicular bile salt export pump: a potential mechanism for hepatic adverse reactions. *Clin Pharmacol Ther* 69:223-31

56. Karthik SV, Casson D. 2005. Erythromycin-associated cholestatic hepatitis and liver dysfunction in children: the British experience. *J Clin Gastroenterol* 39:743-4

57. Dawson S, Stahl S, Paul N, Barber J, Kenna JG. 2012. In vitro inhibition of the bile salt export pump correlates with risk of cholestatic drug-induced liver injury in humans. *Drug Metab Dispos* 40:130-8

58. Morgan RE, Trauner M, van Staden CJ, Lee PH, Ramachandran B, et al. 2010. Interference with bile salt export pump function is a susceptibility factor for human liver injury in drug development. *Toxicol Sci* 118:485-500

59. Koeck K, Ferslew BC, Netterberg I, Yang K, Urban TJ, et al. 2012. Inhibition of the hepatic basolateral bile acid transporter MRP4 predicts cholestatic drug-induced liver injury (DILI). *Hepatology* 56:1530

60. Alvarez AI, Real R, Perez M, Mendoza G, Prieto JG, Merino G. 2010. Modulation of the activity of ABC transporters (P-glycoprotein, MRP2, BCRP) by flavonoids and drug response. *J Pharm Sci* 99:598-617

61. Gandhi YA, Morris ME. 2009. Structure-activity relationships and quantitative structure-activity relationships for breast cancer resistance protein (ABCG2). *AAPS J* 11:541-52

62. Natarajan K, Xie Y, Baer MR, Ross DD. 2012. Role of breast cancer resistance protein (BCRP/ABCG2) in cancer drug resistance. *Biochem Pharmacol* 83:1084-103

63. Broccatelli F, Carosati E, Neri A, Frosini M, Goracci L, et al. 2011. A novel approach for predicting P-glycoprotein (ABCB1) inhibition using molecular interaction fields. *J Med Chem* 54:1740-51

64. Sakurai A, Kurata A, Onishi Y, Hirano H, Ishikawa T. 2007. Prediction of drug-induced intrahepatic cholestasis: in vitro screening and QSAR analysis of drugs inhibiting the human bile salt export pump. *Expert Opin Drug Saf* 6:71-86

65. Ozawa N, Shimizu T, Morita R, Yokono Y, Ochiai T, et al. 2004. Transporter database, TP-Search: a web-accessible comprehensive database for research in pharmacokinetics of drugs. *Pharm Res* 21:2133-4

66. Saier MH, Jr., Yen MR, Noto K, Tamang DG, Elkan C. 2009. The Transporter Classification Database: recent advances. *Nucleic Acids Res* 37:D274-8

67. Ren Q, Chen K, Paulsen IT. 2007. TransportDB: a comprehensive database resource for cytoplasmic membrane transport systems and outer membrane channels. *Nucleic Acids Res* 35:D274-9

68. Yee SW, Chen L, Giacomini KM. 2010. Pharmacogenomics of membrane transporters: past, present and future. *Pharmacogenomics* 11:475-9

69. Sedykh A, Fourches D, Duan J, Hucke O, Garneau M, et al. 2012. Human Intestinal Transporter Database: QSAR Modeling and Virtual Profiling of Drug Uptake, Efflux and Interactions. *Pharm Res*

70. Kindla J, Muller F, Mieth M, Fromm MF, Konig J. 2011. Influence of non-steroidal anti-inflammatory drugs on organic anion transporting polypeptide (OATP) 1B1- and OATP1B3-mediated drug transport. *Drug Metab Dispos* 39:1047-53

71. Vallejo M, Briz O, Serrano MA, Monte MJ, Marin JJ. 2006. Potential role of trans-inhibition of the bile salt export pump by progesterone metabolites in the etiopathogenesis of intrahepatic cholestasis of pregnancy. *J Hepatol* 44:1150-7

72. Stieger B, Fattinger K, Madon J, Kullak-Ublick GA, Meier PJ. 2000. Drug- and estrogen-induced cholestasis through inhibition of the hepatocellular bile salt export pump (Bsep) of rat liver. *Gastroenterology* 118:422-30

73. Gertz M, Cartwright CM, Hobbs MJ, Kenworthy KE, Rowland M, et al. 2013. Cyclosporine Inhibition of Hepatic and Intestinal CYP3A4, Uptake and Efflux Transporters: Application of PBPK Modeling in the Assessment of Drug-Drug Interaction Potential. *Pharm Res* 30:761-80

74. Shitara Y, Nagamatsu Y, Wada S, Sugiyama Y, Horie T. 2009. Long-lasting inhibition of the transporter-mediated hepatic uptake of sulfobromophthalein by cyclosporin a in rats. *Drug Metab Dispos* 37:1172-8

75. Sterz K, Mollmann L, Jacobs A, Baumert D, Wiese M. 2009. Activators of P-glycoprotein: Structure-activity relationships and investigation of their mode of action. *ChemMedChem* 4:1897-911

76. Heredi-Szabo K, Jemnitz K, Kis E, Ioja E, Janossy J, et al. 2009. Potentiation of MRP2/Mrp2-mediated estradiol-17beta-glucuronide transport by drugs--a concise review. *Chem Biodivers* 6:1970-4

77. Kauffmann HM, Keppler D, Kartenbeck J, Schrenk D. 1997. Induction of cMrp/cMoat gene expression by cisplatin, 2-acetylaminofluorene, or cycloheximide in rat hepatocytes. *Hepatology* 26:980-5

78. Perloff MD, Von Moltke LL, Marchand JE, Greenblatt DJ. 2001. Ritonavir induces P-glycoprotein expression, multidrug resistance-associated protein (MRP1) expression, and drug transporter-mediated activity in a human intestinal cell line. *J Pharm Sci* 90:1829-37

79. Suzuki H, Sugiyama Y. 2002. Single nucleotide polymorphisms in multidrug resistance associated protein 2 (MRP2/ABCC2): its impact on drug disposition. *Adv Drug Deliv Rev* 54:1311-31

80. Staud F, Pavek P. 2005. Breast cancer resistance protein (BCRP/ABCG2). *Int J Biochem Cell Biol* 37:720-5

81. Cascorbi I, Haenisch S. 2010. Pharmacogenetics of ATP-binding cassette transporters and clinical implications. *Methods Mol Biol* 596:95-121

82. Keitel V, Kartenbeck J, Nies AT, Spring H, Brom M, Keppler D. 2000. Impaired protein maturation of the conjugate export pump multidrug resistance protein 2 as a consequence of a deletion mutation in Dubin-Johnson syndrome. *Hepatology* 32:1317-28

83. Keitel V, Nies AT, Brom M, Hummel-Eisenbeiss J, Spring H, Keppler D. 2003. A common Dubin-Johnson syndrome mutation impairs protein maturation and transport activity of MRP2 (ABCC2). *Am J Physiol Gastrointest Liver Physiol* 284:G165-74

84. Hirouchi M, Suzuki H, Itoda M, Ozawa S, Sawada J, et al. 2004. Characterization of the cellular localization, expression level, and function of SNP variants of MRP2/ABCC2. *Pharm Res* 21:742-8

85. Megaraj V, Zhao T, Paumi CM, Gerk PM, Kim RB, Vore M. 2011. Functional analysis of nonsynonymous single nucleotide polymorphisms of multidrug resistance-associated protein 2 (ABCC2). *Pharmacogenet Genomics* 21:506-15

86. Ryu S, Kawabe T, Nada S, Yamaguchi A. 2000. Identification of basic residues involved in drug export function of human multidrug resistance-associated protein 2. *J Biol Chem* 275:39617-24

87. Sookoian S, Castano G, Gianotti TF, Gemma C, Pirola CJ. 2009. Polymorphisms of MRP2 (ABCC2) are associated with susceptibility to nonalcoholic fatty liver disease. *J Nutr Biochem* 20:765-70

88. Elens L, Tyteca D, Panin N, Courtoy P, Lison D, et al. 2011. Functional defect caused by the 4544G>A SNP in ABCC2: potential impact for drug cellular disposition. *Pharmacogenet Genomics* 21:884-93

89. Choi JH, Ahn BM, Yi J, Lee JH, Nam SW, et al. 2007. MRP2 haplotypes confer differential susceptibility to toxic liver injury. *Pharmacogenet Genomics* 17:403-15

90. Nguyen TD, Markova S, Liu W, Gow JM, Baldwin RM, et al. 2012. Functional characterization of ABCC2 promoter polymorphisms and allele-specific expression. *Pharmacogenomics J*

91. Laechelt S, Turrini E, Ruehmkorf A, Siegmund W, Cascorbi I, Haenisch S. 2011. Impact of ABCC2 haplotypes on transcriptional and posttranscriptional gene regulation and function. *Pharmacogenomics J* 11:25-34

92. Lang T, Hitzl M, Burk O, Mornhinweg E, Keil A, et al. 2004. Genetic polymorphisms in the multidrug resistance-associated protein 3 (ABCC3, MRP3) gene and relationship to its mRNA and protein expression in human liver. *Pharmacogenetics* 14:155-64

93. Doerfel C, Rump A, Sauerbrey A, Gruhn B, Zintl F, Steinbach D. 2006. In acute leukemia, the polymorphism -211C>T in the promoter region of the multidrug resistance-associated protein 3 (MRP3) does not determine the expression level of the gene. *Pharmacogenet Genomics* 16:149-50

94. Gradhand U, Tegude H, Burk O, Eichelbaum M, Fromm MF, Konig J. 2007. Functional analysis of the polymorphism -211C>T in the regulatory region of the human ABCC3 gene. *Life Sci* 80:1490-4

95. Kobayashi K, Ito K, Takada T, Sugiyama Y, Suzuki H. 2008. Functional analysis of nonsynonymous single nucleotide polymorphism type ATP-binding cassette transmembrane transporter subfamily C member 3. *Pharmacogenet Genomics* 18:823-33

96. Sasaki T, Hirota T, Ryokai Y, Kobayashi D, Kimura M, et al. 2011. Systematic screening of human ABCC3 polymorphisms and their effects on MRP3 expression and function. *Drug Metab Pharmacokinet* 26:374-86

97. Abla N, Chinn LW, Nakamura T, Liu L, Huang CC, et al. 2008. The human multidrug resistance protein 4 (MRP4, ABCC4): functional analysis of a highly polymorphic gene. *J Pharmacol Exp Ther* 325:859-68

98. Ansari M, Sauty G, Labuda M, Gagne V, Laverdiere C, et al. 2009. Polymorphisms in multidrug resistance-associated protein gene 4 is associated with outcome in childhood acute lymphoblastic leukemia. *Blood* 114:1383-6

99. Bruggemann M, Trautmann H, Hoelzer D, Kneba M, Gokbuget N, Raff T. 2009. Multidrug resistance-associated protein 4 (MRP4) gene polymorphisms and treatment response in adult acute lymphoblastic leukemia. *Blood* 114:5400-1; author reply 1-2

100. Wada M. 2006. Single nucleotide polymorphisms in ABCC2 and ABCB1 genes and their clinical impact in physiology and drug response. *Cancer Lett* 234:40-50

101. Elens L, Capron A, Kerckhove VV, Lerut J, Mourad M, et al. 2007. 1199G>A and 2677G>T/A polymorphisms of ABCB1 independently affect tacrolimus concentration in hepatic tissue after liver transplantation. *Pharmacogenet Genomics* 17:873-83

102. Owen A, Goldring C, Morgan P, Chadwick D, Park BK, Pirmohamed M. 2005. Relationship between the C3435T and G2677T(A) polymorphisms in the ABCB1 gene and P-glycoprotein expression in human liver. *Br J Clin Pharmacol* 59:365-70

103. Song P, Lamba JK, Zhang L, Schuetz E, Shukla N, et al. 2006. G2677T and C3435T genotype and haplotype are associated with hepatic ABCB1 (MDR1) expression. *J Clin Pharmacol* 46:373-9

104. Ieiri I. 2012. Functional significance of genetic polymorphisms in P-glycoprotein (MDR1, ABCB1) and breast cancer resistance protein (BCRP, ABCG2). *Drug Metab Pharmacokinet* 27:85-105

105. Mizuarai S, Aozasa N, Kotani H. 2004. Single nucleotide polymorphisms result in impaired membrane localization and reduced atpase activity in multidrug transporter ABCG2. *Int J Cancer* 109:238-46

106. Cascorbi I. 2006. Role of pharmacogenetics of ATP-binding cassette transporters in the pharmacokinetics of drugs. *Pharmacol Ther* 112:457-73

107. Zollner G, Fickert P, Silbert D, Fuchsbichler A, Marschall HU, et al. 2003. Adaptive changes in hepatobiliary transporter expression in primary biliary cirrhosis. *J Hepatol* 38:717-27

108. Zollner G, Fickert P, Zenz R, Fuchsbichler A, Stumptner C, et al. 2001. Hepatobiliary transporter expression in percutaneous liver biopsies of patients with cholestatic liver diseases. *Hepatology* 33:633-46

109. Ros JE, Libbrecht L, Geuken M, Jansen PL, Roskams TA. 2003. High expression of MDR1, MRP1, and MRP3 in the hepatic progenitor cell compartment and hepatocytes in severe human liver disease. *J Pathol* 200:553-60

110. Zollner G, Wagner M, Fickert P, Silbert D, Gumhold J, et al. 2007. Expression of bile acid synthesis and detoxification enzymes and the alternative bile acid efflux pump MRP4 in patients with primary biliary cirrhosis. *Liver Int* 27:920-9

111. Gradhand U, Lang T, Schaeffeler E, Glaeser H, Tegude H, et al. 2008. Variability in human hepatic MRP4 expression: influence of cholestasis and genotype. *Pharmacogenomics J* 8:42-52

112. Hanada K, Nakai K, Tanaka H, Suzuki F, Kumada H, et al. 2012. Effect of nuclear receptor downregulation on hepatic expression of cytochrome P450 and transporters in chronic hepatitis C in association with fibrosis development. *Drug Metab Pharmacokinet* 27:301-6

113. Kurzawski M, Dziedziejko V, Post M, Wojcicki M, Urasinska E, et al. 2012. Expression of genes involved in xenobiotic metabolism and transport in end-stage liver disease: up-regulation of ABCC4 and CYP1B1. *Pharmacol Rep* 64:927-39

114. Ogasawara K, Terada T, Katsura T, Hatano E, Ikai I, et al. 2010. Hepatitis C virus-related cirrhosis is a major determinant of the expression levels of hepatic drug transporters. *Drug Metab Pharmacokinet* 25:190-9

115. Hinoshita E, Taguchi K, Inokuchi A, Uchiumi T, Kinukawa N, et al. 2001. Decreased expression of an ATP-binding cassette transporter, MRP2, in human livers with hepatitis C virus infection. *J Hepatol* 35:765-73

116. Borel F, Han R, Visser A, Petry H, van Deventer SJ, et al. 2012. Adenosine triphosphate-binding cassette transporter genes up-regulation in untreated hepatocellular carcinoma is mediated by cellular microRNAs. *Hepatology* 55:821-32

117. Bonin S, Pascolo L, Croce LS, Stanta G, Tiribelli C. 2002. Gene expression of ABC proteins in hepatocellular carcinoma, perineoplastic tissue, and liver diseases. *Mol Med* 8:318-25

118. Keitel V, Burdelski M, Warskulat U, Kuhlkamp T, Keppler D, et al. 2005. Expression and localization of hepatobiliary transport proteins in progressive familial intrahepatic cholestasis. *Hepatology* 41:1160-72

119. Kipp H, Arias IM. 2002. Trafficking of canalicular ABC transporters in hepatocytes. *Annu Rev Physiol* 64:595-608

120. Wakabayashi Y, Kipp H, Arias IM. 2006. Transporters on demand: intracellular reservoirs and cycling of bile canalicular ABC transporters. *J Biol Chem* 281:27669-73

121. Kipp H, Arias IM. 2000. Intracellular trafficking and regulation of canalicular ATP-binding cassette transporters. *Semin Liver Dis* 20:339-51

122. Kipp H, Pichetshote N, Arias IM. 2001. Transporters on demand: intrahepatic pools of canalicular ATP binding cassette transporters in rat liver. *J Biol Chem* 276:7218-24

123. Kipp H, Arias IM. 2000. Newly synthesized canalicular ABC transporters are directly targeted from the Golgi to the hepatocyte apical domain in rat liver. *J Biol Chem* 275:15917-25

124. Wojtal KA, de Vries E, Hoekstra D, van Ijzendoorn SC. 2006. Efficient trafficking of MDR1/P-glycoprotein to apical canalicular plasma membranes in HepG2 cells requires PKA-RIIalpha anchoring and glucosylceramide. *Mol Biol Cell* 17:3638-50

125. Fu D, van Dam EM, Brymora A, Duggin IG, Robinson PJ, Roufogalis BD. 2007. The small GTPases Rab5 and RalA regulate intracellular traffic of P-glycoprotein. *Biochim Biophys Acta* 1773:1062-72

126. Ferrandiz-Huertas C, Fernandez-Carvajal A, Ferrer-Montiel A. 2011. Rab4 interacts with the human P-glycoprotein and modulates its surface expression in multidrug resistant K562 cells. *Int J Cancer* 128:192-205

127. Ji B, Ito K, Sekine S, Tajima A, Horie T. 2004. Ethacrynic-acid-induced glutathione depletion and oxidative stress in normal and Mrp2-deficient rat liver. *Free Radic Biol Med* 37:1718-29

128. Mottino AD, Crocenzi FA, Pozzi EJ, Veggi LM, Roma MG, Vore M. 2005. Role of microtubules in estradiol-17beta-D-glucuronide-induced alteration of canalicular Mrp2 localization and activity. *Am J Physiol Gastrointest Liver Physiol* 288:G327-36

129. Sekine S, Mitsuki K, Ito K, Kugioka S, Horie T. 2012. Sustained intrahepatic glutathione depletion causes proteasomal degradation of multidrug resistance-associated protein 2 in rat liver. *Biochim Biophys Acta* 1822:980-7

130. Kojima H, Nies AT, Konig J, Hagmann W, Spring H, et al. 2003. Changes in the expression and localization of hepatocellular transporters and radixin in primary biliary cirrhosis. *J Hepatol* 39:693-702

131. Kojima H, Sakurai S, Uemura M, Kitamura K, Kanno H, et al. 2008. Disturbed colocalization of multidrug resistance protein 2 and radixin in human cholestatic liver diseases. *J Gastroenterol Hepatol* 23:e120-8

132. Sekine S, Ito K, Horie T. 2008. Canalicular Mrp2 localization is reversibly regulated by the intracellular redox status. *Am J Physiol Gastrointest Liver Physiol* 295:G1035-41

133. Mottino AD, Cao J, Veggi LM, Crocenzi F, Roma MG, Vore M. 2002. Altered localization and activity of canalicular Mrp2 in estradiol-17beta-D-glucuronide-induced cholestasis. *Hepatology* 35:1409-19

134. Sekine S, Ito K, Saeki J, Horie T. 2011. Interaction of Mrp2 with radixin causes reversible canalicular Mrp2 localization induced by intracellular redox status. *Biochim Biophys Acta* 1812:1427-34

135. Crocenzi FA, Sanchez Pozzi EJ, Ruiz ML, Zucchetti AE, Roma MG, et al. 2008. Ca(2+)-dependent protein kinase C isoforms are critical to estradiol 17beta-D-glucuronide-induced cholestasis in the rat. *Hepatology* 48:1885-95

136. Rost D, Kloeters-Plachky P, Stiehl A. 2008. Retrieval of the rat canalicular conjugate export pump Mrp2 is associated with a rearrangement of actin filaments and radixin in bile salt-induced cholestasis. *Eur J Med Res* 13:314-8

137. Boaglio AC, Zucchetti AE, Sanchez Pozzi EJ, Pellegrino JM, Ochoa JE, et al. 2010. Phosphoinositide 3-kinase/protein kinase B signaling pathway is involved in estradiol 17beta-D-glucuronide-induced cholestasis: complementarity with classical protein kinase C. *Hepatology* 52:1465-76

138. Boaglio AC, Zucchetti AE, Toledo FD, Barosso IR, Sanchez Pozzi EJ, et al. 2012. ERK1/2 and p38 MAPKs are complementarily involved in estradiol 17ss-D-glucuronide-induced cholestasis: crosstalk with cPKC and PI3K. *PLoS One* 7:e49255

139. Schonhoff CM, Gillin H, Webster CR, Anwer MS. 2008. Protein kinase Cdelta mediates cyclic adenosine monophosphate-stimulated translocation of sodium taurocholate cotransporting polypeptide and multidrug resistant associated protein 2 in rat hepatocytes. *Hepatology* 47:1309-16

140. Mohrmann K, van Eijndhoven MA, Schinkel AH, Schellens JH. 2005. Absence of N-linked glycosylation does not affect plasma membrane localization of breast cancer resistance protein (BCRP/ABCG2). *Cancer Chemother Pharmacol* 56:344-50

141. Nakagawa H, Wakabayashi-Nakao K, Tamura A, Toyoda Y, Koshiba S, Ishikawa T. 2009. Disruption of N-linked glycosylation enhances ubiquitin-mediated proteasomal degradation of the human ATP-binding cassette transporter ABCG2. *FEBS J* 276:7237-52

142. Draheim V, Reichel A, Weitschies W, Moenning U. 2010. N-glycosylation of ABC transporters is associated with functional activity in sandwich-cultured rat hepatocytes. *Eur J Pharm Sci* 41:201-9

143. Fernandez SB, Hollo Z, Kern A, Bakos E, Fischer PA, et al. 2002. Role of the N-terminal transmembrane region of the multidrug resistance protein MRP2 in routing to the apical membrane in MDCKII cells. *J Biol Chem* 277:31048-55

144. Zhang P, Tian X, Chandra P, Brouwer KL. 2005. Role of glycosylation in trafficking of Mrp2 in sandwich-cultured rat hepatocytes. *Mol Pharmacol* 67:1334-41

145. Hoque MT, Cole SP. 2008. Down-regulation of Na+/H+ exchanger regulatory factor 1 increases expression and function of multidrug resistance protein 4. *Cancer Res* 68:4802-9

146. Hayashi H, Naoi S, Nakagawa T, Nishikawa T, Fukuda H, et al. 2012. Sorting nexin 27 interacts with multidrug resistance-associated protein 4 (MRP4) and mediates internalization of MRP4. *J Biol Chem* 287:15054-65

147. Zamek-Gliszczynski MJ, Kalvass JC, Pollack GM, Brouwer KL. 2009. Relationship between drug/metabolite exposure and impairment of excretory transport function. *Drug Metab Dispos* 37:386-90

148. Vlaming ML, van Esch A, Pala Z, Wagenaar E, van de Wetering K, et al. 2009. Abcc2 (Mrp2), Abcc3 (Mrp3), and Abcg2 (Bcrp1) are the main determinants for rapid elimination of methotrexate and its toxic metabolite 7-hydroxymethotrexate in vivo. *Mol Cancer Ther* 8:3350-9

149. Vlaming ML, Pala Z, van Esch A, Wagenaar E, de Waart DR, et al. 2009. Functionally overlapping roles of Abcg2 (Bcrp1) and Abcc2 (Mrp2) in the elimination of methotrexate and its main toxic metabolite 7-hydroxymethotrexate in vivo. *Clin Cancer Res* 15:3084-93

150. Vlaming ML, Pala Z, van Esch A, Wagenaar E, van Tellingen O, et al. 2008. Impact of Abcc2 (Mrp2) and Abcc3 (Mrp3) on the in vivo elimination of methotrexate and its main toxic metabolite 7-hydroxymethotrexate. *Clin Cancer Res* 14:8152-60

151. de Waart DR, Vlaming ML, Kunne C, Schinkel AH, Oude Elferink RP. 2009. Complex pharmacokinetic behavior of ezetimibe depends on abcc2, abcc3, and abcg2. *Drug Metab Dispos* 37:1698-702

152. van Waterschoot RA, Eman RM, Wagenaar E, van der Kruijssen CM, Rosing H, et al. 2009. ABCC2, ABCC3, and ABCB1, but not CYP3A, Protect against Trabectedin-Mediated Hepatotoxicity. *Clin Cancer Res* 15:7616-23

153. Lee JK, Leslie EM, Zamek-Gliszczynski MJ, Brouwer KL. 2008. Modulation of trabectedin (ET-743) hepatobiliary disposition by multidrug resistance-associated proteins (Mrps) may prevent hepatotoxicity. *Toxicol Appl Pharmacol* 228:17-23

154. Matsushima S, Maeda K, Hayashi H, Debori Y, Schinkel AH, et al. 2008. Involvement of multiple efflux transporters in hepatic disposition of fexofenadine. *Mol Pharmacol* 73:1474-83

155. Matsushima S, Maeda K, Ishiguro N, Igarashi T, Sugiyama Y. 2008. Investigation of the inhibitory effects of various drugs on the hepatic uptake of fexofenadine in humans. *Drug Metab Dispos* 36:663-9

156. Cvetkovic M, Leake B, Fromm MF, Wilkinson GR, Kim RB. 1999. OATP and P-glycoprotein transporters mediate the cellular uptake and excretion of fexofenadine. *Drug Metab Dispos* 27:866-71

157. Ward ES, Pollack GM, Brouwer KL. 2000. Probenecid-associated alterations in valproic acid pharmacokinetics in rats: can in vivo disposition of valproate glucuronide be predicted from in vitro formation data? *Drug Metab Dispos* 28:1433-9

158. Lam JL, Okochi H, Huang Y, Benet LZ. 2006. In vitro and in vivo correlation of hepatic transporter effects on erythromycin metabolism: characterizing the importance of transporter-enzyme interplay. *Drug Metab Dispos* 34:1336-44

159. Fan J, Maeng HJ, Pang KS. 2010. Interplay of transporters and enzymes in the Caco-2 cell monolayer: I. effect of altered apical secretion. *Biopharm Drug Dispos* 31:215-27

160. Pang KS, Maeng HJ, Fan J. 2009. Interplay of transporters and enzymes in drug and metabolite processing. *Mol Pharm* 6:1734-55

161. Lee JK, Marion TL, Abe K, Lim C, Pollock GM, Brouwer KL. 2010. Hepatobiliary disposition of troglitazone and metabolites in rat and human sandwich-cultured hepatocytes: use of Monte Carlo simulations to assess the impact of changes in biliary excretion on troglitazone sulfate accumulation. *J Pharmacol Exp Ther* 332:26-34

162. Hennessy M, Spiers JP. 2007. A primer on the mechanics of P-glycoprotein the multidrug transporter. *Pharmacol Res* 55:1-15

163. Stein WD. 1997. Kinetics of the multidrug transporter (P-glycoprotein) and its reversal. *Physiol Rev* 77:545-90

164. Korzekwa KR, Nagar S, Tucker J, Weiskircher EA, Bhoopathy S, Hidalgo IJ. 2012. Models to predict unbound intracellular drug concentrations in the presence of transporters. *Drug Metab Dispos* 40:865-76

165. Ihrke G, Martin GV, Shanks MR, Schrader M, Schroer TA, Hubbard AL. 1998. Apical plasma membrane proteins and endolyn-78 travel through a subapical compartment in polarized WIF-B hepatocytes. *J Cell Biol* 141:115-33

166. Aoyama N, Tokumo H, Ohya T, Chandler K, Holzbach RT. 1991. A novel transcellular transport pathway for non-bile salt cholephilic organic anions. *Am J Physiol* 261:G305-11

167. Aoyama N, Ohya T, Chandler K, Gresky S, Holzbach RT. 1991. Transcellular transport of organic anions in the isolated perfused rat liver: the differential effects of monensin and colchicine. *Hepatology* 14:1-9

168. Van ISC, Maier O, Van Der Wouden JM, Hoekstra D. 2000. The subapical compartment and its role in intracellular trafficking and cell polarity. *J Cell Physiol* 184:151-60

169. Wustner D, Mukherjee S, Maxfield FR, Muller P, Herrmann A. 2001. Vesicular and nonvesicular transport of phosphatidylcholine in polarized HepG2 cells. *Traffic* 2:277-96

170. Nies AT, Cantz T, Brom M, Leier I, Keppler D. 1998. Expression of the apical conjugate export pump, Mrp2, in the polarized hepatoma cell line, WIF-B. *Hepatology* 28:1332-40

171. Breuninger LM, Paul S, Gaughan K, Miki T, Chan A, et al. 1995. Expression of multidrug resistance-associated protein in NIH/3T3 cells confers multidrug resistance associated with increased drug efflux and altered intracellular drug distribution. *Cancer Res* 55:5342-7

172. Boyer JL, Soroka CJ. 1995. Vesicle targeting to the apical domain regulates bile excretory function in isolated rat hepatocyte couplets. *Gastroenterology* 109:1600-11

173. Giacomini KM, Huang SM, Tweedie DJ, Benet LZ, Brouwer KL, et al. 2010. Membrane transporters in drug development. *Nat Rev Drug Discov* 9:215-36

174. Swift B, Pfeifer ND, Brouwer KL. 2010. Sandwich-cultured hepatocytes: an in vitro model to evaluate hepatobiliary transporter-based drug interactions and hepatotoxicity. *Drug Metab Rev* 42:446-71

175. Tchaparian EH, Houghton JS, Uyeda C, Grillo MP, Jin L. 2011. Effect of culture time on the basal expression levels of drug transporters in sandwich-cultured primary rat hepatocytes. *Drug Metab Dispos* 39:2387-94

176. Kotani N, Maeda K, Watanabe T, Hiramatsu M, Gong LK, et al. 2011. Culture period-dependent changes in the uptake of transporter substrates in sandwich-cultured rat and human hepatocytes. *Drug Metab Dispos* 39:1503-10

177. Li N, Palandra J, Nemirovskiy OV, Lai Y. 2009. LC-MS/MS mediated absolute quantification and comparison of bile salt export pump and breast cancer resistance protein in livers and hepatocytes across species. *Anal Chem* 81:2251-9

178. Li N, Zhang Y, Hua F, Lai Y. 2009. Absolute difference of hepatobiliary transporter multidrug resistance-associated protein (MRP2/Mrp2) in liver tissues and isolated hepatocytes from rat, dog, monkey, and human. *Drug Metab Dispos* 37:66-73

179. Li N, Singh P, Mandrell KM, Lai Y. 2010. Improved extrapolation of hepatobiliary clearance from in vitro sandwich cultured rat hepatocytes through absolute quantification of hepatobiliary transporters. *Mol Pharm* 7:630-41

180. Karlgren M, Vildhede A, Norinder U, Wisniewski JR, Kimoto E, et al. 2012. Classification of inhibitors of hepatic organic anion transporting polypeptides (OATPs): influence of protein expression on drug-drug interactions. *J Med Chem* 55:4740-63

181. Swift B, Yue W, Brouwer KL. 2010. Evaluation of (99m)technetium-mebrofenin and (99m)technetium-sestamibi as specific probes for hepatic transport protein function in rat and human hepatocytes. *Pharm Res* 27:1987-98

182. Jemnitz K, Veres Z, Tugyi R, Vereczkey L. 2010. Biliary efflux transporters involved in the clearance of rosuvastatin in sandwich culture of primary rat hepatocytes. *Toxicol In Vitro* 24:605-10

183. Boyer JL, Gautam A, Graf J. 1988. Mechanisms of bile secretion: insights from the isolated rat hepatocyte couplet. *Semin Liver Dis* 8:308-16

184. Shinoda Y, Suematsu M, Wakabayashi Y, Suzuki T, Goda N, et al. 1998. Carbon monoxide as a regulator of bile canalicular contractility in cultured rat hepatocytes. *Hepatology* 28:286-95

185. Hoffmaster KA, Zamek-Gliszczynski MJ, Pollack GM, Brouwer KL. 2005. Multiple transport systems mediate the hepatic uptake and biliary excretion of the metabolically stable opioid peptide [D-penicillamine2,5]enkephalin. *Drug Metab Dispos* 33:287-93

186. Liu X, LeCluyse EL, Brouwer KR, Lightfoot RM, Lee JI, Brouwer KL. 1999. Use of Ca2+ modulation to evaluate biliary excretion in sandwich-cultured rat hepatocytes. *J Pharmacol Exp Ther* 289:1592-9

187. Pfeifer ND, Brouwer KLR. 2013. A Novel Method to Elucidate the Relative Contributions of Basolateral Efflux Clearance (CL_{BL}) versus Biliary Clearance (CL_{bile}) of Rosuvastatin in the Sandwich-cultured Hepatocyte (SCH) Model American Association of Pharmaceutical Scientists (AAPS) Workshop on Drug Transporters in ADME, N. Bethesda, MD, Poster M1025.

188. Yang K, Brouwer KLR. 2012. Pharmacokinetic Modeling and Simulation Study to Predict the Impact of Troglitazone (TGZ) on the Hepatobiliary Disposition of Taurocholate (TC) in Rat Sandwich-Cultured Hepatocytes (SCH). AAPS Annual Meeting, Chicago, IL, Poster M1324.

189. Brouwer KL, Thurman RG. 1996. Isolated perfused liver. *Pharm Biotechnol* 8:161-92

190. Akita H, Suzuki H, Sugiyama Y. 2001. Sinusoidal efflux of taurocholate is enhanced in Mrp2-deficient rat liver. *Pharm Res* 18:1119-25

191. Zamek-Gliszczynski MJ, Bedwell DW, Bao JQ, Higgins JW. 2012. Characterization of SAGE Mdr1a (P-gp), Bcrp, and Mrp2 knockout rats using loperamide, paclitaxel, sulfasalazine, and carboxydichlorofluorescein pharmacokinetics. *Drug Metab Dispos* 40:1825-33

192. Zhang D, Frost CE, He K, Rodrigues AD, Wang X, et al. 2013. Investigating the Enteroenteric Recirculation of Apixaban, a Factor Xa Inhibitor: Administration of Activated Charcoal to Bile Duct-Cannulated Rats and Dogs Receiving an Intravenous Dose and Use of Drug Transporter Knockout Rats. *Drug Metab Dispos*

193. Huang L, Be X, Tchaparian EH, Colletti AE, Roberts J, et al. 2012. Deletion of Abcg2 has differential effects on excretion and pharmacokinetics of probe substrates in rats. *J Pharmacol Exp Ther* 343:316-24

194. Ohtsuki S, Uchida Y, Kubo Y, Terasaki T. 2011. Quantitative targeted absolute proteomics-based ADME research as a new path to drug discovery and development: methodology, advantages, strategy, and prospects. *J Pharm Sci* 100:3547-59

195. Agarwal S, Uchida Y, Mittapalli RK, Sane R, Terasaki T, Elmquist WF. 2012. Quantitative proteomics of transporter expression in brain capillary endothelial cells isolated from P-glycoprotein (P-gp), breast cancer resistance protein (Bcrp), and P-gp/Bcrp knockout mice. *Drug Metab Dispos* 40:1164-9

196. Uchida Y, Ohtsuki S, Kamiie J, Terasaki T. 2011. Blood-brain barrier (BBB) pharmacoproteomics: reconstruction of in vivo brain distribution of 11 P-glycoprotein substrates based on the BBB transporter protein concentration, in vitro intrinsic transport activity, and unbound fraction in plasma and brain in mice. *J Pharmacol Exp Ther* 339:579-88

197. Shawahna R, Uchida Y, Decleves X, Ohtsuki S, Yousif S, et al. 2011. Transcriptomic and quantitative proteomic analysis of transporters and drug metabolizing enzymes in freshly isolated human brain microvessels. *Mol Pharm* 8:1332-41

198. Uchida Y, Ohtsuki S, Katsukura Y, Ikeda C, Suzuki T, et al. 2011. Quantitative targeted absolute proteomics of human blood-brain barrier transporters and receptors. *J Neurochem* 117:333-45

199. Kamiie J, Ohtsuki S, Iwase R, Ohmine K, Katsukura Y, et al. 2008. Quantitative atlas of membrane transporter proteins: development and application of a highly sensitive simultaneous LC/MS/MS method combined with novel in-silico peptide selection criteria. *Pharm Res* 25:1469-83

200. Kimoto E, Yoshida K, Balogh LM, Bi YA, Maeda K, et al. 2012. Characterization of Organic Anion Transporting Polypeptide (OATP) Expression and Its Functional Contribution to the Uptake of Substrates in Human Hepatocytes. *Mol Pharm*

201. Li N, Bi YA, Duignan DB, Lai Y. 2009. Quantitative expression profile of hepatobiliary transporters in sandwich cultured rat and human hepatocytes. *Mol Pharm* 6:1180-9

202. Li N, Nemirovskiy OV, Zhang Y, Yuan H, Mo J, et al. 2008. Absolute quantification of multidrug resistance-associated protein 2 (MRP2/ABCC2) using liquid chromatography tandem mass spectrometry. *Anal Biochem* 380:211-22

203. Jones HM, Barton HA, Lai Y, Bi YA, Kimoto E, et al. 2012. Mechanistic pharmacokinetic modeling for the prediction of transporter-mediated disposition in humans from sandwich culture human hepatocyte data. *Drug Metab Dispos* 40:1007-17

204. Bi YA, Kimoto E, Sevidal S, Jones HM, Barton HA, et al. 2012. In vitro evaluation of hepatic transporter-mediated clinical drug-drug interactions: hepatocyte model optimization and retrospective investigation. *Drug Metab Dispos* 40:1085-92

205. Barton HA, Lai Y, Goosen TC, Jones HM, El-Kattan AF, et al. 2013. Model-based approaches to predict drug-drug interactions associated with hepatic uptake transporters: preclinical, clinical and beyond. *Expert Opin Drug Metab Toxicol* 9:459-72

206. Li M, Yuan H, Li N, Song G, Zheng Y, et al. 2008. Identification of interspecies difference in efflux transporters of hepatocytes from dog, rat, monkey and human. *Eur J Pharm Sci* 35:114-26

207. Hirano M, Maeda K, Shitara Y, Sugiyama Y. 2004. Contribution of OATP2 (OATP1B1) and OATP8 (OATP1B3) to the hepatic uptake of pitavastatin in humans. *J Pharmacol Exp Ther* 311:139-46

208. Yamada A, Maeda K, Kamiyama E, Sugiyama D, Kondo T, et al. 2007. Multiple human isoforms of drug transporters contribute to the hepatic and renal transport of olmesartan, a selective antagonist of the angiotensin II AT1-receptor. *Drug Metab Dispos* 35:2166-76

209. Asaka J, Terada T, Tsuda M, Katsura T, Inui K. 2007. Identification of essential histidine and cysteine residues of the H+/organic cation antiporter multidrug and toxin extrusion (MATE). *Mol Pharmacol* 71:1487-93

210. Otsuka M, Matsumoto T, Morimoto R, Arioka S, Omote H, Moriyama Y. 2005. A human transporter protein that mediates the final excretion step for toxic organic cations. *Proc Natl Acad Sci U S A* 102:17923-8

211. Tsuda M, Terada T, Asaka J, Ueba M, Katsura T, Inui K. 2007. Oppositely directed H+ gradient functions as a driving force of rat H+/organic cation antiporter MATE1. *Am J Physiol Renal Physiol* 292:F593-8

212. Terada T, Masuda S, Asaka J, Tsuda M, Katsura T, Inui K. 2006. Molecular cloning, functional characterization and tissue distribution of rat H+/organic cation antiporter MATE1. *Pharm Res* 23:1696-701

213. Tsuda M, Terada T, Mizuno T, Katsura T, Shimakura J, Inui K. 2009. Targeted disruption of the multidrug and toxin extrusion 1 (mate1) gene in mice reduces renal secretion of metformin. *Mol Pharmacol* 75:1280-6

214. Nakamura T, Yonezawa A, Hashimoto S, Katsura T, Inui K. 2010. Disruption of multidrug and toxin extrusion MATE1 potentiates cisplatin-induced nephrotoxicity. *Biochem Pharmacol* 80:1762-7

215. Higgins JW, Bedwell DW, Zamek-Gliszczynski MJ. 2012. Ablation of both organic cation transporter (OCT)1 and OCT2 alters metformin pharmacokinetics but has no effect on tissue drug exposure and pharmacodynamics. *Drug Metab Dispos* 40:1170-7

216. Wang W, Seward DJ, Li L, Boyer JL, Ballatori N. 2001. Expression cloning of two genes that together mediate organic solute and steroid transport in the liver of a marine vertebrate. *Proc Natl Acad Sci U S A* 98:9431-6

217. Seward DJ, Koh AS, Boyer JL, Ballatori N. 2003. Functional complementation between a novel mammalian polygenic transport complex and an evolutionarily ancient organic solute transporter, OSTalpha-OSTbeta. *J Biol Chem* 278:27473-82

CHAPTER 2

Effect of Ritonavir on ^{99m}Technetium-Mebrofenin Disposition in Humans: A Semi-PBPK Modeling and *In Vitro* Approach to Predict Transporter-Mediated DDIs

Introduction

Transport proteins present in clearance organs, specifically liver and kidney, are a well-recognized source of potential drug-drug interactions (DDIs)(1; 2). Inhibition of uptake and/or efflux transporters in the polarized cells of clearance organs may alter drug exposure in the organ, in the systemic circulation, or in both, leading to changes in efficacy and/or toxicity(3; 4). Changes in systemic exposure may be detected from the blood concentration-time curve, whereas organ exposure is more difficult to assess. However, assessing organ drug exposure is important in order to understand, in a comprehensive manner, the effects of altered transport function and identify the specific site(s) and magnitude of DDIs.

Scintigraphic imaging is a non-invasive technique that can be employed to determine organ exposure(5). ^{99m}Technetium (^{99m}Tc)-labeled compounds, coupled with gamma scintigraphy, have been used to estimate the hepatic exposure of drugs by assessing alterations in hepatic uptake and excretion(6; 7), and to evaluate the involvement of specific transport proteins(8; 9). Changes in systemic and organ exposure, as well as biliary excretion of ^{99m}Tc-labeled compounds, can be quantified using a previously validated method for bile collection, including a correction for gallbladder ejection fraction(10). An integrated approach incorporating pharmacokinetic modeling and simulation of clinical data (biliary excretion, systemic and organ exposure) can then guide *in vitro* investigations to elucidate sites and

This chapter has been published in *Clinical Pharmacology and Therapeutics: Pharmacometrics and Systems Pharmacology* (2: e20, 2013) and is presented in the style of that journal.

mechanisms of DDIs.

In vitro systems are commonly used to evaluate transporter function, and predict or confirm DDIs(11). Membrane vesicles prepared from transfected cell lines are useful to characterize substrate specificity and inhibitory potential of a given transport protein in isolation, although the relative contribution of individual transport proteins to overall hepatic uptake or excretion is difficult to elucidate using these artificial systems. A more representative, organ-specific, whole-cell system, such as sandwich-cultured hepatocytes (SCH), can be used to investigate the relative contribution of hepatic uptake and canalicular excretion processes to overall biliary clearance, and to estimate intracellular drug concentrations(11; 12).

^{99m}Tc-Mebrofenin (Choletec®), a metabolically stable iminodiacetic acid (IDA) analogue, is an imaging agent utilized in nuclear medicine to diagnose structural and functional disorders of the hepatobiliary network and gallbladder(13-15). The efficient vectorial transport of ^{99m}Tc-mebrofenin from blood into liver is mediated by the organic anion transporting polypeptides, OATP1B1 and OATP1B3(9; 16; 17); ^{99m}Tc-mebrofenin is preferentially excreted into bile unchanged by the canalicular efflux transporter multidrug resistance protein 2 (MRP2)(9; 16; 18). ^{99m}Tc-Mebrofenin also can be excreted from hepatocytes back into blood by MRP3(9). The important role of MRP2-mediated biliary excretion as the rate-limiting step for ^{99m}Tc-mebrofenin elimination *in vivo* is evidenced by increased and prolonged hepatic exposure of ^{99m}Tc-mebrofenin and other IDA analogues in preclinical species (TR$^-$ rats) and humans (Dubin-Johnson syndrome) with genetic impairment of Mrp2/MRP2(14; 18-21). Probe substrates to assess transport function *in vivo* are a highly sought-after clinical tool; ^{99m}Tc-mebrofenin has been proposed as a probe substrate for MRP2(11) but has yet to be tested in a clinical DDI study.

Ritonavir, an HIV protease inhibitor, is a typical component of anti-retroviral therapy. Ritonavir is administered as a "boosting" agent in combination with other protease inhibitors to exploit the inhibition of intestinal P-gp transport and metabolic enzymes, thereby increasing the bioavailability of anti-retroviral medications administered concomitantly(22; 23). Ritonavir is also a substrate and inhibitor of the biliary transporter MRP2(24; 25), with an IC_{50} reported as low as 50nM in teleost fish(26).

Consequently, we hypothesized that concomitant ritonavir administration would decrease the biliary excretion of ^{99m}Tc-mebrofenin, thereby increasing hepatic exposure. Ritonavir also has been reported to inhibit hepatic OATPs/Oatps, with an IC_{50} ranging from 0.25-2.5μM(27; 28). Therefore, at higher concentrations, ritonavir may inhibit ^{99m}Tc-mebrofenin hepatic uptake, thereby increasing systemic exposure.

These studies employed ^{99m}Tc-mebrofenin as a probe for transport-mediated hepatobiliary clearance, with and without ritonavir as a "perpetrator" of DDIs. The blood, liver and bile dataset was used to develop a semi-physiologically-based pharmacokinetic (semi-PBPK) model to describe ^{99m}Tc-mebrofenin disposition in humans, including clearance pathways mediated by transport proteins, and to elucidate potential site(s) and mechanism(s) of the ^{99m}Tc-mebrofenin-ritonavir DDI. *In vitro* studies were conducted using relevant model systems for hepatobiliary transport in humans to substantiate the results of pharmacokinetic modeling and simulation. We report a translational approach and suggested framework for the use of ^{99m}Tc-mebrofenin as a clinical probe to evaluate DDIs in hepatobiliary transport.

Results

Effect of ritonavir on ^{99m}Tc-mebrofenin disposition in human subjects

^{99m}Tc-Mebrofenin (mean ±SD) blood concentration-time curves are shown in Figure 2.1A, after administration of a 2.5mCi intravenous dose to 18 healthy volunteers either (a) alone (control; n=8), (b) 2h after a single, 200mg oral ritonavir dose (n=7), or (c) following 300mg oral ritonavir doses administered at 14 and 2h prior to ^{99m}Tc-mebrofenin (n=3). ^{99m}Tc-Mebrofenin blood concentrations declined rapidly, with prompt distribution into the liver, followed by a slower terminal elimination phase. Pharmacokinetic parameters resulting from noncompartmental analysis are summarized in Table 2.1; area under the ^{99m}Tc-mebrofenin blood concentration-time curve ($AUC_{blood,0-\infty}$) was significantly greater, by approximately two-fold, in subjects treated with 2x300mg ritonavir compared to control. Observed ritonavir plasma concentrations ranged from 236 to 16,100ng/mL (0.33 to 20μM; Table 2.1). Ritonavir concentrations in plasma (and bile) were significantly greater in subjects pre-treated with 2x300mg ritonavir compared to a single 200mg dose (Table 2.1).

Biliary recovery of ^{99m}Tc-mebrofenin was corrected for gallbladder ejection fraction (EF), with an EF ranging from 8 to 96% (Table 2.1). Biliary recovery was similar between treatment groups, at 75±12, 59±11 and 72±2% of the administered dose in control, 200mg and 2x300mg ritonavir groups, respectively (Table 2.1). Urinary recovery of ^{99m}Tc-mebrofenin (approximately 1% of the administered dose) was negligible and unaffected by ritonavir treatment.

Hepatic imaging of ^{99m}Tc-mebrofenin over 180min revealed rapid uptake by the liver (Figure 2.1B). The time of maximum liver concentration ($t_{max,liver}$) was 11±3, 11±4, and 10±1min in control, 200mg and 2x300mg ritonavir groups, respectively (Table 2.1). This agrees well with the reported value of 11min(14; 29). The elimination half-life based on hepatic time-activity curves from the current study, determined from 30-60min by nonlinear regression, was 19±5, 19±5 and 18±1min in control, 200mg and 2x300mg ritonavir groups, respectively (Table 2.1), compared to previous reports of ~15min(14; 29). Subjects greater than 20% of ideal body weight were excluded in the present study to minimize individual differences in body mass and composition, which could result in variable attenuation of the scintigraphic imaging data. Activity at liver t_{max} was 1950±252, 2003±274 and 1890±508 counts per second in control, 200mg and 2x300mg ritonavir groups, respectively (Figure 2.1B and Table 2.1). There was no apparent difference in ^{99m}Tc-mebrofenin overall liver exposure in the presence or absence of ritonavir based on the mean liver activity profiles.

The ^{99m}Tc-mebrofenin liver-to-blood ratio was calculated using blood sampling points and corresponding liver activity from scintigraphic imaging data (Figure 2.1C). The peak at 40min and subsequent decline suggested more complicated disposition than a mammillary two-compartment model representing blood and liver with constant first-order transfer rates as previously described(9; 14; 29).

Pharmacokinetic modeling

A semi-PBPK model was developed to describe ^{99m}Tc-mebrofenin activity in blood, liver and bile (Figure 2.2). The extrahepatic compartment in the semi-PBPK model represented a high-volume, slowly-perfused tissue(s), with an apparent permeability-limited uptake and egress. Parameters representing transport-mediated clearance mechanisms were obtained by fitting the model to data from the two

subjects with available individual attenuation-corrected liver scintigraphy data (Figure 2.2, Table 2.2; see Supplemental Materials for details). A separate model fit and parameter set were obtained for the mean control group data (biliary recovery, blood and liver concentrations) because the "representative" control subject for which attenuation-corrected data was obtained exhibited the highest biliary recovery of all values observed. Since liver data across all subjects was not corrected for attenuation, an attenuation correction factor was included as a parameter in the model and estimated to scale counts/sec data to activity in nCi/g liver (Table 2.2).

Sensitivity Analysis

Sensitivity analysis of parameter estimates on model output was conducted as described in Supplemental Material, with resulting changes in predicted blood and liver exposure and biliary excretion shown in Figure 2.3. Blood exposure was most sensitive to inhibition of hepatic uptake. However, impaired hepatic uptake also would be expected to decrease hepatic exposure and biliary excretion. No single parameter change explained the observed increase in ^{99m}Tc-mebrofenin blood exposure in the absence of changes in hepatic exposure or biliary excretion, indicating that a combination of factors was necessary to describe the effect of ritonavir. Hepatic exposure was particularly sensitive to impaired biliary clearance (hepatocyte-to-bile), which supports the conclusions from the clinical study that ritonavir did not significantly decrease ^{99m}Tc-mebrofenin biliary clearance. In contrast, the model was relatively insensitive to changes in efflux from tissue (hepatic or extrahepatic) back into blood.

Simulations

Simulations were conducted to explore various scenarios representing the potential impact of ritonavir on ^{99m}Tc-mebrofenin disposition. Decreased ^{99m}Tc-mebrofenin uptake and increased sinusoidal efflux only from the hepatic compartment (Figure 2.4, black dashed lines) adequately described blood and liver concentrations, but predicted a decrease in biliary excretion. This decrease was not observed in the clinical study. Decreased ^{99m}Tc-mebrofenin uptake and increased efflux back into blood from both the hepatic and extrahepatic compartments were required in simulations to describe the increase in ^{99m}Tc-

mebrofenin systemic exposure observed in the presence of 2x300 mg ritonavir, with minimal impact on hepatic exposure and biliary recovery (Figure 2.4, gray dashed lines).

In Vitro Studies

The effect of ritonavir on ATP-dependent uptake of ^{99m}Tc-mebrofenin by membrane vesicles prepared from human embryonic kidney cells (HEK293) transiently transfected with MRP2 was determined, as reported previously(9). Membrane vesicles were incubated for 3 min at 37°C with 50μCi/mL ^{99m}Tc-mebrofenin in the presence of ritonavir. Ritonavir 5 and 50μM inhibited ATP-dependent uptake of ^{99m}Tc-mebrofenin into MRP2-expressing HEK293 membrane vesicles by 32±15 and 60±2% of control, respectively (mean±SD in triplicate). By comparison, 50μM MK571, a prototypical MRP inhibitor, reduced ATP-dependent transport of ^{99m}Tc-mebrofenin by 88±2%(9).

The effect of ritonavir on ^{99m}Tc-mebrofenin accumulation and biliary excretion in human sandwich-cultured hepatocytes (SCH) was determined (Figure 2.5). Ritonavir inhibited ^{99m}Tc-mebrofenin accumulation in cells+bile and cells in a concentration-dependent manner (Figure 2.5A), with an IC_{50} of 3.46 ±1.53μM on total uptake (cells+bile), based on the extracellular dosing concentration. In contrast, ritonavir had no effect on the biliary excretion index (BEI) of ^{99m}Tc-mebrofenin in SCH, consistent with the clinical data and associated pharmacokinetic analysis suggesting that ritonavir did not affect ^{99m}Tc-mebrofenin biliary clearance. Intracellular ritonavir concentrations were estimated to facilitate comparison with membrane vesicle data. Hepatocellular accumulation of ritonavir during the 10-min uptake study in human SCH was 5-10 fold higher than the dosing concentration (Figure 2.5B), based on estimates of cellular volume reported previously(30). Based on total cellular accumulation of ritonavir (up to 100μM) in human SCH, and the estimated IC_{50} value (5-50μM) against MRP2-mediated ^{99m}Tc-mebrofenin transport determined in membrane vesicles, ritonavir would be expected to inhibit ^{99m}Tc-mebrofenin biliary excretion in SCH. However, ritonavir was extensively bound in lysates from human hepatocytes (f_u=0.024 ±0.006). Thus, correcting for the intracellular unbound concentration revealed that the effective cellular concentration of ritonavir was lower than the concentration necessary to significantly inhibit MRP2.

Discussion

This work highlights how *in vitro* and *in silico* approaches, including pharmacokinetic modeling and simulation, as well as transport studies conducted in relevant model systems, can be used to predict the site(s) and potential impact of hepatic transporter-mediated DDIs in humans *in vivo*. Furthermore, this clinical study demonstrates the utility of ^{99m}Tc-mebrofenin as a model organic anion to evaluate DDIs in transporter-mediated hepatobiliary clearance. To our knowledge, this is the first study that utilizes liver scintigraphy data to evaluate a hepatic DDI, and incorporates blood, bile and urine data in humans to develop a comprehensive pharmacokinetic model describing ^{99m}Tc-mebrofenin disposition.

Previously published data involving administration of ^{99m}Tc-mebrofenin (and other IDA derivatives) in humans or animals focused on the time-activity data in blood and liver up to 60min(14; 31-34). A two-compartment model representing blood and liver reasonably approximated 0-60min time-activity data in these studies(31; 32). However, extending the time course of blood and liver observations to 180min clearly demonstrates more complex pharmacokinetic behaviour; the statistically-significant, two-fold increase in ^{99m}Tc-mebrofenin systemic exposure without accompanying changes in hepatic exposure or biliary recovery observed following ritonavir administration (2x300mg) is not consistent with a 2-compartment model. ^{99m}Tc-Mebrofenin did not accumulate in extrahepatic tissues within the gamma camera field-of-view, yet the liver-to-blood ratio and incomplete recovery of total activity in urine and bile suggested an extrahepatic component to ^{99m}Tc-mebrofenin disposition. Therefore, a modeling and simulation approach was undertaken to describe ^{99m}Tc-mebrofenin disposition and elucidate the probable sites of the ^{99m}Tc-mebrofenin-ritonavir interaction.

^{99m}Tc-Mebrofenin rapidly and extensively distributed to the liver. The ^{99m}Tc-mebrofenin hepatic extraction ratio was 0.80±0.16 [(mean±SD), range 0.55-1] in control subjects, based on the observed clearance from noncompartmental analysis (Cl_{total}/Q_h; Table 2.1). In contrast to previous reports estimating-hepatic extraction at nearly 100% (29), this suggests that ^{99m}Tc-mebrofenin hepatic clearance would be susceptible to changes in hepatic uptake. This is consistent with the observed changes in ^{99m}Tc-

mebrofenin disposition following ritonavir administration, which resulted from inhibition of uptake into both hepatic and extrahepatic sites of distribution.

Total plasma concentrations of ritonavir, measured at the beginning and end of the 3-h study period (2 and 5h following ritonavir administration) ranged from 236 to 16,100ng/mL (0.33 to 20μM). Intestinal absorption of ritonavir was estimated to contribute ~12,000 and 18,000ng/mL (17 and 25μM) to the incoming portal blood for the 200 and 300mg doses, respectively, using the previously reported approach ($k_a \bullet Dose \bullet F_a/Q_h$, where k_a represents the absorption rate constant and F_a represents the fraction absorbed)(35). The maximum estimated portal vein concentration (up to 45μM) exceeded the IC_{50} for ^{99m}Tc-mebrofenin uptake in human SCH (~3.5μM). Even though ritonavir is highly protein bound (plasma $f_u \cong 0.01$), unbound concentrations were predicted to be in the range of concentrations expected to inhibit hepatic uptake. Human SCH data, correlated well with the clinical data and pharmacokinetic modeling indicating that ritonavir inhibited ^{99m}Tc-mebrofenin hepatic uptake, with no effects on biliary excretion. The present study suggests that ritonavir may inhibit the hepatic uptake of other OATP substrates resulting in increased systemic exposure, similar to previous reports (25; 28; 36). The magnitude of this increase and altered exposure in hepatic and extrahepatic tissues will depend on the substrate- and tissue-specific involvement of transport-mediated distribution and clearance, and the effect of ritonavir on these processes. In addition to inhibition of uptake, parameter estimates (Table 2.2) suggest enhanced hepatic basolateral efflux ($PS_{eff,h}$) , which may be explained by increased basolateral transporter expression (e.g. MRP3 or MRP4) and/or increased unbound fraction of ^{99m}Tc-mebrofenin in the liver.

Good agreement was found between observed CL_{total} of ^{99m}Tc-mebrofenin (15.9±3.2 mL/min/kg in control group, Table 2.1) and predicted CL_{uptake} based on *in vitro* uptake in human SCH (10.6±3.1 mL/min/kg, Supplemental Material). Similarly, predicted $CL_{biliary}$, based on data obtained in human SCH, was 4.4±1.5 mL/min/kg, compared to the observed $CL_{biliary}$ of 12.5±2.5 mL/min/kg in control subjects. The *in vitro* intrinsic CL_{uptake} was ~50-fold lower than the corresponding value (PS_{inf}) estimated by the semi-PBPK model, which agrees well with reported scaling factors for hepatic uptake clearance in SCH

(37-39). It should be noted that the *in vitro* CL_{uptake} of ^{99m}Tc-mebrofenin in human SCH, along with the calculated IC_{50} value of ritonavir on ^{99m}Tc-mebrofenin accumulation, represents the net effect of all sinusoidal uptake and efflux transporters [e.g., at least OATP1B1, OATP1B3 and MRP3(9; 17)] involved in the hepatocellular disposition of ^{99m}Tc-mebrofenin.

Impaired function of MRP2 in humans and Mrp2 in preclinical species has been reported to delay elimination of ^{99m}Tc-mebrofenin and other IDA derivatives from the liver, with a significant increase in hepatic exposure and time to half-maximal concentration(14; 18-21). Sensitivity analysis and simulations using data from the current study also confirmed that hepatic exposure was highly sensitive to biliary clearance; even modest (2-fold) changes in this parameter should have an apparent effect on the slope of the liver time-activity curves. These data imply that ^{99m}Tc-mebrofenin clearance from liver to bile in the current study was not influenced significantly by ritonavir, even though ritonavir is an MRP2 inhibitor. Previous reports of Mrp2/MRP2 inhibition by ritonavir utilizing a non-mammalian model system [killifish isolated proximal tubules(26)] and mammalian systems (rat and human SCH), confirmed species- and substrate-specific interaction potential(25). Studies in human SCH, coupled with MRP2 membrane vesicles and ritonavir binding to human hepatocyte lysates, corroborate the lack of effect of ritonavir on ^{99m}Tc-mebrofenin biliary excretion observed in the clinical study, suggesting that the reported approach using complementary *in vitro* systems is useful to predict transporter-mediated DDIs in biliary excretion. Although total ritonavir accumulation in SCH exceeded the estimated IC_{50} for ^{99m}Tc-mebrofenin transport into MRP2-expressing membrane vesicles, extensive hepatic binding explains why intracellular ritonavir concentrations were insufficient to inhibit ^{99m}Tc-mebrofenin excretion into bile in humans. These findings demonstrate the importance of correcting for the intracellular unbound concentration when translating between isolated expression systems and whole cell models or *in vivo* intracellular targets. This study also emphasizes the importance of using appropriate *in vitro* systems and specific substrate-inhibitor combinations to accurately assess DDI potential.

In the present study, decreased hepatic uptake of ^{99m}Tc-mebrofenin in the presence of ritonavir led to increased systemic exposure but did not result in altered hepatic exposure or biliary excretion. These

findings are counter-intuitive until one considers the effect of ^{99m}Tc-mebrofenin extrahepatic distribution, which also is subject to alteration by ritonavir, based on the modeling and simulation results. Inhibition of ^{99m}Tc-mebrofenin uptake in both hepatic and extrahepatic sites of distribution would collectively increase systemic exposure such that decreased uptake would yield little net change in tissue exposure ($dX_{tissue}/dt=C_{systemic}\bullet CL_{uptake}$). This concept recently was demonstrated for metformin in the setting of impaired transport function in liver and kidney(40). The extrahepatic distribution of ^{99m}Tc-mebrofenin is not surprising; semi- or whole-body PBPK models have been applied to a number of large and/or anionic drugs(41-44). An outstanding question from this clinical study is the identity of the extrahepatic site(s) of ^{99m}Tc-mebrofenin distribution, accounting for ~10-40% of the administered dose at 180min. Observed ^{99m}Tc-mebrofenin activity was confined to the liver and gallbladder regions during the scintigraphic imaging, thereby excluding other tissues within the gamma camera field-of-view, which included the bulk of the torso and resident organ systems, as potential distribution sites. Human skeletal muscle expresses transport proteins that have been implicated in drug distribution and toxicity(45; 46). Further studies are required to confirm the identity of other tissue(s) involved in the extrahepatic distribution of ^{99m}Tc-mebrofenin.

The availability of quantitative (attenuation corrected) scintigraphy data in humans marks a major advance in the use of imaging agents to assess organ/tissue exposure. Although the methods have existed for many years, they are under-utilized and provide a rich data set that is ideal for pharmacokinetic modeling. The present clinical study has further characterized ^{99m}Tc-mebrofenin as a clinical probe of transporter-mediated hepatobiliary clearance, and demonstrated the need to quantify ^{99m}Tc-mebrofenin in blood and urine beyond 180min to further characterize the terminal elimination phase. A semi-PBPK modeling and *in vitro* systems approach elucidated unforeseen mechanisms underlying a transporter-mediated DDI at both hepatic and extrahepatic sites of ^{99m}Tc-mebrofenin distribution. *In vitro* studies confirmed the conclusions from modeling and simulation that ritonavir inhibited ^{99m}Tc-mebrofenin hepatic uptake, but not biliary excretion, at clinically relevant concentrations. This complimentary set of *in vivo* and *in vitro* studies demonstrates that reliable predictions of transporter-mediated hepatic DDIs

can be achieved when data from appropriate *in vitro* models (*e.g.,*-assessment of inhibitory potential in relevant systems; biliary excretion assessed in SCH) are integrated with knowledge regarding drug disposition (*e.g.,* hepatic and extrahepatic distribution; plasma and intracellular binding) utilizing a quantitative systems approach.

Methods

Clinical Protocol

A randomized, open-label, two arm, parallel study, approved by the University of North Carolina Institutional Review Board (IRB), was conducted in the Clinical and Translational Research Center. Written informed consent was obtained from all subjects prior to enrollment. Healthy male and female subjects (19-29yrs of age), within 20% of ideal body weight (51-91kg), were admitted to the CTRC the evening before the procedure (see Supplemental Materials for detailed demographic information).

A customized oroenteric tube was positioned in the upper small intestine, using the protocol described previously(10). Following tube placement, the balloon was inflated with 20mL of air, and then subjects were positioned under a gamma camera in the supine position. A 2.5mCi intravenous bolus dose of ^{99m}Tc-mebrofenin was administered via an indwelling catheter placed in a forearm vein; subjects randomized to the ritonavir-treated group also swallowed two 100mg capsules of ritonavir before placement of the oroenteric tube, which occurred approximately 2hr prior to ^{99m}Tc-mebrofenin administration. Blood samples were collected from a catheter placed in the arm opposite of ^{99m}Tc-mebrofenin administration at baseline, and at designated time points up to 180min after administration of the ^{99m}Tc-mebrofenin dose. Biliary secretions were aspirated continuously via the oroenteric catheter and pooled over predetermined intervals throughout the study. Urine was collected at baseline and pooled over 180min. Anterior and posterior scintigraphic images of the abdomen were acquired dynamically in the ^{99m}Tc window (140KeV ±15%) at 1-min intervals using a dual headed gamma camera. Two hours after ^{99m}Tc-mebrofenin administration, 0.02µg/kg cholecystokinin octapeptide (CCK-8, Kinevac®) was administered as a 30-min intravenous infusion. The gallbladder ejection fraction (EF) was calculated from the abdominal scintigraphy images and total biliary recovery of ^{99m}Tc-mebrofenin was corrected for

EF to minimize inter-subject variability associated with gallbladder response to CCK-8 as described previously(10). Blood, bile and urine samples were analyzed for ^{99m}Tc-mebrofenin radioactivity with a sodium iodide well counter, and corrected for decay (^{99m}Tc $t_{1/2}$=6.01 hr). Bile samples associated with bulk gallbladder emptying following CCK-8 administration at 120min, as well as plasma samples at 0 and 180min (approximately 120 and 300min post ritonavir dose) were analyzed for ritonavir by HPLC or LC-MS/MS as described previously(47; 48). ^{99m}Tc-Mebrofenin activity was determined in counts/min (CPM) from the geometric mean of the anterior and posterior scintigraphic images, thereby normalizing for the abdominal thickness of the individual subject. Liver time-activity curves were generated by scaling activity in a region of interest (ROI) over the right upper quadrant to activity in the whole liver based on the initial uptake phase, thereby excluding gallbladder interference from the 0-180min liver activity curve.

Protocol Modifications

Upon approval by the UNC IRB, the clinical protocol was modified to include an increased dose of ritonavir: 300mg (three, 100mg capsules) upon admission and before oroenteric tube placement (approximately 14 and 2hr, respectively, prior to ^{99m}Tc-mebrofenin administration). The 2x300mg ritonavir regimen was intended to increase plasma ritonavir concentrations to a steady-state and reduce inter-subject variability observed in the group of subjects treated with the single 200mg dose regimen. In addition, a transmission-emission acquisition was performed before injection of ^{99m}Tc-mebrofenin for the final control and ritonavir-treated subjects using a cobalt-57 flood source to determine the effect of photon attenuation, as described in Supplemental Materials.

Pharmacokinetic Analysis

The area under the blood concentration-time curve (AUC) for ^{99m}Tc-mebrofenin was determined by noncompartmental analysis using WinNonlin Phoenix, v6.1 (St. Louis, MO). $AUC_{0\text{-}180\ min}$ and $AUC_{0\text{-}\infty}$ were calculated using the linear trapezoidal rule; extrapolation to infinity was determined by the slope from linear regression of the last 3-6 time points.

A semi-PBPK model was developed to describe ^{99m}Tc-mebrofenin distribution and elimination (Figure 2.2), consisting of a central (blood) compartment, 5-compartment liver representing the "dispersion" model of hepatic elimination, and extrahepatic tissue compartment. Transfer between blood and tissue was denoted by transport-mediated clearance processes; passive diffusion was assumed to be negligible, based on data reported previously from *in vitro* systems(9; 17). Differential equations describing the disposition of ^{99m}Tc-mebrofenin and the modeling procedures are detailed in Supplemental Materials.

In Vitro Studies

Hepatocytes were purchased from Celsis In Vitro Technologies (Baltimore, MD) or kindly provided by Life Technologies (Research Triangle Park, NC), and Triangle Research Labs (Research Triangle Park, NC) and plated on 24-well Biocoat™ plates and overlaid with Matrigel™ as described previously(12). Hepatocyte donors consisted of two Caucasians and one African-American, ranging from 46-59yrs of age, and BMI from 25.6-29.8kg/m^2. Cell cultures were maintained and accumulation studies were conducted in SCH with 0.5μCi/mL ^{99m}Tc-mebrofenin in the presence or absence of ritonavir, as described previously(12), and further detailed in Supplemental Material.

Membrane vesicles were prepared from MRP2 over-expressing HEK293 cells and transport assays were carried out by a rapid filtration method as described previously(9; 49).

Human hepatocytes from two donors were used to determine the extent of ritonavir binding to cellular components by equilibrium dialysis as described previously(50). Pellets containing ten million hepatocytes were diluted in 10 volumes of phosphate buffer and homogenized by probe sonication. Ritonavir was added to a concentration of 1μM, and aliquots (n=3) were loaded into a 96-well equilibrium dialysis apparatus (HTDialysis, LLC; Gales Ferry, CT) and dialyzed against phosphate buffer for 6h with shaking at 37°C. Ritonavir was quantitated by LC-MS/MS, and the unbound fraction was corrected for dilution as described previously(50):

$$\text{Undiluted fu} = \frac{1/D}{\left(\left(1/\text{fu}_{\text{measured}}\right) - 1\right) + 1/D}$$

Where D is the dilution factor.

Statistical Analysis

Statistically significant differences in pharmacokinetic parameters across all three treatment groups were assessed by ANOVA on ranks, adjusted using Dunnett's multiple comparisons test. Comparison of ritonavir concentrations between the two ritonavir-treated groups was performed using Wilcoxon Rank Sum. The criterion for significance in all cases was $p<0.05$.

Study Highlights

Evaluation of altered intracellular drug concentrations due to hepatic transporter-mediated DDIs is limited due to lack of probes and methodology to assess hepatic exposure and hepatobiliary transport function in humans. This novel approach utilized the hepatobiliary imaging agent ^{99m}Tc-mebrofenin as a probe to evaluate clinical DDIs in hepatic transport. Modeling/simulation evaluated sites/mechanisms of the ^{99m}Tc-mebrofenin-ritonavir DDI. Quantitative scintigraphy data using imaging agents to assess tissue exposure provided a rich dataset for modeling, which revealed a novel ^{99m}Tc-mebrofenin extrahepatic distribution compartment. Semi-PBPK simulations emphasized the impact of extrahepatic ^{99m}Tc-mebrofenin distribution and transporter-mediated DDIs on systemic and tissue exposure. *In vitro* data substantiated *in vivo* effects and modeling conclusions. This work emphasized modeling, assessment of inhibitory potential in relevant *in vitro* systems, and intracellular unbound concentrations to predict complex hepatic DDIs. We report a translational approach and suggested framework for use of ^{99m}Tc-mebrofenin as a clinical probe to evaluate hepatobiliary transport DDIs.

Figure 2.1. ^{99m}Tc-Mebrofenin (A) blood concentration versus time curves; (B) liver scintigraphy versus time curves by treatment group (gray shaded area represents mean ±SD of control); (C) liver-to-plasma ratio versus time curves; mean data by treatment group. Data are presented as group means [±SD in (A) and (B)]; gray = control group, open/dashed = 200mg ritonavir group, closed/solid = 2x300mg ritonavir group.

A.

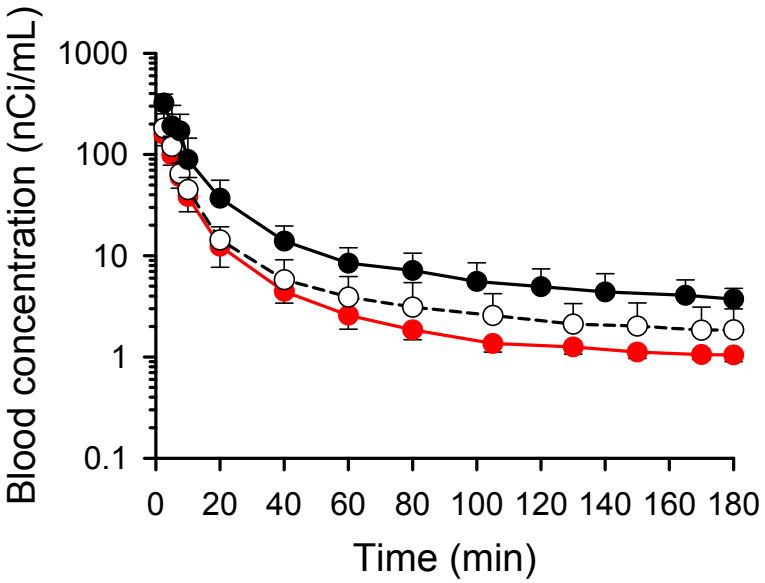

B.

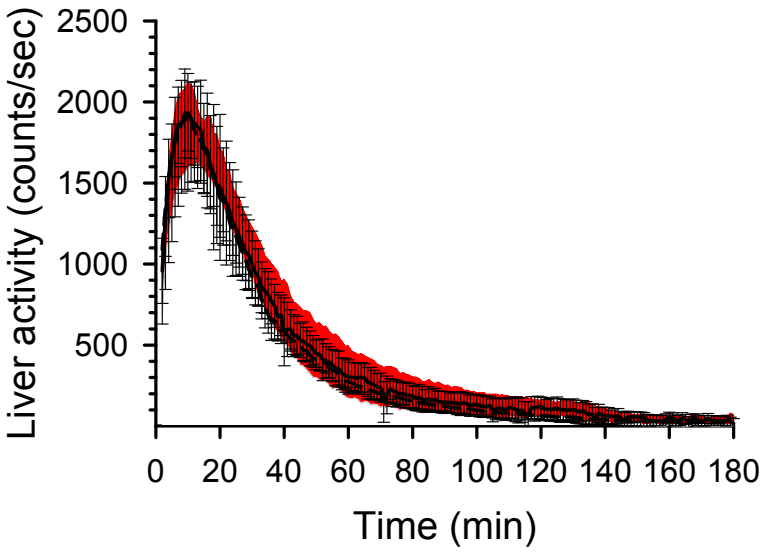

C.

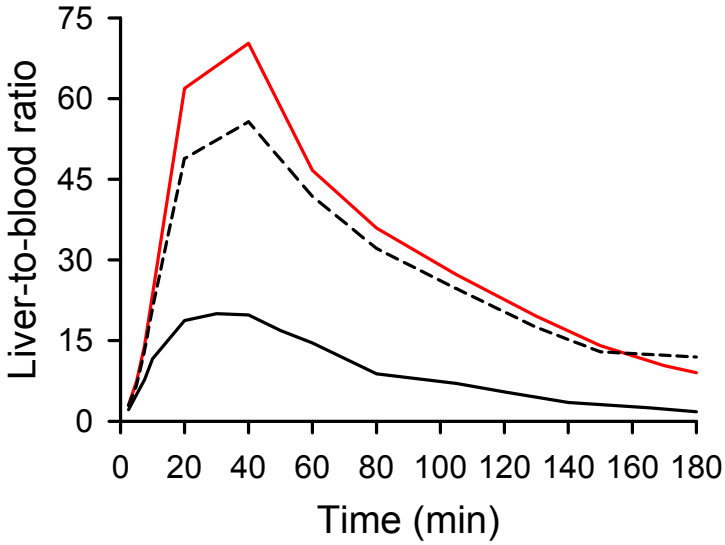
Liver-to-blood ratio
75
60
45
30
15
0
0
20
40
60
80
100
120
140
160
180
Time (min)

Figure 2.2. Semi-PBPK model scheme (A) representing ^{99m}Tc-mebrofenin disposition in humans [Q denotes blood flow (mL/min), subscripts represent tissue or vascular compartments, as follows: liver (h), bile (bile), extrahepatic ("other") tissue (o); clearance values are designated as CL_{uptake} for influx from blood into tissue, CL_{efflux} for efflux from tissue to blood, and $CL_{biliary}$ for excretion from liver into bile]. Simulations based on the semi-PBPK model and observed blood, liver and bile curves for ^{99m}Tc-mebrofenin in subjects with quantitative scintigraphy data for (B) subject 8 (control), and (C) subject 17 (2x300mg ritonavir). Circles represent observed blood samples, solid lines represent simulated blood concentrations, + symbols represent observed liver concentrations from attenuation-corrected (quantitative) scintigraphy data of the liver ROI, dashed lines represent simulated liver concentrations, squares represent observed mass recovered in bile (corrected for gallbladder ejection fraction), and dotted lines represent simulated biliary excretion data.

A.

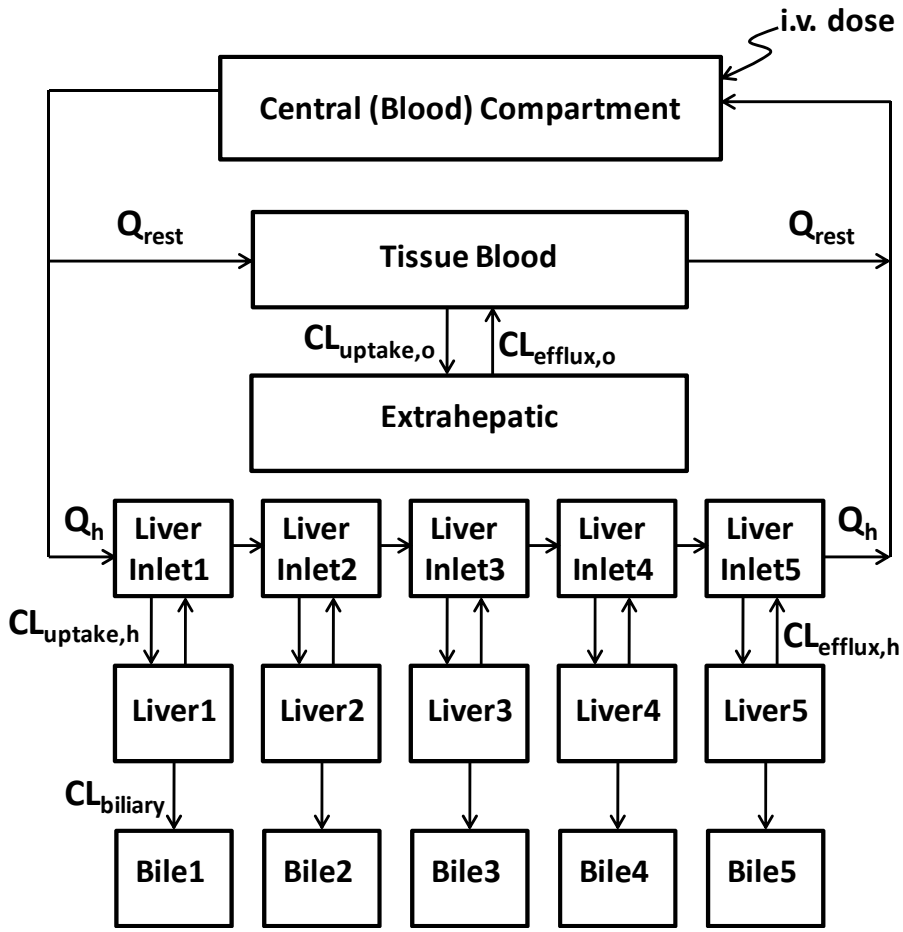

B.

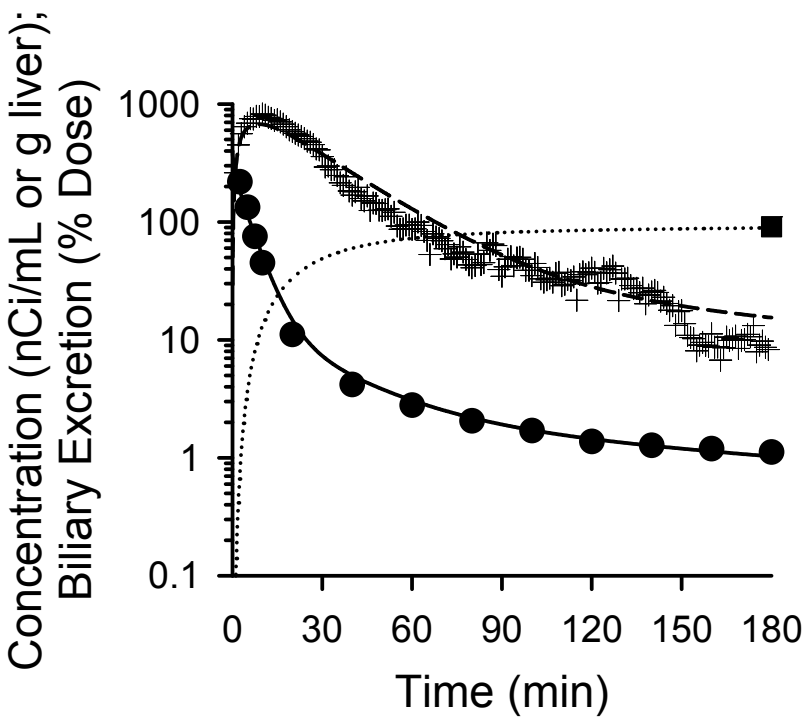
Concentration (nCi/mL or g liver);
Biliary Excretion (% Dose)
1000
100
10
1
0.1
0
30
60
90
120
150
180
Time (min)

C.

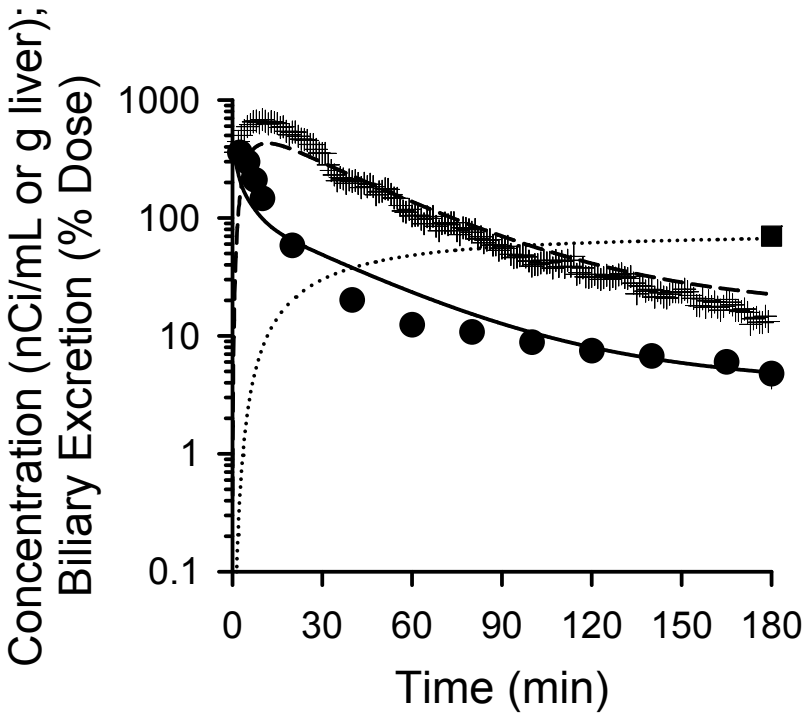
Concentration (nCi/mL or g liver);
Biliary Excretion (% Dose)
1000
100
10
1
0.1
0
30
60
90
120
150
180
Time (min)

Figure 2.3. Sensitivity analysis of parameter estimates determined from the semi-PBPK model (Figure 2.2; Table 2.2). Parameters were altered 10-fold in either direction of the values estimated for mean control data (Table 2.2), and the fold-change in the predicted study endpoints [^{99m}Tc-mebrofenin central compartment (blood) exposure, hepatic exposure, and biliary excretion] were examined. Solid lines represent influx clearance (CL_{uptake}) from blood into tissue, dashed lines represent efflux clearance (CL_{efflux}) from tissue to blood, and gray lines represent biliary excretion from liver into bile ($CL_{biliary}$).

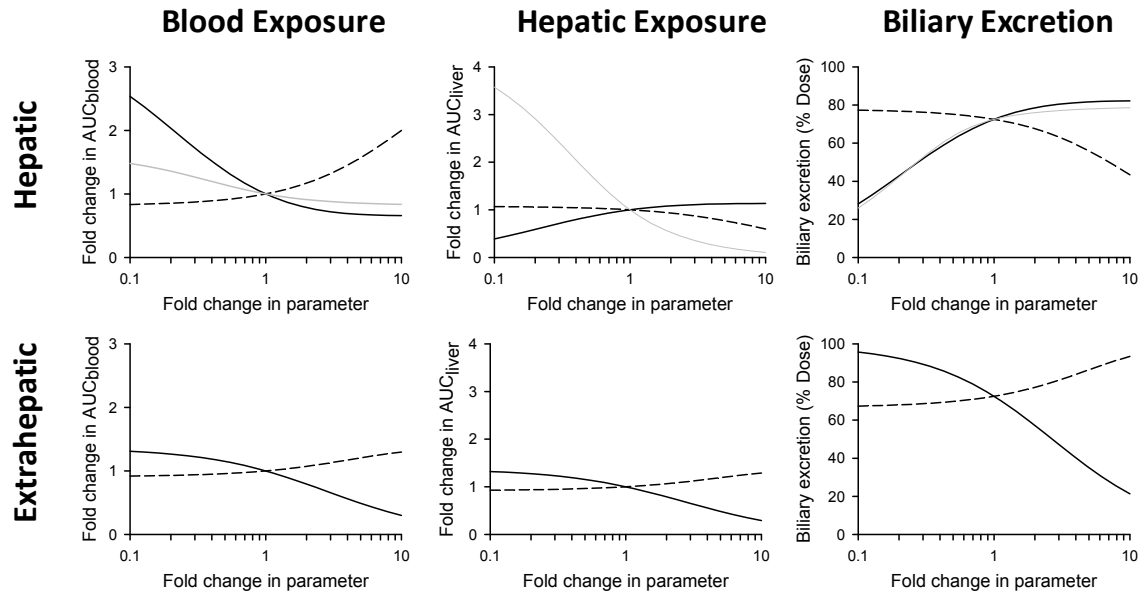

Figure 2.4. Simulations based on the ^{99m}Tc-mebrofenin semi-PBPK model scheme (Figure 2.2) for ^{99m}Tc-mebrofenin (A) blood and (B) liver concentration-time data, and (C) cumulative % dose excreted in bile resulting from parameters describing mean control data (Table 2.2) and the following changes in transport-mediated processes, alone and in combination. Mean control data (red); 1/3 $CL_{uptake,h}$ + 3x $CL_{efflux,h}$ (blue); 1/2 $CL_{uptake,h}$ and $CL_{uptake,o}$ + 2x $CL_{efflux,h}$ and $CL_{efflux,o}$ (dashed black); 1/2 $CL_{biliary}$ (solid black); mean control data without extrahepatic compartment (gray).

A.

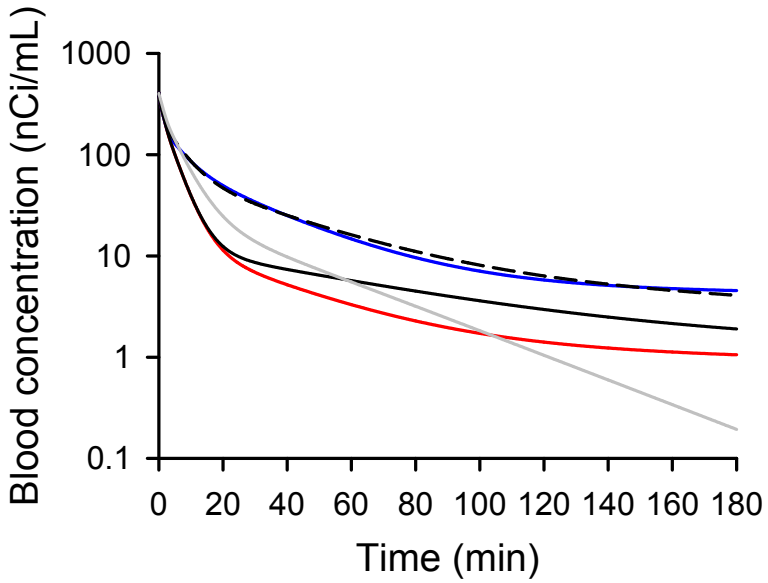

B.

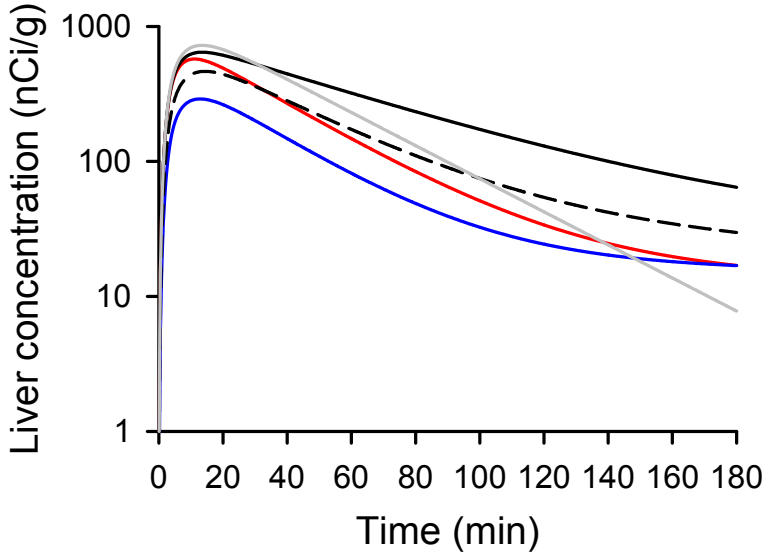

C.

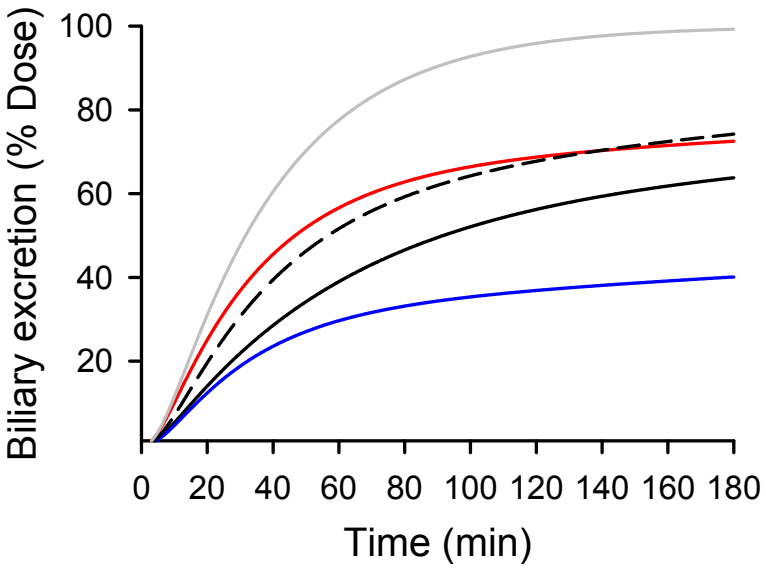
Biliary excretion (% Dose)
100
80
60
40
20
0
20
40
60
80
100
120
140
160
180
Time (min)

Figure 2.5. Human sandwich-cultured hepatocytes (SCH) were incubated for 10min at 37°C with 0.5μCi/mL ^{99m}Tc-mebrofenin in standard (cells+bile) or Ca^{+}-free (cells) HBSS (B-CLEAR®) alone and with various concentrations of ritonavir in SCH from 3 separate donors, in triplicate. (A) ^{99m}Tc-Mebrofenin accumulation and biliary excretion index (BEI) in cells+bile (closed bars) and cells (open bars) in the presence of increasing concentrations of extracellular ritonavir. ^{99m}Tc-Mebrofenin BEI values (above the bars) represent mean data. (B) Ritonavir accumulation in hepatocytes (Ca^{2+}-free HBSS) when co-administered with ^{99m}Tc-mebrofenin, represented as intracellular total concentration ($C_{cell,total}$), as described in Methods. ^{99m}Tc-Mebrofenin and ritonavir accumulation data are represented as mean±S.E.M. of 3 separate donors in triplicate (5μM data are mean±range of 2 donors, in triplicate).

A.

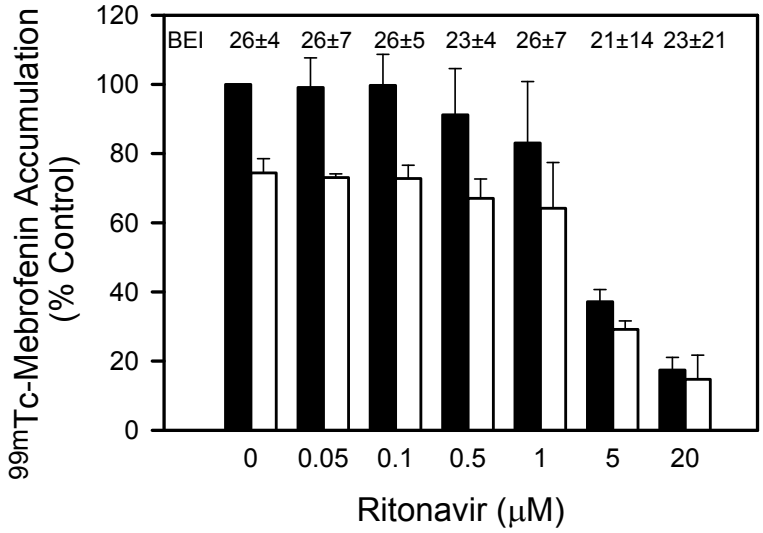

B.

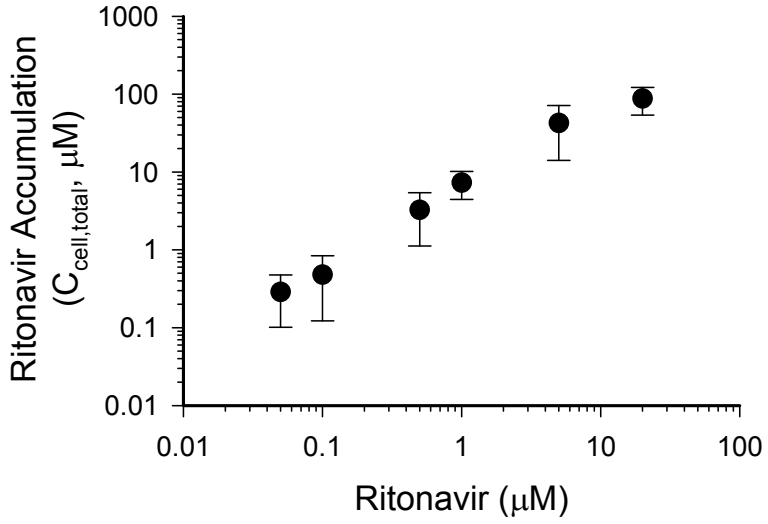
Ritonavir Accumulation
($C_{cell,total}$, μM)
1000
100
10
1
0.1
0.01
0.01
0.1
1
10
100
Ritonavir (μM)

Table 2.1. Pharmacokinetics of ^{99m}Tc-mebrofenin in control and ritonavir pre-treated subjects. All parameters refer to ^{99m}Tc-mebrofenin, except as noted; data are expressed as geometric mean (mean±SD).

	^{99m}Tc-Mebrofenin alone								
	1	*2*	*3*	*4*	*5*	*6*	*7*	*8*	*GeoMean (Mean ±SD)*
Administered Dose (μCi)	2432	2279	2427	2372	2498	2245	2226	2719	2395 (2400 ±162)
Ejection Fraction	0.67	0.78	0.94	0.54	0.86	0.88	0.96	0.54	0.75 (0.77 ±0.17)
Biliary Recovery (% Dose)	62	63	80	59	80	87	76	91	74 (75 ±12)
Urinary Recovery (% Dose)	0.9	0.8	1.0	0.7	0.3	0.0	0.0	0.7	NE (0.56 ±0.41)
$AUC_{0\text{-}180}$ (nCi·min/mL)	1314	1806	1893	1726	1765	2182	1429	2190	1763 (1788 ±313)
$AUC_{0\text{-}\infty}$ (nCi·min/mL)	1473	2044	2022	1928	2071	2294	1576	2356	1948 (1970 ±311)
Cl_{total} (mL/min/kg)	18.6	18.9	13.9	15.0	15.4	10.9	20.7	14.1	15.6 (15.9 ±3.2)
$Cl_{biliary}$ (mL/min/kg)	12.8	13.4	11.8	9.93	14.3	9.87	17.4	13.8	12.7 (12.5 ±2.5)
$t_{max,liver}$ (min)	13	10	11	11	10	17	10	9	11 (11 ±3)
$t_{1/2,liver,30\text{-}60min}$ (min)	23	13	18	20	17	30	15	16	18 (19 ±5)
$X_{max,liver}$ (counts/sec)	1744	2432	1822	1926	1836	1698	1912	2227	1936 (1950 ±252)
$C_{plasma,0min}$ RTV (ng/mL)	-	-	-	-	-	-	-	-	-
$C_{plasma,180min}$ RTV (ng/mL)	-	-	-	-	-	-	-	-	-
$C_{bile,120\text{-}140min}$ RTV (ng/mL)	-	-	-	-	-	-	-	-	-

NE, not estimable; * p <0.05 compared to control, adjusted; † p <0.05, 200 mg vs. 2x300 mg ritonavir

			200 mg Ritonavir						*2x300 mg Ritonavir*		
9	*10*	*11*	*12*	*13*	*14*	*15*	*GeoMean (Mean ±SD)*	*16*	*17*	*18*	*GeoMean (Mean ±SD)*
2317	2542	2450	2331	2404	2453	2484	2425 (2426 ±81)	2472	2543	2369	2460 (2461 ±87)
0.80	0.20	0.94	0.75	0.72	0.72	0.89	0.66 (0.72 ±0.24)	0.61	0.08	0.90	0.35 (0.53 ±0.42)
40	53	62	63	75	62	56	58 (59 ±11)	74	70	73	72 (72 ±2)
1.0	0.6	0.5	1.5	0.9	0.8	3.3	1.0 (1.2 ±1.0)	1.0	1.0	1.5	1.1 (1.2 ±0.3)
1611	3704	1545	2419	1529	3447	2728	2280 (2426 ±914)	3516	5844	2247	3587 (3869 ±1825)
1847	3947	1714	2662	1724	4189	3226	2587 (2759 ±1055)	4090	6483	2819	4212* (4464 ±1861)
13.8	8.62	20.6	17.3	17.8	8.41	13.3	13.6 (14.3 ±4.6)	11.0	5.10	12.3	8.83 (9.46 ±3.8)
6.30	4.83	14.3	12.0	15.1	6.30	8.86	8.89 (9.67 ±4.1)	9.52	3.93	11.2	7.49 (8.23 ±3.8)
9	10	20	8	12	10	9	11 (11 ±4)	9	11	9	10 (10 ±1)
30	21	13	17	15	22	18	19 (19 ±5)	18	20	17	18 (18 ±1)
1633	2145	2379	2195	2005	1663	1998	1986 (2003 ±274)	2473	1548	1648	1848 (1890 ±508)
837	1095	666	3338	`954	4234	265	1150 (1740 ±1630)	6670	12100	6200	7940† (8320 ±3280)
810	1361	475	1823	`469	4343	236	996 (1510 ±1500)	4910	16100	3950	6780 (8320 ±6760)
1858	2466	728	2232	1345	2319	1381	1640 (1760 ±640)	18300	13700	33200	20300† (21700 ±10200)

Table 2.2. Parameter estimates derived from the ^{99m}Tc-mebrofenin semi-PBPK model based on the scheme depicted in Figure 2.2A.

Parameter*	Subject 8 (Control)	Subject 17 (2x300 mg Ritonavir)	Mean Data (Control Subjects)
$CL_{uptake,h}$	91	49	88
$CL_{efflux,h}$	1.2	7.4	1.7
$CL_{biliary}$	3.3	2.5	2.2
$CL_{uptake,o}$	9.4	7.0	15
$CL_{efflux,o}$	6.7	3.0	2.3
ACF†	9.1‡	9.8‡	10.6

*Clearance values (L/min) are designated as CL_{uptake} for influx from blood into tissue, CL_{efflux} for efflux from tissue to blood, and $CL_{biliary}$ for excretion from liver to bile.

†ACF = Attenuation Correction Factor; ‡mean value over 180-min study period.

Supplemental Material

Materials and Methods

Attenuation Correction

A transmission-emission acquisition was performed before injection of ^{99m}Tc-mebrofenin for the final control and ritonavir-treated subjects using a cobalt-57 flood source (Isotope Products Laboratories, Burbank, CA) positioned posteriorly, and gamma rays were detected in the cobalt window (122KeV±15%) for 10min on the anterior detector in the absence and presence of the subject. A subject-specific correction matrix was obtained as the quotient of the two-dimensional transmission-emission acquisition of the cobalt-57 flood source without (I_o) and with the subject (I), as described previously (51; 52). The geometric mean of the anterior and posterior ^{99m}Tc-mebrofenin gamma scintigraphy images was multiplied by the subject-specific correction matrix. Time-activity curves (in counts per second) were generated for the liver (excluding the gall bladder) using Syngo MI applications version 6.5.9.19 (Siemens, New York, NY). The generated time-activity curves were converted from CPM to μCi ^{99m}Technetium using a factor of 854 CPM/μCi based on standards and pilot experiments with an anthropomorphic torso phantom^{TM} (Data Spectrum Corporation, Hillsborough, NC).

Semi-PBPK Model Development

A semi-PBPK model was developed to describe the distribution and elimination of ^{99m}Tc-mebrofenin (Figure 2.2). This model consisted of a central compartment describing the blood concentration-time curve after an intravenous bolus dose, as well as hepatic and extrahepatic tissue compartments linked to the central compartment by blood flow and a tissue-specific vascular space. Transfer between blood and tissue, as well as biliary excretion, were denoted by clearance parameters representing transport-mediated processes. Passive diffusion was assumed to be negligible, based on data reported previously from *in vitro* systems(9, 17). The following differential equations described ^{99m}Tc-mebrofenin disposition:

$$dX_b/dt = Q_h \bullet [X_{i,5}/(V_i/5)] + Q_o \bullet (X_{b,o}/V_{b.o}) - (X_b/V_b) \bullet (Q_h+Q_o) \qquad X_b° = dose$$

$$dX_{i1}/dt = Q_h \bullet (X_b/V_b) + f_h \bullet (CL_{efflux,h}/5) \bullet [X_{h1}/(V_h/5)] - Q_h \bullet (X_i/V_i) - f_b \bullet (CL_{uptake,h} \bullet /5) \bullet (X_i/V_i)$$

$$dX_{i,n}/dt = Q_h \bullet [X_{i,n-1}/(V_i/5)] + f_h \bullet (CL_{efflux,h}/5) \bullet [X_{h,1}/(V_h/5)] - [X_{i,n}/(V_i/5)] \bullet [Q_h + f_b \bullet (CL_{uptake,h} \bullet /5)]$$

$$dX_{h,n}/dt = f_b \bullet [X_{i,n}/(V_i/5)] \bullet (CL_{uptake,h}/5) - f_h \bullet [X_{h,n}/(V_h/5)] \bullet [(CL_{efflux,h}/5)+(CL_{biliary}/5)]$$

$$dX_{bile,n}/dt = f_h \bullet [X_{h,n}/(V_h/5)] \bullet (CL_{biliary}/5)$$

$$dX_{b,o}/dt = Q_o \bullet (X_b/V_b) + CL_{efflux,o} \bullet f_o \bullet (X_o/V_o) - Q_o \bullet (X_{b,o}/V_{b.o}) - CL_{uptake,o} \bullet f_b \bullet (X_{b,o}/V_{b.o})$$

$$dX_o/dt = CL_{uptake,o} \bullet f_b \bullet (X_{b,o}/V_{b.o}) - CL_{efflux,o} \bullet f_o \bullet (X_o/V_o)$$

Where Q denotes blood flow (mL/min), V represents tissue volume (mL), X and f the mass (nCi) and unbound fraction of ^{99m}Tc-mebrofenin, respectively. Subscripts represent tissue or vascular compartments, as follows: blood (b), liver (h), liver vascular (inlet) component (i), bile (bile), liver sub-compartment (n), extrahepatic ("other") tissue (o), and extrahepatic vascular (blood) component (b,o). Clearance values are designated as CL_{uptake} for influx from blood into tissue, CL_{efflux} for efflux from tissue to blood, and $CL_{biliary}$ for excretion from liver into bile. Physiological parameters for tissue volumes (V) and blood flows (Q) were obtained from the literature (53; 54) and summarized in Table 2.4.

The unbound fraction of ^{99m}Tc-mebrofenin in blood (f_b) was determined by ultrafiltration using 40-60 min plasma samples to allow for protein binding equilibration and ensure that ^{99m}Tc-mebrofenin activity in the ultrafiltrate exceeded the minimum sensitivity of the detector. The plasma samples were centrifuged at 600*xg* for 10min at room temperature. The plasma was placed in Centrifree® micropartition devices and centrifuged in a fixed angle rotor at 1380x*g* at room temperature for 5 min to pass <10% of the original volume through the filter. Samples of plasma (total concentration in the presence of protein) and ultrafiltrate (unbound concentration) were collected post-centrifugation and analyzed with a sodium iodide well counter. ^{99m}Tc-Mebrofenin f_b of 0.03 was determined as the product of the unbound fraction and total concentration in the plasma, divided by the total concentration in the blood. The unbound fraction of ^{99m}Tc-mebrofenin in all other tissues was assumed to be the same as blood.

Differential equations describing the disposition of ^{99m}Tc-mebrofenin in each of the compartments were fit simultaneously to the blood, bile, and liver quantitative scintigraphy data using WinNonlin Phoenix, v6.3 (Pharsight, St. Louis, MO) to obtain estimated parameters representing transport-mediated clearance processes. All processes were assumed to be linear under the present experimental conditions [trace amounts of ^{99m}Tc-mebrofenin were administered (2.5mCi=~194nmol)] and therefore, only first-order rate constants were included in the model. Liver data was reduced to 2, 4, 6, 8, 10, 15, 20, 30, 40, 50, 60, 80, 100, 120, 140, 160, 175 min to reflect a similar sampling intensity as the blood compartment. The model also was fit to mean control data to obtain parameter estimates representing average biliary recovery and extrahepatic distribution. In order to account for the semi-quantitative mean liver scintigraphy data, an extra term was added to the function input representing an *in silico* attenuation correction factor (ACF). The *in silico* ACF represents the time-averaged effect of the two-dimensional correction matrix on total liver counts; the resulting parameter estimate was in good agreement with the value obtained from the two subjects with attenuation-corrected scintigraphy data using the cobalt-57 flood source.

Sensitivity analysis of parameter estimates on model output (blood, liver and bile time-activity profiles) was conducted in Berkeley-Madonna v.8.3.11. Parameters representing transport-mediated clearance processes were adjusted in isolation up to 10-fold in either direction of the values describing mean control data (Table 2.2), with resulting changes in predicted blood and liver exposure and biliary excretion (t=0-180min) shown in Figure 2.3. Sensitivity of one or more model output (blood, liver, bile) to a given parameter indicates relative confidence in the parameter value estimate. In contrast, poor confidence is implicated when sensitivity analysis reveals the parameter could take on a range of values with little or no change in relevant model results.

Simulation experiments were conducted in Berkeley Madonna to explore various scenarios representing the potential impact of ritonavir on ^{99m}Tc-mebrofenin disposition. In addition, simulations provide a comparison of the full 180-min profiles versus the time-averaged parameters (AUCs) and cumulative biliary recovery represented in the sensitivity analysis. The specifc combinations and

magnitude of parameter changes were selected to represent the potential impact of ritonavir on ^{99m}Tc-mebrofenin disposition based on results of sensitivity analysis (Figure 2.3) and semi-PBPK model fit and parameter estimates (Table 2.2).

Human SCH Studies

[^{3}H]Taurocholate and [^{3}H]rosuvastatin (1μM; ~100nCi/mL) were used as positive controls to ensure functional uptake and biliary excretion of each SCH preparation (Table 2.5). Samples were quantified using a sodium iodide well counter for ^{99m}Tc-mebrofenin activity, LC-MS/MS analysis for ritonavir, and liquid scintillation counting for [^{3}H]taurocholate and [^{3}H]rosuvastatin. Transport function was normalized to the protein content of each preparation, and intracellular ritonavir concentrations were calculated using a value of 7.5μL/mg protein(29). The inhibitory effect of ritonavir on ^{99m}Tc-mebrofenin accumulation was evaluated using GraphPad Prism to calculate the IC_{50} in each hepatocyte preparation, fixing the initial (no inhibitor) and maximal effect at 100 and 0%, respectively. ^{99m}Tc-Mebrofenin *in vitro* biliary clearance ($CL_{biliary}$) and biliary excretion index (BEI) were calculated using B-CLEAR technology(55). *In vitro* uptake clearance (CL_{uptake}) was calculated based on total accumulation in standard HBSS, as described previously(12). *In vitro* clearance values (μL/min/mg protein) were scaled to kilograms of body weight using the following conversions: 0.85 mg protein/million cells(29), 100 million cells/g liver, and 25.7 g liver/kg body weight(12). Predicted *in vivo* clearance values were estimated according to the well-stirred model of hepatic disposition (Table 2.6).

Table 2.3. Demographic information for clinical study participants.

	^{99m}Tc-Mebrofenin alone							
	1	*2*	*3*	*4*	*5*	*6*	*7*	*8*[*]
Age (yrs)	23	21	20	19	20	23	21	29
Weight (kg)	88.6	59.0	86.5	82.0	78.6	90.2	68.2	81.9
Gender	M	M	M	M	M	M	M	M
Ethnicity[†]	O	C	O	C	L	B	C	C

[*]Subjects for which quantitative scintigraphy data were obtained using the cobalt-57 flood source.
[†]Self-Identified Race/Ethnicity: A – Asian, B – Black/African-American, C – Caucasian, L – Latino/-a, O - Other

200 mg Ritonavir							*2x300 mg Ritonavir*		
9	*10*	*11*	*12*	*13*	*14*	*15*	*16*	*17*[*]	*18*
23	20	24	24	26	20	20	24	21	21
90.9	74.7	69.3	50.6	78.4	69.6	57.8	54.8	76.9	68.6
M	M	M	F	M	M	F	F	M	F
O	B	C	A	C	C	B	A	C	C

Table 2.4. Physiologic parameters for semi-PBPK model (53; 54)

Physiologic Parameters	**Value**
Volume:	g or mL/kg body weight
Blood (total)	75
Liver	26
Extrahepatic	400
Tissue vascular space:	
Liver	7
Extrahepatic	0.75
Blood Flow:	mL/min/kg
Liver	20
Extrahepatic (remaining cardiac output)	55

Table 2.5. Total accumulation (cells+bile, standard HBSS) and BEI of [^{3}H]taurocholate and [^{3}H]rosuvastatin (1μM; ~100nCi/mL) in 24-well human SCH. Accumulation data represent mean ± SD of n=3 human liver donors.

Compound	Total Accumulation	BEI	*In Vitro* CL_{uptake}	*In Vitro* $CL_{biliary}$
	pmol/mg P	*%*	*mL/min/kg*	
[^{3}H]Taurocholate	131.5 ± 29.5	77.4 ± 15.6	29.3 ± 6.6	22.6 ± 6.8
[^{3}H]Rosuvastatin	68.8 ± 19.6	30.5 ± 7.7	15.3 ± 4.4	4.7 ± 2.0

Table 2.6. ^{99m}Tc-Mebrofenin *in vitro* intrinsic clearance values and predicted *in vivo* clearance from data generated in human SCH. Data represent mean ± SD of n=3 human liver donors.

Clearance Value	*In Vitro* Intrinsic Clearance	Predicted *In Vivo* Clearance
	mL/min/kg	
CL_{uptake}	23.7 ± 12.1	10.6 ± 3.1
$CL_{biliary}$	5.8 ± 2.4	4.4 ± 1.5

REFERENCES

1. Administration USFaD. 2012. Guidance for Industry: Drug Interaction Studies - Study Design, Data Analysis, Implications for Dosing, and Labeling Recommendations. ed. FaDAF U.S. Department of Health and Human Services, Center for Drug Use and Evaluation (CDER). Silver Spring, MD

2. Agency EM. 2012. Guideline on the Investigation of Drug Interactions. ed. CfHMP (CHMP). London, United Kingdon

3. Funk C. 2008. The role of hepatic transporters in drug elimination. *Expert Opinion on Drug Metabolism & Toxicology* 4:363-79

4. Pauli-Magnus C, Meier PJ. 2006. Hepatobiliary transporters and drug-induced cholestasis. *Hepatology* 44:778-87

5. Hendrikse NH, Franssen EJ, van der Graaf WT, Vaalburg W, de Vries EG. 1999. Visualization of multidrug resistance in vivo. *Eur J Nucl Med* 26:283-93

6. Michael M, Thompson M, Hicks R, Mitchell P, Ellis A, et al. 2006. Relationship of hepatic functional imaging to irinotecan pharmacokinetics and genetic parameters of drug elimination. *Journal of Clinical Oncology* 24:4228-35

7. Wong M, Balleine RL, Blair EY, McLachlan AJ, Ackland SP, et al. 2006. Predictors of vinorelbine pharmacokinetics and pharmacodynamics in patients with cancer. *Journal of Clinical Oncology* 24:2448-55

8. Chen CC, Meadows B, J. R, Kalafsky G, Fojo T, et al. 1997. Detection of in vivo P-glycoprotein inhibition by PSC 833 using Tc-99m sestamibi. *Clinical Cancer Research* 3:545-52

9. Ghibellini G, Leslie EM, Pollack GM, Brouwer KLR. 2008. Use to Tc-99m mebrofenin as a clinical probe to assess altered hepatobiliary transport: integration of in vitro, pharmacokinetic modeling, and simulation studies. *Pharmaceutical research* 25:1851-60

10. Ghibellini G, Johnson BM, Kowalsky RJ, Heizer WD, Brouwer KLR. 2004. A novel method for the determination of biliary clearance in humans. *AAPS Journal* 6:Article 33

11. Giacomini KM, Huang SM, Tweedie DJ, Benet LZ, Brouwer KL, et al. 2010. Membrane transporters in drug development. *Nat Rev Drug Discov* 9:215-36

12. Swift B, Pfeifer ND, Brouwer KL. 2010. Sandwich-cultured hepatocytes: an in vitro model to evaluate hepatobiliary transporter-based drug interactions and hepatotoxicity. *Drug metabolism reviews* 42:446-71

13. Balon HR, Fink-Bennett DM, Brill DR, Fig LM, Freitas JE, et al. 1997. Procedure guideline for hepatobiliary scintigrahy. *Journal of Nuclear Medicine* 38:1654-7

14. Doo E, Krishnamurthy GT, Eklem MJ, Gilbert S, Brown PH. 1991. Quantification of hepatobiliary function as an integral part of imaging with technetium-99m-mebrofenin in health and disease. *J Nucl Med* 32:48-57

15. Loberg MD, Cooper M, Harvey E, Callery P, Faith W. 1976. Development of new radiopharmaceuticals based on N-substitution of iminodiacetic acid. *J Nucl Med* 17:633-8

16. Swift B, Yue W, Brouwer KL. 2010. Evaluation of (99m)technetium-mebrofenin and (99m)technetium-sestamibi as specific probes for hepatic transport protein function in rat and human hepatocytes. *Pharmaceutical research* 27:1987-98

17. de Graaf W, Hausler S, Heger M, van Ginhoven TM, van Cappellen G, et al. 2011. Transporters involved in the hepatic uptake of (99m)Tc-mebrofenin and indocyanine green. *Journal of hepatology* 54:738-45

18. Bhargava KK, Joseph B, Ananthanarayanan M, Balasubramaniyan N, Tronco GG, et al. 2009. Adenosine triphosphate-binding cassette subfamily C member 2 is the major transporter of the hepatobiliary imaging agent (99m)Tc-mebrofenin. *J Nucl Med* 50:1140-6

19. Pinos T, Figueras C, Herranz R. 1991. Scintigraphic diagnosis of Dubin-Johnson syndrome: DISIDA is also useful. *Am J Gastroenterol* 86:1687-8

20. Hendrikse NH, Kuipers F, Meijer C, Havinga R, Bijleveld CM, et al. 2004. In vivo imaging of hepatobiliary transport function mediated by multidrug resistance associated protein and P-glycoprotein. *Cancer chemotherapy and pharmacology* 54:131-8

21. Pinos T, Constansa JM, Palacin A, Figueras C. 1990. A new diagnostic approach to the Dubin-Johnson syndrome. *Am J Gastroenterol* 85:91-3

22. Hirsch MS. 2008. Initiating therapy: when to start, what to use. *J. Infect. Dis.* 15:S252-60

23. Vourvahis M, Kashuba AD. 2007. Mechanisms of pharmacokinetic and pharmacodynamic drug interactions associated with ritonavir-enhanced tipranavir. *Pharmacotherapy* 27:888-909

24. Huisman MT, Smit JW, Crommentuyn KM, Zelcer N, Wiltshire HR, et al. 2002. Multidrug resistance protein 2 (MRP2) transports HIV protease inhibitors, and transport can be enhanced by other drugs. *AIDS* 16:2295-301

25. Ye ZW, Camus S, Augustijns P, Annaert P. 2010. Interaction of eight HIV protease inhibitors with the canalicular efflux transporter ABCC2 (MRP2) in sandwich-cultured rat and human hepatocytes. *Biopharm Drug Dispos* 31:178-88

26. Gutmann H, Fricker G, Drewe J, Toeroek M, Miller DS. 1999. Interactions of HIV Protease Inhibitors with ATP-Dependent Drug Export Proteins. *Molecular Pharmacology* 56:383-9

27. Ye ZW, Augustijns P, Annaert P. 2008. Cellular accumulation of cholyl-glycylamido-fluorescein in sandwich-cultured rat hepatocytes: kinetic characterization, transport mechanisms, and effect of human immunodeficiency virus protease inhibitors. *Drug metabolism and disposition: the biological fate of chemicals* 36:1315-21

28. Annaert P, Ye ZW, Stieger B, Augustijns P. 2010. Interaction of HIV protease inhibitors with OATP1B1, 1B3, and 2B1. *Xenobiotica; the fate of foreign compounds in biological systems* 40:163-76

29. Krishnamurthy S, Krishnamurthy GT. 1989. Technetium-99m-iminodiacetic acid organic anions: review of biokinetics and clinical application in hepatology. *Hepatology* 9:139-53

30. Lee JaB, K.R. 2010. Determination of Intracellular Volume of Rat and Human Sandwich-Cultured Hepatocytes (Abstract ID 1595). *The Toxicologist, Supplement to Toxicological Sciences* 114:339

31. Chervu LR, Nunn AD, Loberg MD. 1982. Radiopharmaceuticals for hepatobiliary imaging. *Semin Nucl Med* 12:5-17

32. Hawkins RA, Hall T, Gambhir SS, Busuttil RW, Huang SC, et al. 1988. Radionuclide evaluation of liver transplants. *Semin Nucl Med* 18:199-212

33. Brown PH, Juni JE, Lieberman DA, Krishnamurthy GT. 1988. Hepatocyte versus biliary disease: a distinction by deconvolutional analysis of technetium-99m IDA time-activity curves. *J Nucl Med* 29:623-30

34. Peters AM, Myers MJ, Mohammadtaghi S, Mubashar M, Mathie RT. 1998. Bidirectional transport of iminodiacetic organic anion analogues between plasma and hepatocyte. *Eur J Nucl Med* 25:766-73

35. Ito K, Chiba K, Horikawa M, Ishigami M, Mizuno N, et al. 2002. Which concentration of the inhibitor should be used to predict in vivo drug interactions from in vitro data? *AAPS PharmSci* 4:E25

36. van Heeswijk RP, Bourbeau M, Campbell P, Seguin I, Chauhan BM, et al. 2006. Time-dependent interaction between lopinavir/ritonavir and fexofenadine. *Journal of clinical pharmacology* 46:758-67

37. Jones HM, Barton HA, Lai Y, Bi YA, Kimoto E, et al. 2012. Mechanistic pharmacokinetic modeling for the prediction of transporter-mediated disposition in humans from sandwich culture human hepatocyte data. *Drug metabolism and disposition: the biological fate of chemicals* 40:1007-17

38. Menochet K, Kenworthy KE, Houston JB, Galetin A. 2012. Use of mechanistic modeling to assess interindividual variability and interspecies differences in active uptake in human and rat hepatocytes. *Drug metabolism and disposition: the biological fate of chemicals* 40:1744-56

39. Abe K, Bridges AS, Yue W, Brouwer KL. 2008. In vitro biliary clearance of angiotensin II receptor blockers and 3-hydroxy-3-methylglutaryl-coenzyme A reductase inhibitors in sandwich-cultured rat hepatocytes: comparison with in vivo biliary clearance. *The Journal of pharmacology and experimental therapeutics* 326:983-90

40. Higgins JW, Bedwell DW, Zamek-Gliszczynski MJ. 2012. Ablation of both organic cation transporter (OCT)1 and OCT2 alters metformin pharmacokinetics but has no effect on tissue drug exposure and pharmacodynamics. *Drug metabolism and disposition: the biological fate of chemicals* 40:1170-7

41. Watanabe T, Kusuhara H, Maeda K, Shitara Y, Sugiyama Y. 2009. Physiologically based pharmacokinetic modeling to predict transporter-mediated clearance and distribution of pravastatin in humans. *The Journal of pharmacology and experimental therapeutics* 328:652-62

42. Poirier A, Funk C, Scherrmann JM, Lave T. 2009. Mechanistic modeling of hepatic transport from cells to whole body: application to napsagatran and fexofenadine. *Molecular pharmaceutics* 6:1716-33

43. Jones HM, Parrott N, Jorga K, Lave T. 2006. A novel strategy for physiologically based predictions of human pharmacokinetics. *Clin Pharmacokinet* 45:511-42

44. Kawai R, Mathew D, Tanaka C, Rowland M. 1998. Physiologically based pharmacokinetics of cyclosporine A: extension to tissue distribution kinetics in rats and scale-up to human. *The Journal of pharmacology and experimental therapeutics* 287:457-68

45. Takeda M, Noshiro R, Onozato ML, Tojo A, Hasannejad H, et al. 2004. Evidence for a role of human organic anion transporters in the muscular side effects of HMG-CoA reductase inhibitors. *Eur J Pharmacol* 483:133-8

46. Knauer MJ, Urquhart BL, Meyer zu Schwabedissen HE, Schwarz UI, Lemke CJ, et al. 2010. Human skeletal muscle drug transporters determine local exposure and toxicity of statins. *Circ Res* 106:297-306

47. Rezk NL, Crutchley RD, Yeh RF, Kashuba ADM. 2006. Full validation of an analytical method for the HIV-protease inhibitor atazanavir in combination with 8 other antiretroviral agents and its applicability to therapeutic drug monitoring. *Therapeutic Drug Monitoring* 28:517-25

48. Jung BH, Rezk NL, Bridges AS, Corbett AH, Kashuba AD. 2007. Simultaneous determination of 17 antiretroviral drugs in human plasma for quantitative analysis with liquid chromatography-tandem mass spectrometry. *Biomed Chromatogr* 21:1095-104

49. Leslie EM, Mao Q, Oleschuk CJ, Deeley RG, Cole SP. 2001. Modulation of multidrug resistance protein 1 (MRP1/ABCC1) transport and atpase activities by interaction with dietary flavonoids. *Molecular pharmacology* 59:1171-80

50. Kalvass JC, Maurer TS. 2002. Influence of nonspecific brain and plasma binding on CNS exposure: implications for rational drug discovery. *Biopharm Drug Dispos* 23:327-38

51. Delpon G, Ferrer L, Lisbona A, Bardies M. 2003. Impact of scatter and attenuation corrections for iodine-131 two-dimensional quantitative imaging in patients. *Cancer Biother Radiopharm* 18:191-9

52. Miller C, Filipow L, Jackson S, Riauka T. 1996. Planar imaging quantification using 3D attenuation correction data and Monte Carlo simulated buildup factors. *Phys Med Biol* 41:1401-23

53. Davies B, Morris T. 1993. Physiological parameters in laboratory animals and humans. *Pharm Res* 10:1093-5

54. Brown RP, Delp MD, Lindstedt SL, Rhomberg LR, Beliles RP. 1997. Physiological parameter values for physiologically based pharmacokinetic models. *Toxicol Ind Health* 13:407-84

55. Liu X, Chism JP, LeCluyse EL, Brouwer KR, Brouwer KL. 1999. Correlation of biliary excretion in sandwich-cultured rat hepatocytes and in vivo in rats. *Drug metabolism and disposition: the biological fate of chemicals* 27:637-44

CHAPTER 3

Determination of Intracellular Unbound Concentrations and Subcellular Localization of Drugs in Rat Sandwich-Cultured Hepatocytes Compared to Liver Tissue

Introduction

The impact of drugs on intracellular targets of efficacy and/or toxicity, as well as routes of elimination, is driven by local unbound concentrations ($C_{unbound}$) according to the "free drug hypothesis"(1). Prediction of clinical efficacy, toxicity and drug-drug interactions (DDIs) could be improved by accounting for $C_{unbound}$ *in vitro* and *in vivo*(2-4). Furthermore, subcellular drug distribution may aid prediction and/or correlation of efficacy and/or toxicity and risk assessment for drugs(5-7). Measurement of blood or plasma $C_{unbound}$ is convenient and may correlate with tissue concentrations for compounds with sufficient passive permeability. However, for hydrophilic compounds (highly polar or ionized at physiologic pH) that rely on uptake/efflux transporters for distribution and do not readily cross membrane barriers, the ratio of intracellular and extracellular (blood or plasma) $C_{unbound}$ ($Kp_{u,u}$) may be highly disparate.

$Kp_{u,u}$ has been used extensively in CNS pharmacokinetics-pharmacodynamics (PK/PD) to elucidate the role of blood-brain barrier penetration and transport(8), as well as correlate *in vivo* effects with *in vitro* potency(9-11). Figure 3.1 illustrates the concept of $Kp_{u,u}$ as it applies to hepatobiliary drug disposition. The important role of the organic anion transporting polypeptides (OATPs) has been recognized in recent years, highlighting the need to elucidate the role of active uptake in the hepatic accumulation of drugs(12; 13). Compounds that are taken up efficiently into hepatocytes may exhibit a

---

This work has been presented, in part, at the AAPS Annual Meeting, Chicago, IL, October 15-18, 2012 and has been submitted to *Drug Metabolism and Disposition.*

$Kp_{u,u}$>>1(12; 14). Indeed, any situation in which the net rate of appearance exceeds elimination under steady-state conditions might result in a $Kp_{u,u}$>>1; this would include formation of metabolites, which are often polar, poorly permeable compounds that rely on active transport for elimination. $Kp_{u,u}$<<1 in the liver indicates that the net effects of elimination (efflux, metabolism) outweigh appearance in the tissue/cellular compartment (low passive permeability and/or rate-limited influx). While a $Kp_{u,u}$<<1 is common in the context of CNS exposure, where net efflux processes often dominate drug disposition as a mechanism of tissue protection/exclusion, a $Kp_{u,u}$>>1 is expected to be more common in the liver due to its major role in drug elimination (biotransformation, biliary excretion), which is driven by (hepato)cellular concentrations.

Hepatic intracellular $C_{unbound}$, $Kp_{u,u}$ and subcellular localization information has improved predictions and/or explained seemingly discrepant PK/PD relationships with a variety of endpoints including efficacy(12), toxicity(15), and drug disposition, including drug transport(16), metabolism(17-20), and related DDIs(15; 21-23). Intracellular $C_{unbound}$ in the relevant compartment(s) and subcellular localization of drugs are challenging to accurately measure, and our understanding of intracellular drug disposition in the liver remains rudimentary. A versatile and reliable method to determine these parameters in a relevant hepatic *in vitro* model would be of value in order to differentiate the contribution of active uptake vs. binding/sequestration as mechanisms of hepatocellular accumulation, and to assess routes and rates of elimination (e.g., metabolism, biliary excretion)(2; 13; 24; 25).

Isolated perfused livers (IPLs) are considered the "gold standard" for studying the hepatobiliary system in isolation, without the influence of extrahepatic components(26). Unfortunately, the IPL system has a number of drawbacks, including a limited experimental period (≤~2 h), the time- and labor-intensive nature of the procedure, and limited applicability to non-rodent species including humans. Sandwich-cultured hepatocytes (SCH) are a common *in vitro* model used to assess the role of hepatic uptake and excretory function, including DDIs and transporter-metabolism interplay(27). Methods to estimate subcellular distribution and intracellular $C_{unbound}$ in the SCH model have not been developed.

The objective of this work was to determine the intracellular $C_{unbound}$ and subcellular localization of drugs in SCH compared to liver tissue from IPLs. A set of probe drugs with distinct mechanisms of hepatocellular uptake and accumulation was selected for investigation. Ritonavir inhibits drug transport and metabolism *in vitro* and *in vivo*, and accumulates in liver tissue(28). Surprisingly, the mechanism(s) underlying the cellular uptake and accumulation of ritonavir, and the intracellular $C_{unbound}$ for prediction of DDIs, have not been reported(29). Rosuvastatin, an HMG-CoA reductase inhibitor with a primary site of action in hepatocytes, is efficiently taken up by OATPs and accumulates within hepatocytes, with an expected $Kp_{u,u}$>1. Pafuramidine, the prodrug of furamidine, is the only orally-active agent that has shown efficacy in clinical trials for the treatment of first-stage (hemolymphatic) human African trypanosomiasis(30). Furamidine is formed in the liver via sequential metabolism, and must be excreted from hepatocytes into the systemic circulation to exert antiparasitic activity. This set of drugs provided a useful range of tissue accumulation, hepatic unbound fraction (f_u), subcellular distribution, and $Kp_{u,u}$ values for comparison of methods to determine hepatocellular $C_{unbound}$.

Materials and Methods

Materials

All chemicals were purchased from Sigma-Aldrich (St. Louis, MO) unless otherwise stated. Rosuvastatin(31) and the deuterated internal standard were purchased from Moravek Biochemicals (Brea, CA). Ritonavir(28) was purchased from Toronto Research Chemicals (Toronto, ON, Canada. Furamidine, the prodrug pafuramidine, and internal standard (deuterium-labeled furamdine) were synthesized in the laboratory of Dr. David W. Boykin, as reported previously(32).

Tissue Accumulation.

Male Wistar rats (Charles River Labs, Wilmington, MA) were used for IPL studies. Rats were allowed free access to water and food, and acclimated for a minimum of 1 week prior to experimentation. All animal procedures complied with the guidelines of the Institutional Animal Care and Use Committee (University of North Carolina, Chapel Hill, NC). All procedures were performed under full anesthesia with ketamine/xylazine (140/8mg/kg i.p.). Livers were perfused in a single-pass manner (30 mL/min continually

oxygenated Krebs-Ringer bicarbonate buffer in the presence of 5 μM taurocholate to maintain bile flow); following a 15-min equilibration period, ritonavir (1 μM) or rosuvastatin (1 μM) was included in the perfusate for 30-min, and then the livers were flushed briefly with blank buffer. Pafuramidine (10 μM) was perfused in a recirculating liver system for 120 min as reported previously(32). Livers were harvested and stored whole at -80°C until homogenization and analysis.

Rat hepatocytes were seeded in 6-well BioCoat plates (BD Biosciences, San Jose, CA) and overlaid with Matrigel basement membrane matrix (BD Biosciences, San Jose, CA) in a sandwich-cultured configuration and maintained as described previously(27). Day 4 rat SCH were pre-incubated for 10 min in Ca^{2+}-free Hanks Balanced Salt Solution (HBSS; B-CLEAR® technology) to open tight junctions and prevent accumulation in bile canalicular spaces, and then treated with 1 μM ritonavir or [^{3}H]rosuvastatin (100 nCi/mL; American Radiolabeled Chemicals, Inc., St. Louis, MO) for 10 min at 37°C as described previously(27). Starting on day 3, pafuramidine was incubated for 24 h at 10 μM to allow complete formation and equilibration of furamidine, as previously reported(32), followed by a 5-min incubation in Ca^{2+}-free HBSS. In all cases, incubation medium was collected at the end of the incubation period, and cells were washed three times in ice-cold HBSS.

Fractionation.

Liver tissue was homogenized in 3-5 volumes of fractionation buffer (250 mM sucrose, 10 mM HEPES, 10 mM KCl, 1 mM EDTA, 1.5 mM $MgCl_2$, 1 mM DTT, Roche cOmplete Protease Inhibitor Cocktail) using a Potter-Elvehjem homogenizer. Following treatment with the drug of interest, all wells of the 6-well SCH plate were harvested and pooled by scraping each well sequentially into 1 mL fractionation buffer. Collected cells in buffer were homogenized by passing 10 times through a 27g needle, resting 10 min on ice, followed by an additional 10 passes. Following homogenization to disrupt cell membranes, the resulting crude lysates (liver and SCH) were sampled and reserved to perform analysis for total and unbound drug concentrations, protein content and enzyme activity assays. The remaining lysate was subjected to stepwise differential centrifugation as published previously(33) to separate the following cellular components: 10 min at 600x*g* (nuclei and cellular debris), 10,000x*g* (mitochondria), 35,000*xg* (lysosomes

and other medium-sized membrane-bound bodies), 60 min at 100,000x*g* (microsomes, membrane fraction) with the resulting supernatant representing the cytosolic fraction. All spins <100,000x*g* were repeated after resuspending the pellet in 5 (liver) or 0.2 (SCH) mL of fractionation buffer; resulting supernatants were pooled before moving on to subsequent centrifugation steps. Pellets were resuspended in fractionation buffer [10 mL for liver tissue and 0.3 (600x*g*) or 0.15 (>600x*g*) mL for SCH] for analysis of drug and protein content and enzyme activities.

Protein content of each fraction was determined using the Pierce BCA Protein Assay (Thermo Fisher Scientific Inc, Rockford, IL). Separation and recovery of subcellular fractions was assessed by measuring lactate dehydrogenase (LDH) activity as a cytosolic marker using a Cytotoxicity Detection kit (Roche Diagnostics, Indianapolis, IN), and acid phosphatase activity as a lysosomal marker using an Acid Phosphatase kit (Sigma, St. Louis, MO). Succinate dehydrogenase activity was measured to assess the presence of mitochondria as described previously(34), adapted to a microplate format as follows: 5 µL sample volume was combined with 60 µL 10 mM sodium succinate in 50 mM phosphate buffer and incubated for 60 min at 37°C, followed by the addition of 20 µL 2.5 mg/mL *p*-iodonitrotetrazolium and incubation for another 15 min. The reaction was quenched by the addition of 0.2 mL of 5:5:1 (v/v/w) ethanol/ethyl acetate/trichloroacetic acid and absorbance was determined at 492 nm on a plate-based spectrophotometer (BioTek PowerWave HT, Winooski, VT). Similarly, glucose-6-phosphatase activity was measured to assess the presence of microsomes as described previously(35), adapted to a microplate format as follows: 10 µL sample volume was plated in duplicate and combined with 10 µL 20 mM Tris-HCl, pH 7.3, with and without 50 mM glucose-6-phosphate (Na^+ salt, Sigma, St. Louis, MO) and incubated for 30 min at 37°C. Inorganic phosphate standards were prepared from 0.1-2 mM and added to the plate (20 µL) at the end of the incubation. The reaction was terminated by the addition of 200 µL detection reagent [3:1 1 mg/mL malachite green (oxalate salt, Sigma, St. Louis, MO) in 1 N HCl/4.2% (w/v) ammonium molybdate in 5 N HCl] to samples and standards, followed immediately by the addition of 10 µL 0.05% (v/v) Tween-20. The reaction mixture was shaken briefly and allowed to equilibrate for 10-15 min, and absorbance was determined at 660 nm on a plate-based spectrophotometer. Phosphate formation

was calculated as the difference between samples incubated with and without glucose-6-phosphate substrate to correct for endogenous phosphate content in the samples. Recovery of each fraction was calculated as the percentage of the total organelle-specific enzyme activity detected in each subfraction compared to the whole lysate.

Binding.

Binding was determined in whole tissue lysates and cytosolic fractions by equilibrium dialysis. Initial studies were performed to determine the time to equilibrium and test for protein leakage or potential volume shifts with whole liver tissue (data not shown). Aliquots were loaded into a 96-well equilibrium dialysis apparatus (HTDialysis, LLC; Gales Ferry, CT) and dialyzed against phosphate buffer for 6 h with shaking at 37°C. Binding replicates (n=3) consisted of 3-fold dilutions of each sample (1-, 3-, and 9-fold original sample). The unbound fraction (f_u) was back-extrapolated to account for dilution during the homogenization/fractionation process, as well as subsequent dilutions, as described previously(36):

$$\text{Undiluted fu} = \frac{1/D}{\left(\left(1/fu_{measured}\right) - 1\right) + 1/D}$$

This approach provides the best precision in the linear range, and that precision is lost when the measured unbound fraction becomes high ($f_{u,measured}$ is >80%). Where $f_{u,measured}$ was >80% at the lowest dilution, the value is reported as "greater than" the undiluted f_u calculated according to the equation above.

Sample Analysis

Ritonavir, rosuvastatin and furamidine were quantified by LC-MS/MS as described previously; rosuvastatin was quantified by liquid scintillation counting for SCH studies.(37-40) Total cellular concentrations in SCH were calculated by dividing the quantified substrate mass in the whole lysate by 7.4 μL/mg protein in SCH, the estimated hepatocellular volume determined by [^{3}H]3-O-methyl-D-glucose.(40)

Data Analysis.

The observed partition coefficient ($Kp_{observed}$) was calculated as the total tissue concentration (liver or SCH) divided by the perfusate (IPL) or buffer (SCH) total concentration, respectively. The predicted partition coefficient ($Kp_{predicted}$) was calculated as the reciprocal of the unbound fraction, including the

subcellular distribution in the case of the cytosolic fraction [$1/f_u$ or $1/(f_{cytosol}xf_{u,cytosol})$], where $f_{cytosol}$ represents the fraction of the total drug mass in the tissue recovered in the cytosol. The unbound tissue concentration was calculated as the product of the total tissue concentration and the unbound fraction determined in whole lysate ($C_{unbound}=f_u \bullet C_{tissue}$), including the subcellular distribution in the case of the cytosolic fraction ($C_{unbound}=f_{cytosol} \bullet f_{u,cytosol} \bullet C_{tissue}$). The ratio of intracellular and extracellular $C_{unbound}$ ($Kp_{u,u}$) was calculated as the unbound tissue concentration divided by the unbound concentration in perfusate or buffer ($f_{u,buffer}$ was assumed to be 1 in the absence of protein in both systems).

Results

In order to characterize the subcellular distribution of the probe compounds, differential centrifugation was performed on lysates from whole liver tissue and SCH following drug treatment. Marker enzyme activities specific to mitochondria, lysosomes, endoplasmic reticulum (microsomes) and cytosol were examined in tissue lysate and subfractions to assess the purity and recovery of the various fractions. The distribution of these organelles in subfractions of whole liver tissue and SCH is shown in Figure 3.2. Using whole liver tissue, separation of subfractions was demonstrated, with organelle-specific enzyme activity detected in the expected fractions. Following fractionation of SCH lysates, the majority of membrane-bound organelles (including mitochondria and microsomes) were recovered in the initial low-speed spin (600 *xg*). Cytosolic separation and recovery was efficient and successful, as shown in Figure 3.2.D with ~90% of the total LDH activity in the crude lysate recovered in the cytosolic fraction of SCH lysates.

Recovery of the probe drugs in all fractions was compared to the total mass in the whole lysate prior to fractionation. Recovery of probe drugs after fractionation of whole liver tissue and SCH was approximately 100% (±10%). The average subcellular distribution of each drug in whole tissue and SCH is shown in Figure 3.3. In all cases, the coefficient of variation was less than 20% when at least 10% of the drug was recovered in a given fraction. In whole liver tissue, approximately 36% of the ritonavir was found in the cytosolic fraction, 31% in the microsomal fraction, and 18% in the mitochondrial fraction, with the remainder distributed fairly evenly among the remaining fractions. In SCH lysates, cytosolic

recovery of ritonavir was similar to that in whole liver tissue (43%). The remaining ritonavir was recovered primarily in the initial low-speed spin, consistent with binding/sequestration to organelles (including microsomes), which were difficult to separate in SCH lysates. Rosuvastatin distribution was confined primarily to the cytosol, with recovery of 72% in the cytosolic fraction of whole liver tissue, and 88% in SCH lysates. Rosuvastatin distribution to specific organelles was minimal (<11%). Furamidine was localized in the mitochondrial (43%), nuclear (18%) and lysosomal (15%) fractions of tissue lysate from the rat IPL; the remaining material was recovered in the cytosolic fraction, with minimal localization in the microsomal fraction. Furamidine was recovered predominantly (85%) in the initial low-speed spin (600 *xg*) following fractionation of SCH lysates, with minor recovery in the remaining fractions, including cytosol (3%). This is consistent with extensive binding and/or sequestration within membrane-bound organelles (including mitochondria), which were recovered in the 600 *xg* pellet following initial centrifugation of SCH lysates.

Concentrations of probe drugs in tissue, along with binding data and calculated concentration ratios (Kp and $Kp_{u,u}$) are listed in Table 3.1. Total tissue accumulation (Kp) ranged over three orders of magnitude in the compound set selected for investigation. Ritonavir binding was extensive in whole liver tissue and SCH (f_u of 1.0±0.1% and 3.0±1.0%, respectively). Predicted accumulation ($Kp_{predicted}$) of ritonavir based on binding and subcellular distribution (91-100 in IPL, 22-35 in SCH) was in good agreement with observed accumulation ($Kp_{observed}$; 110 and 33 in IPL and SCH, respectively). The estimated intracellular $C_{unbound}$ approximated the extracellular concentration, resulting in a $Kp_{u,u}$ of ~1, suggesting that binding to cellular components can explain the observed tissue accumulation. Rosuvastatin displayed moderate accumulation in liver tissue and SCH ($Kp_{observed}$ of 33 and 17 respectively) in the absence of extensive binding and/or sequestration. $Kp_{predicted}$ (~3-4 in IPL and SCH) underestimated the observed accumulation, as might be expected for a compound that is a substrate for hepatic uptake transporters. The estimated intracellular $C_{unbound}$ and resulting $Kp_{u,u}$ (~8-11) suggested accumulation of unbound rosuvastatin within the liver. Calculation of a precise $Kp_{u,u}$ in SCH was complicated by the low degree of binding in diluted SCH lysate and cytosolic fraction, but accumulation

of unbound drug was evident based on a $Kp_{u,u}$ value >5-6. Furamidine accumulation was extensive in whole liver tissue and SCH (Kp of 8400 and 6900, respectively). While furamidine also was extensively bound or sequestered, $Kp_{predicted}$ underestimated the observed accumulation by more than 10-fold. The estimated intracellular $C_{unbound}$ and resulting $Kp_{u,u}$ (>16) confirmed accumulation of unbound drug within hepatocytes.

Discussion

The present study evaluated the use of an organ-specific *in vitro* model system to estimate $C_{unbound}$, and predict cellular partitioning and accumulation of drugs. The SCH system exhibits properly localized and functional transport proteins, metabolic and regulatory machinery. This system may be able to recapitulate the relevant cellular disposition of drugs whose distribution is influenced by the interplay of these processes in hepatocytes *in vivo*.

Total accumulation ($Kp_{observed}$) in whole tissue was well predicted by the SCH model (within 2-3 fold) for the limited compound set selected for investigation. A system that enables accurate estimates of hepatic Kp values would be a valuable addition to physiologically-based pharmacokinetic (PBPK) modeling efforts. Although tissue partitioning can be predicted using physicochemical properties, such as the method of Rodgers and Rowland(41; 42), exceptions and inaccuracies inevitably exist, particularly for compounds that may rely on active processes, such as transport and/or metabolism.

While the Kp value is useful for estimating overall tissue, it does not provide information on the mechanism(s) of tissue accumulation. For mechanistic information, one must assess tissue binding and subcellular distribution. In the case where binding does not explain the observed tissue accumulation, $Kp_{u,u}$ is an informative parameter for describing the potential role of active uptake. However, a $Kp_{u,u} \approx 1$ does not necessarily imply that passive processes (*e.g.*, diffusion) are solely responsible for hepatocellular distribution. While it is tempting to dismiss the potential contribution of active transport for such compounds, it is possible that a net balance exists between uptake and efflux processes. In such a case, impaired transport function (e.g., DDIs, genetic variation, and/or disease states) may result in altered hepatic and/or systemic exposure, with corresponding implications for changes in efficacy, toxicity, and

DDI potential. For example, ritonavir undergoes active hepatic transport even though the calculated $Kp_{u,u}$ is ~1. Although the role of active uptake in the hepatobiliary disposition of ritonavir has not been reported conclusively, ritonavir is a competitive inhibitor of OATP-mediated uptake, as well as P-gp and MRP-mediated efflux *in vitro*(43-45). Despite the fact that ritonavir accumulates in the liver (reported literature ranges from 10-100 fold(28)) and is excreted into bile in rats, dogs and humans(28), we recently demonstrated that ritonavir did not inhibit MRP2-mediated biliary excretion of the imaging agent, ^{99m}Tc-mebrofenin in humans(23). This apparent *in vitro-in vivo* disconnect was reconciled by accounting for the $C_{unbound}$ of ritonavir in hepatocytes relative to its inhibitory potency against MRP2(23).

Rosuvastatin accumulation in whole liver ($Kp_{observed}$ = 33) and SCH ($Kp_{observed}$ = 17) was in good agreement with the previously reported range of 18- to 45-fold up to 8 h after oral administration in rats(31). Although rosuvastatin binding did account for a portion of tissue accumulation ($Kp_{predicted}$ ~3-4), the majority of accumulation was due to unbound drug ($Kp_{u,u}$ of 8 to 11), consistent with efficient hepatic uptake and rate-limited efflux as described previously(31; 46). Rosuvastatin binding data in SCH demonstrated a limitation of the required dilution of small tissue samples when performing these studies in *in vitro* systems. For compounds that are not extensively bound ($f_{u,measured}$ >80%), dilution of SCH samples resulted in observed binding data that were difficult to extrapolate accurately. Therefore, the resulting $Kp_{u,u}$ value is a conservative minimum and potentially underestimates the true value by up to 2-3-fold. Rosuvastatin was selected as a model drug that is efficiently taken up by OATPs, which drives accumulation of unbound drug within hepatocytes, with an expected $Kp_{u,u}$ significantly greater than 1.

As previously reported, extensive and prolonged hepatic accumulation of the active metabolite, furamidine, was observed in both rat IPLs and SCH(32). Previous studies using differential centrifugation to separate fractions revealed that furamidine was localized primarily in the mitochondrial fraction of the liver and kidney(47). Similarly, furamidine was localized primarily in the mitochondrial fraction (43%) following subcellular fractionation of tissue lysate from the rat IPL. Despite extensive binding and sequestration, these processes underpredict the observed accumulation in liver tissue. Accumulation of unbound furamidine ($Kp_{u,u}$) was predicted to be >16-fold, suggesting permeability-

limited efflux of this charged metabolite formed in the hepatocyte. The extensive hepatic binding/sequestration may limit the systemic exposure to furamidine; in contrast, a structural analogue had a 5-fold greater hepatic f_u, which could contribute, in part, to the enhanced systemic exposure of this agent compared to furamidine(32).

Subcellular fractionation has not been reported previously in SCH. Similar to partitioning, it would be useful to determine subcellular localization and sequestration in a relevant *in vitro* system. This is particularly true of the liver, where drug-induced liver injury via idiosyncratic hepatocellular injury is the most frequent cause of regulatory action on drugs, including failure to approve, labeling changes, and withdrawal from the market(48). Hepatotoxic drugs are known to cause hepatocellular injury through diverse pathways, including organelle-specific sequestration and toxicity, such as phopholipidosis (lysosomes)(5) and mitochondrial disruption/dysfunction(6; 49), among others(7). Although isolation of subcellular fractions consisting of membrane-bound organelles proved challenging in SCH, cell lysis, release and isolation of soluble cytosolic proteins and contents was successful, as determined by LDH activity and rosuvastatin recovery. Enzyme markers of subcellular components were recovered primarily in the initial, low-speed centrifugation step from SCH lysates, indicating that these organelles were retained in large, dense conglomerates. It is possible that the collagen matrix, indispensible to the sandwich configuration, prevented the plasma membrane from separating enough to release larger, membrane-bound bodies. This limitation may provide an advantage for rapid isolation of the cytosolic fraction in SCH. These data suggest that a single, low-speed (600x*g*) spin, which can be performed on any benchtop microcentrifuge, will reliably exclude cellular organelles from the resulting supernatant of SCH lysate. This single step method has the additional advantage of minimizing potential redistribution of drugs during multiple centrifugation steps and associated dilutions. Although the specific site(s) of subcellular sequestration would remain unknown, extensive distribution/recovery of drug in the pellet could indicate the need to consider intracellular pharmacokinetics. Meanwhile, the cytosolic fraction would contain the unbound drug content in the tissue ($f_{cytosol}$), which could be assessed formally by determining the extent of binding to cytosolic protein ($f_{u,cytosol}$), as reported in the present studies.

A number of potential limitations are associated with the subcellular fractionation approach, including: a) Some degree of cross-contamination among isolated cellular fractions. This can be assessed primarily by recovery of marker enzyme activity specific for each organelle, but adds significant time- and labor-intensive efforts to sample analysis. b) Potential disruption of binding equilibrium between cellular compartments during the fractionation process. Tissue homogenization and fractionation inherently involve dilution, which can shift binding equilibrium. Despite the potential limitations of the reported method, assessment of intracellular $C_{unbound}$ and mechanisms of hepatic accumulation is challenging and *in vitro* methods are needed for general application to compounds that are not amenable to visualization, such as fluorescence. Other methods are rarely used and not without limitations, such as assessment of cellular accumulation at 4 versus 37°C(12). The assumption of the latter method is that all active processes are inert at 4°C, and that cellular accumulation represents passive equilibration of unbound drug. However, the effect of temperature and potential artifacts on non-specific binding(50-52) and membrane fluidity and partitioning(53-55) are well-established.

Hepatic intracellular $C_{unbound}$, $Kp_{u,u}$ and subcellular localization can be used to improve prediction of clinical efficacy, toxicity and drug-drug interactions (DDIs). A straightforward *in vitro* method was developed to determine hepatocellular accumulation of total and unbound drug in the SCH model. This method was used successfully to differentiate the contribution of active transport vs. binding/sequestration as mechanisms of hepatocellular accumulation for a set of probe drugs with distinct mechanisms of hepatocellular uptake and accumulation.

Table 3.1. Total tissue concentrations, unbound fraction and calculated tissue-to-medium or -perfusate partition coefficients (Kp and $Kp_{u,u}$).

Outcome	Ritonavir		Rosuvastatin		Furamidine	
	IPL	***SCH***	***IPL***	***SCH***	***IPL***	***SCH***
C_{tissue} (μM)	56	15±2	18	17±3	24[b]	1500±500
C_{medium} (μM)	0.49	0.47±0.12	0.54	1	0.0032[c]	0.27±.19
$Kp_{observed}$	110	33	33	17	8400[c]	6900
Whole lysate:[a]						
f_u (%)	1.0±0.1	3.0±1.0	23±1	>36[d]	0.3±0.1[b]	0.9±0.2
$Kp_{predicted}$	100	35	4.3	<2.8	330	110
$C_{u,tissue}$ (μM)	0.56	0.46±0.16	4.1	>6.1	0.073	14±6
$Kp_{u,u}$	1.1	1.1	7.9	>6.1	23	53
Cytosol:[a]						
f_u (%)	3.3±0.2	11±1	46±8	>34[d]	6.2±1.2[b]	11±4
$Kp_{predicted}$	91	22	3.3	<3.4	81	330
$C_{u,tissue}$ (μM)	0.62	0.76±0.31	5.9	>5.0	0.30	4.3±1.6
$Kp_{u,u}$	1.3	1.7	11	>5.0	93	16

[a] $Kp_{predicted}$ and $C_{u,tissue}$ calculated for lysate and cytosol as described in Methods.
[b] From Yan, et al.(32)
[c] Taking into account f_u of 44% in perfusate, containing 20% whole blood.
[d] Undiluted f_u and subsequent calculations represented by inequalities when $f_{u,measured}$ >80%, as described in Methods.

Figure 3.1. The tissue-to-plasma unbound concentration ratio ($Kp_{u,u}$) applied to hepatobiliary drug disposition.

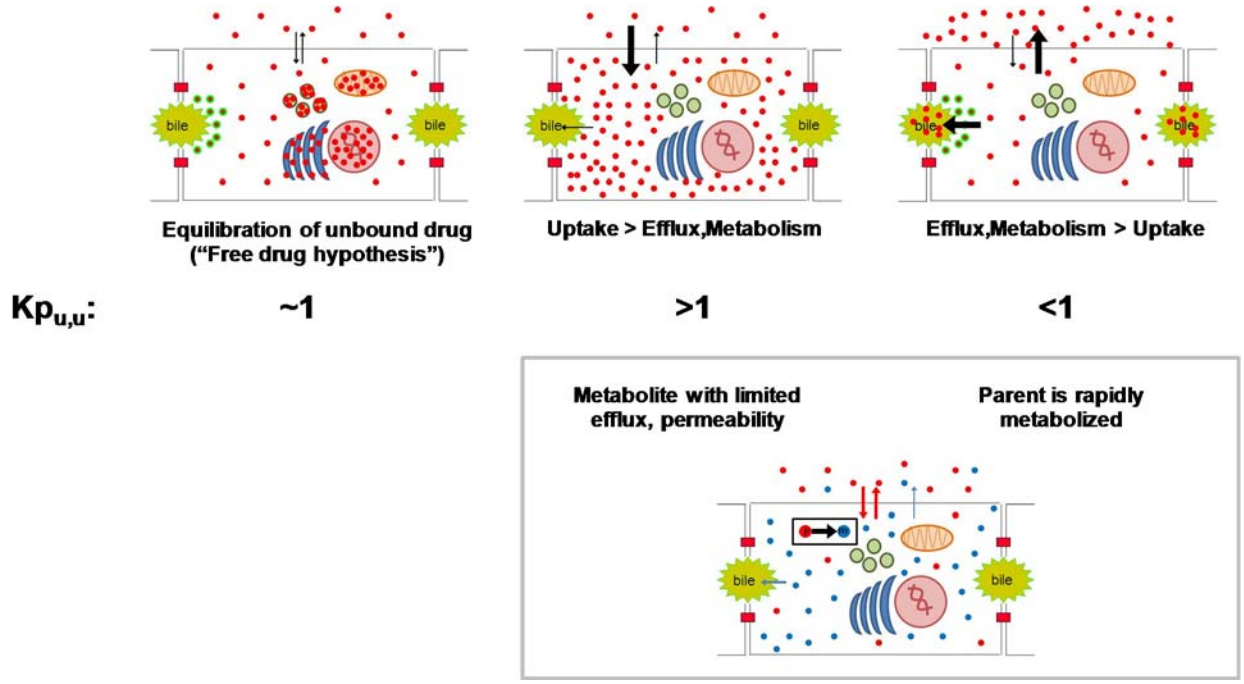

Figure 3.2. Distribution and recovery of organelle-specific marker enzyme activity following differential centrifugation of whole liver tissue (A) and SCH (B). Data are expressed as % total activity in the initial lysate, mean±SD of n=3 (whole liver) or n=9 (SCH).

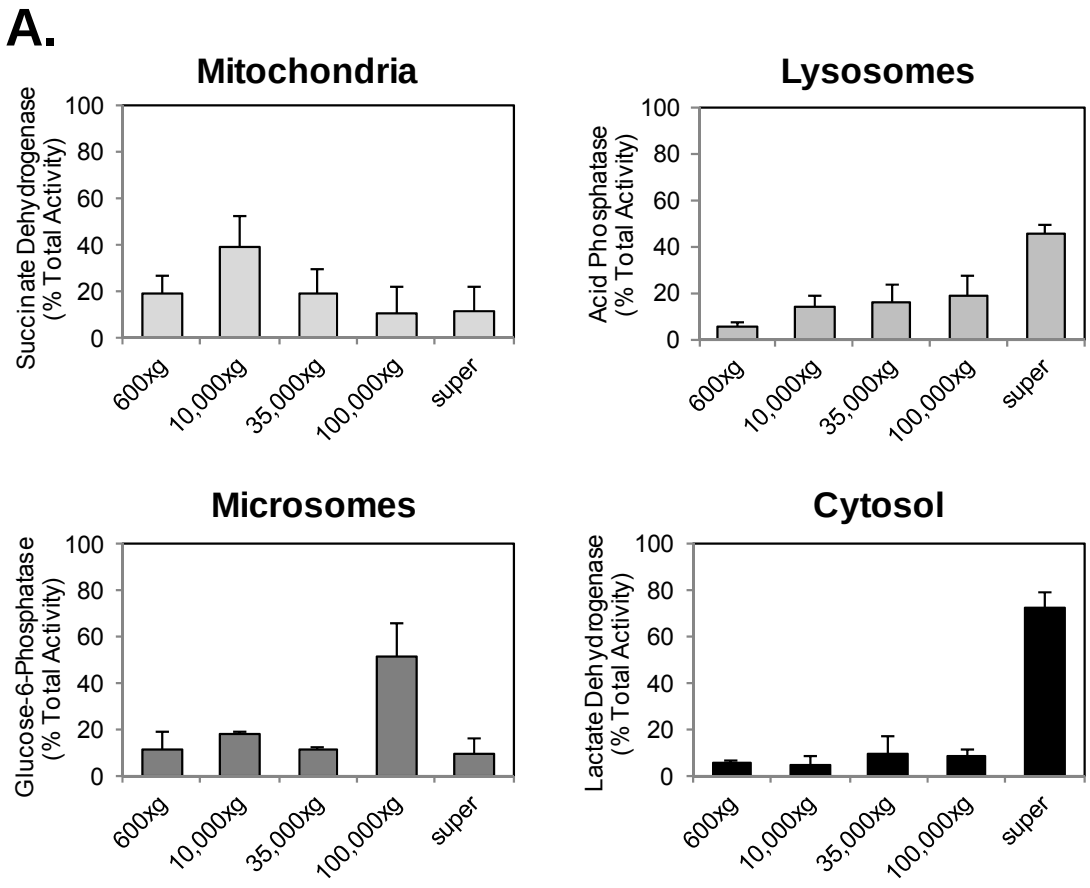

B.

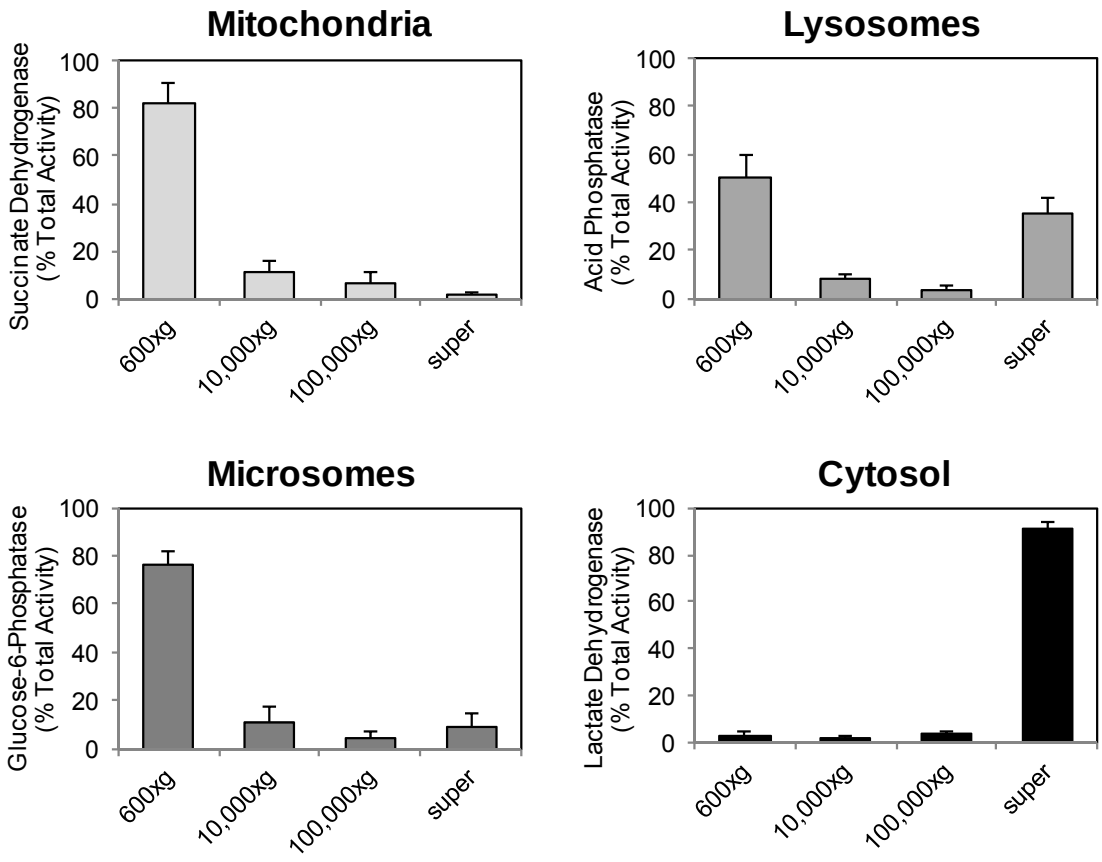
Mitochondria
Succinate Dehydrogenase (% Total Activity)
100
80
60
40
20
0
600xg
10,000xg
100,000xg
super
Lysosomes
Acid Phosphatase (% Total Activity)
Microsomes
Glucose-6-Phosphatase (% Total Activity)
Cytosol
Lactate Dehydrogenase (% Total Activity)

Figure 3.3. Subcellular distribution and recovery of ritonavir, rosuvastatin and furamidine following differential centrifugation of whole liver tissue and SCH. Data are presented as % recovery of total material in lysate. Open = 600x*g* pellet, light gray = 10,000x*g* pellet, mid-gray = 35,000x*g* pellet, dark gray = 100,000x*g* pellet, black = 100,000x*g* supernatant.

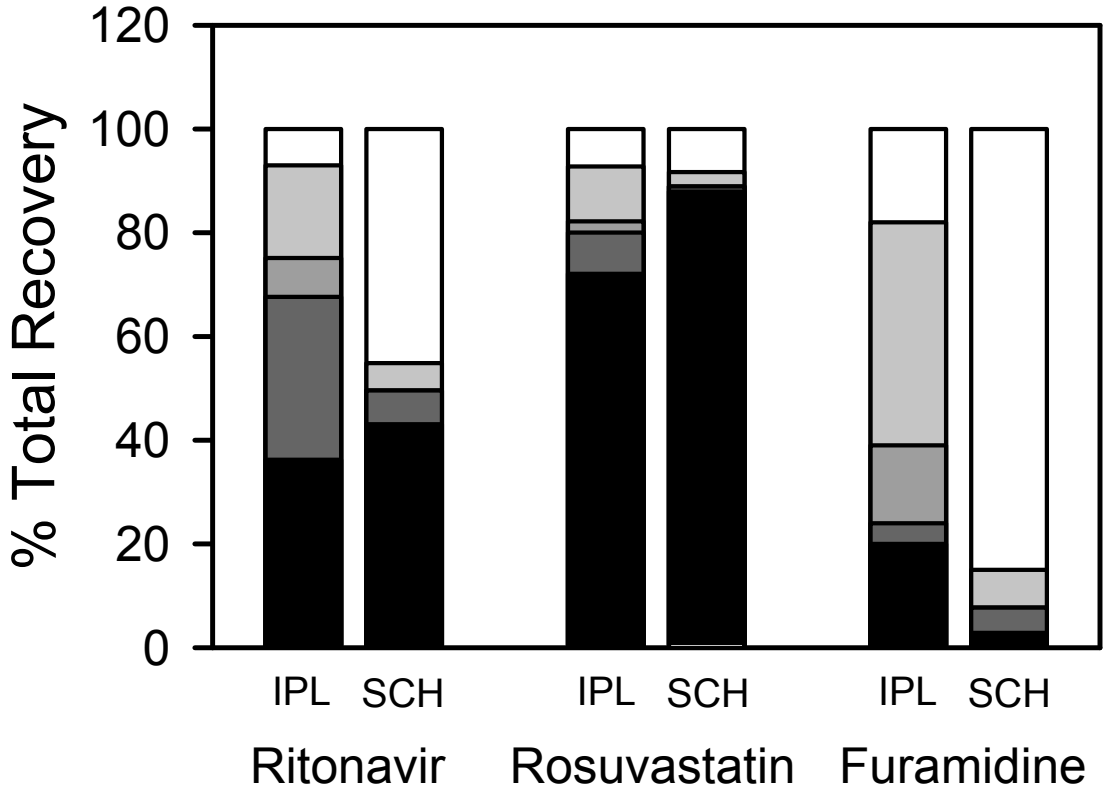

REFERENCES

1. Smith DA, Di L, Kerns EH. 2010. The effect of plasma protein binding on in vivo efficacy: misconceptions in drug discovery. *Nat Rev Drug Discov* 9:929-39

2. Zhou F, Zhang J, Li P, Niu F, Wu X, et al. 2011. Toward a new age of cellular pharmacokinetics in drug discovery. *Drug metabolism reviews* 43:335-45

3. Zha W, Zha BS, Zhou F, Zhou H, Wang G. 2012. The cellular pharmacokinetics of HIV protease inhibitors: current knowledge and future perspectives. *Curr Drug Metab* 13:1174-83

4. Zhang J, Zhou F, Lu M, Ji W, Niu F, et al. 2012. Pharmacokinetics-pharmacology disconnection of herbal medicines and its potential solutions with cellular pharmacokinetic-pharmacodynamic strategy. *Curr Drug Metab* 13:558-76

5. Reasor MJ, Kacew S. 2001. Drug-induced phospholipidosis: are there functional consequences? *Exp Biol Med (Maywood)* 226:825-30

6. Labbe G, Pessayre D, Fromenty B. 2008. Drug-induced liver injury through mitochondrial dysfunction: mechanisms and detection during preclinical safety studies. *Fundam Clin Pharmacol* 22:335-53

7. Gunawan BK, Kaplowitz N. 2007. Mechanisms of drug-induced liver disease. *Clin Liver Dis* 11:459-75

8. Gupta A, Chatelain P, Massingham R, Jonsson EN, Hammarlund-Udenaes M. 2006. Brain distribution of cetirizine enantiomers: comparison of three different tissue-to-plasma partition coefficients: K(p), K(p,u), and K(p,uu). *Drug metabolism and disposition: the biological fate of chemicals* 34:318-23

9. Liu X, Chen C, Smith BJ. 2008. Progress in brain penetration evaluation in drug discovery and development. *The Journal of pharmacology and experimental therapeutics* 325:349-56

10. Read KD, Braggio S. 2010. Assessing brain free fraction in early drug discovery. *Expert Opin Drug Metab Toxicol* 6:337-44

11. Hammarlund-Udenaes M, Friden M, Syvanen S, Gupta A. 2008. On the rate and extent of drug delivery to the brain. *Pharmaceutical research* 25:1737-50

12. Shitara Y, Maeda K, Ikejiri K, Yoshida K, Horie T, Sugiyama Y. 2013. Clinical significance of organic anion transporting polypeptides (OATPs) in drug disposition: their roles in hepatic clearance and intestinal absorption. *Biopharm Drug Dispos* 34:45-78

13. Giacomini KM, Huang SM, Tweedie DJ, Benet LZ, Brouwer KL, et al. 2010. Membrane transporters in drug development. *Nat Rev Drug Discov* 9:215-36

14. Yamazaki M, Kobayashi K, Sugiyama Y. 1996. Primary active transport of pravastatin across the liver canalicular membrane in normal and mutant Eisai hyperbilirubinaemic rats. *Biopharm Drug Dispos* 17:645-59

15. Chen YJ, Huang SM, Liu CY, Yeh PH, Tsai TH. 2008. Hepatobiliary excretion and enterohepatic circulation of colchicine in rats. *International journal of pharmaceutics* 350:230-9

16. Kudo N, Sakai A, Mitsumoto A, Hibino Y, Tsuda T, Kawashima Y. 2007. Tissue distribution and hepatic subcellular distribution of perfluorooctanoic acid at low dose are different from those at high dose in rats. *Biol Pharm Bull* 30:1535-40

17. Obach RS. 1996. The importance of nonspecific binding in in vitro matrices, its impact on enzyme kinetic studies of drug metabolism reactions, and implications for in vitro-in vivo correlations. *Drug metabolism and disposition: the biological fate of chemicals* 24:1047-9

18. Obach RS. 1997. Nonspecific binding to microsomes: impact on scale-up of in vitro intrinsic clearance to hepatic clearance as assessed through examination of warfarin, imipramine, and propranolol. *Drug metabolism and disposition: the biological fate of chemicals* 25:1359-69

19. Obach RS. 1999. Prediction of human clearance of twenty-nine drugs from hepatic microsomal intrinsic clearance data: An examination of in vitro half-life approach and nonspecific binding to microsomes. *Drug metabolism and disposition: the biological fate of chemicals* 27:1350-9

20. Deshmukh SV, Harsch A. Direct determination of the ratio of unbound fraction in plasma to unbound fraction in microsomal system (fu p/fu mic) for refined prediction of phase I mediated metabolic hepatic clearance. *J Pharmacol Toxicol Methods* 63:35-9

21. Yamano K, Yamamoto K, Kotaki H, Sawada Y, Iga T. 1999. Quantitative prediction of metabolic inhibition of midazolam by itraconazole and ketoconazole in rats: implication of concentrative uptake of inhibitors into liver. *Drug metabolism and disposition: the biological fate of chemicals* 27:395-402

22. Sato K, Mizuki Y, Komuro S. 2010. Consideration of reliable concentrations for prediction of change in enzyme activity by mechanism-based inactivation using physiologically-based pharmacokinetic model simulations. *Drug metabolism and pharmacokinetics* 25:335-42

23. Pfeifer ND, Goss SL, Swift B, Ghibellini G, Ivanovic M, et al. 2013. Effect of Ritonavir on 99mTechnetium-Mebrofenin Disposition in Humans: A Semi-PBPK Modeling and In Vitro Approach to Predict Transporter-Mediated DDIs. *CPT: pharmacomet. syst. pharmacol.* 2:e20

24. Lam JL, Okochi H, Huang Y, Benet LZ. 2006. In vitro and in vivo correlation of hepatic transporter effects on erythromycin metabolism: characterizing the importance of transporter-enzyme interplay. *Drug metabolism and disposition: the biological fate of chemicals* 34:1336-44

25. Chu X, K. Korzekwa, R. Elsby, K. Fenner, A. Galetin, Y. Lai, P. Matsson, A. Moss, S. Nagar, G.R. Rosania, Y. Sugiyama, K.L.R. Brouwer. 2013. Intracellular Drug Concentrations and Transporters:

Measurement, Modeling and Implications in the Liver. *Clinical pharmacology and therapeutics* (Submitted for Review)

26. Brouwer KL, Thurman RG. 1996. Isolated perfused liver. *Pharmaceutical biotechnology* 8:161-92

27. Swift B, Pfeifer ND, Brouwer KL. 2010. Sandwich-cultured hepatocytes: an in vitro model to evaluate hepatobiliary transporter-based drug interactions and hepatotoxicity. *Drug metabolism reviews* 42:446-71

28. Denissen JF, Grabowski BA, Johnson MK, Buko AM, Kempf DJ, et al. 1997. Metabolism and disposition of the HIV-1 protease inhibitor ritonavir (ABT-538) in rats, dogs, and humans. *Drug metabolism and disposition: the biological fate of chemicals* 25:489-501

29. Griffin L, Annaert P, Brouwer KL. 2011. Influence of drug transport proteins on the pharmacokinetics and drug interactions of HIV protease inhibitors. *Journal of pharmaceutical sciences* 100:3636-54

30. Paine MF, Wang MZ, Generaux CN, Boykin DW, Wilson WD, et al. 2010. Diamidines for human African trypanosomiasis. *Curr Opin Investig Drugs* 11:876-83

31. Nezasa K, Takao A, Kimura K, Takaichi M, Inazawa K, Koike M. 2002. Pharmacokinetics and disposition of rosuvastatin, a new 3-hydroxy-3-methylglutaryl coenzyme A reductase inhibitor, in rat. *Xenobiotica; the fate of foreign compounds in biological systems* 32:715-27

32. Yan GZ, Brouwer KL, Pollack GM, Wang MZ, Tidwell RR, et al. 2011. Mechanisms underlying differences in systemic exposure of structurally similar active metabolites: comparison of two preclinical hepatic models. *The Journal of pharmacology and experimental therapeutics* 337:503-12

33. Ward ES, Pollack GM, Brouwer KL. 2000. Probenecid-associated alterations in valproic acid pharmacokinetics in rats: can in vivo disposition of valproate glucuronide be predicted from in vitro formation data? *Drug metabolism and disposition: the biological fate of chemicals* 28:1433-9

34. Gong Y, Zhao Z, McConn DJ, Beaudet B, Tallman M, et al. 2007. Lysosomes contribute to anomalous pharmacokinetic behavior of melanocortin-4 receptor agonists. *Pharmaceutical research* 24:1138-44

35. Ockerman PA. 1967. Glucose-6-phosphatase assay on microgram amounts of liver tissue. *Clinica chimica acta; international journal of clinical chemistry* 17:201-6

36. Kalvass JC, Maurer TS, Pollack GM. 2007. Use of plasma and brain unbound fractions to assess the extent of brain distribution of 34 drugs: comparison of unbound concentration ratios to in vivo p-glycoprotein efflux ratios. *Drug metabolism and disposition: the biological fate of chemicals* 35:660-6

37. Rezk NL, White NR, Jennings SH, Kashuba AD. 2009. A novel LC-ESI-MS method for the simultaneous determination of etravirine, darunavir and ritonavir in human blood plasma. *Talanta* 79:1372-8

38. Yan GZ, Brouwer KL, Pollack GM, Wang MZ, Tidwell RR, et al. Mechanisms underlying differences in systemic exposure of structurally similar active metabolites: comparison of two preclinical hepatic models. *The Journal of pharmacology and experimental therapeutics* 337:503-12

39. Abe K, Bridges AS, Yue W, Brouwer KL. 2008. In vitro biliary clearance of angiotensin II receptor blockers and 3-hydroxy-3-methylglutaryl-coenzyme A reductase inhibitors in sandwich-cultured rat hepatocytes: comparison with in vivo biliary clearance. *The Journal of pharmacology and experimental therapeutics* 326:983-90

40. Lee JK, Brouwer KR. 2010. Determination of Intracellular Volume of Rat and Human Sandwich-Cultured Hepatocytes (Abstract ID 1595). *The Toxicologist, Supplement to Toxicological Sciences* 114:339

41. Rodgers T, Leahy D, Rowland M. 2005. Physiologically based pharmacokinetic modeling 1: predicting the tissue distribution of moderate-to-strong bases. *Journal of pharmaceutical sciences* 94:1259-76

42. Rodgers T, Rowland M. 2006. Physiologically based pharmacokinetic modelling 2: predicting the tissue distribution of acids, very weak bases, neutrals and zwitterions. *Journal of pharmaceutical sciences* 95:1238-57

43. Vourvahis M, Kashuba AD. 2007. Mechanisms of pharmacokinetic and pharmacodynamic drug interactions associated with ritonavir-enhanced tipranavir. *Pharmacotherapy* 27:888-909

44. Gutmann H, Fricker G, Drewe J, Toeroek M, Miller DS. 1999. Interactions of HIV protease inhibitors with ATP-dependent drug export proteins. *Molecular pharmacology* 56:383-9

45. Annaert P, Ye ZW, Stieger B, Augustijns P. 2010. Interaction of HIV protease inhibitors with OATP1B1, 1B3, and 2B1. *Xenobiotica; the fate of foreign compounds in biological systems* 40:163-76

46. Nezasa K, Higaki K, Matsumura T, Inazawa K, Hasegawa H, et al. 2002. Liver-specific distribution of rosuvastatin in rats: comparison with pravastatin and simvastatin. *Drug metabolism and disposition: the biological fate of chemicals* 30:1158-63

47. Midgley I, Fitzpatrick K, Taylor LM, Houchen TL, Henderson SJ, et al. 2007. Pharmacokinetics and metabolism of the prodrug DB289 (2,5-bis[4-(N-methoxyamidino)phenyl]furan monomaleate) in rat and monkey and its conversion to the antiprotozoal/antifungal drug DB75 (2,5-bis(4-guanylphenyl)furan dihydrochloride). *Drug metabolism and disposition: the biological fate of chemicals* 35:955-67

48. Watkins PB, Seligman PJ, Pears JS, Avigan MI, Senior JR. 2008. Using controlled clinical trials to learn more about acute drug-induced liver injury. *Hepatology* 48:1680-9

49. Pessayre D. 2007. Role of mitochondria in non-alcoholic fatty liver disease. *J Gastroenterol Hepatol* 22 Suppl 1:S20-7

50. Igari Y, Sugiyama Y, Awazu S, Hanano M. 1981. Interspecies difference in drug protein binding-temperature and protein concentration dependency: effect on calculation of effective protein fraction. *Journal of pharmaceutical sciences* 70:1049-53

51. Kodama H, Kodama Y, Shinozawa S, Kanemaru R, Todaka K, Mitsuyama Y. 1999. Temperature effect on serum protein binding kinetics of phenytoin in monotherapy patients with epilepsy. *European journal of pharmaceutics and biopharmaceutics : official journal of Arbeitsgemeinschaft fur Pharmazeutische Verfahrenstechnik e.V* 47:295-8

52. Zeitlinger MA, Derendorf H, Mouton JW, Cars O, Craig WA, et al. 2011. Protein binding: do we ever learn? *Antimicrobial agents and chemotherapy* 55:3067-74

53. Palmeira CM, Oliveira CR. 1992. Partitioning and membrane disordering effects of dopamine antagonists: influence of lipid peroxidation, temperature, and drug concentration. *Arch Biochem Biophys* 295:161-71

54. Herbette L, Katz AM, Sturtevant JM. 1983. Comparisons of the interaction of propranolol and timolol with model and biological membrane systems. *Molecular pharmacology* 24:259-69

55. Liu XY, Yang Q, Kamo N, Miyake J. 2001. Effect of liposome type and membrane fluidity on drug-membrane partitioning analyzed by immobilized liposome chromatography. *J Chromatogr A* 913:123-31

CHAPTER 4

Basolateral Efflux Transporters Contribute Significantly to the Excretion of Rosuvastatin in Rat and Human Hepatocytes: Characterization of Basolateral vs. Biliary Clearance Using a Novel Protocol in Sandwich-Cultured Hepatocytes

Introduction

Hepatic transport plays an important role in the pharmacokinetics and pharmacodynamics of rosuvastatin (RSV), with the liver serving as the primary organ of efficacy and elimination. Hepatic clearance accounts for 72% of total RSV clearance following an intravenous dose in humans.(1) A number of transport proteins mediating RSV disposition in the liver have been characterized. Active uptake into hepatocytes is mediated by multiple OATP isoforms; NTCP also has been reported to play a role (2-4). MRP2 and BCRP are the major canalicular proteins responsible for the biliary excretion of RSV (2; 5-8). The role of basolateral transport proteins in the efflux of RSV from hepatocytes back into sinusoidal blood has not been examined. This is clinically relevant because impaired hepatic transport due to drug-drug interactions (DDIs) and genetic polymorphisms has been shown to alter the pharmacokinetics of RSV (2; 5; 7; 9-12). Some of these changes have been associated with altered efficacy (LDL-lowering) of RSV (13; 14), while increased systemic exposure has been associated with the life-threatening rhabdomyolysis related to statin use in general (15; 16). Candidate basolateral efflux transporters for RSV include MRP3 and MRP4, which have been shown to mediate basolateral excretion of drugs and metabolites, particularly as a compensatory route of excretion under cholestatic

[1]This work has been presented, in part, at the AAPS Workshop on Drug Transporter in ADME, N. Bethesda, MD, March 18-20, 2013 and will be submitted to *Journal of Pharmacology and Experimental Therapeutics.*

conditions (17-20). SLC51 (polyspecific organic solute carrier, OSTα/β), is localized at the basolateral membrane of the liver and small intestine, where it plays a role in bile acid transport; the ability of OSTα/β to efflux drugs such as RSV has not been investigated(21).

Many transport proteins involved in the hepatobiliary disposition of RSV are also present in the small intestine. Thus, the effects of impaired transport function on oral absorption vs. hepatic elimination can be challenging to deconvolve. For example, the ~2-fold increase in RSV systemic exposure in individuals carrying a BCRP polymorphism associated with decreased transport function has been attributed to the effects of intestinal BCRP and a resulting increase in oral absorption (7; 11). However, a similar increase in RSV systemic exposure was observed in Mrp2- and Bcrp-deficient animal models following intravenous administration (2). This could be attributed to translocation of RSV from the hepatocyte back into the systemic circulation in the setting of impaired biliary excretion. The role of the basolateral efflux pathway in mediating altered hepatic vs. systemic exposure in the setting of impaired biliary excretion has not been characterized thoroughly.

The quantitative impact of excretory transport modulation on the hepatic, systemic, and biliary exposure to xenobiotics and derived metabolites was formalized recently by our research team (22). Experimental data and theoretical relationships indicated that the fold change in exposure is governed by the relationship, $1/(1 - f_e)$, where f_e is the fraction excreted by a particular transport protein. Loss-of-function of a transport pathway associated with a $f_e < 0.5$ will have minimal consequences on exposure, but substantial changes can be expected in response to loss-of-function of one or more transport pathways with $f_e > 0.5$. It should be noted that the impact of f_e on exposure depends on the compartment of interest (systemic, hepatic or bile), the directionality of the impaired efflux pathway (canalicular or sinusoidal), and the existence of an alternative route of excretion. When a transport protein is impaired, the increased excretion in the alternative direction is a function of the fraction of total hepatocellular clearance mediated by the impaired pathway. For example, in the case of impaired (') biliary clearance (CL_{Bile}) the resulting increase in basolateral (BL) excretion and systemic exposure can be estimated from $\Delta f_{e,BL} = (CL_{Bile} - CL_{Bile}') / (CL_{Bile} + CL_{BL})$, where $(CL_{Bile} + CL_{BL})$ is the baseline (pre-impairment) total cellular

excretory clearance (CL_{Total}). The increase in hepatocellular exposure resulting from impaired efflux can be estimated from $\Delta f_{e,Total} = (CL_{Total} - CL_{Total}') / CL_{Total}$, assuming that there are no compensatory changes in uptake or metabolism. Therefore, accurate predictions of altered hepatic and systemic exposure in the setting of impaired excretory transport require an understanding of the contributions of basolateral and biliary clearance.

The present experiments were designed to quantify the contribution of the basolateral efflux pathway to the hepatocellular elimination of RSV. The role of basolateral efflux was investigated in single-pass rat isolated perfused livers (IPLs) and an uptake/efflux protocol was developed in rat and human sandwich-cultured hepatocytes (SCH). This novel protocol allowed tight junction modulation and measurement of RSV accumulation in cells+bile and cells throughout the experimental time course without compromising cell viability or function as a result of prolonged exposure to $-Ca^{2+}$ conditions; quantification of RSV cellular efflux after the loading phase can be measured directly using this protocol. The ability of the basolateral efflux proteins MRP3 and MRP4 to transport RSV in humans was evaluated in membrane vesicles prepared from overexpressing HEK293 cells. These methods, combined with pharmacokinetic (PK) modeling, revealed that basolateral and biliary clearance represent alternative elimination routes with a quantitatively similar contribution to the overall hepatocellular excretion of RSV in rat and human hepatocytes.

Materials and Methods

Materials

All chemicals were purchased from Sigma-Aldrich (St. Louis, MO) unless otherwise stated. Non-radiolabeled RSV and the deuterated internal standard (d_6-RSV) were purchased from Moravek Biochemicals (Brea, CA). [^{3}H]Estradiol-17-β-D-glucuronide ($E_2$17G) and [^{3}H]dehydroepiandrosterone sulfate (DHEAS) were purchased from Perkin Elmer (Waltham, MA); [^{3}H]RSV was purchased from American Radiolabeled Chemicals, Inc. (St. Louis, MO). GF120918 (elacridar) was a generous gift from GlaxoSmithKline (Research Triangle Park, NC).

Animals

Male Wistar wild-type (WT) rats (250-350 g) from Charles River Labs (Wilmington, MA) or male Mrp2-deficient (TR^-) rats bred at the University of North Carolina (250—350 g; breeding stock obtained from Dr. Mary Vore, University of Kentucky, Lexington, KY) were used as donors for hepatocyte and isolated perfused liver (IPL) studies. Rats were allowed free access to water and food, and acclimated for a minimum of 1 week prior to experimentation. All animal procedures complied with the guidelines of the Institutional Animal Care and Use Committee (University of North Carolina, Chapel Hill, NC). All procedures were performed under full anesthesia with ketamine/xylazine (140/8 mg/kg i.p.).

Sandwich-cultured Hepatocytes (SCH)

Freshly isolated rat and human hepatocytes were seeded in 24-well BioCoat plates (BD Biosciences, San Jose, CA) at a density of 0.35×10^6 cells/well (WT rat and human) or 0.2×10^6 cells/well (TR^- rat) and overlaid with Matrigel basement membrane matrix (BD Biosciences, San Jose, CA) in a sandwich configuration and maintained as described previously (23). Human hepatocytes were kindly provided by Life Technologies (Research Triangle Park, NC) from a 55 year old female Caucasian donor with a BMI 30.8 kg/m^2. On day 4 (rat) or day 7 (human), SCH were pre-incubated for 10 min in 0.5 mL/well standard (Ca^{2+}-containing) or Ca^{2+}-free Hanks Balanced Salt Solution (HBSS) to maintain or open tight junctions, respectively (B-CLEAR® technology, Qualyst Transporter Solutions, Research Triangle Park, NC). Subsequently, SCH were treated with 0.1 or 1 μM [^{3}H]RSV (100 nCi/mL) in the absence or presence of GF120918 (0.5 μM), in standard HBSS for 20 min at 37°C. After the 20-min uptake phase, buffers containing RSV were removed, cells were washed twice with 37°C standard or Ca^{2+}-free HBSS buffer without RSV, and the third application of buffer was added to SCH for the 15-min efflux phase (Fig. 4.1A). For conditions in the presence of inhibitor, 0.5 μM GF120918 was maintained in the incubation buffer for the duration of the experiment (pre-incubation, uptake and efflux phases). Preliminary studies indicated that 0.5 μM GF120918 was sufficient to inhibit RSV biliary excretion in SCH with minimal impact on uptake. RSV accumulation in cells+bile, cells, and medium (standard HBSS or Ca^{2+}-free HBSS buffer) during uptake (2, 5, 10, and 20 min) and efflux (2, 5, 10, and 15 min) phases were determined by

terminal sampling of n=3 wells at each time point. In all cases, incubation medium was collected at the end of the incubation period, and cells were washed twice in ice-cold HBSS. Cells were solubilized in 0.3 mL 0.5% Triton X-100 and radioactivity in cell lysates and buffer samples was quantified by liquid scintillation counting (Packard TriCarb, Perkin-Elmer, Waltham, MA). Preliminary studies were performed to confirm that cell viability and tight junction modulation were maintained throughout the experimental uptake/efflux protocol described above and in Fig. 4.1 using 1 μM carboxydichlorofluorescein diacetate (CDFDA). The fluorescence intensity in bile networks was observed by serial imaging using a Zeiss Axiovert 100TV inverted fluorescent microscope (Carl Zeiss Inc., Thornwood, NY). Leakage of lactate dehydrogenase (LDH) into buffer during the uptake/efflux protocol was determined using the LDH Cytotoxicity Detection Kit (Roche Diagnostics, Indianapolic, IN). LDH release was evaluated as a percentage of total cellular LDH content, represented by values measured after complete cell lysis using 0.5% Triton X-100.

Isolated Perfused Livers (IPLs)

WT and TR^- rat livers were perfused in a single-pass manner as described previously (24; 25). Briefly, following cannulation of the portal vein and bile duct, livers were perfused *in situ* with continuously-oxygenated Krebs-Ringer bicarbonate buffer (35 mL/min) in the presence of 5 μM taurocholate to maintain bile flow. Livers were removed from the body cavity and placed in a humidified perfusion chamber heated to maintain liver temperature at 37°C. After a 15-min equilibration period, the perfusate for the 60-min loading phase contained RSV (0.5 μM); at 60 min, the perfusate was switched back to RSV-free, and was continued for an additional 30 min. For conditions in the presence of inhibitor, the inflow perfusate contained 0.5 μM GF120918 for the duration of the experiment (15-min equilibration period followed by a 90-min perfusion). The concentration of GF120918 was based on preliminary studies in SCH (see above). Liver viability was assessed by monitoring inflow perfusion pressure (<15 mm H_2O), gross morphology, and maintenance of bile flow (within 30% of the baseline rate during the equilibration period). Bile and perfusate were collected over 5-min intervals, and bile volume was determined

gravimetrically in pre-weighed tubes. After perfusion, livers were blotted dry, weighed, and stored at -80°C until analysis.

Membrane Vesicles

Human MRP3 plasmid (pcNDA3.1(-)-MRP3) and MRP4 plasmid (pcDNA3.1(-)-MRP4) were kindly provided by Dr. Susan Cole (Queen's University, Kingston, Canada) and Dr. Dietrich Keppler (German Cancer Research Center, Heidelberg, Germany), respectively. Transiently transfected HEK293T cells were generated and membrane vesicles were prepared as described previously (26). Transport experiments were carried out by a rapid filtration assay as described previously (27). Briefly, membrane vesicles (10 μg protein) were incubated at 37°C with test compound in Tris-sucrose buffer (TSB; 50 mM Tris-HCl, 250 mM sucrose, 10 mM $MgCl_2$, 10 mM creatine phosphate, 100 μg/mL creatine kinase, 4 mM ATP or AMP) and 20 μM [^{3}H]$E_2$17βG (0.4 μCi/mL) for MRP3, 2 μM [^{3}H]DHEAS (0.7 μCi/mL) for MRP4, or 0.1-100 μM [^{3}H]RSV (0.5 μCi/mL), in a volume of 50 μL. After incubation for 10 min, the reaction was stopped by the addition of 0.45 mL ice-cold TSB and immediately applied to a glass fiber filter (type A/E, Pall Corp., Port Washington, NY) and washed twice with 2 mL ice-cold TSB. Filters were mixed by vortex in 5 mL of scintillation fluid and radioactivity was quantified by liquid scintillation counting (Packard TriCarb, Perkin-Elmer, Waltham, MA). The ATP-dependent uptake of substrate was calculated by subtracting substrate uptake in the presence of AMP from substrate uptake in the presence of ATP. Membrane vesicles from non-transfected (NT) cells were used to demonstrate the potential endogenous ATP-dependent uptake of probe substrates. Inhibition data are presented as the percentage of the prototypical substrate ($E_2$17βG or DHEAS) uptake in membrane vesicles prepared from cells overexpressing MRP3 or MRP4. Transport of RSV by MRP4 is presented as ATP-dependent uptake, after subtracting endogenous ATP-dependent uptake in NT vesicles. All data are expressed as mean ±SD of triplicate determinations in a single experiment.

Bioanalysis

RSV was quantified by LC-MS/MS as described previously for samples derived from IPL studies; [^{3}H]RSV was quantified by liquid scintillation counting for SCH studies (4). The RSV calibration curve

was constructed over a standard range of 1-1000 nM based on peak area ratios of analyte and internal standard. The pentanoic acid metabolite of RSV was identified by high resolution LC-MS/MS (TOF/TOF) using an ABSciex API5600 TripleTOF mass spectrometer (Fig. 4.3). Although absolute quantification of the pentanoic acid derivative of RSV was not possible due to the lack of an analytical standard, relative changes in this metabolite were determined by normalizing the peak area of the extracted (TOF) parent ion chromatogram with the extracted (TOF) parent ion of the internal standard. The concentration of RSV pentanoic acid was estimated by the calibration curve generated using the peak area of RSV normalized by the peak area of the internal standard under the assumption that RSV and the pentanoic acid metabolite of RSV have similar ionization efficiencies.

Pharmacokinetic Modeling

Pharmacokinetic modeling and simulation were used to evaluate RSV disposition in rat SCH and IPLs, and to determine the effects of GF120918 and loss of Mrp2 function on RSV hepatobiliary disposition. Models incorporating various combinations of linear and/or non-linear parameters governing RSV flux were fit to mass (SCH) or rate (IPL) versus time data from individual experiments (Fig. 4.4). The model fitting was performed with WinNonlin Phoenix, v6.1 (St. Louis, MO) using the stiff estimation method and a mixed (additive and proportional) model to estimate residual error. The following differential equations, which were developed based on the model scheme depicted in Fig. 4.1B, were fit simultaneously to data generated in SCH in the presence of intact and disrupted bile canaliculi:

Mass in buffer (Standard HBSS):

$$\frac{dX^{+}_{Buffer}}{dt} = CL_{BL} \times C^{+}_{Cell} + K_{Flux} \times X_{Bile} - CL_{Uptake} \times C^{+}_{Buffer} - K_{Wash} \times X^{+}_{Buffer} \qquad X^{+}_{Buffer}{}^{\circ} = X_{dose}$$

Mass in buffer (Ca^{2+}-free HBSS):

$$\frac{dX^{-}_{Buffer}}{dt} = (CL_{BL} + CL_{Bile}) \times C^{-}_{Cell} - CL_{Uptake} \times C^{-}_{Buffer} - K_{Wash} \times X^{-}_{Buffer} \qquad X^{-}_{Buffer}{}^{\circ} = X_{dose}$$

Mass in cells:

$$\frac{dX^{+or-}_{Cell}}{dt} = CL_{Uptake} \times C^{+or-}_{Buffer} - (CL_{BL} + CL_{Bile}) \times C^{+or-}_{Cell} \qquad X^{+or-}_{Cell}{}^{\circ} = 0$$

Mass in bile (Standard HBSS):

$$\frac{dX_{Bile}}{dt} = CL_{Bile} \times C^{+}_{Cell} - K_{Flux} \times X_{Bile} \qquad X_{Bile}^{\circ} = 0$$

Mass in cells+bile (Standard HBSS):

$$\frac{dX_{Cells+Bile}}{dt} = \frac{dX_{Bile}}{dt} + \frac{dX^{+}_{Cell}}{dt}$$

where variables and parameters are defined as in Fig. 4.2A. In order to account for removal of the RSV dose from the buffer compartment during wash step, K_{wash} was activated for 1.5 minutes at the end of the 20-min uptake phase and fixed at $1x10^4$ min^{-1} based on simulations. C_{Cell} represents the intracellular concentration, calculated as X_{Cell}/V_{Cell}, where cellular volume (V_{Cell}) was estimated based on the protein content of each preparation, using a value of 7.4 μL/mg protein.(28) C_{Buffer} represents the buffer concentration, calculated as X_{Buffer}/V_{Buffer} where the buffer volume (V_{Buffer}) was constant (0.5 mL). Initial parameter estimates were obtained from noncompartmental analysis of SCH data, where CL_{Uptake} was estimated from the initial (2 min) uptake data, $CL_{Uptake} = (dX_{cells+bile}/dt)/C_{Buffer}$, and CL_{BL} and CL_{Bile} were estimated from efflux phase data under calcium-free conditions, where $(CL_{BL} + CL_{Bile}) = X^{-}_{Buffer,0\text{-}15min}/AUC_{cells,0\text{-}15min}$. K_{Flux} , which represents the flux of substrate out of bile networks in standard HBSS conditions, was estimated initially from simulations using Berkeley-Madonna.

The model scheme depicting the single-pass IPL system (Fig. 4.2) consisted of an extracellular (sinusoidal/perfusate) compartment, liver tissue, and a bile compartment, each divided into 5 subcompartments in the semiphysiologically-based approximation of the dispersion model, as reported by Watanabe et al.(29) The model was fit simultaneously to biliary excretion rate and appearance in outflow perfusate rate versus time data, as well as terminal recovery of RSV and the pentanoic acid metabolite in liver tissue. Differential equations describing the model scheme in Fig. 4.2 are as follows:

Extracellular liver 1:

$$\frac{dX_{EC,1}}{dt} = Q \times C_{in} + \frac{CL_{BL}}{5} \times C_{u,L1} - \frac{CL_{Uptake}}{5} \times C_{EC,1} - Q \times C_{EC,1}$$

Extracellular liver 2-5:

$$\frac{dX_{EC,n}}{dt} = Q \times C_{EC,n-1} + \frac{CL_{BL}}{5} \times C_{u,L,n} - \frac{CL_{Uptake}}{5} \times C_{EC,n} - Q \times C_{EC,n}$$

Intracellular liver 1-5:

$$\frac{dX_{Liver,n}}{dt} = \frac{CL_{Uptake}}{5} \times \left[\left(\frac{CL_{BL}}{5}\right) + \left(\frac{CL_{Met}}{5}\right) + \left(\frac{CL_{Other}}{5}\right)\right] \times C_{u,L,n} - \frac{C_{u,L,n} \times (V_{max}/5)}{(K_m + C_{u,L,n})}$$

Bile 1-5:

$$\frac{dX_{Bile,n}}{dt} = \frac{C_{u,L,n} \times (V_{max}/5)}{(K_m + C_{u,L,n})}$$

where variables and parameters are defined as in Fig. 4.2 with further explanation as follows. C_{EC} is the extracellular concentration, calculated as $X_{EC,n}/(V_{EC}/5)$ and V_{EC} is the extracellular volume of the liver, which was assumed to be in equilibration with the sinusoidal space and estimated at 20% of the total liver mass, as reported previously (5; 29). Q is the perfusate flow rate of 35 mL/min, and C_{in} is the concentration of RSV in the perfusate, measured for each preparation; binding of RSV to the perfusion tubing and apparatus was <10% and not considered further. $C_{u,L}$ is the unbound intracellular concentration of RSV in the liver based on binding of RSV to rat liver tissue, which was determined by equilibrium dialysis with an unbound fraction of 0.25, corrected for dilution. The total intracellular liver concentration was calculated as $X_{liver,n}/(V_L/5)$ where V_L is the intracellular volume, calculated as total liver mass minus the V_{EC}. The RSV concentration resulting in half-maximal biliary excretion (K_m) was set to 10 μM based on the reported affinity of RSV for Mrp2 and Bcrp in isolated expression systems (8; 30). The $CEC_5 \times Q$ was fit to the observed appearance rate in outflow perfusate, while the sum of the excretion rate in bile (dX_{bile}/dt) for liver subcompartments 1-5 was fit to the observed biliary excretion rate. Initial parameter estimates were obtained from a combination of direct extrapolation of IPL data and simulations in Berkeley-Madonna. V_{max} was estimated initially as the steady-state excretion rate in bile based on unbound liver concentrations from mass balance of ~3-5 times the K_m for biliary excretion process (10 μM). CL_{Uptake} was estimated initially from the observed hepatic extraction (E_h) at the initial time point in outflow perfusate (0-15 min),

and subsequently extrapolated using the well-stirred model, assuming hepatic intrinsic clearance represents uptake clearance, according to the following equations:

$$E_h = (C_{in}-C_{out})/C_{in}$$

$$E_h = CL_{int}/(Q+CL_{int})$$

$$CL_{Uptake} = CL_{int} = E_h \times Q/(1-E_h)$$

Based on two independent reports of RSV uptake in freshly-isolated, suspended WT rat hepatocytes, CL_{Uptake} was fixed at 40 mL/min/g liver (31; 32), which was very close to the CL_{Uptake} estimated from TR^- liver preparations in the current study (50 mL/min/g liver). Metabolic clearance to the pentanoic acid derivative (CL_{Met}) and other potential metabolites (CL_{Other}) were estimated initially from simulations in Berkeley-Madonna.

Transporter-mediated clearance values (CL_{Uptake}, CL_{BL} and CL_{Bile}) estimated from pharmacokinetic modeling of RSV SCH and IPL data were compared and scaling factors were reported for the WT Control conditions. The scaling factors represent the respective clearance value in IPL divided by the corresponding value in SCH.

Data Analysis

The effect of Mrp2 status (WT or TR^-) and GF120918 on RSV disposition in SCH and IPL experiments was determined by one-way ANOVA with Tukey's post-hoc test. The effect of Mrp2 status was evaluated at each level of inhibitor (absent or present) and the effect of GF120918 was evaluated at each level of Mrp2 status (WT or TR^-).

Results

SCH

Preliminary studies were conducted to establish that the novel uptake/efflux protocol described in Fig. 4.1A maintained tight junction modulation in the absence of Ca^{2+} throughout the experimental time course without compromising cell viability. Following carboxydichlorofluorescein diacetate (CDFDA) administration, fluorescence microscopy confirmed that CDF did not accumulate in bile networks during the 20-min uptake phase following preincubation in Ca^{2+}-free HBSS. Less than 5% of total cellular LDH

content was released over the experimental time course (data not shown). The mass-time profiles of RSV in cells+bile, cells and buffer during the uptake/efflux protocol are plotted in Fig. 4.4. RSV accumulation in cells+bile and cells increased during the uptake phase and decreased during the efflux phase, while appearance in the buffer increased during the efflux phase. RSV accumulation in bile networks (the difference between accumulation in cells+bile and cells) was reduced in Mrp2-deficient TR^- SCH, and biliary excretion nearly was ablated in TR^- SCH in the presence of GF120918. Parameter estimates recovered from fitting the differential equations based on the model scheme in Fig. 4.1B to these data are listed in Table 4.1. CL_{Bile} was significantly different between groups (F-value 38.2, $p<0.0001$). The effect of Mrp2 status (WT vs. TR^-) was statistically significant in the absence and presence of GF120918, while the effect of GF120918 was statistically significant in WT hepatocytes but not in the TR^- hepatocytes. The CL_{BL} term was significantly different between groups (F-value=3.92, $p<0.048$). However, the individual effect of animal and GF120918 failed to reach significance after correcting for multiple comparisons. There was a trend toward decreased CL_{Uptake} and increased CL_{BL} in TR^- compared to WT hepatocytes in both the absence and presence of GF120918. Interestingly, GF120918 tended to decrease both CL_{Uptake} and CL_{BL} in WT and TR^- SCH. The K_{Flux} term was significantly different between groups (F-value=7.22, $p<0.01$); K_{Flux} was significantly increased in TR^- SCH in the absence of GF120918. The effect of GF120918 was statistically significant in TR^- but not WT SCH. Importantly, parameter estimates revealed that CL_{BL} and CL_{Bile} have a similar contribution to the total cellular excretion of RSV in WT SCH in the absence of GF120918.

Uptake of 1 μM RSV and subsequent efflux was examined in SCH from one human liver (Fig. 4.5). Parameter estimates recovered from fitting the differential equations based on the model scheme depicted in Fig. 4.1B to these data are listed in Table 4.1. CL_{Uptake} was at least an order of magnitude greater than the efflux pathways (CL_{BL} and CL_{Bile}), which were of similar magnitude; CL_{BL} was approximately 2-fold greater than CL_{Bile}. K_{Flux} was similar to the value observed in rat SCH.

IPLs

Outflow perfusate concentrations of RSV ranged from 0.003 to 0.23 μM in WT and TR$^-$ IPLs. The rates of RSV appearance in bile and outflow perfusate are plotted in Fig. 4.6; recovery of RSV and the pentanoic acid metabolite at the end of the perfusion are summarized in Fig. 4.7. Interestingly, the initial appearance rate of RSV in the outflow perfusate was reduced in TR$^-$ IPLs (Fig 4.6.C and D). Addition of GF120918 did not reduce further the appearance rate of RSV in outflow perfusate of TR$^-$ IPLs. The recovery of RSV in perfusate tended to be reduced in TR$^-$ compared to WT livers in the absence of GF120918, and also by GF120918 in WT livers (F-value=5.54, p=0.039). However, the individual effects of Mrp2 status and GF120918 failed to reach significance after correcting for multiple comparisons. Biliary excretion of RSV was not affected by GF120918 in WT livers, while the effect of GF120918 on reduced biliary recovery in TR$^-$ IPLs was statistically significant. The effect of Mrp2 status on RSV biliary excretion was statistically significant in the presence of GF120918, but not in the absence of GF120918. The recovery of RSV in liver tissue at the end of the 90-min perfusion was significantly greater in TR$^-$ compared to WT livers in the absence and presence of GF120918 (Fig. 4.7). Total recovery of the dose in perfusate, bile and liver tissue at the end of the 90-min studies was nearly complete following perfusion of WT livers, and reduced significantly in TR$^-$ livers in the absence and presence of GF120918. This reduction in total recovery was offset, in part, by the presence of the pentanoic acid metabolite in TR$^-$ liver tissue. Concentrations of the pentanoic acid metabolite were low in perfusate and bile samples, representing <2% of the total dose over the course of the study. As such, the pentanoic acid metabolite was reported only in the liver tissue. The pentanoic acid derivative comprised approximately 40% of total RSV content in TR$^-$ liver tissue, or 16% of the administered RSV, at the end of the perfusion; no other specific metabolites were identified by LC-MS/MS.

Parameter estimates recovered from fitting the differential equations based on the model scheme depicted in Fig. 4.2 to the data are listed in Table 4.2. The estimated maximal velocity (V_{max}) of the biliary excretion process and resulting biliary clearance of RSV ($CL_{Bile} = V_{max}/K_m$) were significantly reduced in TR$^-$ compared to WT IPLs in the absence and presence of GF120918. GF120918 reduced

V_{max} significantly in TR^- but not WT IPLs. CL_{BL} was significantly greater in WT compared to TR^- livers in the absence of GF120918. GF120918 tended to reduce CL_{BL} in WT IPLs, with no additional effect in TR^- IPLs. The CL_{Met} and CL_{Other} tended to be increased in TR^- compared to WT IPLs, and the presence of GF120918 also tended to increase the metabolic clearance ($F=5.62$, $p=0.023$ and $F=4.57$, $p=0.038$, for CL_{Met} and CL_{Other}, respectively; differences failed to reach significance after correcting for multiple comparisons). Comparing transport-mediated clearance rates between WT (Control) SCH and IPL data (Tables 4.1 and 4.2) resulted in empirical scaling factors of 4.2 for CL_{Uptake} (40 mL/min/g liver in IPL vs. 9.5 mL/min/g liver in SCH), 6.4 for CL_{BL} (0.21 vs. 1.4 mL/min/g liver in SCH compared to IPLs), and 1.1 [0.23 mL/min/g liver in SCH vs. 0.26 mL/min/g liver (V_{max}/K_m) in IPLs] for CL_{Bile}.

MRP3- and MRP4-Mediated Transport in Membrane Vesicles

The inhibitory potential and substrate specificity of RSV for MRP3 and MRP4 was evaluated using membrane vesicles prepared from non-transfected (NT) and MRP-overexpressing HEK293 cells. Pilot studies confirmed ATP-dependent uptake was linear up to 5 and 2 min for the prototypical MRP3 and MRP4 probe substrates, $E_2$17G and DHEAS, respectively (data not shown). ATP-dependent uptake determined at 1 min was concentration-dependent with a K_m and V_{max} of 23±5 μM and 1700±200 pmol/min/mg protein, respectively, for $E_2$17G, and 2.9±0.2 μM and 390±40 pmol/min/mg protein, respectively, for DHEAS (mean±SD). Co-incubation with 50 μM RSV inhibited ATP-dependent transport of the prototypical MRP3 and MRP4 probe substrates, $E_2$17G (20 μM) and DHEAS (2 μM), by 76 and 88%, respectively (Fig. 4.8A and B). By comparison, ATP-dependent transport of $E_2$17G (20 μM) and DHEAS (2 μM) was 77 and 88% lower in NT membrane vesicles, and decreased by 98 and 105% in the presence of the potent pan-MRP inhibitor, MK571 (50 μM, Fig. 4.8A and B). ATP-dependent transport of 0.1 μM RSV was linear up to ~1 min, and was greater in membrane vesicles from HEK293 cells overexpressing MRP4 and MRP3 compared to NT cells (Fig. 4.8C). Uptake of RSV at 1 min in membrane vesicles from MRP4-overexpressing cells was concentration-dependent with a K_m and V_{max} of 21±7 μM and 1140±210 pmol/min/mg protein for MRP4 (Fig. 4.8D). Despite inhibition of MRP3-mediated $E_2$17G transport by 50 μM RSV (Fig. 4.8A) and apparent MRP3-dependent RSV uptake at low

concentrations (Fig. 4.8C), ATP-dependent uptake of RSV over a range of concentrations in membrane vesicles from MRP3-overexpressing cells was not significantly greater than uptake into vesicles prepared from NT cells (data not shown).

Discussion

The present studies suggest for the first time a significant role for basolateral efflux in the hepatobiliary disposition of RSV in rat and human hepatocytes. Uptake and efflux profiles observed in SCH with tight junction modulation extended over 35 min, and the behavior of the system under these conditions, also has not been reported previously. The novel uptake and efflux protocol in SCH, combined with pharmacokinetic modeling, revealed that CL_{BL} and CL_{Bile} represent alternative pathways with a quantitatively similar contribution to the total hepatocellular excretion of RSV under normal conditions in rat and human SCH. The effects of modulating Mrp2 and Bcrp function using TR^- SCH and GF120918, respectively, were consistent with IPL data and previous reports suggesting that each transporter contributes to a similar degree, and together comprise approximately 90-95% of RSV biliary excretion in rats. GF120918 tended to inhibit both CL_{Uptake} and CL_{BL} in rat SCH experiments, consistent with the promiscuous nature, or overlap in affinity, of transporter substrates and inhibitors. In TR^- rat SCH, CL_{Uptake} tended to decrease and CL_{BL} tended to increase, consistent with the hepatoprotective compensatory changes that would be expected in the setting of impaired biliary excretion. Indeed, it has been shown that Ntcp expression is downregulated and Mrp3 upregulated in TR^- compared to WT livers (33).

It is clear that differences exist in the handling of RSV by WT and TR^- livers beyond the expected decrease in biliary excretion rate resulting from loss of Mrp2 function (Figs. 4.6 and 4.7, Table 4.2). In particular, there is a delay in the attainment of steady-state appearance rate of RSV in the outflow perfusate of TR^- livers during the loading phase. Qualitatively, this would be expected assuming RSV accumulation in the liver and saturation of the biliary excretion capacity, as represented by the model structure and resulting parameter estimates (Fig. 4.2, Table 4.2). Quantitatively, it is curious that the excretion rate in the outflow perfusate remains lower in TR^- compared to WT throughout the loading

phase despite increased hepatocellular concentrations driving the efflux process(es). This finding is consistent with the hypothesis that the basolateral efflux of RSV may be impaired in TR^- livers. Indeed, the CL_{BL} was significantly reduced in TR^- compared to WT livers in the absence of GF120918. Basolateral efflux is regarded commonly as a compensatory route of elimination to protect hepatocytes in the setting of cholestasis or otherwise impaired biliary excretion (17-20). Proteins that have been suggested to have compensatory/hepatoprotective roles in this manner include Mrp3 and Mrp4, which are known to be upregulated in animals with impaired biliary excretion; Mrp3 exhibits increased expression in TR^- rat livers, and Mrp4 expression is increased following bile duct ligation (33; 34). Therefore, it would be expected that basolateral efflux and resulting outflow perfusate rates would be greater in TR^- livers. Impaired basolateral efflux of RSV in TR^- IPLs could be attributed to accumulation of endogenous anions (*e.g.*, bilirubin glucuronides, glutathione, and bile acids) resulting from loss-of-function of Mrp2 (35); these anions would be expected to compete with RSV for basolateral excretion(36). The absence of impaired basolateral efflux in TR^- SCH may be due to decreased accumulation of endogenous anions *in vitro*. Although the SCH system retains much of the synthetic function of the liver *in vivo*, bile acids and bilirubin are extensively recycled from the intestine, which is absent in the SCH model (37; 38). Exogenous bile acid administration in SCH has been reported to amplify the toxicity of known BSEP inhibitors (39). Scaling of transporter-mediated RSV clearance values between SCH and IPLs was confined to the WT Control conditions because of the differences observed between SCH and IPLs in the effect of Mrp2 status on CL_{BL}. CL_{BL} was decreased ~6-fold (0.21 vs. 1.4 mL/min/g liver) in SCH compared to IPLs, suggesting a corresponding decrease in expression of the transporter(s) mediating basolateral efflux of RSV; available data suggest that Mrp4 protein expression remains constant or is decreased over days in culture(23). The ~4-fold decrease in CL_{Uptake} in SCH compared to IPLs (9.5 vs. 40 mL/min/g liver) corresponds with reduced Oatp expression over days in culture in rat SCH(40). Interestingly, the CL_{Bile} translated almost directly [0.23 mL/min/g liver in SCH vs. 0.26 mL/min/g liver (V_{max}/K_m) in IPLs]. Although Bcrp and Mrp2 protein expression have been reported to increase and

decrease, respectively (~2-3 fold) in SCH over days in culture, these changes may offset each other with respect to RSV biliary clearance(41; 42).

Following i.v. administration of RSV to healthy humans, approximately 72% of the dose was eliminated by the liver, with an estimated hepatic extraction (E_h) of 0.63 (1). Similarly, the mean E_h observed at steady-state (30-60 min) in WT rat IPLs without GF120918 in the current studies was 0.66. However, perfusate outflow profiles in the current studies using WT and TR^- rat IPLs clearly indicated that RSV is almost completely extracted by the liver in a single-pass, and that appearance in outflow perfusate is a result of basolateral efflux. This is evident from the low initial appearance rate of RSV in outflow perfusate, especially from the TR^- IPLs, and the absence of a "drop-off" in outflow perfusate upon switching to blank buffer for the 30-min efflux phase in single-pass IPL studies(25; 43). As evident from the disparate initial appearance rate in outflow perfusate, initial estimates of CL_{Uptake} were up to 5-fold greater in TR^- compared to WT rat liver preparations. Uptake in TR^- livers would not be expected to be greater than WT; if anything, uptake mechanisms (*e.g.*, Ntcp) are known to be downregulated in a compensatory/hepatoprotective manner in relation to loss-of-function of Mrp2 (33). Rather, it was assumed that rapid attainment of steady-state in the outflow perfusate of WT liver preparations precluded accurate estimation of the initial uptake rate. These studies demonstrate for the first time the important role of hepatic basolateral efflux in mediating systemic exposure of RSV. The importance of basolateral efflux of RSV is further documented by inhibition of this efflux pathway, either by GF120918 in WT IPLs, or in TR^- compared to WT IPLs.

RSV is not metabolized extensively in humans; approximately 90% of the dose was recovered as parent drug (44). The primary metabolite is N-desmethyl-RSV, formed by CYP2C9. In rats, RSV metabolism plays a larger role, with metabolites accounting for ~50% of plasma and liver content(2; 45). Biotransformation of RSV in rats is not mediated extensively by Cyps. Rather, the primary metabolite is the pentanoic acid derivative, presumably formed by β-oxidation of the fatty acid chain (45). Results of the present study confirmed the presence of RSV pentanoic acid as the primary metabolite, contributing ~40% of total content in both WT and TR^- livers, consistent with previous reports (2; 45). Measurement

of total radioactivity in SCH experiments precluded comparisons between IPL and *in vitro* studies. However, the increase in hepatic accumulation of RSV and the pentanoic acid metabolite of RSV in TR^- compared to WT IPLs is consistent with impaired RSV excretion and "shunting" to the metabolic pathway(s); alternatively, excretion of RSV pentanoic acid may be impaired in TR^- rat hepatocytes. A similar effect of increased hepatic exposure was observed for erythromycin and its N-desmethyl metabolite when co-administered with GF120918 in cultured hepatocytes and whole animals (46).

Interestingly, in a whole animal study with WT Sprague-Dawley and Mrp2-deficient Eisai hyperbilirubinemic rats (EHBR), liver concentrations of RSV were not significantly increased in EHBR animals (2). Biliary clearance (liver-to-bile) was decreased, and systemic exposure was increased more than 3-fold. While this may suggest efficient hepatic basolateral efflux of RSV in the setting of impaired biliary excretion, decreased renal elimination in EHBR rats may contribute to the increased systemic exposure. An important advantage of the IPL model is that the role of hepatic processes can be evaluated in isolation from other organ systems. RSV disposition was reported recently in recirculating perfused WT and TR^- IPLs (5). Increased tissue accumulation was observed in TR^- compared to WT livers, similar to the present study. However, the role of basolateral excretion was not considered. Indeed, the pharmacokinetic model used to analyze and interpret the data did not allow for translocation of RSV from liver tissue back into perfusate. The single-pass IPL system used in the present study allows for direct evaluation of basolateral excretion from liver to perfusate.

Finally, two candidate transporters that could be responsible for the basolateral excretion of RSV were examined in the membrane vesicle system. RSV (50 μM) inhibited the transport of protypical substrates, $E_2$17βG and DHEAS, in membrane vesicles from HEK293 cells overexpressing MRP3 and MRP4, respectively, at a similar level as the prototypical pan-MRP inhibitor MK-571 (Figs. 4.8A and B). Further studies were performed to evaluate RSV as a substrate, showing that time- and ATP-dependent uptake in membrane vesicles prepared from MRP3- and MRP4-overexpressing cells was greater than in vesicles from non-transfected (NT) cells (Fig. 4.8C). Based on kinetic analysis, RSV was transported by MRP4 with a Km ~20 μM. Unbound RSV concentrations in human liver are likely to be below this K_m

value, despite efficient hepatic uptake and accumulation. The mean steady-state RSV total plasma C_{max} is ~50 ng/mL (0.1 μM) following an 80 mg daily oral dose (47; 48), while accumulation of total RSV (Kp) in human and rat hepatocytes *in vitro* is ~20-fold in this and other reports (31), and accumulation in rat liver *in vivo* is ~20-45 fold (45). The involvement of other transport proteins cannot be ruled out. In fact, SCH and IPL data in the present studies suggest that ~50% of basolateral efflux in rat liver is mediated by mechanism(s) unaffected by GF120918 or intracellular accumulation of endogenous anions in TR^- rat hepatocytes.

A novel uptake and efflux protocol was developed in SCH that revealed the significant contribution of basolateral efflux to the hepatocellular excretion of RSV in rat and human hepatocytes. When combined with a modeling approach, this experimental paradigm can be used to elucidate the relative contribution of basolateral efflux clearance as well as biliary clearance. As shown in SCH and IPLs, basolateral efflux of RSV is altered by co-administration with GF120918, and in TR^- hepatocytes. RSV is a substrate for human MRP4, which likely contributes to the basolateral efflux of RSV in human liver. MRP4-mediated efflux of RSV may be impaired due to patient-specific factors such as DDIs, genetic variation and/or disease states. Altered function may lead to changes in systemic and hepatic exposure of RSV, with implications for the pharmacologic effect and safety of this commonly-used drug.

Table 4.1. Summary of recovered parameter estimates based on the model scheme depicted in Figure 4.1B describing rosuvastatin disposition in rat wild-type (WT) and Mrp2-deficient (TR^-) sandwich-cultured hepatocytes (SCH) in the absence (Control) or presence of GF120918, and rosuvastatin disposition in human SCH.

	CL_{Uptake}	CL_{BL}	CL_{Bile}	K_{Flux}
Conditions:	*(mL/min/g liver)*	*(mL/min/g liver)*	*(mL/min/g liver)*	*(min^{-1})*
WT SCH				
Control	9.5 ± 2.7	0.21 ± 0.07	0.23 ± 0.04	0.057 ± 0.029
+GF120918	7.9 ± 1.0	0.16 ± 0.03	0.079 ± 0.017†	0.046 ± 0.007
TR^- SCH				
Control	7.6 ± 1.2	0.34 ± 0.09	0.089 ± 0.025*	0.093 ± 0.008*
+GF120918	6.6 ± 1.6	0.27 ± 0.06	0.018 ± 0.015*	0.049 ± 0.027†
Human SCH	1.8 ± 0.1	0.095 ± 0.013	0.053 ± 0.010	0.042 ± 0.008

Data are presented as mean ± SD of individual fits from n=3-4 rat SCH preparations, or ± SD of the parameter estimate from a single preparation of human SCH

* $p<0.05$, adjusted: Effect of Mrp2 status (WT vs. TR^-) is statistically significant within the same level of inhibitor (+ or –GF120918); $^{\dagger}p<0.05$, adjusted: Effect of GF120918 (absence vs, presence) is statistically significant within the same level of Mrp2 status (WT or TR^-).

Table 4.2. Summary of recovered parameter estimates based on the model scheme depicted in Figure 4.2 describing rosuvastatin disposition in wild-type (WT) and Mrp2-deficient (TR^-) isolated perfused livers in the absence (Control) or presence of GF120918.

	CL_{BL}	V_{max}	CL_{Met}	CL_{Other}
Conditions:	*(mL/min/g liver)*	*(nmol/min/g liver)*	*(µL/min/g liver)*	*(µL/min/g liver)*
WT				
Control	1.4 ± 0.3	2.6 ± 1.2	0.83 ± 0.25	16 ± 22
+GF120918	0.83 ± 0.29	3.2 ± 0.7	1.3 ± 0.5	24 ± 34
TR^-				
Control	0.55 ± 0.19*	1.3 ± 0.1*	3.2 ± 1.5	46 ± 13
+GF120918	0.51 ± 0.13	0.26 ± 0.08*†	4.2 ± 1.7	85 ± 27

Mean ± SD of n=3 livers;

CL_{Uptake} was fixed at 40 mL/min/g liver (Nezasa et al., 2003,Yabe et al., 2011);
K_m was fixed at 10 µM based on the reported affinity of RSV for Mrp2 and Bcrp (Deng et al., 2008,Huang et al., 2006).

*$p<0.05$, adjusted: Effect of Mrp2 status (WT vs. TR^-) is statistically significant within the same level of inhibitor (+ or –GF120918); † $p<0.05$, adjusted: Effect of GF120918 (absence vs, presence) is statistically significant within the same level of Mrp2 status (WT or TR^-),.

Figure 4.1. A. Scheme depicting uptake/efflux protocol in sandwich-cultured hepatocytes (SCH). Gray shading represents inclusion of substrate in the Hanks' Balanced Salt Solution (HBSS) buffer during the uptake phase. **B.** Model schemes depicting the disposition of rosuvastatin in SCH studies. X denotes mass of rosuvastatin, V denotes compartmental volume, C denotes compartmental concentration; subscripts on mass, bile and concentration terms denote the corresponding compartment in the model scheme; superscripts represent the presence (+; intact tight junctions, cells+bile) and absence (-; modulated tight juntions, cells) of Ca^{2+} in the incubation buffer; clearance values are designated as CL_{Uptake} for uptake from buffer into hepatocytes, CL_{BL} for efflux from hepatocytes into buffer, CL_{Bile} for efflux from hepatpocytes into bile spaces, and K_{Flux} for flux from bile spaces into buffer.

A.

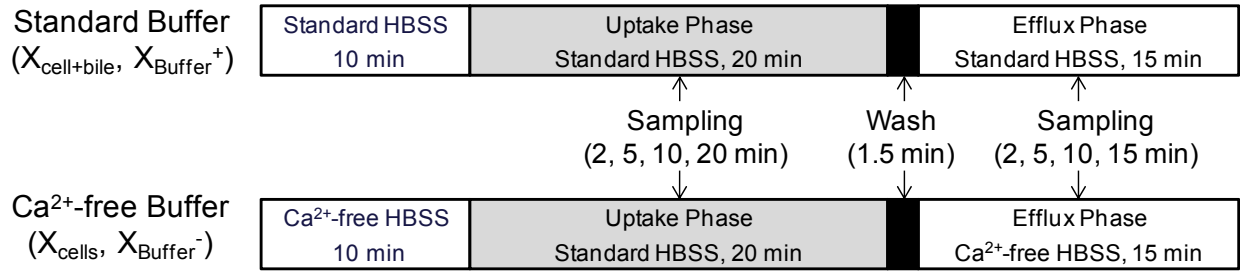

B.

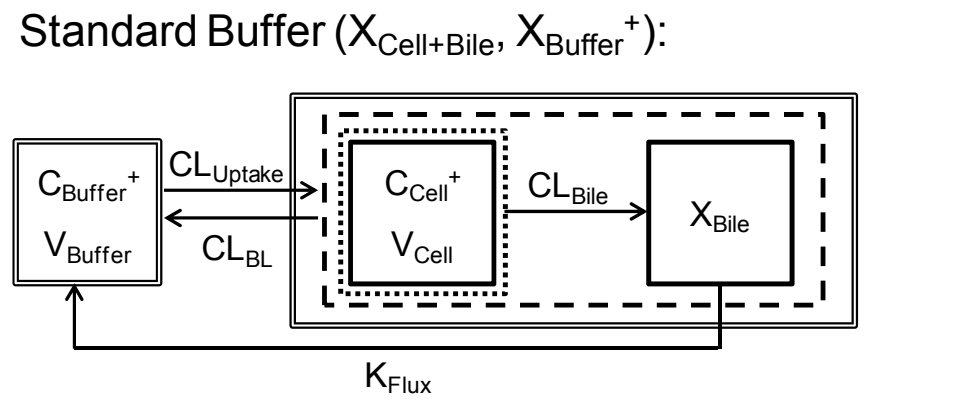

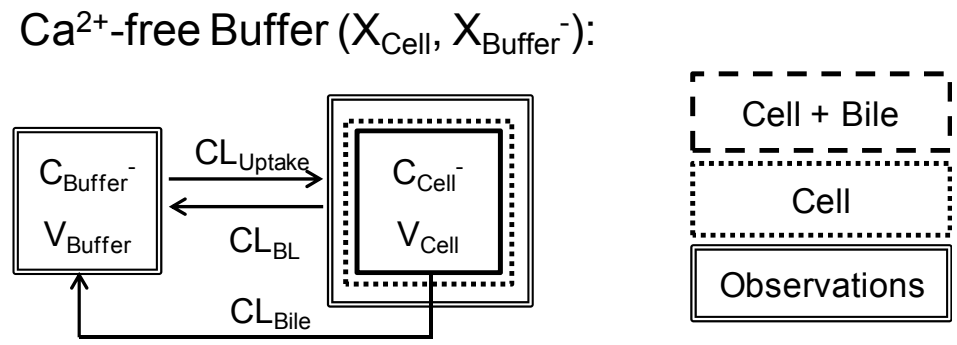

Figure 4.2. A. Scheme depicting the experimental protocol in isolated perfused livers (IPLs). **B.** Model scheme depicting the disposition of rosuvastatin in rat IPL studies. Q denotes the flow rate of perfusate, X denotes mass of RSV, V denotes compartmental volume, C denotes compartmental concentration; subscripts on mass, bile and concentration terms denote the corresponding compartment in the model scheme, as follows: inflow perfusate (in), outflow perfusate (out), extracellular compartment (EC, assumed to be in rapid equilibration with the perfusate), intracellular liver compartment (L), and bile (Bile); clearance values are designated as CL_{Uptake} for RSV uptake from the extracellular to intracellular liver compartment, CL_{BL} for RSV efflux from the intracellular to extracellular liver compartment, CL_{Met} for conversion from RSV to the pentanoic acid metabolite, and CL_{Other} for RSV conversion to metabolites other than the pentanoic acid derivative; V_{max} is the maximum velocity of RSV biliary excretion, K_m is the RSV concentration resulting in half-maximal biliary excretion.

A.

Equilibration Phase	Loading Phase	Efflux Phase
15 min	+ 0.5 M RSV, 60 min	30 min

B.

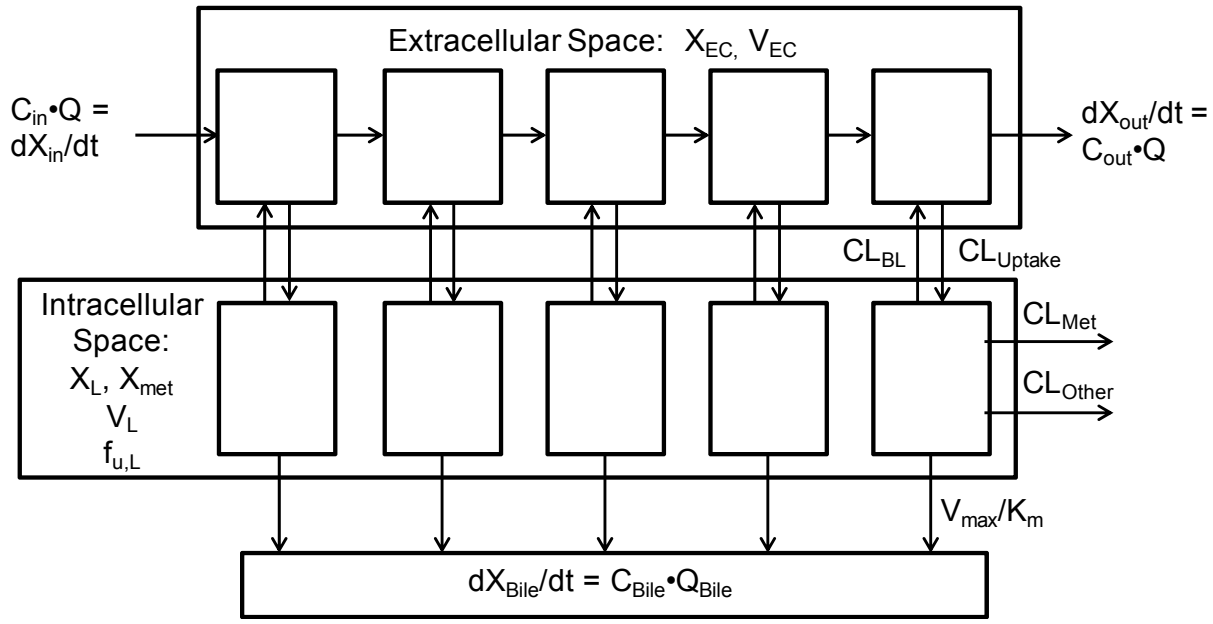

Figure 4.3. A. Extracted ion current (XIC) chromatograph of rosuvastatin (blue, 482.2 0.05 amu), rosuvastatin pentanoic acid (purple, 422.20 0.05 amu), and d_6-rosuvastatin (internal standard, red, 488.20 0.05 amu) in TR^- Control liver tissue compared to blank liver tissue (inset). **B.** High resolution product ion spectra of rosuvastatin (top), d_6-rosuvastatin (middle), and rosuvastatin pentanoic acid (bottom). Note the expected Δ6 amu between the products of rosuvastatin and its internal standard (258.14/264.17, 300.15/306.19, 314.14/320.20, 378.12/384.16, 404.19/410.23, 422.15/428.19 and 446.15/452.19). Common product ions formed from rosuvastatin and the pentanoic acid metabolite (242.10, 256.12 and 270.17 amu) are independent of the changes within the carboxylic acid side chain. Additionally, the paired product ions, 402.19/404.19 for rosuvastatin and 342.17/344.17 for the metabolite, represent loss of CH_4O_2S while maintaining the Δ60 amu ($C_2H_4O_2$) between rosuvastatin and the pentanoic acid metabolite.

A.

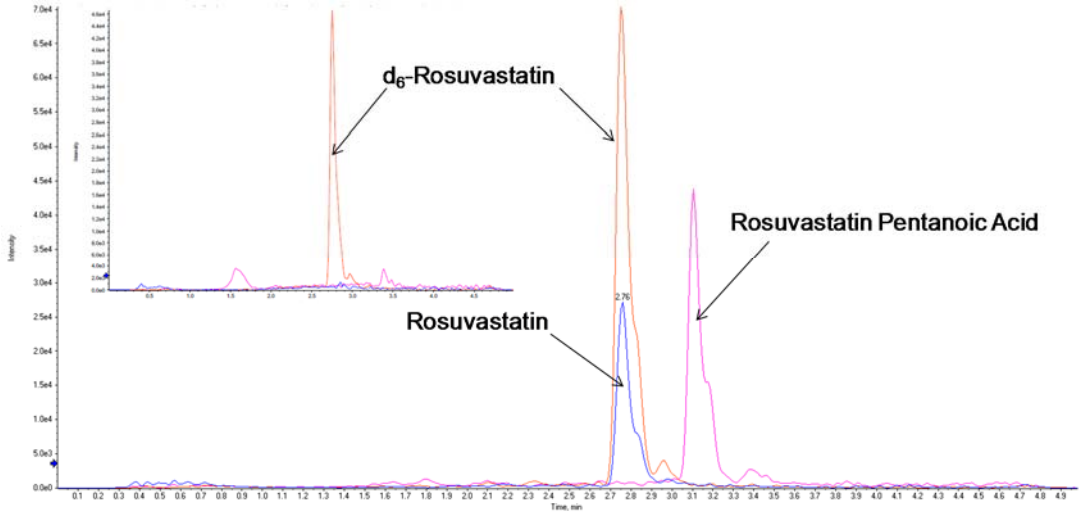

B.

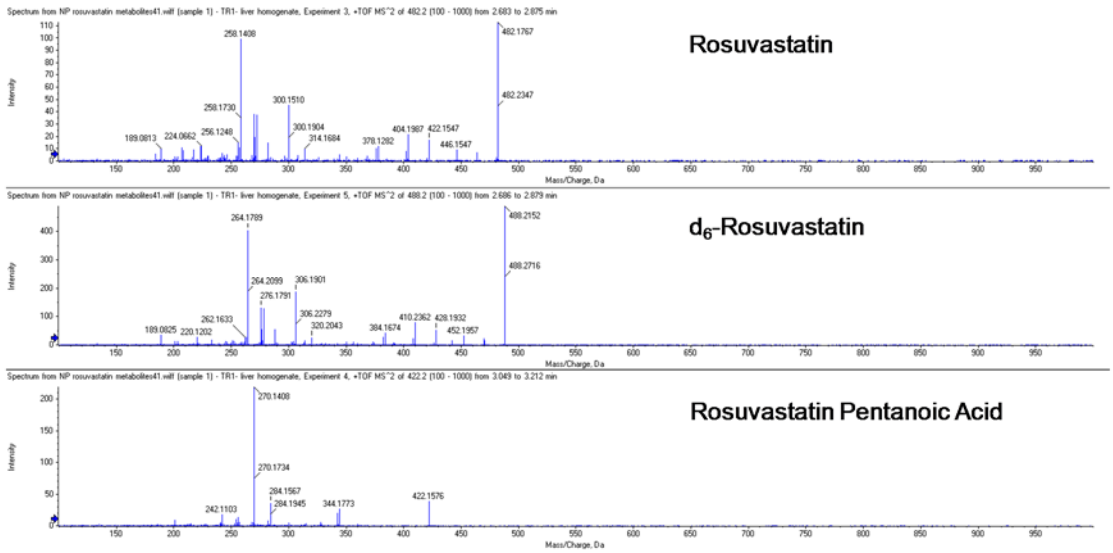

Figure 4.4. [^{3}H]Rosuvastatin (RSV) mass versus time data in wild-type (WT) and Mrp2-deficient (TR$^-$) rat SCH in the absence (Control) or presence of GF120918 during the uptake and efflux phase. Closed symbols/solid lines represent [^{3}H]RSV in cells+bile (standard HBSS) and open symbols/dashed lines represent [^{3}H]RSV in cells (-Ca^{2+} HBSS). The simulated mass-time profiles were generated from the relevant equations based on the model scheme depicted in Figure 4.1B and the final parameter estimates reported in Table 4.1. Data (pmol/well) are reported as mean±SEM (n=3-4 SCH preparations in triplicate per group).

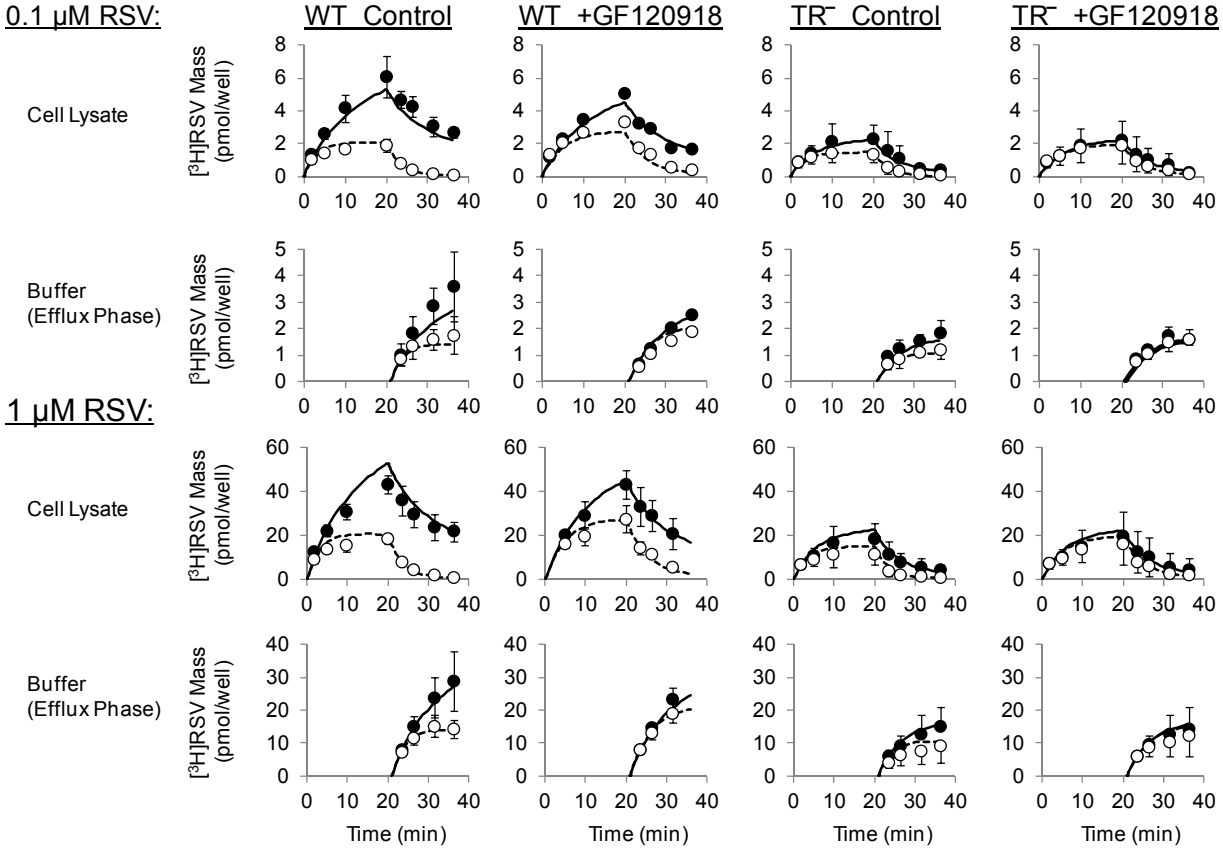

Figure 4.5. [^{3}H]Rosuvastatin (RSV) mass versus time data in human SCH during the uptake and efflux phase. Closed symbols/solid lines represent [^{3}H]RSV mass in cells+bile (standard HBSS) and open symbols/dashed lines represent [^{3}H]RSV mass in cells (-Ca^{2+} HBSS). The simulated mass-time profiles were generated from the relevant equations based on the model scheme depicted in Figure 4.1B and the final parameter estimates reported in Table 4.1. Data (pmol/well) are reported as mean±SD (n=1 human SCH preparation, in triplicate).

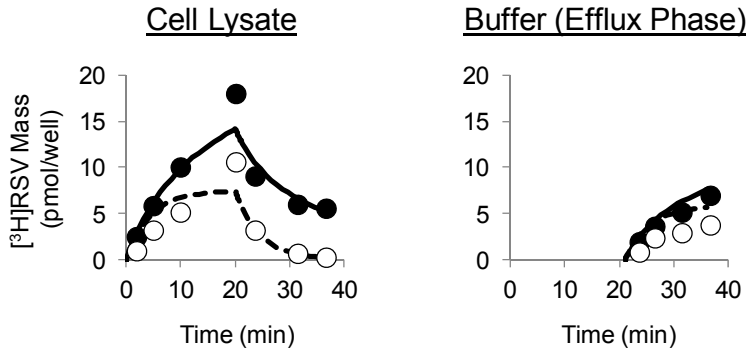

Figure 4.6. Rosuvastatin (RSV) biliary excretion (**A.** and **B.**) and outflow perfusate (**C.** and **D.**) rate versus time data in isolated perfused livers from wild-type (WT: **A.** and **C.**) and Mrp2-deficient (TR^-: **B.** and **D.**) rats in the absence (open symbols; dashed line) or presence (closed symbols; solid line) of GF120918. The simulated excretion rate-time profiles were generated from the relevant equations based on the model scheme in Figure 4.2 and the final parameter estimates reported in Table 4.2. Data are presented as mean±SD (n=3 livers).

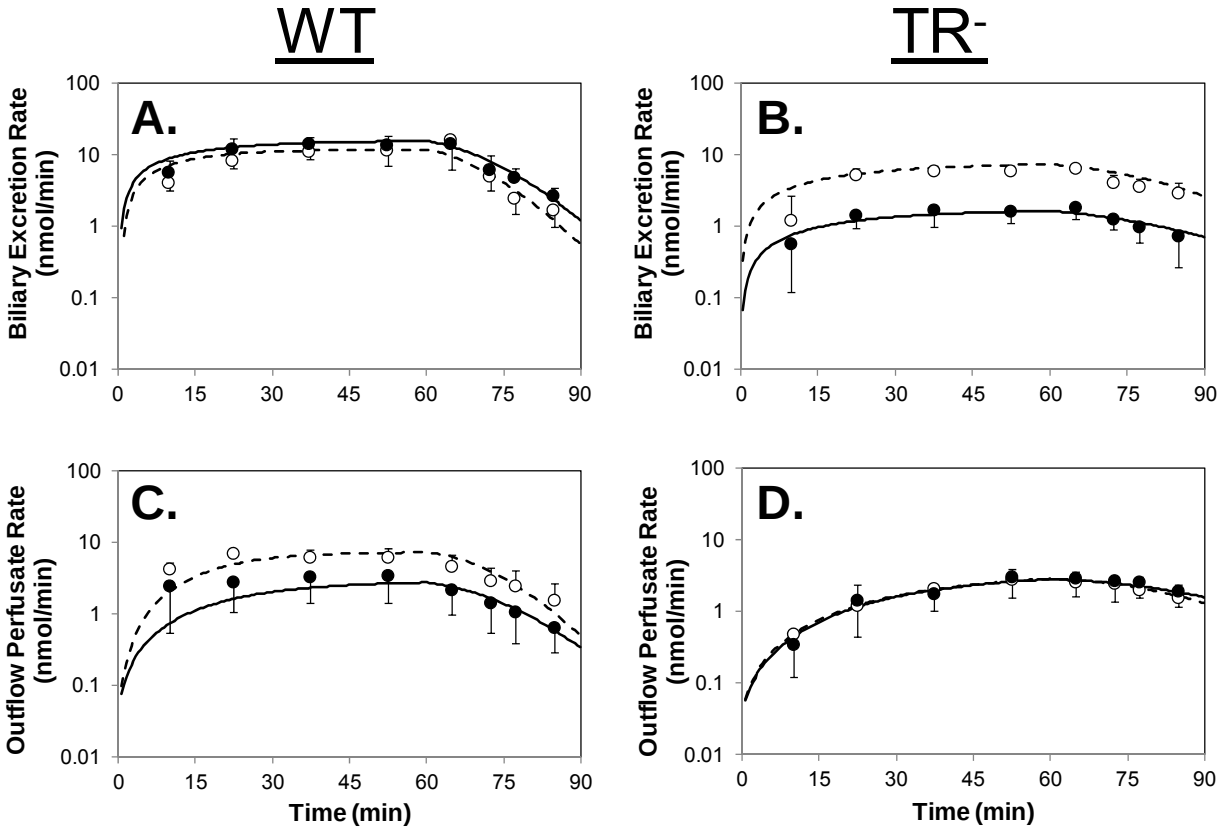

Figure 4.7. Recovery of rosuvastatin (solid bars) and rosuvastatin pentanoic acid (gray bars) in perfusate, liver and bile, as well as total recovery from wild-type (WT) and Mrp2-deficient (TR^-) isolated perfused livers in the absence or presence of GF120918. Data are reported as the mean percentage ± SD based on the total dose administered to each liver (n=3 per group) recovered at the end of the 90-min perfusion. For recovery of parent drug: *$p<0.05$, adjusted: Effect of Mrp2 status (WT vs. TR^-) is statistically significant within the same level of inhibitor (+ or –GF120918),; † $p<0.05$, adjusted: Effect of GF120918 (absence vs, presence) is statistically significant within the same level of Mrp2 status (WT or TR^-). For recovery of the metabolite: ‡$p<0.05$, adjusted: Effect of Mrp2 status (WT vs. TR^-) is statistically significant within the same level of inhibitor (+ or –GF120918).

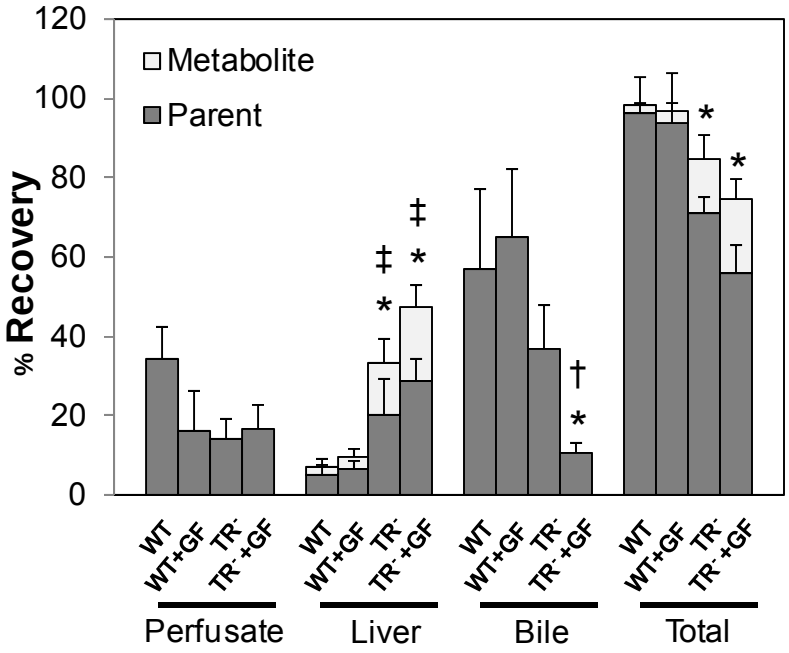

Figure 4.8. ATP-dependent uptake of (**A**) 20 μM [^{3}H]$E_2$17G (MRP3) or (**B**) 2 μM [^{3}H]DHEAS (MRP4) in membrane vesicles from non-transfected (NT) and MRP3- or MRP4-overexpressing (control) HEK293 cells, respectively, and inhibition by 50 μM rosuvastatin (RSV) and MK571. (**C**) Time-dependent transport of [^{3}H]RSV in membrane vesicles from NT (●) MRP3- (▲) and MRP4-transfected (■) cells. (**D**) Concentration-dependent transport of RSV in membrane vesicles from MRP4-transfected HEK293 cells, and corresponding V_{max} and K_m values obtained from nonlinear regression analysis. In all cases, data represent mean ± SD of triplicate measurements in a single experiment.

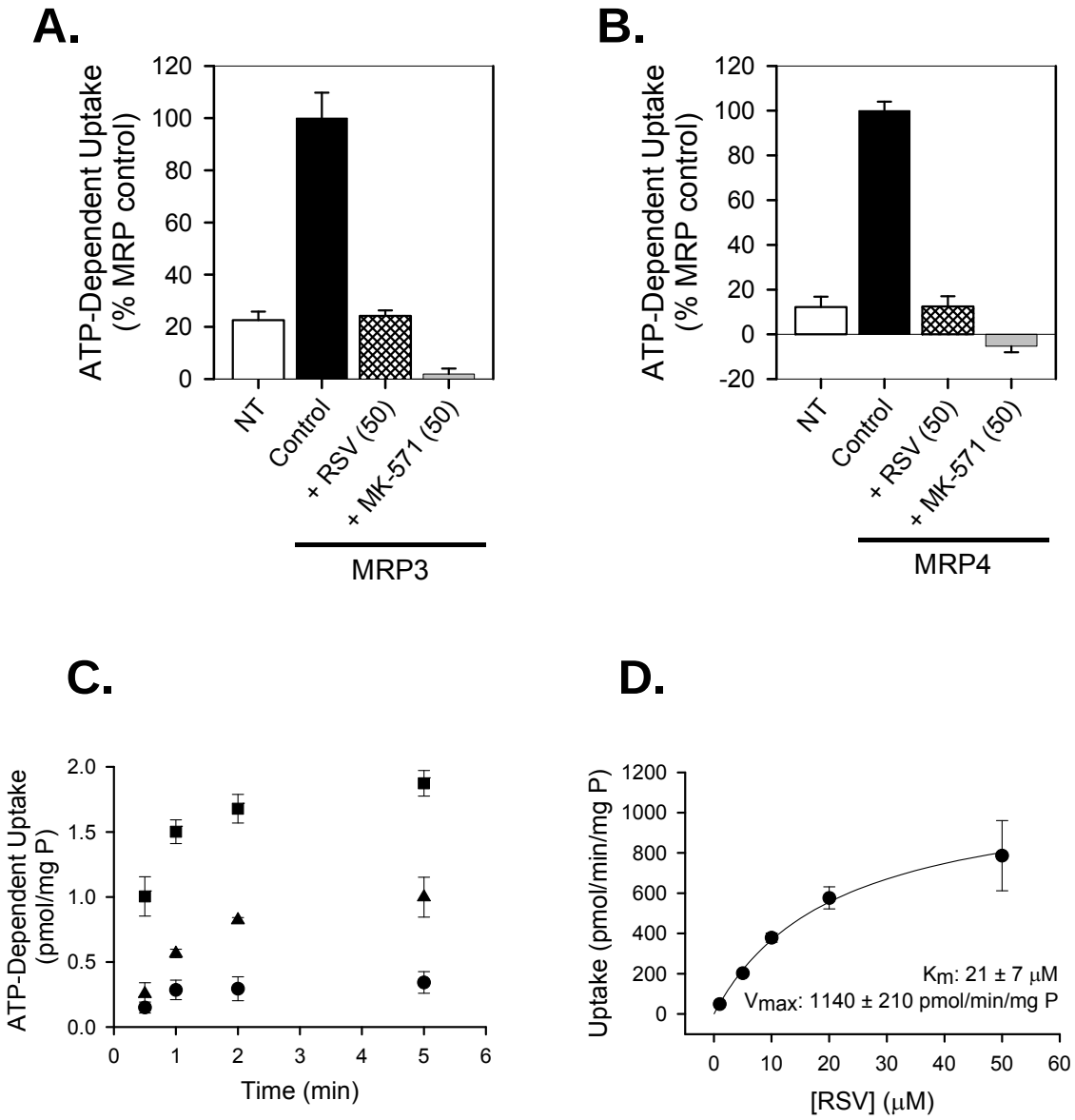

REFERENCES

1. Martin PD, Warwick MJ, Dane AL, Brindley C, Short T. 2003. Absolute oral bioavailability of rosuvastatin in healthy white adult male volunteers. *Clin Ther* 25:2553-63

2. Kitamura S, Maeda K, Wang Y, Sugiyama Y. 2008. Involvement of multiple transporters in the hepatobiliary transport of rosuvastatin. *Drug metabolism and disposition: the biological fate of chemicals* 36:2014-23

3. Ho RH, Tirona RG, Leake BF, Glaeser H, Lee W, et al. 2006. Drug and bile acid transporters in rosuvastatin hepatic uptake: function, expression, and pharmacogenetics. *Gastroenterology* 130:1793-806

4. Abe K, Bridges AS, Yue W, Brouwer KL. 2008. In vitro biliary clearance of angiotensin II receptor blockers and 3-hydroxy-3-methylglutaryl-coenzyme A reductase inhibitors in sandwich-cultured rat hepatocytes: comparison with in vivo biliary clearance. *The Journal of pharmacology and experimental therapeutics* 326:983-90

5. Hobbs M, Parker C, Birch H, Kenworthy K. 2012. Understanding the interplay of drug transporters involved in the disposition of rosuvastatin in the isolated perfused rat liver using a physiologically-based pharmacokinetic model. *Xenobiotica; the fate of foreign compounds in biological systems* 42:327-38

6. Jemnitz K, Veres Z, Tugyi R, Vereczkey L. 2010. Biliary efflux transporters involved in the clearance of rosuvastatin in sandwich culture of primary rat hepatocytes. *Toxicol In Vitro* 24:605-10

7. Keskitalo JE, Zolk O, Fromm MF, Kurkinen KJ, Neuvonen PJ, Niemi M. 2009. ABCG2 polymorphism markedly affects the pharmacokinetics of atorvastatin and rosuvastatin. *Clinical pharmacology and therapeutics* 86:197-203

8. Huang L, Wang Y, Grimm S. 2006. ATP-dependent transport of rosuvastatin in membrane vesicles expressing breast cancer resistance protein. *Drug metabolism and disposition: the biological fate of chemicals* 34:738-42

9. Simonson SG, Raza A, Martin PD, Mitchell PD, Jarcho JA, et al. 2004. Rosuvastatin pharmacokinetics in heart transplant recipients administered an antirejection regimen including cyclosporine. *Clinical pharmacology and therapeutics* 76:167-77

10. Schneck DW, Birmingham BK, Zalikowski JA, Mitchell PD, Wang Y, et al. 2004. The effect of gemfibrozil on the pharmacokinetics of rosuvastatin. *Clinical pharmacology and therapeutics* 75:455-63

11. Zhang W, Yu BN, He YJ, Fan L, Li Q, et al. 2006. Role of BCRP 421C>A polymorphism on rosuvastatin pharmacokinetics in healthy Chinese males. *Clinica chimica acta; international journal of clinical chemistry* 373:99-103

12. Kiser JJ, Gerber JG, Predhomme JA, Wolfe P, Flynn DM, Hoody DW. 2008. Drug/Drug interaction between lopinavir/ritonavir and rosuvastatin in healthy volunteers. *J Acquir Immune Defic Syndr* 47:570-8

13. Simonson SG, Martin PD, Mitchell P, Schneck DW, Lasseter KC, Warwick MJ. 2003. Pharmacokinetics and pharmacodynamics of rosuvastatin in subjects with hepatic impairment. *Eur J Clin Pharmacol* 58:669-75

14. Tomlinson B, Hu M, Lee VW, Lui SS, Chu TT, et al. 2010. ABCG2 polymorphism is associated with the low-density lipoprotein cholesterol response to rosuvastatin. *Clinical pharmacology and therapeutics* 87:558-62

15. Hamilton-Craig I. 2001. Statin-associated myopathy. *The Medical journal of Australia* 175:486-9

16. Thompson PD, Clarkson P, Karas RH. 2003. Statin-associated myopathy. *JAMA : the journal of the American Medical Association* 289:1681-90

17. Scheffer GL, Kool M, de Haas M, de Vree JM, Pijnenborg AC, et al. 2002. Tissue distribution and induction of human multidrug resistant protein 3. *Lab Invest* 82:193-201

18. Denk GU, Soroka CJ, Takeyama Y, Chen WS, Schuetz JD, Boyer JL. 2004. Multidrug resistance-associated protein 4 is up-regulated in liver but down-regulated in kidney in obstructive cholestasis in the rat. *Journal of hepatology* 40:585-91

19. Gradhand U, Lang T, Schaeffeler E, Glaeser H, Tegude H, et al. 2008. Variability in human hepatic MRP4 expression: influence of cholestasis and genotype. *The pharmacogenomics journal* 8:42-52

20. Chai J, He Y, Cai SY, Jiang Z, Wang H, et al. 2012. Elevated hepatic multidrug resistance-associated protein 3/ATP-binding cassette subfamily C 3 expression in human obstructive cholestasis is mediated through tumor necrosis factor alpha and c-Jun NH2-terminal kinase/stress-activated protein kinase-signaling pathway. *Hepatology* 55:1485-94

21. Ballatori N, Li N, Fang F, Boyer JL, Christian WV, Hammond CL. 2009. OST alpha-OST beta: a key membrane transporter of bile acids and conjugated steroids. *Frontiers in bioscience : a journal and virtual library* 14:2829-44

22. Zamek-Gliszczynski MJ, Kalvass JC, Pollack GM, Brouwer KL. 2009. Relationship between drug/metabolite exposure and impairment of excretory transport function. *Drug metabolism and disposition: the biological fate of chemicals* 37:386-90

23. Swift B, Pfeifer ND, Brouwer KL. 2010. Sandwich-cultured hepatocytes: an in vitro model to evaluate hepatobiliary transporter-based drug interactions and hepatotoxicity. *Drug metabolism reviews* 42:446-71

24. Brouwer KL, Thurman RG. 1996. Isolated perfused liver. *Pharmaceutical biotechnology* 8:161-92

25. Chandra P, Johnson BM, Zhang P, Pollack GM, Brouwer KL. 2005. Modulation of hepatic canalicular or basolateral transport proteins alters hepatobiliary disposition of a model organic anion in the isolated perfused rat liver. *Drug metabolism and disposition: the biological fate of chemicals* 33:1238-43

26. Leslie EM, Mao Q, Oleschuk CJ, Deeley RG, Cole SP. 2001. Modulation of multidrug resistance protein 1 (MRP1/ABCC1) transport and atpase activities by interaction with dietary flavonoids. *Molecular pharmacology* 59:1171-80

27. Ghibellini G, Leslie EM, Pollack GM, Brouwer KL. 2008. Use of tc-99m mebrofenin as a clinical probe to assess altered hepatobiliary transport: integration of in vitro, pharmacokinetic modeling, and simulation studies. *Pharmaceutical research* 25:1851-60

28. Lee JK, Brouwer KR. 2010. Determination of Intracellular Volume of Rat and Human Sandwich-Cultured Hepatocytes (Abstract ID 1595). *The Toxicologist, Supplement to Toxicological Sciences* 114:339

29. Watanabe T, Kusuhara H, Maeda K, Shitara Y, Sugiyama Y. 2009. Physiologically based pharmacokinetic modeling to predict transporter-mediated clearance and distribution of pravastatin in humans. *The Journal of pharmacology and experimental therapeutics* 328:652-62

30. Deng JW, Shon JH, Shin HJ, Park SJ, Yeo CW, et al. 2008. Effect of silymarin supplement on the pharmacokinetics of rosuvastatin. *Pharmaceutical research* 25:1807-14

31. Nezasa K, Higaki K, Takeuchi M, Nakano M, Koike M. 2003. Uptake of rosuvastatin by isolated rat hepatocytes: comparison with pravastatin. *Xenobiotica; the fate of foreign compounds in biological systems* 33:379-88

32. Yabe Y, Galetin A, Houston JB. 2011. Kinetic characterization of rat hepatic uptake of 16 actively transported drugs. *Drug metabolism and disposition: the biological fate of chemicals* 39:1808-14

33. Johnson BM, Zhang P, Schuetz JD, Brouwer KL. 2006. Characterization of transport protein expression in multidrug resistance-associated protein (Mrp) 2-deficient rats. *Drug metabolism and disposition: the biological fate of chemicals* 34:556-62

34. Mennone A, Soroka CJ, Cai SY, Harry K, Adachi M, et al. 2006. Mrp4-/- mice have an impaired cytoprotective response in obstructive cholestasis. *Hepatology* 43:1013-21

35. Chan LM, Lowes S, Hirst BH. 2004. The ABCs of drug transport in intestine and liver: efflux proteins limiting drug absorption and bioavailability. *European journal of pharmaceutical sciences : official journal of the European Federation for Pharmaceutical Sciences* 21:25-51

36. Rius M, Hummel-Eisenbeiss J, Hofmann AF, Keppler D. 2006. Substrate specificity of human ABCC4 (MRP4)-mediated cotransport of bile acids and reduced glutathione. *American journal of physiology. Gastrointestinal and liver physiology* 290:G640-9

37. Monte MJ, Marin JJ, Antelo A, Vazquez-Tato J. 2009. Bile acids: chemistry, physiology, and pathophysiology. *World journal of gastroenterology : WJG* 15:804-16

38. Chiang JY. 2009. Bile acids: regulation of synthesis. *Journal of lipid research* 50:1955-66

39. Ogimura E, Sekine S, Horie T. 2011. Bile salt export pump inhibitors are associated with bile acid-dependent drug-induced toxicity in sandwich-cultured hepatocytes. *Biochemical and biophysical research communications* 416:313-7

40. Tchaparian EH, Houghton JS, Uyeda C, Grillo MP, Jin L. 2011. Effect of culture time on the basal expression levels of drug transporters in sandwich-cultured primary rat hepatocytes. *Drug metabolism and disposition: the biological fate of chemicals* 39:2387-94

41. Li N, Singh P, Mandrell KM, Lai Y. 2010. Improved extrapolation of hepatobiliary clearance from in vitro sandwich cultured rat hepatocytes through absolute quantification of hepatobiliary transporters. *Molecular pharmaceutics* 7:630-41

42. Li N, Bi YA, Duignan DB, Lai Y. 2009. Quantitative expression profile of hepatobiliary transporters in sandwich cultured rat and human hepatocytes. *Molecular pharmaceutics* 6:1180-9

43. Akita H, Suzuki H, Sugiyama Y. 2001. Sinusoidal efflux of taurocholate is enhanced in Mrp2-deficient rat liver. *Pharmaceutical research* 18:1119-25

44. Martin PD, Warwick MJ, Dane AL, Hill SJ, Giles PB, et al. 2003. Metabolism, excretion, and pharmacokinetics of rosuvastatin in healthy adult male volunteers. *Clin Ther* 25:2822-35

45. Nezasa K, Takao A, Kimura K, Takaichi M, Inazawa K, Koike M. 2002. Pharmacokinetics and disposition of rosuvastatin, a new 3-hydroxy-3-methylglutaryl coenzyme A reductase inhibitor, in rat. *Xenobiotica; the fate of foreign compounds in biological systems* 32:715-27

46. Lam JL, Okochi H, Huang Y, Benet LZ. 2006. In vitro and in vivo correlation of hepatic transporter effects on erythromycin metabolism: characterizing the importance of transporter-enzyme interplay. *Drug metabolism and disposition: the biological fate of chemicals* 34:1336-44

47. Warwick MJ, Dane AL, Raza A, Schneck DW. 2000. Single- and multiple-dose pharmacokinetics and safety of the new HMG-CoA reductase inhibitor ZD4522 (Abstract). *Atherosclerosis* 151:39

48. Cooper KJ, Martin PD, Dane AL, Warwick MJ, Raza A, Schneck DW. 2003. Lack of effect of ketoconazole on the pharmacokinetics of rosuvastatin in healthy subjects. *British journal of clinical pharmacology* 55:94-9

CHAPTER 5

Summary and Future Directions

The general focus of this dissertation research has been the study and characterization of hepatobiliary clearance of drugs in humans and preclinical species. The contribution of multiple transport proteins in mediating altered hepatic and/or systemic exposure in the setting of impaired transport function remains poorly characterized. To address this knowledge gap, a series of experiments was designed and conducted using a variety of model systems, ranging from membrane vesicles that allowed the investigation of single transport proteins in isolation, to sandwich-cultured hepatocytes (SCH) containing the full complement of transport mechanisms expected *in vivo*, scaling up to isolated perfused rat livers, and finally *in vivo* studies in human subjects; a truly translational approach. A number of probe drugs were employed to evaluate transporter function in these experimental systems. This research has focused primarily on three drugs: ^{99m}Technetium-mebrofenin (Choletec®), ritonavir (Norvir®), and rosuvastatin (Crestor®).

^{99m}Tc-Mebrofenin (MEB) is a metabolically stable iminodiacetic acid (IDA) analogue and imaging agent, used to diagnose structural and functional disorders of the hepatobiliary network and gallbladder(1-3). The efficient vectorial transport of MEB from blood into liver is mediated by the organic anion transporting polypeptides, OATP1B1 and OATP1B3(4-6) and the canalicular efflux transporter multidrug resistance protein 2 (MRP2)(4; 5; 7). Ritonavir (RTV) was developed as an HIV protease inhibitor, but its extensive clinical use as a component of anti-retroviral therapy is to "boost" concentrations of other protease inhibitors by exploiting its ability to inhibit metabolic enzymes and intestinal p-glycoprotein (P-gp), thereby increasing the bioavailability of medications administered

concomitantly(8; 9). RTV also has been reported to inhibit hepatic OATP-/Oatp-(10; 11) and MRP-mediated transport *in vitro*(8; 11; 12), accumulate in liver tissue(13) and undergo biliary excretion in rats, dogs and humans(13). Hepatic transport plays an important role in the pharmacokinetics and pharmacodynamics of rosuvastatin (RSV), an HMG-CoA reductase inhibitor, with the liver serving as the primary organ of pharmacologic action and elimination. Hepatic uptake of RSV is mediated by multiple OATP isoforms, and reportedly by the sodium-taurocholate cotransporting polypeptide (NTCP)(14-16), while MRP2 and breast cancer resistance protein (BCRP) are primarily responsible for the biliary excretion of RSV(14; 17-20). Impaired function of these transporters via drug-drug interactions (DDIs) and genetic polymorphisms has been shown to have important consequences for the pharmacokinetics (14; 17; 19; 21-24) and pharmacodynamics (LDL-lowering)(25; 26) of RSV.

This research project has made a number of valuable contributions and advances to current and longstanding issues in the field of drug transport and pharmacokinetics. As with any scientific investigation at the doctoral level, this research has generated at least as many questions as it has answers. The following is a summary of the contributions and opportunities for further exploration based on the original aims of this research project.

Effect of Ritonavir on ^{99m}Technetium-Mebrofenin Disposition in Humans: A Semi-PBPK Modeling and In Vitro Approach to Predict Transporter-Mediated DDIs (Chapter 2)

Probe substrates to assess transport function and organ exposure *in vivo* are a highly sought-after clinical tool; MEB has been proposed as a probe substrate for MRP2(27) but had not been tested in a clinical DDI study prior to this work. This was the first study that utilized liver scintigraphy data to evaluate a hepatic DDI in humans, while incorporating blood, bile and urine data to develop a comprehensive pharmacokinetic model describing MEB disposition. The objective of using MEB as a probe substrate and "victim" of a transporter-mediated DDI at the level of biliary excretion was to demonstrate that such interactions can lead to elevated liver concentrations, with implications for safety and efficacy of drugs. Instead, coadministration of RTV led to a statistically-significant, two-fold increase in MEB systemic exposure without accompanying changes in hepatic exposure or biliary recovery. This finding was unexpected, but led to a number of novel discoveries.

This work has further characterized MEB as a clinical probe of transporter-mediated hepatobiliary clearance. Previous reports of MEB (or other IDA derivative) administration in humans or animals was limited to ≤60 min(2; 28-31), in which a two-compartment model representing blood and liver reasonably approximated time-activity data(28; 29). However, results of the present study, in which a statistically-significant, two-fold increase in MEB systemic exposure was observed without accompanying changes in hepatic exposure or biliary recovery following RTV administration (2x300mg), cannot be described by a 2-compartment model. A semi-PBPK modeling and *in vitro* systems translational approach suggested a transporter-mediated DDI involving tissue uptake at both hepatic and extrahepatic sites of MEB distribution. Rather than a specific MRP2 probe, this clinical study demonstrated the utility of MEB as a model organic anion to evaluate DDIs in overall (uptake and efflux) transporter-mediated hepatobiliary clearance.

Estimated unbound hepatic portal vein concentrations of RTV achieved in the clinical study (0.2-0.5 μM) were in the range that would be expected to inhibit OATP-mediated uptake (0.25-2.5μM)(10; 11). Studies in human SCH predicted the clinical study result that RTV was a more potent inhibitor of

hepatic uptake, as compared to biliary excretion, of MEB. Inhibition of MRP2-mediated MEB transport by RTV in a membrane vesicle assay suggested that the IC_{50} was between 5-50 μM, instead of the reported value of 50 nM in teleost fish(12). Despite this discrepancy, RTV accumulation within human SCH, and estimated *total* cellular concentrations (up to 100 μM), predicted that RTV would impair the biliary excretion of MEB. By assessing nonspecific binding of RTV to cell lysates (f_u ~0.02) and incorporating the estimated intracellular unbound concentration (2 μM maximum), we were able to translate data between *in vitro* systems, which predicted the *in vivo* results. This research contributed specific data to the literature regarding the use of RTV as an inhibitor of hepatic transport processes. More importantly, these high-impact studies outlined an overall paradigm for reliable predictions of transporter-mediated hepatic DDIs using data from appropriate *in vitro* models (*e.g.,*-assessment of inhibitory potential in relevant systems; biliary excretion assessed in SCH) integrated with knowledge regarding drug disposition (*e.g.,* hepatic and extrahepatic distribution; plasma and intracellular binding).

The experimental paradigm described in the current work - using *in vitro* human systems and accounting for intracellular unbound inhibitor concentrations - can be used to identify a substrate/inhibitor combination and target concentrations to design subsequent clinical studies. This approach is being pursued in collaboration with the Health and Environmental Sciences Institute (HESI) liver imaging group, as demonstrated by the recent report by Slizgi, et al(32). In addition to MEB, other probe substrates are being considered, including gadoxetate and PET agents such as fluorine-labeled bile acids. Potential inhibitors include rifampicin, diclofenac, ketoprofen, and fusidate. All are known to inhibit MRP2, and are being evaluated for their effects on hepatic uptake. The ideal inhibitor would demonstrate selective inhibition of biliary excretion and basolateral efflux, with a minimal impact on hepatic uptake.

As noted in the current work: "The availability of quantitative (attenuation corrected) scintigraphy data in humans marks a major advance in the use of imaging agents to assess organ/tissue exposure. Although the methods have existed for many years, they are under-utilized and provide a rich data set that is ideal for pharmacokinetic modeling." In addition to this key methodological advance, other improvements could be made in future studies to improve the robustness of generated data. One addition

would be to obtain the liver volume for individual subjects using a brief CT scan. Determination of hepatic blood flow for individual subjects also would be ideal; however, accurate and reliable methods for this assessment are not readily available. Such measurements could improve the PBPK modeling approach by reducing the uncertainty in these parameters, which are currently estimated based on weight-based (allometric) scaling of reported population distributions. This would reduce inter-subject variability in the parameter estimates obtained for the clearance values of interest (*e.g.*, hepatic uptake, biliary excretion).

One of the novel findings of the PBPK modeling approach was the proposed extrahepatic distribution of MEB. An outstanding question from this clinical study is the identity of the extrahepatic site(s) of MEB distribution, which accounted for approximately 10-40% of the administered dose at 180 min. MEB activity was confined to the liver and gallbladder in scintigraphic imaging data, thereby excluding other tissues and organs within the gamma camera field-of-view as potential sites of distribution, including the bulk of the torso and resident organ systems. Interestingly, parallel changes in the hepatic and extrahepatic compartments (impaired uptake and enhanced efflux) were required to explain altered MEB disposition following pre-treatment with 2x300 mg RTV. This suggested that similar mechanisms may mediate hepatic and extrahepatic MEB distribution. Human skeletal muscle has been shown to express a number of uptake and efflux transport proteins involved in drug disposition, including OAT1, OAT3, OATP2B1 and MRP1, -4 and -5 (33; 34). The presence of transport proteins, in particular OATP2B1, may play a role in accumulation of MEB in muscle tissue. In addition, the large relative volume of muscle tissue (~40% body weight) makes muscle a plausible target tissue for distribution. However, further studies are required to confirm that muscle or other tissue(s) account for the extrahepatic distribution of MEB. Whole-body gamma scintigraphic imaging of animal models (rat or mouse) and/or tissue collection and analysis would be a logical place to start with respect to identifying the potential extraheptic site(s) of MEB distribution.

Determination of Intracellular Unbound Concentrations and Subcellular Localization of Drugs in Rat Sandwich-Cultured Hepatocytes Compared to Liver Tissue (Chapter 3)

The methods applied in Aim 1 to estimate the intracellular unbound concentration of RTV in human SCH were further developed in Aim 2 using rat SCH and whole liver tissue. A set of probe drugs with diverse mechanisms of hepatocellular accumulation and disposition were employed. In addition to RTV and RSV, which have been described above, these studies evaluated furamidine, which is formed in the liver from the prodrug, pafuramidine, via sequential metabolism. Furamidine is excreted from hepatocytes into the systemic circulation to exert antiparasitic activity(35). This set of drugs provided a diverse range of tissue accumulation, hepatic unbound fraction (f_u), subcellular distribution, and ratio of intracellular and extracellular unbound concentration ($Kp_{u,u}$) values for comparison of methods to determine hepatocellular unbound concentrations ($C_{unbound}$). A novel application of classic approaches used to determine whole tissue distribution (differential centrifugation, equilibrium dialysis) was investigated in the SCH model system. The current work highlights the finding that total tissue accumulation and intracellular unbound concentration can be reasonably predicted using the SCH model. Importantly, the reported methods and resulting parameters, particularly the hepatic f_u and $Kp_{u,u}$, can be used to elucidate the relative contribution of active transport vs. binding/sequestration as potential mechanisms of hepatocellular accumulation, while providing a straightforward approach to estimate these parameters, which are needed for accurate *in vitro-in vivo* extrapolations.

For example, the estimated intracellular $C_{unbound}$ approximated the extracellular concentration of RTV, resulting in a $Kp_{u,u}$ of ~1, suggesting that binding to cellular components can explain the observed tissue accumulation. Although RSV binding did account for a portion of tissue accumulation ($Kp_{predicted}$ ~3-4), the majority of accumulation was due to unbound drug ($Kp_{u,u}$ of 8 to 11), consistent with efficient hepatic uptake and rate-limited efflux. RSV was selected as a model drug that is efficiently taken up by OATPs, which drive accumulation of unbound drug within hepatocytes, and has an expected $Kp_{u,u}$ significantly greater than one. In addition to extensive binding and sequestration, accumulation of unbound furamidine ($Kp_{u,u}$) was >16-fold, suggesting permeability-limited efflux of this charged

metabolite formed in the hepatocyte. It remains to be seen whether the similarity between predicted Kp, $Kp_{u,u}$ and $C_{unbound}$ values generated in SCH and whole liver tissue for these probe drugs would be observed for additional drugs that exhibit a wide range of physicochemical properties.

Subcellular fractionation has not been reported previously in SCH. Although isolation of subcellular fractions consisting of membrane-bound organelles proved challenging in SCH, cell lysis, release and isolation of soluble cytosolic proteins and contents was successful. Enzyme markers of subcellular components were recovered primarily in the initial, low-speed centrifugation step from SCH lysates, indicating that these organelles were retained in large, dense conglomerates. This limitation may provide an advantage for rapid isolation of the cytosolic fraction in SCH. These data suggest that a single, low-speed (600x*g*) spin, which can be performed on any benchtop microcentrifuge, will reliably exclude cellular organelles from the resulting supernatant of SCH lysate. This single-step method has the additional advantage of minimizing potential redistribution of drugs during multiple centrifugation steps and associated dilutions. Although the specific site(s) of subcellular sequestration would remain unknown, extensive distribution/recovery of drug in the pellet would indicate the need to consider intracellular pharmacokinetics.

One postulated reason for difficulty in isolating subcellular fractions in SCH may be the collagen matrix, which may prevent dissociation of the plasma membrane required to release larger, membrane-bound organelles. This could be tested by treating the collected (scraped) SCH cell pellet with collagenase prior to lysis, followed bydifferential centrifugation. While this approach may allow successful separation of subcellular fractions, the utility following drug treatment may be limited. Treated SCH are washed and kept on ice for subsequent handling (lysis, fractionation) in part to minimize transport, metabolism and other potential mechanisms of altered cellular distribution. However, collagenase treatment would require an incubation period at elevated temperatures under which these processes would again become active, likely resulting in an undesired redistribution of drugs.

Given the challenge in isolating subcellular fractions in SCH, another direction for future work is to investigate mechanisms of hepatocellular accumulation and localization in SCH using techniques other

than differential centrifugation. For example, the sequestration of cationic drugs in lysosomes vs. mitochondria is an area of considerable interest in drug discovery. Cationic drug accumulation is commonly attributed to ion trapping due to the lysosomal pH and/or mitochondrial electrochemical gradients(36-41). While it is true that physicochemical properties are predictive of cationic sequestration/accumulation to a certain extent(36; 41), even advanced pharmacophore models often fail to successfully predict drug sequestration over diverse chemical space *within* a single organelle (lysosomes or mitochondria), let alone mitochondrial *versus* lysosomal(36-38; 40; 41). Therefore, empiric experimental methods are still needed to predict and explain subcellular distribution and related implications for drug safety, efficacy and disposition.

This could be explored using a method analogous to the B-CLEAR® technology, where the presence and absence of Ca^{2+} in the incubation buffer is used to evaluate the difference between accumulation in cells+bile and cells, respectively. Similarly, one could use chemicals that are known to abolish the pH gradient in lysosomes and/or the electrochemical gradient in mitochondria. Examples of compounds that abolish the lysosomal pH gradient include ammonium chloride, concanamycin A and monensin(39; 41), while uncoupling agents that disrupt the inner mitochondrial membrane electrochemical potential include 2,4-dinitrophenol and FCCP (carbonylcyanide-p-trifluoromethoxyphenylhydrazone) (41). Experiments might involve pre-incubating SCH in the presence and absence of the modulating agent, followed by incubation with the compound of interest. The difference in cellular accumulation at steady-state in the presence and absence of the lysosomal or mitochondrial modulator would indicate the extent of accumulation that can be attributed to the organelle or mechanism(s) being modulated. This should be performed ideally under conditions in which the tight junctions have been disrupted (-Ca^{2+} conditions) so that only cellular content/accumulation is being evaluated. However, caution should be exercised in modulating mitochondrial electrochemical or lysosomal pH gradients. Care should be taken to carefully evaluate and characterize the SCH system under these conditions, including measures of cell viability (*e.g.*, LDH) and function (*e.g.*, prototypical transport substrates such as taurocholate and/or rosuvastatin).

Similarly, subcellular disposition of anionic drugs might be explored with respect to accumulation and transport within the vesicle network. As integral membrane proteins, transporters are inserted immediately upon synthesis (under normal circumstances), and transferred to the plasma membrane through dynamic and complex vesicle trafficking pathways(42-46). Similarly, plasma membrane regions and their contents are continuously cycled on and off the membrane, leading to intracellular pools of transporter-containing vesicles(47; 48). As a result, substrates for efflux transporters constantly are accumulating within these vesicles. This has been shown with fluorescent substrates, where characteristic punctate vesicular structures have been observed that are absent in Mrp2-deficient cells and sensitive to known MRP2 inhibitors, such as cyclosporine A(47; 49; 50). This pathway has been shown for a number of substrates, including taurocholate(48; 51). Vesicle trafficking in hepatocytes is known to be altered by a number of disease states (including TR^- rat liver as a model of Dubin-Johnson syndrome in humans) and drugs (e.g., monensin, colchicine, taurocholate) by both cytoskeletal-(actin/myosin) dependent and independent mechanisms(47; 51-56). Vesicle trafficking also may play a role in taurocholate disposition in rat SCH(57). Our ability to ascertain the contribution of the vesicle trafficking process and subcellular space to total cellular drug content and excretion may improve our understanding and prediction of drug interactions. For example, the observed biliary excretion rate may be a combination of terminal release (efflux) of accumulated drug from fusion of subapical vesicles with the canalicular membrane and direct transporter-mediated efflux across the canalicular membrane(47; 56). Vesicular fusion and direct transporter flux may occur at very different rates across the canalicular membrane. One could modulate this pathway in SCH using known inhibitors of the vesicle trafficking process, such as monensin or colchicine. Again, care must be taken to characterize the SCH system under these conditions. Visual techniques such as microscopy using fluorescent compounds such as carboxydichlorofluorescein diacetate (CDFDA), bile acid derivatives (*e.g.*, CGamF) or other compounds also may be effective in determining the potential for these types of modulatory effects in SCH.

Basolateral Efflux Contributes Significantly to the Hepatocellular Excretion of Rosuvastatin: Characterization of Basolateral vs. Biliary Clearance Using a Novel Protocol in Rat and Human Sandwich-Cultured Hepatocytes (Chapter 4)

Transport proteins mediating the hepatic uptake and biliary excretion of RSV have been fairly well-characterized(14-20). Less well-known is the role of basolateral efflux of RSV from hepatocytes back into sinusoidal blood. Wild-type (WT) and Mrp2-deficient (TR^-) rat livers were perfused in a single-pass manner with RSV in the presence and absence of the dual P-gp/Bcrp inhibitor, GF120918 (elacridar), for a 60-min loading phase, followed by a 30-min washout phase to determine the degree of basolateral and biliary efflux of RSV; a pharmacokinetic model was fit to the resulting data. As expected, the biliary clearance (CL_{Bile}) of RSV was reduced in TR^- compared to WT livers, and GF120918 further reduced CL_{Bile} and biliary recovery in TR^- livers. Interestingly, the appearance rate of RSV in outflow perfusate and the resulting basolateral clearance (CL_{BL}) estimate were reduced by GF120918 in WT livers, and also in TR^- compared to WT livers. These data, along with the lack of an immediate drop-off in RSV perfusate concentrations upon switching from the loading to the efflux phase, indicated that RSV is almost completely taken up by hepatocytes and that appearance of RSV in outflow perfusate is due almost exclusively to basolateral efflux. In fact, modeling results suggested that CL_{BL} and CL_{Bile} represent alternative pathways with a similar contribution to the total hepatocellular excretion of RSV. This is a novel finding, and suggests that hepatic exposure of RSV is unlikely to be elevated greatly in the setting of impaired biliary efflux, unless basolateral efflux is also impaired. Serendipitously, data in TR^- livers appeared to represent the case of impaired basolateral *and* biliary efflux, resulting in significantly elevated (~4-fold) hepatic exposure of RSV. In addition to RSV, hepatic concentrations and recovery of the pentanoic acid metabolite of RSV were significantly greater (>5-fold) in TR^- compared to WT livers.

Although RSV is not reported to be extensively metabolized in humans(58), metabolism plays a larger role in rats, with ~50% of plasma and liver content accounted for by metabolites.(14; 59) These studies confirmed the presence of RSV pentanoic acid as the primary metabolite, contributing ~40% of total RSV content in both WT and TR^- livers, consistent with previous reports(14; 59). This is the first

study to corroborate the structural identity of the pentanoic acid metabolite of RSV by mass spectrometry; previous reports suggested the identity of the metabolite by thin-layer chromatography of the pure standard co-spotted with blood, liver and bile samples from rats administered radiolabeled RSV. Increased hepatic accumulation of RSV and the pentanoic acid metabolite in TR^- compared to WT livers was consistent with impaired excretion and "shunting" to the metabolic pathway(s).

A novel uptake and efflux protocol, coupled with pharmacokinetic modeling, was developed in order to elucidate the relative contribution of CL_{BL} and CL_{Bile} to the hepatocellular elimination of the model drug, RSV, in the SCH model. Although several strategies using the SCH model have been published to assess efflux by preloading the cells and quantifying substrate in cells+bile, cells, and/or buffer during an efflux phase(5; 18), the system remains poorly characterized under these conditions. A major contribution of the present work was to characterize the behavior of the SCH system under various uptake/efflux scenarios and differentiate the contributions of CL_{BL} and CL_{Bile} from flux out of bile spaces (K_{Flux}) in the presence of Ca^{2+} (cells+bile) (60-64) using a modeling approach. Based on this approach, RSV disposition in rat SCH was in agreement with perfused liver data, demonstrating that CL_{BL} and CL_{Bile} represent alternative pathways with a quantitatively similar contribution to total hepatocellular excretion of RSV.

In order to translate the relevance of these findings from rat to humans, RSV transport was evaluated in human SCH and membrane vesicles prepared from HEK293 cells overexpressing human MRP3 and MRP4. Results of these studies revealed, for the first time, that RSV is an inhibitor of MRP3 and MRP4, and an efficient substrate of MRP4 (K_m = 21±7 μM), which likely contributes to the basolateral efflux of RSV from hepatocytes in humans. A pilot study in human SCH using the novel uptake/efflux protocol, coupled with pharmacokinetic modeling, revealed that, as in rats, CL_{BL} and CL_{Bile} represent alternative pathways for hepatocellular excretion of RSV; in human SCH, CL_{BL} was nearly 2-fold CL_{Bile}.

One limitation of the novel uptake/efflux protocol and pharmacokinetic modeling approach is that the resulting parameter estimates for sinusoidal uptake and efflux clearance represent *net* uptake and

efflux, respectively. Addition of a passive diffusion term to the current model scheme results in parameter identifiability/covariance issues without additional experimental conditions under which active transport processes are rendered inoperable. While no conditions exist that are ideal for isolating the passive diffusion component of transporter substrates, this is an area that may explored in the future. The best possible approach may be to coadminister one or more inhibitors of transport mechanisms (*e.g.*, rifamycin, rifampicin, CsA). Other approaches, such as ATP depletion and incubations on ice, are less attractive due to limitations including compromised cell viability (ATP depletion) and temperature effects on non-specific binding(65-67), membrane fluidity and partitioning(68-70).

Evidence of the role of transport in the basolateral efflux pathway of RSV can be strengthened by demonstrating that modulation of basolateral efflux results in altered hepatic and/or systemic exposure of drugs. Recent efforts in the Brouwer lab have included screening drugs for inhibitory potential against MRP4(71). One of the identified, potent inhibitors could be coadministered with RSV in SCH and/or IPLs to demonstrate the effect of a known MRP4 inhibitor on hepatobiliary disposition of RSV. However, the impact of an MRP4 inhibitor on overall cellular exposure would depend on the relative contribution of the impaired pathway to total excretory clearance (CL_{BL}+CL_{Bile}). For RSV, you would need to impair Mrp2 & Bcrp in addition to Mrp4 in order to detect a change in cellular exposure in rat SCH, since CL_{Bile} represents approximately one-half of total efflux clearance based on the data generated in this dissertation research. Inhibition of Mrp4 alone would not be expected to result in significant alterations in cellular exposure, because the MRP4-mediated portion of total excretory clearance is approximately one-fourth of total efflux clearance. Kynuremic acid recently was reported as a potent substrate and inhibitor of BCRP and MRP4 using membrane vesicle systems(72). This would seem to be an ideal compound to coadminister with RSV, similar to the current work that used GF120918 as an inhibitor of BCRP and P-gp. One caveat is that kynuremic acid must be able to enter the hepatocyte in order to inhibit efflux mechanisms. While this compound is likely a substrate for OAT2 and/or OATPs, the uptake/accumulation of kynuremic acid would need to be verified in hepatocytes. Even though it might inhibit hepatic uptake, the novel uptake/efflux protocol and modeling approach developed in this

aim should be able to deconvolute the resulting SCH data successfully. Finally, kynuremic acid is highly bound to plasma proteins, so it may bind extensively to cellular components; preliminary experiments such as those developed in Aim 2 should be conducted to determine the feasibility of this inhibitor based on the intracellular $C_{unbound}$ that is determined to inhibit hepatocellular efflux processes.

This dissertation focused on two general themes involving hepatobiliary drug disposition: hepatocellular exposure and multiplicity of transport. MEB, RTV and RSV were characterized further as probes with respect to their hepatocellular exposure and interaction with multiple hepatic transport proteins. This research has resulted in a number of important and novel contributions that have advanced both preclinical and clinical (translational) tools available to study hepatic drug transport. These developments will significantly enhance the ability to assess and predict altered hepatobiliary drug disposition due to drug interactions, disease states, or other patient-specific factors, and will ultimately lead to improved safety and efficacy of medications.

REFERENCES

1. Balon HR, Fink-Bennett DM, Brill DR, Fig LM, Freitas JE, et al. 1997. Procedure guideline for hepatobiliary scintigrahy. *Journal of Nuclear Medicine* 38:1654-7

2. Doo E, Krishnamurthy GT, Eklem MJ, Gilbert S, Brown PH. 1991. Quantification of hepatobiliary function as an integral part of imaging with technetium-99m-mebrofenin in health and disease. *J Nucl Med* 32:48-57

3. Loberg MD, Cooper M, Harvey E, Callery P, Faith W. 1976. Development of new radiopharmaceuticals based on N-substitution of iminodiacetic acid. *J Nucl Med* 17:633-8

4. Ghibellini G, Leslie EM, Pollack GM, Brouwer KLR. 2008. Use to Tc-99m mebrofenin as a clinical probe to assess altered hepatobiliary transport: integration of in vitro, pharmacokinetic modeling, and simulation studies. *Pharmaceutical research* 25:1851-60

5. Swift B, Yue W, Brouwer KL. 2010. Evaluation of (99m)technetium-mebrofenin and (99m)technetium-sestamibi as specific probes for hepatic transport protein function in rat and human hepatocytes. *Pharmaceutical research* 27:1987-98

6. de Graaf W, Hausler S, Heger M, van Ginhoven TM, van Cappellen G, et al. 2011. Transporters involved in the hepatic uptake of (99m)Tc-mebrofenin and indocyanine green. *Journal of hepatology* 54:738-45

7. Bhargava KK, Joseph B, Ananthanarayanan M, Balasubramaniyan N, Tronco GG, et al. 2009. Adenosine triphosphate-binding cassette subfamily C member 2 is the major transporter of the hepatobiliary imaging agent (99m)Tc-mebrofenin. *J Nucl Med* 50:1140-6

8. Vourvahis M, Kashuba AD. 2007. Mechanisms of pharmacokinetic and pharmacodynamic drug interactions associated with ritonavir-enhanced tipranavir. *Pharmacotherapy* 27:888-909

9. Hirsch MS. 2008. Initiating therapy: when to start, what to use. *J Infect Dis* 197 Suppl 3:S252-60

10. Ye ZW, Augustijns P, Annaert P. 2008. Cellular accumulation of cholyl-glycylamido-fluorescein in sandwich-cultured rat hepatocytes: kinetic characterization, transport mechanisms, and effect of human immunodeficiency virus protease inhibitors. *Drug metabolism and disposition: the biological fate of chemicals* 36:1315-21

11. Annaert P, Ye ZW, Stieger B, Augustijns P. 2010. Interaction of HIV protease inhibitors with OATP1B1, 1B3, and 2B1. *Xenobiotica; the fate of foreign compounds in biological systems* 40:163-76

12. Gutmann H, Fricker G, Drewe J, Toeroek M, Miller DS. 1999. Interactions of HIV protease inhibitors with ATP-dependent drug export proteins. *Molecular pharmacology* 56:383-9

13. Denissen JF, Grabowski BA, Johnson MK, Buko AM, Kempf DJ, et al. 1997. Metabolism and disposition of the HIV-1 protease inhibitor ritonavir (ABT-538) in rats, dogs, and humans. *Drug metabolism and disposition: the biological fate of chemicals* 25:489-501

14. Kitamura S, Maeda K, Wang Y, Sugiyama Y. 2008. Involvement of multiple transporters in the hepatobiliary transport of rosuvastatin. *Drug metabolism and disposition: the biological fate of chemicals* 36:2014-23

15. Ho RH, Tirona RG, Leake BF, Glaeser H, Lee W, et al. 2006. Drug and bile acid transporters in rosuvastatin hepatic uptake: function, expression, and pharmacogenetics. *Gastroenterology* 130:1793-806

16. Abe K, Bridges AS, Yue W, Brouwer KL. 2008. In vitro biliary clearance of angiotensin II receptor blockers and 3-hydroxy-3-methylglutaryl-coenzyme A reductase inhibitors in sandwich-cultured rat hepatocytes: comparison with in vivo biliary clearance. *The Journal of pharmacology and experimental therapeutics* 326:983-90

17. Hobbs M, Parker C, Birch H, Kenworthy K. 2012. Understanding the interplay of drug transporters involved in the disposition of rosuvastatin in the isolated perfused rat liver using a physiologically-based pharmacokinetic model. *Xenobiotica; the fate of foreign compounds in biological systems* 42:327-38

18. Jemnitz K, Veres Z, Tugyi R, Vereczkey L. 2010. Biliary efflux transporters involved in the clearance of rosuvastatin in sandwich culture of primary rat hepatocytes. *Toxicol In Vitro* 24:605-10

19. Keskitalo JE, Zolk O, Fromm MF, Kurkinen KJ, Neuvonen PJ, Niemi M. 2009. ABCG2 polymorphism markedly affects the pharmacokinetics of atorvastatin and rosuvastatin. *Clinical pharmacology and therapeutics* 86:197-203

20. Huang L, Wang Y, Grimm S. 2006. ATP-dependent transport of rosuvastatin in membrane vesicles expressing breast cancer resistance protein. *Drug metabolism and disposition: the biological fate of chemicals* 34:738-42

21. Simonson SG, Raza A, Martin PD, Mitchell PD, Jarcho JA, et al. 2004. Rosuvastatin pharmacokinetics in heart transplant recipients administered an antirejection regimen including cyclosporine. *Clinical pharmacology and therapeutics* 76:167-77

22. Schneck DW, Birmingham BK, Zalikowski JA, Mitchell PD, Wang Y, et al. 2004. The effect of gemfibrozil on the pharmacokinetics of rosuvastatin. *Clinical pharmacology and therapeutics* 75:455-63

23. Zhang W, Yu BN, He YJ, Fan L, Li Q, et al. 2006. Role of BCRP 421C>A polymorphism on rosuvastatin pharmacokinetics in healthy Chinese males. *Clinica chimica acta; international journal of clinical chemistry* 373:99-103

24. Kiser JJ, Gerber JG, Predhomme JA, Wolfe P, Flynn DM, Hoody DW. 2008. Drug/Drug interaction between lopinavir/ritonavir and rosuvastatin in healthy volunteers. *J Acquir Immune Defic Syndr* 47:570-8

25. Simonson SG, Martin PD, Mitchell P, Schneck DW, Lasseter KC, Warwick MJ. 2003. Pharmacokinetics and pharmacodynamics of rosuvastatin in subjects with hepatic impairment. *Eur J Clin Pharmacol* 58:669-75

26. Tomlinson B, Hu M, Lee VW, Lui SS, Chu TT, et al. 2010. ABCG2 polymorphism is associated with the low-density lipoprotein cholesterol response to rosuvastatin. *Clinical pharmacology and therapeutics* 87:558-62

27. Giacomini KM, Huang SM, Tweedie DJ, Benet LZ, Brouwer KL, et al. 2010. Membrane transporters in drug development. *Nat Rev Drug Discov* 9:215-36

28. Chervu LR, Nunn AD, Loberg MD. 1982. Radiopharmaceuticals for hepatobiliary imaging. *Semin Nucl Med* 12:5-17

29. Hawkins RA, Hall T, Gambhir SS, Busuttil RW, Huang SC, et al. 1988. Radionuclide evaluation of liver transplants. *Semin Nucl Med* 18:199-212

30. Brown PH, Juni JE, Lieberman DA, Krishnamurthy GT. 1988. Hepatocyte versus biliary disease: a distinction by deconvolutional analysis of technetium-99m IDA time-activity curves. *J Nucl Med* 29:623-30

31. Peters AM, Myers MJ, Mohammadtaghi S, Mubashar M, Mathie RT. 1998. Bidirectional transport of iminodiacetic organic anion analogues between plasma and hepatocyte. *Eur J Nucl Med* 25:766-73

32. Slizgi JS, Pfeifer ND, Koeck K, Powell H, Brouwer KLR. 2013. Interaction of MRP2 Inhibitors with Hepatic Organic Anion Transporting Polypeptides (OATP) 1B1, 1B3, and 2B1. In *AAPS Workshop on Drug Transporters in ADME*. N. Bethesda, MD

33. Takeda M, Noshiro R, Onozato ML, Tojo A, Hasannejad H, et al. 2004. Evidence for a role of human organic anion transporters in the muscular side effects of HMG-CoA reductase inhibitors. *Eur J Pharmacol* 483:133-8

34. Knauer MJ, Urquhart BL, Meyer zu Schwabedissen HE, Schwarz UI, Lemke CJ, et al. 2010. Human skeletal muscle drug transporters determine local exposure and toxicity of statins. *Circ Res* 106:297-306

35. Paine MF, Wang MZ, Generaux CN, Boykin DW, Wilson WD, et al. 2010. Diamidines for human African trypanosomiasis. *Curr Opin Investig Drugs* 11:876-83

36. Horobin RW, Trapp S, Weissig V. 2007. Mitochondriotropics: a review of their mode of action, and their applications for drug and DNA delivery to mammalian mitochondria. *Journal of controlled release : official journal of the Controlled Release Society* 121:125-36

37. Rosania GR. 2003. Supertargeted chemistry: identifying relationships between molecular structures and their sub-cellular distribution. *Current topics in medicinal chemistry* 3:659-85

38. Rashid F, Horobin RW, Williams MA. 1991. Predicting the behaviour and selectivity of fluorescent probes for lysosomes and related structures by means of structure-activity models. *The Histochemical journal* 23:450-9

39. Daniel WA, Wojcikowski J. 1999. Lysosomal trapping as an important mechanism involved in the cellular distribution of perazine and in pharmacokinetic interaction with antidepressants. *European neuropsychopharmacology : the journal of the European College of Neuropsychopharmacology* 9:483-91

40. Zheng N, Tsai HN, Zhang X, Rosania GR. 2011. The subcellular distribution of small molecules: from pharmacokinetics to synthetic biology. *Molecular pharmaceutics* 8:1619-28

41. Duvvuri M, Gong Y, Chatterji D, Krise JP. 2004. Weak base permeability characteristics influence the intracellular sequestration site in the multidrug-resistant human leukemic cell line HL-60. *The Journal of biological chemistry* 279:32367-72

42. Ihrke G, Martin GV, Shanks MR, Schrader M, Schroer TA, Hubbard AL. 1998. Apical plasma membrane proteins and endolyn-78 travel through a subapical compartment in polarized WIF-B hepatocytes. *J Cell Biol* 141:115-33

43. Aoyama N, Tokumo H, Ohya T, Chandler K, Holzbach RT. 1991. A novel transcellular transport pathway for non-bile salt cholephilic organic anions. *The American journal of physiology* 261:G305-11

44. Aoyama N, Ohya T, Chandler K, Gresky S, Holzbach RT. 1991. Transcellular transport of organic anions in the isolated perfused rat liver: the differential effects of monensin and colchicine. *Hepatology* 14:1-9

45. Kipp H, Arias IM. 2000. Newly synthesized canalicular ABC transporters are directly targeted from the Golgi to the hepatocyte apical domain in rat liver. *The Journal of biological chemistry* 275:15917-25

46. Van ISC, Maier O, Van Der Wouden JM, Hoekstra D. 2000. The subapical compartment and its role in intracellular trafficking and cell polarity. *Journal of cellular physiology* 184:151-60

47. Wustner D, Mukherjee S, Maxfield FR, Muller P, Herrmann A. 2001. Vesicular and nonvesicular transport of phosphatidylcholine in polarized HepG2 cells. *Traffic* 2:277-96

48. Kipp H, Pichetshote N, Arias IM. 2001. Transporters on demand: intrahepatic pools of canalicular ATP binding cassette transporters in rat liver. *The Journal of biological chemistry* 276:7218-24

49. Nies AT, Cantz T, Brom M, Leier I, Keppler D. 1998. Expression of the apical conjugate export pump, Mrp2, in the polarized hepatoma cell line, WIF-B. *Hepatology* 28:1332-40

50. Breuninger LM, Paul S, Gaughan K, Miki T, Chan A, et al. 1995. Expression of multidrug resistance-associated protein in NIH/3T3 cells confers multidrug resistance associated with increased drug efflux and altered intracellular drug distribution. *Cancer research* 55:5342-7

51. Hung DY, Siebert GA, Chang P, Roberts MS. 2005. Hepatic pharmacokinetics of taurocholate in the normal and cholestatic rat liver. *British journal of pharmacology* 145:57-65

52. Milkiewicz P, Roma MG, Elias E, Coleman R. 2002. Pathobiology and experimental therapeutics in hepatocellular cholestasis: lessons from the hepatocyte couplet model. *Clin Sci (Lond)* 102:603-14

53. Hoque MT, Cole SP. 2008. Down-regulation of Na+/H+ exchanger regulatory factor 1 increases expression and function of multidrug resistance protein 4. *Cancer research* 68:4802-9

54. Gatmaitan ZC, Nies AT, Arias IM. 1997. Regulation and translocation of ATP-dependent apical membrane proteins in rat liver. *The American journal of physiology* 272:G1041-9

55. Stieger B, Meier PJ, Landmann L. 1994. Effect of obstructive cholestasis on membrane traffic and domain-specific expression of plasma membrane proteins in rat liver parenchymal cells. *Hepatology* 20:201-12

56. Boyer JL, Soroka CJ. 1995. Vesicle targeting to the apical domain regulates bile excretory function in isolated rat hepatocyte couplets. *Gastroenterology* 109:1600-11

57. Yang K, Brouwer KLR. 2012. Pharmacokinetic Modeling and Simulation Study to Predict the Impact of Troglitazone (TGZ) on the Hepatobiliary Disposition of Taurocholate (TC) in Rat Sandwich-Cultured Hepatocytes (SCH). In *AAPS Annual Meeting*. Chicago, IL

58. Martin PD, Warwick MJ, Dane AL, Hill SJ, Giles PB, et al. 2003. Metabolism, excretion, and pharmacokinetics of rosuvastatin in healthy adult male volunteers. *Clin Ther* 25:2822-35

59. Nezasa K, Takao A, Kimura K, Takaichi M, Inazawa K, Koike M. 2002. Pharmacokinetics and disposition of rosuvastatin, a new 3-hydroxy-3-methylglutaryl coenzyme A reductase inhibitor, in rat. *Xenobiotica; the fate of foreign compounds in biological systems* 32:715-27

60. Boyer JL, Gautam A, Graf J. 1988. Mechanisms of bile secretion: insights from the isolated rat hepatocyte couplet. *Seminars in liver disease* 8:308-16

61. Shinoda Y, Suematsu M, Wakabayashi Y, Suzuki T, Goda N, et al. 1998. Carbon monoxide as a regulator of bile canalicular contractility in cultured rat hepatocytes. *Hepatology* 28:286-95

62. Hoffmaster KA, Zamek-Gliszczynski MJ, Pollack GM, Brouwer KL. 2005. Multiple transport systems mediate the hepatic uptake and biliary excretion of the metabolically stable opioid peptide [D-penicillamine2,5]enkephalin. *Drug metabolism and disposition: the biological fate of chemicals* 33:287-93

63. Liu X, LeCluyse EL, Brouwer KR, Lightfoot RM, Lee JI, Brouwer KL. 1999. Use of Ca2+ modulation to evaluate biliary excretion in sandwich-cultured rat hepatocytes. *The Journal of pharmacology and experimental therapeutics* 289:1592-9

64. Lee JK, Marion TL, Abe K, Lim C, Pollock GM, Brouwer KL. 2010. Hepatobiliary disposition of troglitazone and metabolites in rat and human sandwich-cultured hepatocytes: use of Monte Carlo simulations to assess the impact of changes in biliary excretion on troglitazone sulfate accumulation. *The Journal of pharmacology and experimental therapeutics* 332:26-34

65. Igari Y, Sugiyama Y, Awazu S, Hanano M. 1981. Interspecies difference in drug protein binding-temperature and protein concentration dependency: effect on calculation of effective protein fraction. *Journal of pharmaceutical sciences* 70:1049-53

66. Kodama H, Kodama Y, Shinozawa S, Kanemaru R, Todaka K, Mitsuyama Y. 1999. Temperature effect on serum protein binding kinetics of phenytoin in monotherapy patients with epilepsy. *European journal of pharmaceutics and biopharmaceutics : official journal of Arbeitsgemeinschaft fur Pharmazeutische Verfahrenstechnik e.V* 47:295-8

67. Zeitlinger MA, Derendorf H, Mouton JW, Cars O, Craig WA, et al. 2011. Protein binding: do we ever learn? *Antimicrobial agents and chemotherapy* 55:3067-74

68. Palmeira CM, Oliveira CR. 1992. Partitioning and membrane disordering effects of dopamine antagonists: influence of lipid peroxidation, temperature, and drug concentration. *Arch Biochem Biophys* 295:161-71

69. Herbette L, Katz AM, Sturtevant JM. 1983. Comparisons of the interaction of propranolol and timolol with model and biological membrane systems. *Molecular pharmacology* 24:259-69

70. Liu XY, Yang Q, Kamo N, Miyake J. 2001. Effect of liposome type and membrane fluidity on drug-membrane partitioning analyzed by immobilized liposome chromatography. *J Chromatogr A* 913:123-31

71. Koeck K, Ferslew BC, Netterberg I, Yang K, Urban TJ, et al. 2012. Inhibition of the hepatic basolateral bile acid transporter MRP4 predicts cholestatic drug-induced liver injury (DILI). *Hepatology* 56:1530

72. Mutsaers H, Dankers A, Wilmer M, van den Heuvel LP, Hoenderop JG, Masereeuw R. 2013. The Novel MRP4 and BCRP Substrate Kynurenic Acid Attenuates Renal Drug Metabolism. In *AAPS Workshop on Drug Transporters in ADME*. N. Betrhesda, MD

APPENDIX

Data Appendix

Figure 2.5

A.

Ritaonvir Dose (µM)	MEB Accumulation (%Control)			
	+Ca		-Ca	
	Mean	SEM	Mean	SEM
0 (Control)	100		74.4	4.1
0.05	99.1	8.6	73.1	1.0
0.1	99.7	8.9	72.8	3.9
0.5	91.2	13.4	67.0	5.6
1	83.1	17.8	64.1	13.3
5	37.2	3.5	29.2	2.4
20	17.4	3.7	14.8	7.0

B.

Ritonavir Dose (µM)	ATP-Dependent Uptake ($C_{cell,total}$, µM)	
	Mean	SD
0.05	0.288	0.186
0.1	0.481	0.359
0.5	3.26	2.14
1	7.31	2.88
5	42.7	28.7
20	87.8	34.0

Figure 3.2

A. Whole Liver Tissue

	Enzyme Activity (% Total in Whole Lysate)							
Centrifugation Step (x *g*)	**Succinate Dehydrogenase**		**Acid Phosphatase**		**Glucose-6-Phosphatase**		**Lactate Dehydrogenase**	
	Mean	**SD**	**Mean**	**SD**	**Mean**	**SD**	**Mean**	**SD**
600	19	8	5.7	1.1	11	8	5.6	0.8
10,000	39	13	14	4	18	1	4.5	4.2
35,000	20	10	16	8	11	1	8.8	7.5
100,000	11	11	19	8	51	15	8.6	2.6
super	12	10	45	3	9.6	6.7	72	6

B. Sandwich-cultured Hepatocytes (SCH)

	Enzyme Activity (% Total in Whole Lysate)							
	Succinate Dehydrogenase		**Acid Phosphatase**		**Glucose-6-Phosphatase**		**Lactate Dehydrogenase**	
	Mean	**SD**	**Mean**	**SD**	**Mean**	**SD**	**Mean**	**SD**
600	82	8	51	9	76	6	3.4	1.5
10,000	11	5	8.1	2.2	11	6	2.1	1.0
100,000	5.9	5.4	3.9	1.8	4.4	3.2	3.7	1.1
super	1.2	1.7	36	7	9.0	5.5	91	3

Figure 3.3

IPL:

	Recovery of Probe Drug (% Total in Whole Lysate)		
Centrifugation Step (x *g*)	**Ritonavir**	**Rosuvastatin**	**Furamidine**
600	19	7.3	18
10,000	39	11	43
35,000	20	2.1	15
100,000	11	7.9	4
super	12	72	20

SCH:

	Recovery of Probe Drug (% Total in Whole Lysate)					
Centrifugation Step (x *g*)	**Ritonavir**		**Rosuvastatin**		**Furamidine**	
	Mean	**SD**	**Mean**	**SD**	**Mean**	**SD**
600	45	8	8.3	0.5	85	1
10,000	5.3	5.2	2.8	0.3	7.3	1.4
100,000	6.5	3.6	1.0	0.1	4.9	1.6
super	43	8	88	1	2.9	0.9

Figure 4.4

0.1 μM [^{3}H]Rosuvastatin, WT (Control)

			[^{3}H]Rosuvastatin Accumulation (pmol/well)							
			Lysate				Buffer			
Study Phase	**Time (min)**		**+Ca^{2+}**		**-Ca^{2+}**		**+Ca^{2+}**		**-Ca^{2+}**	
	(in phase)	**(cumulative)**	**Mean**	**SEM**	**Mean**	**SEM**	**Mean**	**SEM**	**Mean**	**SEM**
Uptake	**2**	**2**	1.36	0.26	1.04	0.23				
	5	**5**	2.59	0.31	1.43	0.13				
	10	**10**	4.13	0.80	1.62	0.10				
	20	**20**	6.06	1.25	1.87	0.36				
Efflux	**2**	**23.5**	4.66	0.49	0.77	0.13	0.99	0.41	0.83	0.23
	5	**26.5**	4.24	0.59	0.38	0.17	1.82	0.64	1.31	0.49
	10	**31.5**	3.03	0.59	0.11	0.04	2.83	0.69	1.57	0.37
	15	**36.5**	2.66	0.32	0.07	0.07	3.60	1.32	1.74	0.73

1 μM [^{3}H]Rosuvastatin, WT (Control)

			[^{3}H]Rosuvastatin Accumulation (pmol/well)							
			Lysate				Buffer			
Study Phase	**Time (min)**		**+Ca^{2+}**		**-Ca^{2+}**		**+Ca^{2+}**		**-Ca^{2+}**	
	(in phase)	**(cumulative)**	**Mean**	**SEM**	**Mean**	**SEM**	**Mean**	**SEM**	**Mean**	**SEM**
Uptake	**2**	**2**	12.49	1.89	8.55	1.38				
	5	**5**	21.87	2.58	13.24	1.65				
	10	**10**	30.51	3.59	15.12	2.51				
	20	**20**	43.05	4.24	18.29	2.38				
Efflux	**2**	**23.5**	35.75	6.85	7.59	1.86	7.68	0.93	7.07	0.85
	5	**26.5**	29.59	5.92	4.00	1.69	14.73	3.27	11.42	2.15
	10	**31.5**	23.46	5.87	1.56	1.27	23.67	5.99	15.09	3.21
	15	**36.5**	21.46	4.28	0.47	0.47	28.58	9.01	14.09	2.81

0.1 μM [^{3}H]Rosuvastatin, WT (+GF120918)

			[^{3}H]Rosuvastatin Accumulation (pmol/well)							
			Lysate				Buffer			
Study Phase	**Time (min)**		**+Ca^{2+}**		**-Ca^{2+}**		**+Ca^{2+}**		**-Ca^{2+}**	
	(in phase)	**(cumulative)**	**Mean**	**SEM**	**Mean**	**SEM**	**Mean**	**SEM**	**Mean**	**SEM**
Uptake	**2**	**2**	1.21		1.35					
	5	**5**	2.29		2.02					
	10	**10**	3.48		2.65					
	20	**20**	4.99		3.27					
Efflux	**2**	**23.5**	3.21		1.71		0.64		0.53	
	5	**26.5**	2.92		1.30		1.23		1.01	
	10	**31.5**	1.75		0.53		2.01		1.52	
	15	**36.5**	1.66		0.36		2.48		1.84	

1 μM [^{3}H]Rosuvastatin, WT (+GF120918)

			[^{3}H]Rosuvastatin Accumulation (pmol/well)							
			Lysate				Buffer			
Study Phase	**Time (min)**		**+Ca^{2+}**		**-Ca^{2+}**		**+Ca^{2+}**		**-Ca^{2+}**	
	(in phase)	**(cumulative)**	**Mean**	**SEM**	**Mean**	**SEM**	**Mean**	**SEM**	**Mean**	**SEM**
Uptake	**2**	**2**								
	5	**5**	19.98	2.59	15.57	1.72				
	10	**10**	29.03	6.17	19.55	4.03				
	20	**20**	42.85	6.55	27.25	6.16				
Efflux	**2**	**23.5**	32.95	8.87	13.96	2.91	7.91	0.87	7.68	1.04
	5	**26.5**	28.73	6.91	10.91	1.57	14.34	1.88	12.92	1.93
	10	**31.5**	20.43	6.98	5.33	1.86	23.03	3.63	18.94	2.99
	15	**36.5**								

0.1 μM [^{3}H]Rosuvastatin, TR$^-$ (Control)

			[^{3}H]Rosuvastatin Accumulation (pmol/well)							
			Lysate				Buffer			
Study Phase	Time (min)		+Ca^{2+}		-Ca^{2+}		+Ca^{2+}		-Ca^{2+}	
	(in phase)	(cumulative)	Mean	SEM	Mean	SEM	Mean	SEM	Mean	SEM
Uptake	2	2	0.87	0.35	0.85	0.29				
	5	5	1.43	0.45	1.14	0.32				
	10	10	2.15	1.08	1.38	0.53				
	20	20	2.26	0.86	1.33	0.47				
Efflux	2	23.5	1.59	1.15	0.55	0.44	0.92	0.10	0.62	0.16
	5	26.5	1.10	0.78	0.29	0.22	1.24	0.32	0.84	0.35
	10	31.5	0.48	0.25	0.13	0.10	1.52	0.26	1.09	0.19
	15	36.5	0.38	0.30	0.07	0.08	1.83	0.45	1.19	0.37

1 μM [^{3}H]Rosuvastatin, TR$^-$ (Control)

			[^{3}H]Rosuvastatin Accumulation (pmol/well)							
			Lysate				Buffer			
Study Phase	Time (min)		+Ca^{2+}		-Ca^{2+}		+Ca^{2+}		-Ca^{2+}	
	(in phase)	(cumulative)	Mean	SEM	Mean	SEM	Mean	SEM	Mean	SEM
Uptake	2	2	6.69	2.20	6.33	1.94				
	5	5	10.34	3.55	8.65	3.08				
	10	10	16.47	7.39	10.99	5.54				
	20	20	18.00	7.56	11.08	4.70				
Efflux	2	23.5	11.23	5.65	3.54	2.22	5.72	1.99	3.86	1.71
	5	26.5	7.60	4.26	1.94	1.41	8.96	3.25	6.34	3.24
	10	31.5	5.36	3.90	0.88	0.79	12.52	5.90	7.40	3.89
	15	36.5	3.90	2.55	0.46	0.47	14.86	5.85	8.80	4.81

0.1 µM [^{3}H]Rosuvastatin, TR$^-$ (+GF120918)

			[^{3}H]Rosuvastatin Accumulation (pmol/well)							
			Lysate				Buffer			
Study Phase	Time (min)		+Ca^{2+}		-Ca^{2+}		+Ca^{2+}		-Ca^{2+}	
	(in phase)	(cumulative)	Mean	SEM	Mean	SEM	Mean	SEM	Mean	SEM
Uptake	2	2	0.84	0.31	0.90	0.37				
	5	5	1.25	0.56	1.27	0.55				
	10	10	1.91	1.01	1.74	0.88				
	20	20	2.18	1.23	1.88	1.07				
Efflux	2	23.5	1.36	1.09	0.93	0.61	0.83	0.19	0.72	0.11
	5	26.5	0.98	0.76	0.64	0.39	1.19	0.16	1.04	0.20
	10	31.5	0.68	0.70	0.42	0.38	1.70	0.37	1.46	0.33
	15	36.5	0.26	0.17	0.18	0.13	1.56	0.38	1.59	0.20

1 µM [^{3}H]Rosuvastatin, TR$^-$ (+GF120918)

			[^{3}H]Rosuvastatin Accumulation (pmol/well)							
			Lysate				Buffer			
Study Phase	Time (min)		+Ca^{2+}		-Ca^{2+}		+Ca^{2+}		-Ca^{2+}	
	(in phase)	(cumulative)	Mean	SEM	Mean	SEM	Mean	SEM	Mean	SEM
Uptake	2	2	6.98	2.53	7.08	2.62				
	5	5	9.92	3.75	9.27	3.10				
	10	10	14.94	7.34	13.38	6.06				
	20	20	19.54	11.21	15.67	9.08				
Efflux	2	23.5	12.39	9.23	7.43	4.62	5.68	1.56	5.90	1.36
	5	26.5	9.79	8.86	5.75	4.50	9.38	2.81	8.66	2.77
	10	31.5	5.49	6.04	2.46	2.46	12.48	5.93	10.04	4.36
	15	36.5	4.09	5.06	1.83	2.00	14.12	6.77	12.18	6.44

Figure 4.5

1 μM [^{3}H]Rosuvastatin, human SCH

			[^{3}H]Rosuvastatin Accumulation (pmol/well)							
			Lysate				Buffer			
Study Phase	**Time (min)**		**+Ca^{2+}**		**-Ca^{2+}**		**+Ca^{2+}**		**-Ca^{2+}**	
	(in phase)	**(cumulative)**	**Mean**	**SEM**	**Mean**	**SEM**	**Mean**	**SEM**	**Mean**	**SEM**
Uptake	**2**	**2**	4.58	2.89	3.23	3.18				
	5	**5**	8.28	2.29	5.67	2.15				
	10	**10**	11.49	2.69	8.41	3.06				
	20	**20**	15.05	3.31	10.20	1.44				
Efflux	**5**	**26.5**	7.55	1.78	5.34	1.98	3.34	0.24	1.97	0.44
	10	**31.5**	4.77	1.31	2.27	1.45	5.24	0.43	3.37	0.52
	15	**36.5**	4.21	1.38	1.29	0.84	6.71	0.44	4.35	0.99

Figure 4.6

Wild-Type (WT)

	Rosuvastatin Appearance Rate (nmol/min)							
	Bile				Perfusate			
Time (min)	Control		+GF120918		Control		+GF120918	
	Mean	SD	Mean	SD	Mean	SD	Mean	SD
5-15	4.15	1.00	5.60	2.80	4.22	0.98	2.40	1.87
15-30	8.40	1.91	12.2	4.6	6.98	0.86	2.79	1.75
30-45	11.2	2.6	14.3	3.3	6.11	1.73	3.24	1.83
45-60	11.3	4.3	13.8	4.2	6.16	2.18	3.36	1.94
60-70	16.1	9.9	14.4	2.6	4.60	1.92	2.17	1.21
70-75	4.92	1.75	6.14	3.54	2.87	1.43	1.39	0.86
75-80	2.44	0.96	4.75	1.60	2.45	1.59	1.06	0.68
80-90	1.65	0.69	2.68	0.74	1.52	1.18	0.627	0.333

Mrp2-Deficient (TR^-)

	Rosuvastatin Appearance Rate (nmol/min)							
	Bile				Perfusate			
Time (min)	Control		+GF120918		Control		+GF120918	
	Mean	SD	Mean	SD	Mean	SD	Mean	SD
5-15	1.20	1.53	0.559	0.437	0.471	0.349	0.346	0.196
15-30	5.17	1.30	1.42	0.49	1.20	0.75	1.41	0.92
30-45	5.86	1.28	1.67	0.71	2.05	1.01	1.78	0.44
45-60	5.92	1.16	1.63	0.52	2.78	1.23	3.05	0.84
60-70	6.44	0.59	1.82	0.55	2.60	0.96	2.93	0.67
70-75	4.05	1.28	1.25	0.33	2.43	1.05	2.66	0.29
75-80	3.58	1.12	0.979	0.392	2.02	0.48	2.58	0.41
80-90	2.92	1.14	0.743	0.473	1.52	0.37	1.91	0.48

Figure 4.7

	Recovery (% Administered Dose)							
	WT (Control)		WT +GF120918		TR$^-$ (Control)		TR$^-$ +GF120918	
	Mean	SD	Mean	SD	Mean	SD	Mean	SD
Rosuvastatin:								
Perfusate	34.1	8.4	16.3	9.8	14.3	4.7	16.5	6.3
Liver	4.9	4.2	6.5	2.0	20.2	9.2	29.0	5.4
Bile	57.1	20.2	65.0	17.3	36.7	11.4	10.4	2.9
Total	96.2	9.4	93.7	12.6	71.1	3.9	55.9	6.9
Rosuvastatin Pentanoic Acid:								
Liver, Total	2.1	0.6	3.3	2.0	13.3	6.1	18.7	5.3

Figure 4.8

A. 20 μM [^{3}H]$E_2$17G

	ATP-Dependent Uptake (% MRP Control)	
	Mean	**SD**
Non-Transfected (NT)	22.6	3.2
Control (MRP3)	100	9.8
+50 μM RSV	24.2	2.0
+50 μM MK-571	1.9	2.1

B. 2 μM [^{3}H]DHEAS

	ATP-Dependent Uptake (% MRP Control)	
	Mean	**SD**
Non-Transfected (NT)	12.2	4.7
Control (MRP4)	100	4.0
+50 μM RSV	12.4	4.6
+50 μM MK-571	-5.3	2.7

C. Time-dependent transport of [^{3}H]Rosuvastatin

	ATP-Dependent [^{3}H]Rosuvastatin Uptake (pmol/mg P)					
Time	**Non-Transfected (NT)**		**MRP3**		**MRP4**	
(min)	**Mean**	**SD**	**Mean**	**SD**	**Mean**	**SD**
0.5	0.150	0.042	0.255	0.086	1.00	0.15
1	0.285	0.075	0.566	0.032	1.50	0.09
2	0.294	0.092	0.823	0.018	1.68	0.11
5	0.342	0.084	0.999	0.153	1.87	0.10

D. Concentration-dependent transport of [^{3}H]Rosuvastatin

	MRP4-Dependent Uptake (pmol/min/mg P)	
[^{3}H]Rosvustatin Concentration (μM)	**Mean**	**SD**
1	49	1
5	203	12
10	379	23
20	577	55
50	786	174